FROSTING IN MEMBRANE ENERGY EXCHANGERS

A Thesis Submitted to the College of

Graduate Studies and Research

In Partial Fulfillment of the Requirements

For the Degree of Doctor of Philosophy

In the Department of Mechanical Engineering

University of Saskatchewan

Saskatoon

By

Mohammad Rafatinasr

PERMISSION TO USE AND DISCLAIMER STATEMENT

In presenting this thesis in partial fulfilment of the requirements for a Postgraduate degree from the University of Saskatchewan, I agree that the Libraries of this University may make it freely available for inspection. I further agree that permission for copying of this thesis in any manner, in whole or in part, for scholarly purposes may be granted by the professor or professors who supervised my thesis work or, in their absence, by the Head of the Department or the Dean of the College in which my thesis work was done. It is understood that any copying or publication or use of this thesis or parts thereof for financial gain shall not be allowed without my written permission. It is also understood that due recognition shall be given to me and to the University of Saskatchewan in any scholarly use which may be made of any material in my thesis.

The Exchanger by used in this thesis were exclusively created by dPoint technologies Inc. to meet the thesis and/or exhibition requirements for the degree of PhD at the University of Saskatchewan. Reference in this thesis/dissertation to any specific commercial products, process, or service by trade name, trademark, manufacturer, or otherwise, does not constitute or imply its endorsement, recommendation, or favoring by the University of Saskatchewan. The views and opinions of the author expressed herein do not state or reflect those of the University of Saskatchewan, and shall not be used for advertising or product endorsement purposes.

Requests for permission to copy or to make other uses of materials in this thesis/dissertation in whole or part should be addressed to:

Head of the Department of mechanical Engineering
57 Campus Drive
University of Saskatchewan
Saskatoon, Saskatchewan S7N 5A9 Canada

or

Dean
College of Graduate Studies and Research
University of Saskatchewan
107 Administration Place
Saskatoon, Saskatchewan S7N 5A2 Canada

ABSTRACT

Frost formation in heat/energy exchangers is undesirable because it may reduce air flow through the exchanger, increase the power consumption of fans, decrease the effectiveness of the exchanger, and in extreme cases, cause physical damage to the exchanger. Frosting is more critical in regions with arctic weather conditions, such as Canada and Northern Europe. Membrane-based energy exchangers are believed to be an important step towards frost free exchangers; however, at the beginning of this PhD study, there was no data available in the open literature documenting frosting in membrane energy exchangers. Therefore, the main goal of this PhD work is to determine if membrane energy exchangers are less susceptible to frosting than conventional heat exchangers.

In this thesis, an in-depth study between conventional cross-flow air-to-air heat exchangers and membrane energy exchangers is conducted to (1) quantify the frosting limit; the operating conditions at which frost first begins in an exchanger, (2) develop a theoretical model to predict the frosting limit, and (3) quantify the energy impact of frosting and defrosting cycles on energy recovery. To meet these objectives, a test facility to test exchangers under frosting and defrosting cycles is developed and different strategies to detect frosting inside the exchangers are investigated. For the first time in the literature, it is shown that the temperature profile at the exhaust outlet can be used as a reliable and quick method to detect frosting. The frosting limit temperature of the energy exchanger is found to be 5℃ to10℃ lower than the frosting limit of the heat exchanger under the same air flow rate and exhaust air relative humidity. Testing the exchangers under both frosting and defrosting conditions shows that the frost accumulation rate is nearly linear with time, while the frost removal rate decreases exponentially with time. Moreover, the frosting rate in the heat exchanger is found to be three times higher than that of the energy exchanger. A theoretical model to predict the frosting limit using the design parameters of the exchangers and the operating conditions is developed. The model is verified with experiments. Both the experimental and theoretical results show that the indoor air moisture content and the outdoor air temperature have significant effects on the frosting limit. Finally, a method to calculate the energy impact of frosting is introduced. Comparison between different frost control strategies in exchangers shows that frost prevention is preferred over repeated cycle of frosting followed by defrosting.

ACKNOWLEDGMENTS

I would like to express my sincere thanks to my supervisor Dr. Carey Simonson for his advice and guidance in this research and in the preparation of this thesis and my advisory committee members for directing me through my PhD studies. I would also like to convey special thanks to my parents, Mehdi and Sedigheh, my fiancé, Natalia, and my siblings for their support and encouragement during my PhD study.

I also express my gratitude to our research group members: Dr. Fauchoux, Dr. Ge, Mr. Fathieh, Dr. Ghadiri-Moghaddam, Dr. Ahmed Abdel-Salam, Mr. Mohamed Rani Abdel-Salam, Ms. Niroumand, Mr. Oghabi, Mr. Kamali, from University of Saskatchewan, Mr. Liu from NTNU, and Mr. Kadylak, Mr. Hizing from dPoint Technologies for their assistance during my research.

I would like to thank the Natural Sciences and Engineering Research Council of Canada (NSERC) for its financial support through the Smart Net-Zero Energy Building Strategic Research Network (SNEBRN), ASHRAE through a grant-in-aid, dPoint Technologies Inc. through a NSERC Engage project, and the University of Saskatchewan through PhD scholarships for graduate studies, travel awards, and Toyota Automotive Engineering award.

DEDICATION

*I dedicate this thesis to my hometown, **Abadan**, and its people including my family who showed me how to love and work hard and having very limited access to education is not an excuse to stop learning.*

TABLE OF CONTENTS

PERMISSION TO USE and DISCLAIMER statement i
ABSTRACT ii
ACKNOWLEDGMENTS iii
DEDICATION iv
TABLE OF CONTENTS v
LIST OF TABLES ix
LIST OF FIGURES x
NOMENCLATURE xv
1 CHAPTER 1: INTRODUCTION 1
1.1 Motivation 1
1.2 Background 3
1.2.1 Frost formation stages 4
1.2.2 Frosting in exchangers 4
1.3 Literature review 5
1.4 Objectives and overview 6
1.4.1 Test facility 7
1.4.2 Experimental frosting limit 7
1.4.3 Theoretical model 7
1.4.4 Energy impact of frosting and defrosting 8
1.5 Publications 8
1.5.1 Journal papers 8
1.5.2 Conference and technical meetings 9
1.6 Thesis Structure 9
1.7 Progress 11
2 CHAPTER 2: A REVIEW OF FROSTING IN AIR-TO-AIR ENERGY EXCHANGERS 12
2.1 Overview 12
2.2 Abstract 13
2.3 Introduction 13
2.4 Air-to-Air Heat/Energy Exchangers 15
2.4.1 Types of air-to-air heat/energy exchangers 15
2.4.2 Performance parameters in air-to-air heat/energy exchangers 16
2.5 Overview of research on frosting in exchangers 18
2.6 Frosting in exchangers 21
2.6.1 Physical process of frost formation in heat/energy exchangers 21
2.7 Research on frost properties 23
2.7.1 Frost formation, structure and location on simple geometries 23
2.7.2 Frost density, thermal conductivity and heat transfer coefficient 25
2.7.3 Frost on extended surfaces 26
2.7.4 Frost deposition pattern 26
2.7.5 Summary 27
2.8 Air-to-air Heat exchangers 28
2.8.1 Frost deposition pattern in exchangers 28
2.8.2 Effectiveness of heat exchangers under frosting 29
2.8.3 Frost location 31
2.8.4 Summary 31

2.9 Air-to-air Energy exchangers 32
2.9.1 Frosting limit 32
2.9.2 Frost type and location 36
2.9.3 Impact of frosting on effectiveness 38
2.9.4 Surface treatment effect 40
2.9.5 Frost detection methods 40
2.10 Defrosting techniques 42
2.10.1 Preheating the inlet air 42
2.10.2 Reducing the supply airflow rate 43
2.10.3 Recirculating warm exhaust air 44
2.10.4 Bypassing the supply air 45
2.10.5 Reducing the effectiveness of the exchanger 45
2.10.6 Auxiliary exchanger or double core heat exchanger 46
2.10.7 Coating on the surface of energy wheels 47
2.10.8 Phase-change materials 48
2.10.9 Moving belt and rollers 49
2.10.10 Design and Installation of Exchangers 49
2.11 Conclusions 52
2.12 Acknowledgement 53
3 CHAPTER 3: EXPERIMENTAL METHODS 54
3.1 Overview 54
3.2 Abstract 55
3.3 Introduction 56
3.4 Experimental methodology and uncertainty analysis 58
3.4.1 Instrumentation and uncertainty analysis 60
3.4.2 Mass and energy balance 63
3.4.3 Methods to detect the onset of frosting 65
3.4.4 Time to detect frosting 69
3.5 Results 70
3.5.1 Verification of experiments 70
3.5.2 Frosting detection methods 72
3.5.3 Time to detect the onset of frosting 84
3.5.4 Comparison of frosting detection methods 85
3.6 Conclusions 89
3.7 Acknowledgment 89
4 CHAPTER 4: THEORETICAL MODEL 90
4.1 Overview 90
4.2 Abstract 91
4.3 Introduction 91
4.4 Mathematical model 95
4.4.1 Assumptions 95
4.4.2 Critical supply (outdoor) air temperature 97
4.4.3 Condensation limit 98
4.4.4 Frosting limits 98
4.5 Experimental Validation 99
4.5.1 Test facility 99

4.5.2 Frosting detection methods 100
4.6 Results and Discussion 102
4.6.1 Model validation: **NTUh** and **NTUm** of heat/energy exchanger 102
4.6.2 Model Validation: Frosting limit 104
4.7 Parametric analysis 108
4.7.1 Effect of NTU on the frosting limit 108
4.7.2 Parametric study on NTU 111
4.8 Summary and Conclusions 113
4.9 Acknowledgements 114
5 CHAPTER 5: FROSTING-DEFROSTING AND REQUIRED DEFROSTING TIME 115
5.1 Overview 115
5.2 Abstract 116
5.3 Introduction 117
5.4 Methodology 119
5.4.1 Test facility 119
5.4.2 Measurement of frost mass 121
5.4.3 Criteria to measure the defrosting time 123
5.4.4 Operating conditions 124
5.4.5 Parameter definitions 125
5.5 Results and discussion 125
5.5.1 Frosting 126
5.5.2 Defrosting 135
5.5.3 Summary and Conclusion 143
5.6 Acknowledgment 144
6 CHAPTER 6: ENERGY IMPACT OF FROSTING 145
6.1 Overview 145
6.2 Abstract 146
6.3 Introduction 146
6.4 Defrosting methods 148
6.4.1 Preheating the outdoor supply air 148
6.4.2 Bypassing the outdoor airflow 149
6.5 Methodology 150
6.5.1 Heat/energy consumption without energy recovery 150
6.5.2 Heat/energy consumption when ignoring frosting effect 152
6.5.3 Heat/energy consumption using pre-heating method 154
6.5.4 Heat/energy consumption using outdoor air bypassing method 156
6.6 Experimental frosting limit and DTR of exchangers 159
6.7 Results and discussions 162
6.8 Conclusions 165
6.9 Acknowledgements 166
7 Chapter 7: SUMMARY AND CONCLUSIONS 167
7.1 SUMMARY AND CONCLUSIONS 167
7.2 Challenges/Limitations 169
7.2.1 Transient Nature of Frosting Tests 169
7.2.2 Heat Loss 169
7.2.3 Calibration 170

7.3 Contributions 170
7.4 FUTURE WORK 171
REFERENCES 172
APPENDIX: permissions to reproduce 179
A.1 Permissions for the manuscripts used in chapters 2,3, 4, and 6 179
A.2 Permission for the manuscript used in chapter 5 180

LIST OF TABLES

Table 2.1. Qualitative comparison between heat and energy exchangers. 41

Table 2.2. Frost control strategies or defrosting techniques in air-to-air heat/energy exchangers. 51

Table 3.1. Physical specifications of the heat and energy exchangers tested. 60

Table 3.2. Uncertainties in measured values. 63

Table 3.3. Total uncertainties in calculated values. 63

Table 3.4. Theoretical performance parameters. 68

Table 3.5. Experimental effectiveness for both the HRV and ERV at AHRI test conditions (i.e., with no frosting before and after the frosting experiments). 70

Table 3.6. Range of operating condition used to compare the different frost detection methods. 72

Table 3.7. Comparison between the frosting detection methods used in this paper. 88

Table 4.1. Physical specification of the heat and energy exchangers tested. 103

Table 4.2. Theoretical performance parameters. 104

Table 4.3. Comparison between the experimental and theoretical effectivenesses. 104

Table 4.4. Uncertainties in measured and calculated values with 95% confidence interval. 106

Table 5.1. Uncertainties in the Measured and Calculated Values. 120

Table 5.2. Physical Specifications of the Heat and Energy Exchangers. 121

Table 5.3. Test plan (highlighted boxes show test that was carried out under these conditions). 125

Table 5.4. Experimental effectiveness for both heat and energy exchangers at AHRI test conditions (no frosting) (Rafati Nasr, Fathieh, et al. 2015). 126

Table 5.5. Operating condition for frosting and defrosting tests. 126

Table 5.6. Summary of the operating conditions for each test. 127

Table 5.7. Summary of the results of the frosting tests. 131

Table 5.8. Summary of the frosting experiments and pressure change during frosting phase. .. 135

Table 5.9. Summary of the experiments during the defrosting phase. 140

Table 6.1. Design parameters for the energy estimation of ventilation. 150

Table 6.2. Tested effectiveness and frost limit of the heat/energy exchanger. 160

Table 6.3. Defrosting tests for a heat exchanger using outdoor air bypassing. 161

Table 6.4. Defrosting tests for an energy exchanger using outdoor air bypassing. 161

LIST OF FIGURES

Figure 1.1. Frosting in a fixed-plate cross-flow heat exchange (photo credit: JLHockman Consulting Inc.)..... 2

Figure 1.2. Climate zones in North America and Europe reprinted with permission from Dr.-Ing. Rainer Pfluger (Pfluger et al. 2015). 2

Figure 1.3. Phase diagram of water (Sonntag et al. 2009). 3

Figure 1.4. A schematic of frost growth in a counter-flow exchanger. 5

Figure 1.5. Overview of the thesis showing the objectives, chapters and their connections. 11

Figure 2.1. Fixed-plate cross-flow heat exchanger (ASHRAE 2012). 15

Figure 2.2. Rotary air-to-air energy exchanger (ASHRAE 2012). 16

Figure 2.3. Distribution of the published work from 1980-2013 on frosting in heat/energy exchangers..... 19

Figure 2.4. Distribution of the published work from 1980-2013 based on the type of heat/energy exchanger. 19

Figure 2.5. Distribution of the published work from 1980-2013 based on the energy transfer method..... 20

Figure 2.6. Distribution of the published work from 1980-2013 based on the content of the research. 20

Figure 2.7. Psychometric chart showing the processes in the exhaust and supply air streams in heat exchangers..... 22

Figure 2.8. Psychometric chart showing the processes in the exhaust and supply air streams in energy exchangers. 22

Figure 2.9. Frost growth process with time (Iragorry et al. 2004). t is time and T is the cold wall surface temperature. 24

Figure 2.10. Streamlines of flow configuration in cross counter-flow heat exchanger under laminar flow regime (Bantle et al. 1987). 29

Figure 2.11. Different regions in a typical cross-flow heat exchanger under frosting (Mercadier et al. 1993). 29

Figure 2.12. Double-pass heat exchanger (Holmberg 1989b). 30

Figure 2.13. Experimental frosting limit for three types of exchangers (Fisk et al. 1984). 33

Figure 2.14. Frosting limit in an energy wheel with an exhaust air inlet of 22 °C and different humilities at different supply air temperature and a humidity ratio of $0.23 g_w/kg_a$ (Bilodeau et al. 1999). 34

Figure 2.15. Results of frosting limits in an energy wheel for different exhaust air relative humidity(Gazi & Simonson 2012). 35

Figure 2.16. Regions in a cross view of the energy wheel with frosting (Holmberg 1989a). 37

Figure 2.17. Moisture content and frost formation across air tubes in energy wheel (Simonson & Besant 1998). 37

Figure 2.18. Latent effectiveness of an energy wheel for different relative humidity values with a supply air temperature of -20 ºC for two different desiccant coatings(Simonson & Besant 1998). 38

Figure 2.19. Schematic of frost thickness in the numerical model by Shang et al. (a) after first frost fracture, (b) just before the frost fracture (Shang et al. 2005). 39

Figure 2.20. Cross-leakage in energy wheels with frost blocking the matrix..... 39

Figure 2.21. Schematic of a bypass system in an exchanger (Bantle et al. 1987). 45

Figure 2.22.An auxiliary exchanger or double core heat exchangers (Kragh et al. 2007). 47

Figure 2.23. A cross flow heat exchanger with PCM (Qarnia et al. 2001)..... 48

Figure 2.24. Defrosting system to partially block supply air channels (Hallgren 1981). 49

Figure 3.1. Schematic of the experimental setup for air-to-air cross-flow exchangers. 59

Figure 3.2. Exchanger design and dimensions..... 60

Figure 3.3. Locations of the thermocouples, pitot tubes, and endoscopes at the outlet of the exchanger. 69

Figure 3.4. Mass and energy inequalities for the heat and energy exchangers under AHRI winter test conditions (no frosting). 71

Figure 3.5. Mass and energy inequalities for the heat and energy exchangers ($TSI = -20$℃ and $RHEI = 20\%$RH). 73

Figure 3.6. Photographs of the exhaust side outlet of the heat exchanger at different times during the experiment ($TSI = -20$℃ and $RHEI = 20\%$RH)..... 74

Figure 3.7. Photographs of the exhaust side outlet of the energy exchanger at different times during the experiment ($TSI = -20$℃ and $RHEI = 20\%$RH)..... 75

Figure 3.8. Change in pressure drop across the exchangers ($TSI = -20$℃ and $RHEI = 20\%$RH). 77

Figure 3.9. Change in Δp during the test (normalized with the uncertainty) showing the time to detect frosting, tf, and the uncertainty in the frosting time (Utf) with the Δp method ($TSI = -20$℃ and $RHEI = 20\%$RH). 78

Figure 3.10. The sensible and latent effectivenesses of the supply and exhaust streams. ($TSI = -20$℃ and $RHEI = 20\%$ RH). The error bars represent the 95% uncertainty bounds of each measurement. 78

Figure 3.11. Normalized $\Delta\varepsilon$ as a function of time showing the time to detect frosting, tf, for the heat and energy exchangers ($TSI = -20$℃ and $RHEI = 20\%$RH). 80

Figure 3.12. Difference between exhaust outlet temperature measured after a mixer ($Tmix$) and average of the 12 thermocouples at the face of the exchanger ($Tave$) during a frosting test ($TSI = -20$℃ and $RHEI = 20\%$RH). 81

Figure 3.13. Normalized ΔT as a function of time showing the time to detect frosting, tf, for the heat and energy exchangers ($TSI = -20$℃ and $RHEI = 20\%$RH). 82

Figure 3.14. Temperature distribution at the exhaust outlet in heat exchanger ($TSI = -20$℃ and $RHEI = 20\%$RH). 83

Figure 3.15. ΔT using thermocouples at different locations ($TSI = -20$℃ and $RHEI = 20\%$ RH). 84

Figure 3.16. Time to detect frosting by different methods for TSI $= -20$℃ and RHEI $= 20\%$RH. 85

Figure 3.17. Frosting detection time, with different methods at different operating conditions. . 85

Figure 3.18. ΔT and ΔP at different operating conditions. The green dots in the figure represents the time (according to the method in figures 3.12 and 3.13) where the frost detection method is able to conclude that frosting is occurring in the exchanger. 87

Figure 4.1. (a) Qualitative temperature distribution and frosting location in a cross-flow exchanger, (b) The channels with highest risk of frosting in a corrugated cross-flow air-to-air exchanger... 95

Figure 4.2. Schematic of the experimental setup for air-to-air cross-flow exchangers. 99

Figure 4.3. Frosting detection method when: $TSI \sim -15$℃, $TEI \sim 22, RHSI \sim 45\%$RH, $RHEI \sim 37\%$RH (a) Pressure drop method, (b) View of the energy exchanger at the end of experiment. 101

Figure 4.4. Tested exchangers and their geometrical parameters. 102

Figure 4.5. Experimental test points showing conditions with and without frosting in the heat exchanger and energy exchanger. 106

Figure 4.6. Experimental frosting limit for heat and energy exchanger. 106

Figure 4.7. Experimental and theoretical frosting limits for the (a) energy exchanger and (b) heat exchanger. 107

Figure 4.8. Effect of NTUh on frosting limit of the energy exchanger. Upper-left area represents the frost zone. 109

Figure 4.9. Effectiveness VS NTU for both sensible and latent heat. 110

Figure 4.10. Effect of NTUm on frosting limit of the energy exchanger. Upper-left area represents the frosting zone. 110

Figure 4.11. Minimum latent effectiveness for frost free energy exchanger versus sensible effectiveness at different TSI 111

Figure 4.12. Effects of different design parameters on $NTUh$. The horizontal axis shows the ratio of the values over base value used in this paper. 112

Figure 4.13. Effects of different design parameters on $NTUm$. The horizontal axis shows the ratio of the values over base value used in this paper. 113

Figure 5.1. Protecting an air-to-air exchanger by preheating the supply air. 118
Figure 5.2. Defrosting an air-to-air exchanger by shutting off the supply air. 118
Figure 5.3. Photograph of the test facility used for frosting and defrosting tests. 120
Figure 5.4. Mass of frost in the heat exchanger and energy exchanger as a function of time for repeated tests. 128
Figure 5.5. Mass of frost in the heat exchanger and energy exchanger as a function of time under different operating conditions. 129
Figure 5.6. Effect of flow rate on frost growth for the heat and energy exchangers. 130
Figure 5.7. The change in the pressure drop across the energy exchanger during one test. 132
Figure 5.8. Mass of frost with time for the heat and energy exchangers for repeated experiments. 136
Figure 5.9. Mass of water/frost in the heat and energy exchangers as a function of time during the defrosting phase. 137
Figure 5.10. Photographs from the heat exchanger exhaust outlet for the test with TSI $= -16^{\circ}$C and RHEI $=$ 34%RH. 138
Figure 5.11. Effect of flow rate on defrosting for the heat and energy exchangers. 139
Figure 5.12. Comparison of required defrosting time for test 15 (HX) and test 7 (EX) using two different criteria. Dashed lines show the time when defrosting is complete. 141
Figure 5.13. Required defrosting time ratio calculated from water mass measurement (mf) and moisture content change (Δw) methods. 142
Figure 6.1. The schematic of a heat/energy recovery system with preheating. 149
Figure 6.2. The schematic of a heat/energy recovery system with outdoor air bypassing. 149
Figure 6.3. The ambient temperature duration curve of Saskatoon and the required heating for ventilation. 151
Figure 6.4. The ambient temperature-enthalpy curve of Saskatoon and the required energy for ventilation. 152
Figure 6.5. The sensible heat recovered by heat exchanger and required heating energy by the re-heater when ignoring frosting effect. 153
Figure 6.6. The energy recovered by energy exchanger and required energy for ventilation air when ignoring frosting effect. 154
Figure 6.7. The recovered heat by heat exchanger and heating requirement by the pre-heater and re-heater when using pre-heating method. 155
Figure 6.8. The recovered energy by energy exchanger and energy requirement by the pre-heater and re-heater and humidifier when using pre-heating method. 156
Figure 6.9. Schematic of the frosting and defrosting periods for heat/energy exchangers. 157
Figure 6.10. The recovered heat by the heat exchanger and the required heating by the re-heater when using outdoor air bypassing. 158

Figure 6.11. The total energy recovered by energy exchanger and additional energy consumption for conditioning the ventilation air when using the outdoor air bypassing..... 159

Figure 6.12. Schematic of the test facility for frosting/defrosting tests of heat/energy exchangers. 160

Figure 6.13. The fitted average effectiveness of heat/energy exchangers at different outdoor temperatures. 161

Figure 6.14. The energy requirement to condition the outdoor air when the outdoor temperature is less than 0ºC. 162

Figure 6.15. The amounts of energy recovery and auxiliary energy requirement for ventilation by (a) heat exchanger (sensible), (b) energy exchanger (total) using different defrosting methods (Saskatoon, Canada). 163

Figure 6.16. The saving percentages by heat/energy exchangers using different defrosting methods in three cold cities. 165

NOMENCLATURE

	Definition	Unit
Acronym		
AHRI	Air-Conditioning, Heating and Refrigeration Institute	
ASHRAE	American Society of Heating, Refrigerating, and Air-Conditioning Engineers	
ASME	American Society of Mechanical Engineers	
CFD	Computational fluid dynamics	
DAQ	Data acquisition system	
ERV	Energy recovery ventilator	
FDP	frost deposition pattern	
HRV	Heat recovery ventilator	
HVAC	heating, ventilation, and air conditioning	
IAQ	Indoor air quality	
NSERC	Natural Sciences and Engineering Research Council of Canada	
PCM	Phase change material	
SNEBRN	Smart Net-Zero Energy Building Strategic Research Network	
English Symbols		
A	Total heat or mass transfer surface area	m^2
a	Half duct channel height in exchanger	mm
B	Bias uncertainty	
b	Half duct channel width in exchanger	mm
C	$\dot{m}c_p$ for sensible, $\dot{m}h_{fg}$ for latent or ṁ for total effectiveness	
C_i	Tracer gas concentration	%
c_P	specific heat capacity of air	kJ/ kg K
c_r	capacity ratio	-
cte	Constant value	
D_{eff}	Effective water vapor diffusivity	m^2/s
D_h	Hydrodynamic diameter of an air channel	mm
DTR	Defrosting time ratio	-
D_{va}	Water vapor diffusivity in the air	m^2/s
D_{wp}	Membrane water vapor diffusivity	m^2/s
EATR	Exhaust air transfer ratio	
EI	Exhaust air inlet	
EO	Exhaust air outlet	
Ex	Energy exchanger	
H	Exchanger height	mm
Hx	Heat exchanger	
h	Enthalpy	kJ/ kg
h	Convective heat transfer coefficient	J/(s m^2 K)
h_{fg}	heat of vaporization of water	kJ/ kg
h_m	Convective mass transfer coefficient	m/s
h_{sf}	Heat of fusion (melting)	kJ/ kg
k	Thermal conductivity	W/(m K)

L	Exchanger depth/ Air channel length	mm
$\dot{m}$	Mass accumulation rate (air, condensed water or frost)	g/min
n	Number of air channels in an exchanger	
NTU	Number of transfer unit	-
Nu	Nusselt number	-
OACF	Outdoor Air Correction Factor	-
p	Pressure	Pa
P	Precision uncertainty	
Q	Volumetric flow rate	L/s
q	Sensible, latent, or total transfer	
Re	Reynolds number	-
RER	Recovery Efficiency Ratio	-
RH	Relative humidity	%
SEE	Standard Error of Estimate	
SI	Supply air inlet	
Sh	Sherwood number	
SO	Supply air outlet	
T	Temperature	^{o}C
t	Time	min
t_f	Time duration it takes to detect frosting	min
U_R	Uncertainty of function R	
U	Overall heat transfer coefficient	
u	Velocity of air in channels	
U_m	Overall convective mass transfer coefficient	
w	Humidity ratio	g_{water}/g_{air}
X	Exchanger width	mm

Greek Symbols

ε	effectiveness	%
Δ	Algebraic difference	
η_{fS}	Supply side fan efficiencies	%
η_{fE}	Exhaust side fan efficiencies	%
ψ	stream line	
α	Apex angle for fin	°
δ	Thickness(membrane, plate, frost)	μm
φ	measured parameters such as T, RH, w	
ϕ	any constant value	
Ω	Heat or mass conductance	
ν	Kinetic viscosity	m^2/s
ρ	Density	kg/m^3
∂ / ∂	Partial derivative	

Subscript

1	First channel in exhaust side close to the supply air
a	Dry air properties
air	Dry air properties

aux	Auxiliary energy
avg	Average value
cr	Critical value to satisfy frosting condition
DF or df	Defrosting
E	Exhaust
EI	exhaust inlet/indoor
f	fin
F or f	Frosting
f/s	Related fluid or solid phase of water
j	Numeric indicator
l	Latent heat
lm	Logarithmic mean
m	Moisture or related to mass transfer of water vapor
max	Maximum
min	Minimum
mix	Fully mixed air properties
p	Plate in exchanger
rec	Recovered (heat/energy)
rh	re-heater
s or h	Sensible heat
S or sup	Supply
sf	Solid to liquid
sg	Solid to gas phase
SI	Supply inlet/outdoor
t	Total heat
tot	Total
∞	Related to the bulk flow
0	Initial value
ΔT	Related to ΔT method

Superscripts

‘	properties under preheating method
“	properties under bypassing method
*	Dimensionless from

CHAPTER 1:

INTRODUCTION

1.1 MOTIVATION

Energy consumption in residential and commercial buildings contributes to more than 30% of greenhouse gas emissions in Canada and 60% of these emissions are from space heating alone (NRC 2011). Also, providing outdoor ventilation air and conditioning the indoor air is crucial to the health and productivity of occupants. One of the ways to reduce energy use and greenhouse gas emissions for space heating and cooling is to incorporate air-to-air heat/energy exchangers into the heating, ventilation, and air conditioning (HVAC) systems. Exchangers, along with fans, filters, casings and control systems, are used in commercial units called Heat/Energy Recovery Ventilators (HRVs/ERVs). These HRVs/ERVs are designed to extract the waste heat from the stale exhaust air leaving the building and use it to warm the fresh ventilation air.

In Canada, the potential to recover energy is the greatest in the winter, when the difference between the indoor and outdoor air temperatures is large; however, during these very cold conditions, frost often forms in HRV/ERV units (Figure 1.1). Frost formation in HRVs/ERVs may reduce the air flow, increase the power consumption of fans, decrease exchanger effectiveness, or cause damage to the exchanger (e.g. deflection of the exchanger plates). This problem is more critical for the regions with arctic weather conditions such as Canada and Northern Europe (in Figure 1.2), especially during the winter.

The problem of frosting in exchangers has received attention for the past four decades; however, the frost protection mechanisms that are used in commercial HRV/ERV units are usually inefficient because they do not account for some of the important factors that govern frosting and defrosting. There is a high demand for making frost-free exchangers and smart frost protection systems, especially in cold regions such as Canada and Northern Europe.

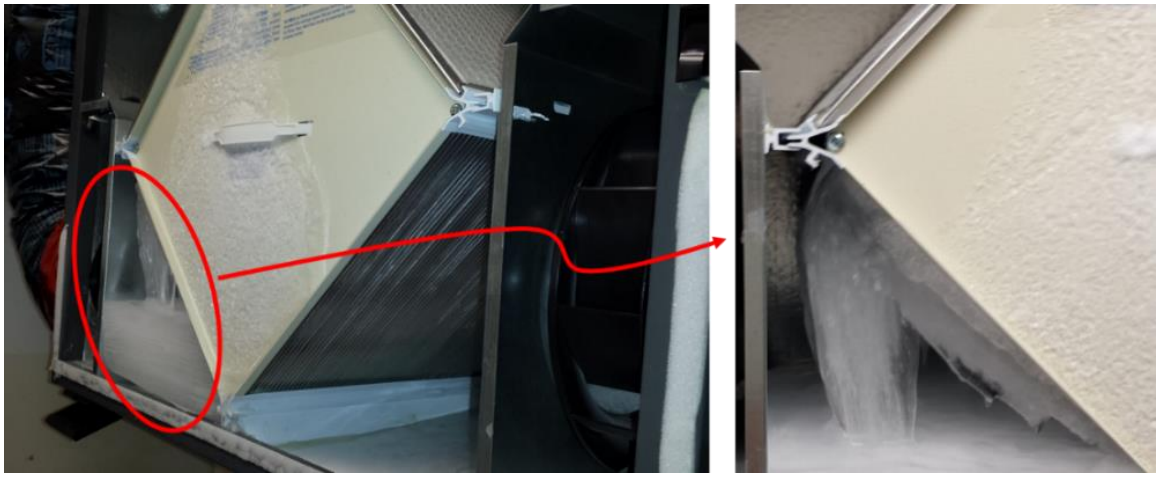

Figure 1.1. Frosting in a fixed-plate cross-flow heat exchange (photo credit: JLHockman Consulting Inc.).

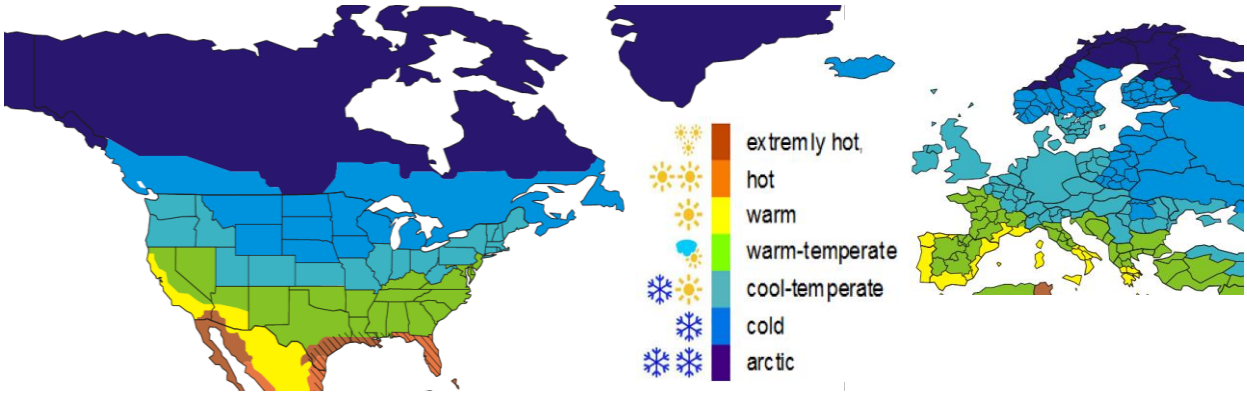

Figure 1.2. Climate zones in North America and Europe reprinted with permission from Dr.-Ing. Rainer Pfluger (Pfluger et al. 2015).

Membrane-based energy exchangers have been on the market for the past decade. In membrane exchangers, the aluminum or plastic plate that is used to separate the air streams in conventional heat exchanger designs is replaced with a membrane that is capable of moisture transfer, in addition to the heat transfer. Moisture transfer through the membrane reduces the risk of condensation and frost formation in exchangers. Studies on energy wheels under frosting conditions have shown that moisture transfer reduces the risk of frosting considerably (Shang et al. 2005; Gazi & Simonson 2012); however, membrane energy exchangers under frosting operating conditions have not been investigated in the literature.

To achieve the goal of efficient HRV/ERV units for cold climates, there is a need to investigate the performance of these units and conduct an energy analysis on them, in simulated cold-climate conditions. The main goal of this PhD research is to assess membrane energy exchangers and their performance under frosting conditions.

1.2 BACKGROUND

The phase diagram of water in Figure 1.3 represents the state of water (solid, liquid or vapor) based on the water vapor pressure and temperature. The liquid-solid boundary in this figure represents the freezing point. Beyond the critical point, water vapor and liquid co-exist, and at the triple point for water all three phases of water are in equilibrium.

When humid air flows over a cold plate, its temperature decreases due to convective heat transfer to the plate. If the temperature of the air goes below its dew point temperature, the water vapor in the air will begin to condense on the surface of the plate. A further temperature reduction will eventually lead to the formation of ice on the surface as the water changes from the liquid state to the solid state. Frost is formed when water changes phase directly from a vapor to a solid state. The presence of the plate, which acts as the nucleation site, is essential for condensation and frosting. In some situations (such as hoar frost), the water droplets floating in the air are super cooled to a temperature lower than the freezing point, due to the lack of a nucleation site. In this case, droplets freeze once they hit a surface. The structure of the frost depends on the vapor temperature, moisture content of the air, surface temperature, surface porosity, and surface adsorption potential on which the frost is deposited.

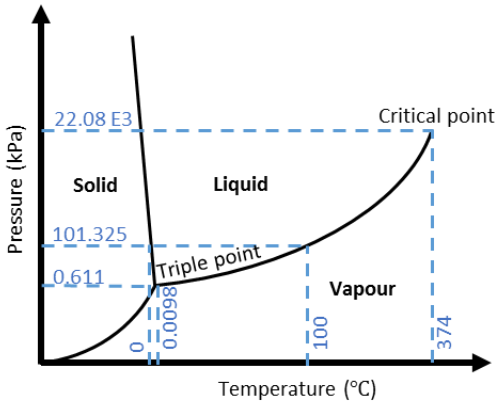

Figure 1.3. Phase diagram of water (Sonntag et al. 2009).

1.2.1 Frost formation stages

Experimental observations of frost on constant temperature surfaces have shown three stages in the frosting process: (1) dropwise condensation, during which very small droplets in the liquid state form on the cold surface. After a specific time, which is called the characteristic time, (2) solidification and tip-growth starts and continues until a transitional time is reached. At the transition time, the frost layer enters (3) the densification and bulk-growth period, where a network of ice branches grow from the main ice particle, forming a homogenous and porous frost structure over the surface.

The structure and characteristics of frost depend on the physical and thermodynamic frost properties of the specific application. Many types of frost which are found in nature, such as "window frost", "hoarfrost", "surface hoar", "frost flowers", and "rime frost" (Caltech 1999), are explained by these stages. However, these classifications are according to frost visual specifications and the natural condition in which these types of frost are formed. In HVAC applications, frost is classified mainly according to thermophysical properties. Depending on the frost type, different correlations have been developed to calculate the frost properties such as thermal conductivity, density, roughness, growth rate, water vapor diffusion coefficient, and porosity (Iragorry et al. 2004). Most of these correlations are based on experiments which indicates that theoretical models are not able to fully predict frost properties.

1.2.2 Frosting in exchangers

Figure 1.4 contains a schematic diagram of frost growth on an air-to-air plate heat/energy exchanger. When the plate temperature is below the freezing point, ice crystals start accumulating on the warm and humid (exhaust) side of the plate and the frost layer thickness increases with time. Due to the thermal resistance of the frost layer, the temperature at the air-frost interface increases as the frost thickness increases. When the interface temperature reaches the melting point, the frost at the interface starts to melt. The liquid water soaks into the frost layer and reduces the thermal resistance of the frost layer which will decrease the temperature at the air-frost interface and result in additional frost deposition. This continuous melting and freezing process eventually results in a dense layer of frost on the plate. In energy exchangers a similar process occurs, however the moisture transfer through the plate reduces the dew point temperature of the warm, humid air

stream. Figure 1.4 summarizes the heat and mass transfer mechanisms in heat and energy exchangers. In this figure, it is assumed that the surface temperature is below the freezing point. It should be kept in mind that frosting is always an unsteady process, and the non-uniformities in frost formation lead to three dimensional flow distribution over the surface which makes modeling of frosting in exchangers very complex.

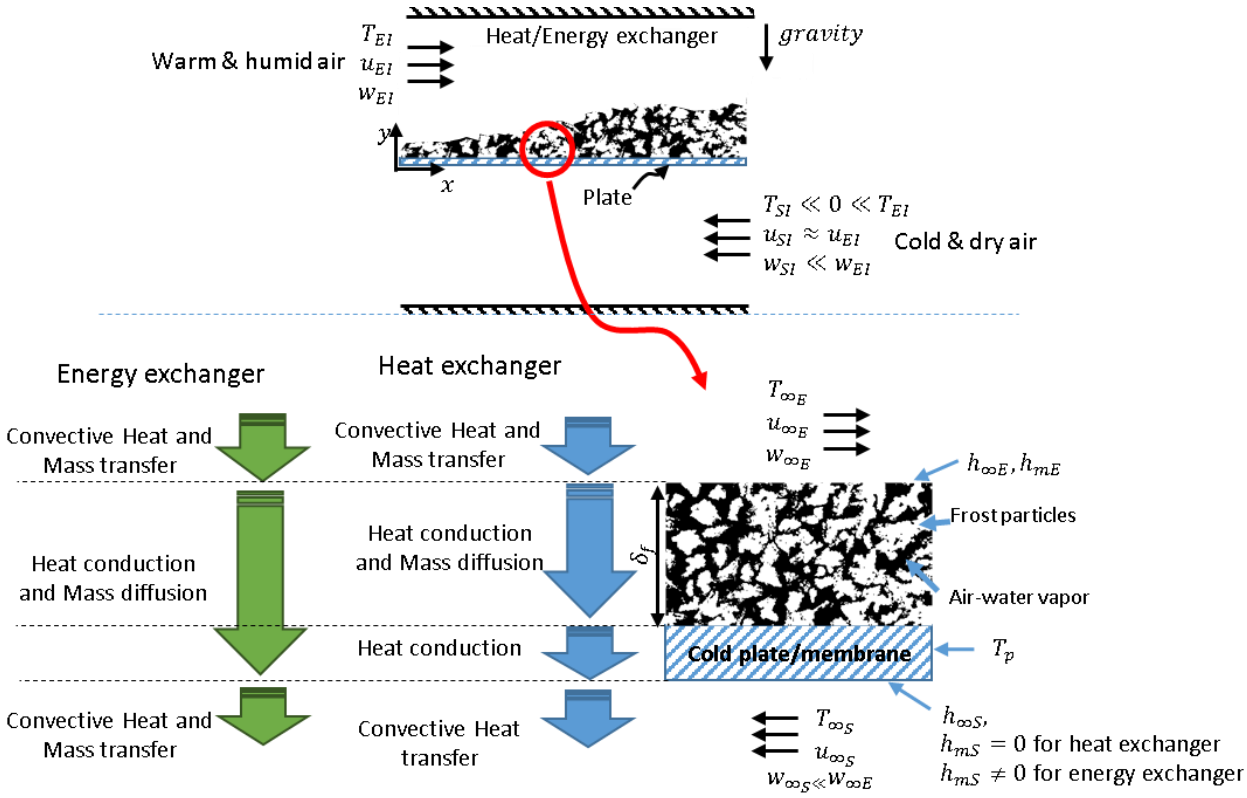

Figure 1.4. A schematic of frost growth in a counter-flow exchanger.

1.3 LITERATURE REVIEW

A comprehensive literature review is conducted to identify the work on frosting in air-to-air heat and energy exchangers. In this regard, common types of air-to-air exchangers such as cross-flow and counter-flow fixed plate exchanger, and heat and energy wheels under frosting conditions are considered. In the counter-flow configuration the two air streams passing through the exchanger in opposite direction in the exchanger and in cross flow configuration the two air stream are perpendicular to each other. In cross-flow exchangers, the two dimensional temperature

distribution of the plates makes the theoretical analysis more complicated. In addition, the methods to control frost in these exchangers are reviewed. This literature review is published as a review journal paper (Rafati Nasr, Fauchoux, Besant, et al. 2014) and is presented in Chapter 2 of this thesis. The main findings from this literature review are that the current frost protection mechanisms do not include important factors that govern frosting and defrosting, which results in a great amount of loss in energy recovery. Another observation is that membrane energy exchangers, which are expected to be more frost resistant compared to similarly designed heat exchangers, have not been investigated under frosting conditions.

1.4 OBJECTIVES AND OVERVIEW

The purpose of this PhD research is to assess membrane energy exchangers and their performance under frosting conditions. Frosting limit is referred to the operating conditions at which frost first begins in an exchanger. Assessment includes but not limited to measurement of frosting limit, sensible and latent effectiveness of exchangers, pressure drop across the exchangers, frost accumulation and frost removal rates during frosting and defrosting cycles, measurement of required duration of defrosting and impact of frosting on the total energy use in buildings.

The following objectives are set to investigate frosting in air-to-air cross-flow heat/energy exchangers:

1. Develop a test facility to investigate frosting in exchangers,
2. Quantify the frosting limit for heat and energy exchangers,
3. Develop a theoretical model to predict the frosting limit for heat and energy exchangers,
4. Evaluate the energy impact of frosting and defrosting phases.

To address each of these objectives and present a credible comparison between heat exchangers and energy exchangers, an energy exchanger and a heat exchanger with identical geometries are tested and analyzed. In the energy exchanger, the separating plate between the two air streams is a polymer membrane which is permeable to water vapor, while in the heat exchanger, the plates are made with an impermeable polymer film with the same thickness as the permeable membrane. More details about these exchangers are provided in Chapter 3.

1.4.1 Test facility

Due to limitations and complexity in the theoretical analysis of frosting, experimental evaluations of heat/energy exchangers under frosting conditions are essential in this research. However, frosting tests are costly, time consuming, and challenging. In addition, the test standards for air-to-air heat and energy exchangers (e.g. ASHRAE 2013; AHRI 2014) do not recommend tests under frosting conditions. Some of the questions which arise in an experimental approach are addressed in Chapters 3 to 5 such as: how to detect frosting in exchangers, what are the key operating conditions that lead to frosting in exchangers, and how to evaluate the transient process of frosting in exchangers. In Chapter 3, a detailed description of the test facility, calibration and uncertainty analysis are presented, and a new method to detect frosting in exchangers is introduced, evaluated and compared with traditional methods.

1.4.2 Experimental frosting limit

In practice, the frosting limit of an exchanger is required to determine whether or not an exchanger is at risk of frosting in a specific application. The literature review in Chapter 2 shows that frosting limits in exchangers are usually reported by supply air (outdoor) temperature. This data is not very useful when the operating conditions in exchangers are different than that in the literature. To find the frosting limit under a wider variety of conditions, the prototype heat exchanger and energy exchanger are tested at various operating conditions. The experimental results for each exchanger are presented in Chapter 4.

1.4.3 Theoretical model

Experimental evaluation of exchangers under frosting conditions is expensive and complex. In addition, experimental test facilities are not always able to cover different sizes and operating conditions for exchangers. Therefore, the third objective of this PhD research is to develop a simplified theoretical model to predict the frosting limit for cross-flow exchangers. In this model, the exchanger's design parameters such as flow rate, channel spacing, size of the exchanger, and membrane vapor transfer properties are taken into account. The experimental frosting limit results are used to verify the model. Using this theoretical model, an in-depth parametric study on exchanger design and operating conditions is done. The simplifying assumptions, verification of the model and the theoretical parametric studies are detailed in Chapter 4.

1.4.4 Energy impact of frosting and defrosting

The main problem with frosting in exchangers is the reduction in energy recovery when the potential to recover energy is highest. To determine how much the energy recovery is affected by frosting, the performance of the exchanger when frost is forming inside the exchanger must be measured. In this regard, the frost accumulation rate and its relation to the effectiveness change and pressure drop across the exchanger core are investigated experimentally. Moreover, the time it takes to remove the frost from the exchanger during defrosting mode according to the operating conditions and type of the exchanger is determined. In Chapter 5, the experimental results from frosting-defrosting modes for the heat exchanger and the energy exchanger are presented.

In the literature, the performance of exchangers under frosting conditions are discussed frequently, while the energy impact of frosting and defrosting on buildings' total heating requirement is missing. For example, when the heating energy consumption for buildings with HRV/ERV units is calculated, effectiveness of the exchanger is often assumed to be constant and the effect of defrosting modes is ignored. In Chapter 6, a method is introduced to estimate the heating energy consumption for buildings for different frost protection strategies and different weather conditions. This method uses both experimental results from this research as well as standard values from the literature.

1.5 PUBLICATIONS

The research outcomes of this PhD work are published or under review in several journals, and presented in several national and international conferences, workshops and technical meetings. At the time of preparation of this thesis, a journal papers is still under review. The list of publications are as follows:

1.5.1 Journal papers

1. Rafati Nasr, M., Simonson, C.J.,. Measurement of required defrosting time for air-to-air heat and energy exchangers, *International Journal of Refrigeration*, (submitted in March 2016) **(Presented in Chapter five of this thesis)**
2. Rafati Nasr, M., Fathieh, F., Kadylak, D., Huizing, R., Simonson, C.J.,. Experimental methods for detecting frosting in cross-flow air-to-air energy exchangers, *Experimental Thermal and Fluid Science*, Experimental Thermal and Fluid Science 77 (2016) 100–115. **(Presented in Chapter three of this thesis)**

3. Liu, P., Rafati Nasr, M., Ge, G., Justo Alonso, M., Mathisen, H.M., Fathieh, F., Simonson, C.J., 2015, A theoretical model to predict frosting limits in cross-flow air-to-air flat plate heat/energy exchangers, *Energy and Building*, 110:404-14. **(Presented in Chapter four of this thesis)**
4. Rafati Nasr, M., Kassai, M., Ge, G., Simonson, C.J., 2015. Evaluation of defrosting methods for air-to-air heat/energy exchangers on energy consumption of ventilation, *Applied Energy*, 151, 32-40. **(Presented in Chapter six of this thesis)**
5. Rafati Nasr, M., Fauchoux, M.T., Besant, R.W., Simonson, C.J., 2014. A review of frosting in air-to-air energy exchangers, *Renewable and Sustainable Energy Reviews*, 30, 538-554. **(Presented in Chapter two of this thesis)**

1.5.2 Conference and technical meetings

6. Rafati Nasr, Simonson, C.J.,. Experimental measurement of frosting limits in cross-flow air-to-air energy exchangers, Technical paper in 2016 ASHRAE winter Conference, January 28-Feb 1, 2017, Las Vegas, USA.
7. Rafati Nasr, M., Fauchoux, M., Kadylak, D., Huizing, R., Simonson, C.J., 2014. Frosting limit in air-to-air membrane energy exchangers, Proceedings of the 10th Nordic Symposium on Building Physics, edited by J. Arfvidsson, L. Harderup, A. Kumlin and B. Rosencrantz, Lund, Sweden, June 15-19, 774-781.
8. Rafati Nasr M., Zhang J.L., Fathieh1, F., Fung, A.S., Simonson, C.J., 2015, Energy impact of frosting and defrosting in HRV/ERVs, Poster presentation in 4th annual meeting of NSERC Smart Net-Zero Energy Building Strategic Research Network (SNEBRN), Saskatoon, Canada.
9. Rafati Nasr M., Liu, P., Simonson, C.J., 2014, Test facility and frosting detection methods for air-to-air energy exchangers, Poster presentation in 3rd annual meeting of NSERC Smart Net-Zero Energy Building Strategic Research Network (SNEBRN), Montreal, Canada.
10. Liu, P., Justo Alonso, M., Mathisen, H.M., Rafatinasr, M., Simonson, C.J. 2014. Frosting limits for counter-flow Membrane Energy Exchanger (MEE) in cold climates Proceedings of Indoor Air Conference 2014, Hong Kong.

1.6 THESIS STRUCTURE

In this thesis, a combination of experiments and theoretical analysis is adopted. The test facility allows testing the exchangers under very low supply temperatures. The experiments include four methods of detecting frost and monitoring the performance of the exchangers (Chapter 3). The frosting limit operating conditions are measured and a theoretical model is developed to predict such conditions (Chapter 4). In addition, the performance of the exchangers under frosting and defrosting phases are evaluated and the required defrosting time, based on the operating conditions,

are calculated (Chapter 5). In Chapter 6, a method to estimate the energy impact of frosting using the frosting limit, operating conditions and the required defrosting time is discussed.

This thesis is structured as a manuscript style thesis. Each chapter from Chapter 2 to Chapter 6 contains a journal paper that is published or under review. All manuscripts have been reformatted from the original version for inclusion in the thesis. In Chapter 4, additional results are added that are not part of the published paper. At the beginning of each chapter an overview of each paper along with the contributions of each author are provided. Each paper addresses the objectives according to Figure 1.5. The diagram depicts the structure of the thesis by showing the objectives and chapters and how they are connected.

1.7 PROGRESS

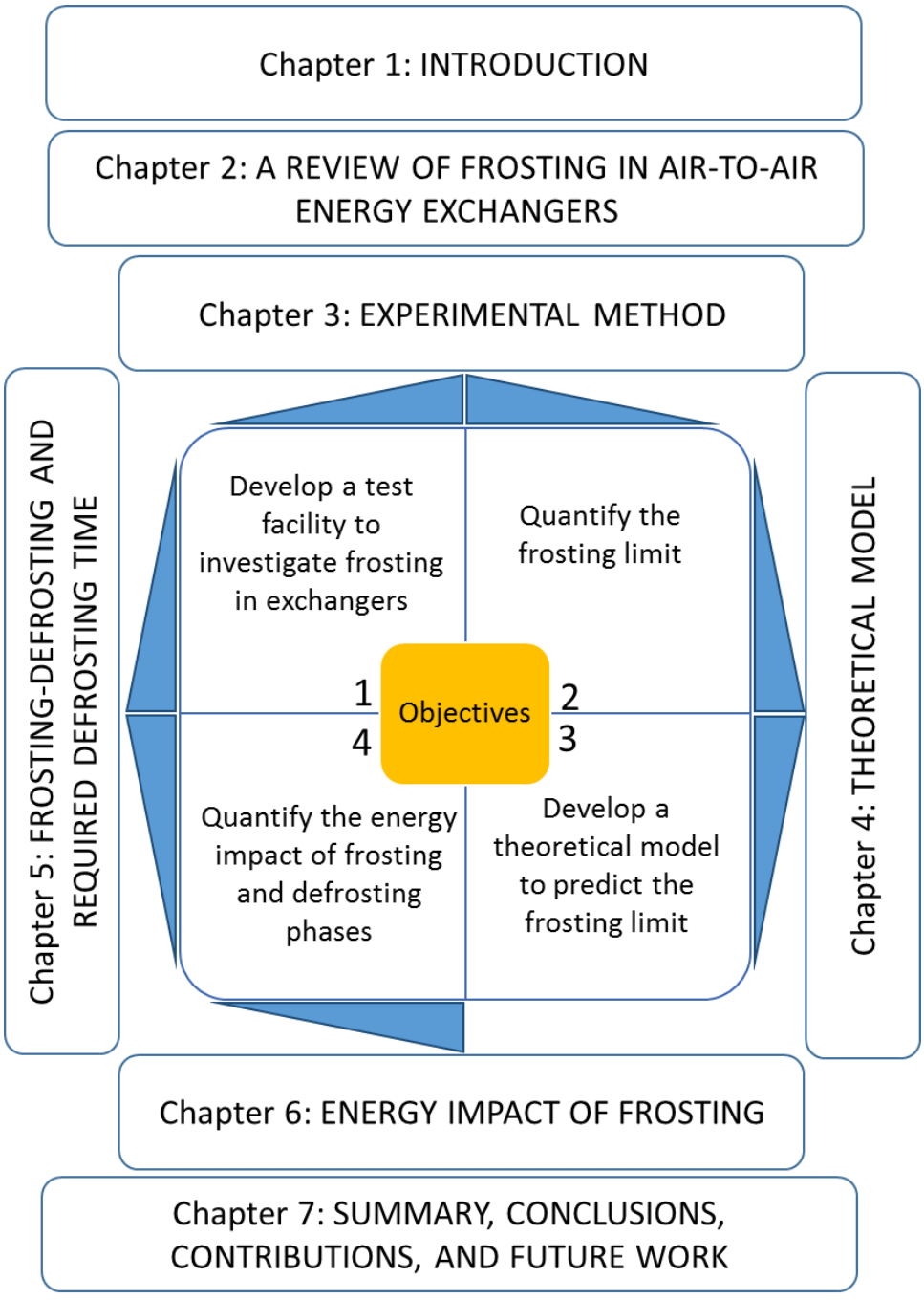

Figure 1.5. Overview of the thesis showing the objectives, chapters and their connections.

CHAPTER 2:

A REVIEW OF FROSTING IN AIR-TO-AIR ENERGY EXCHANGERS

2.1 OVERVIEW

This chapter presents a comprehensive literature review on frosting in air-to-air heat/energy exchangers. Existing air-to-air exchanger technologies and challenges related to their applications in cold climates are reviewed. After a short overview of studies on the physical properties of frosting, such as density and thermal conductivity, frosting patterns in exchangers, exchanger effectiveness under frosting, and the operating conditions when frosting begins in the exchangers are discussed. Finally, different frost control technologies in the literature are evaluated.

The manuscript presented in this chapter is published in Renewable and Sustainable Energy Reviews. Dr. Fauchoux, a post-doctoral fellow, contributed to this manuscript by proofreading the paper, and providing guidance to clarify the discussions and organizations of the topics in the paper. Professor Besant is very experienced in frosting research and helped by identifying many relevant papers and reports for this report, some of which could not be found through online resources. As the lead author, the PhD candidate, Mr. Rafati conducted the literature search, reviewed all the literature, summarized the research into different categories, developed the layout of the paper, wrote the manuscript, requested permission to reuse materials in the literature from the copyright holders, incorporated co-authors comments and addressed the reviewers' comments.

This paper was prepared during the first year of this PhD study, and the findings from this paper were used to develop the objectives of this PhD research, based on the gaps in the current research. It should be noted that very recent work (2014 and after) on membrane energy exchangers under frosting are not addressed in chapter 2. Example includes Liu et al. (2016); Liu et al. (2014); Alonso et al. (2015); Zhang & Fung (2015a); Zhang et al. (2014); Zhang & Fung (2015b).

A review of frosting in air-to-air energy exchangers

(Renewable and Sustainable Energy Reviews 30 (2014) 538–554)

Mohammad Rafatinasr, Melanie Fauchoux, Robert W. Besant, Carey J. Simonson

2.2 ABSTRACT

Air-to-air heat/energy exchangers are often used with heating or cooling systems in buildings to transfer heat and moisture from an airstream at a high temperature or humidity to an airstream at a low temperature or humidity. Frosting inside heat/energy exchangers is common in cold regions such as Canada and northern Europe, and results in a significant decrease in the performance of the exchangers. The desire to improve the performance and control strategies of heat/energy exchangers under cold air conditions has led to significant research and development equipment over the past 30 years, however, from an energy savings point of view, this problem has not been researched in as much detail. In this paper, a detailed review of the research on frosting and defrosting techniques, specifically in air-to-air heat/energy exchangers is presented.

2.3 INTRODUCTION

Global demands for environmentally clean energy and a shortage of energy resources have led to the development of more energy efficient technologies. In cold countries, 30% to 50% of the total energy consumed is used for residential and commercial buildings, and 60% of that is dedicated to space heating and cooling (NRC 2011; Nyman & Simonson 2005). Many studies have focused on ways to reduce the amount of energy used by Heating, Ventilation and Air-conditioning (HVAC) systems (Charneux 2012; Voss et al. 2009; Nyman & Simonson 2005) (Besant & Simonson 2000; Besant & Simonson 2003). Heat/Energy Recovery Ventilators (HRV/ERV) are types of HVAC systems that are designed to reduce energy consumption. An ideal heat/energy exchanger allows sensible and latent (for energy exchangers) heat transfer between supply and exhaust air under all operating conditions without significant cross-contamination. Typical HRV/ERV units contain a heat/energy exchanger, fans, supply and exhaust ducts, air filters, a drainage system and controllers. To design an efficient heat/energy exchanger some factors should

be considered such as, pressure drop, fouling, corrosion, maintenance, controls, condensation and frost formation (ASHRAE 2012).

Frost formation in exchangers is common in cold regions where the outdoor temperature is below -10°C for the majority of the cold season. Conventional problems created by the formation of frost in energy exchangers are:

- Partial or full blockage of air flow passages (Bantle et al. 1987),
- Increase in pressure drop through the exchanger or decrease in air flow rate (Chichindayev 2006; Fisk et al. 1984; Fisk et al. 1985),
- Increase in electric power for the fans (Kragh et al. 2005; Davis 1996),
- Decrease in the heat transfer rate between the two air streams (Fisk et al. 1985) and
- Draught in the space due to low supply air temperatures (Kragh et al. 2005).

Additionally, frosting in heat exchangers has been reported as a reason for operational problems in the air conditioning systems of aircraft (Chichindayev 2006), boats and ships, and electro power systems (Östin & Johannesson 1991). Each of the aforementioned problems can result in a reduction in the effectiveness of the equipment over a short time period or physical damage to the equipment over a longer time.

Energy recovery is most beneficial when the outside air is very cold, because high temperature and humidity differences between the indoor and outdoor air creates the potential for high energy transfer rate and energy savings. However, a considerable reduction in the effectiveness of exchangers under frosting conditions reduces energy recovery, exactly when the most energy can potentially be recovered. In this paper, an overview in the open literature in the category of frosting in heat/energy exchangers is presented. Also, a brief review of the process of frost formation and frost properties on simple surfaces is provided. This paper reviews the open literature in the field of frosting in air-to-air heat/energy exchangers, summarizes the findings of previous research, finds similarities and differences in the results, presents defrosting/frost protection techniques or methods to decrease the negative effect of frosting and finally highlights the gaps in the literature.

2.4 AIR-TO-AIR HEAT/ENERGY EXCHANGERS

Energy can be recovered in the form of sensible (heat transfer) or latent (moisture transfer) or both. In air-to-air exchangers two air streams pass through the exchange without mixing. Depending on the design, energy is transferred directly or indirectly from one air stream to the other. Air-to-air exchangers can be categorized into different groups based on the geometry of the exchanger and the orientation of the airflow. These include fixed plate exchanger, rotary exchanger, run around coils, heat pipe heat exchangers, and twin tower energy recovery loops (Reay 1980; ASHRAE 2012), however plate heat/energy exchangers and heat/energy wheels are more widely used, and thus will be the focus of this paper.

2.4.1 Types of air-to-air heat/energy exchangers

Fixed plate heat/energy exchangers: In this type of exchanger, the supply and exhaust air pass through adjacent channels with parallel surfaces, in counter-flow or cross-flow configurations. If the surfaces are made of an impermeable material (e.g. aluminum or plastic), only heat will transfer between the two streams, while if the surface is a permeable material (e.g. treated paper (Barringer & McGugan 1988), or a semi-permeable membrane (Ge et al. 2013; Zhang 2012) both heat and moisture will transfer between the two streams.

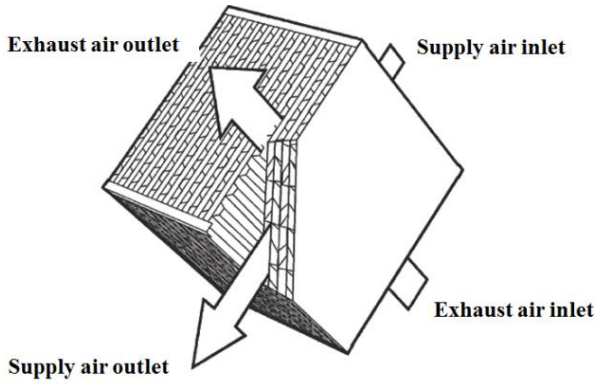

Figure 2.1. Fixed-plate cross-flow heat exchanger (ASHRAE 2012).

Rotary air-to-air heat/energy exchangers (heat/energy wheels): A rotary energy exchanger is made of a rotating cylinder, filled with an air-permeable structure with a high surface area in contact with the air. Supply and exhaust air pass through the wheel, in a counter-flow configuration. Heat/moisture are transferred from one air stream to the surface, then the wheel

rotates 180° and the heat/moisture from the surface are released in to the other air stream (Simonson 2007).

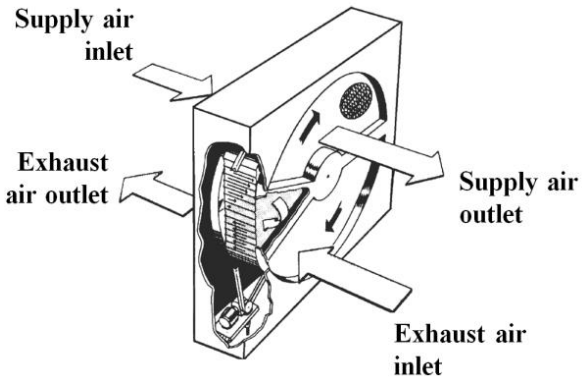

Figure 2.2. Rotary air-to-air energy exchanger (ASHRAE 2012).

2.4.2 Performance parameters in air-to-air heat/energy exchangers

The performance of air-to-air heat/energy exchangers depends on many factors, including inlet conditions, as well design parameters. The performance of exchangers is quantified using the following parameters:

Effectiveness: The main indicator of performance in air-to-air exchangers is the effectiveness: sensible effectiveness for a heat exchanger and both sensible and latent effectivenesses for a energy exchanger. The effectiveness of an exchanger is calculated for the supply and exhaust streams from the following equations (ASHRAE 2013):

$$\varepsilon = \frac{q}{q_{max}} \tag{2-1}$$

$$q = \begin{cases} C_{SO}(\varphi_{SI} - \varphi_{SO}) & \text{supply side} \\ C_{EI}(\varphi_{EO} - \varphi_{EI}) & \text{exhaust side} \end{cases} \tag{2-2}$$

$$q_{max} = C_{min}(\varphi_{SI} - \varphi_{EI}) \tag{2-3}$$

Where ε effectiveness

q sensible, latent, or total energy

φ dry-bulb temperature for sensible effectiveness, humidity ratio for latent effectiveness or enthalpy for total effectiveness

C $\dot{m}_a c_p$ for sensible, $\dot{m}_a h_{fg}$ for latent or $\dot{m}$ for total effectiveness

$\dot{m}_a$ the mass flow rate of dry air

c_p the specific heat of dry air

h_{fg} the heat of vaporization of water

SI, SO, EI, and EO subscript represent supply inlet, supply outlet, exhaust inlet, and exhaust outlet respectively. When no frost, condensation or excessive moisture transfer is present in the exchanger, the effectivenesses on the supply and exhaust sides should be the same.

Outdoor Air Correction Factor (OACF): The outdoor air correction factor is a measure of the leakage between the supply duct and the exhaust duct in an exchanger. If there is no leakage, the value will be one. The outdoor air correction factor is calculated from (ASHRAE 2013):

$$OACF = \frac{\dot{m}_{SI}}{\dot{m}_{SO}} \tag{2-4}$$

Exhaust air transfer ratio: The exhaust air transfer ratio is a scale indicating the amount of leakage of a specific gas from one side to the other defined by (ASHRAE 2013):

$$EATR = \frac{C_{i\_SO} - C_{i\_SI}}{C_{i\_EI} - C_{i\_SI}} \tag{2-5}$$

Where C_i is the tracer gas concentration at each location.

Recovery Efficiency Ratio (RER): The recovery efficiency ratio is a ratio of the energy transferred in the energy exchanger to the energy consumed by the exchanger. It defines by (ASHRAE 2013):

$$RER = \frac{\dot{m}_S(h_{SI} - h_{SO})}{\Delta p_S Q_{SO}/\eta_{fS} + \Delta p_E Q_{EI}/\eta_{fE} + q_{aux}} \tag{2-6}$$

$\Delta p_S$and$\Delta p_E$are the pressure drop across the supply and exhaust side of the exchanger respectively. Q is the volume flow rate, η_{fS} and η_{fE} are the supply and exhaust side fan efficiencies, q_{aux} the auxiliary total power input. In addition to these performance parameters, some important non-dimensional parameters that are used to define exchangers are number of heat transfer units (NTU_h), and capacity ratio (c_r) (ASHRAE 2009):

$$NTU_h = \frac{(UA)_h}{C_{min}} \tag{2-7}$$

$$c_r = \frac{C_{min}}{C_{max}} \tag{2-8}$$

Where U is the overall heat transfer coefficient, A is the heat transfer area associated with U, and C_{min} and C_{max} are the minimum and maximum heat capacity between supply ($C_S = \left(\dot{m}c_p\right)_S$) and exhaust ($C_E = \left(\dot{m}c_p\right)_E$) fluid capacity rate, respectively. Sensible effectiveness (ε_s) can be expressed as a function of NTU and c_r (ASHRAE 2009):

$$\varepsilon_s = f(NTU_h, c_r, \text{flow arrangement}) \tag{2-9}$$

It can be understand from equation (2-9) that effectiveness is independent of exchanger inlet temperatures. The functional relationships in equation (2-9) are provided in (ASHRAE 2009) and other heat transfer books for different flow arrangements. For energy exchangers mass transfer occurs as well as heat transfer. The number of mass transfer units (NTU_m) in energy exchangers is defined by (2-10) (Namvar et al. 2012). In this equation U_m is the overall convective mass transfer coefficient, and $\dot{m}_{min}$ is the minimum mass flow rate between the two air streams.

$$NTU_m = \frac{(UA)_m}{\dot{m}_{min}} \tag{2-10}$$

2.5 OVERVIEW OF RESEARCH ON FROSTING IN EXCHANGERS

In order to provide a review of the current literature on frosting in heat and energy exchangers, a search was performed using an inclusive engineering publication database (www.engineeringvillage.com). Figure 2.3 shows the number of papers published, over five years periods, from 1980 to 2013 related to frost in heat and energy exchangers. It can be seen that frosting in heat/energy exchangers has been a concern for the past 30 years, but has received more attention in the last decade. By categorizing the studies based on the type of heat/energy exchangers in Figure 2.4, it can be seen that most of the research has been on heat pumps and refrigeration systems, and very little research has focused on air-to-air heat/energy exchangers. There are fewer papers on other types of air-to-air exchangers in applications such as electronic device, cars or aircrafts. The remaining papers are grouped in the “not specified” category because

the research was on simple geometries such as frosting on plates or tubes or the application was not clear from the abstract. Considering only the review papers in frosting in heat/energy exchangers in Figure 2.3 showed that no comprehensive review for frosting in air-to-air heat/energy exchangers. Most of reviews are in frosting in heat pumps, or frost properties. This review paper will focus on those papers relating to plate heat exchangers and energy wheels. These devices are described in the next section.

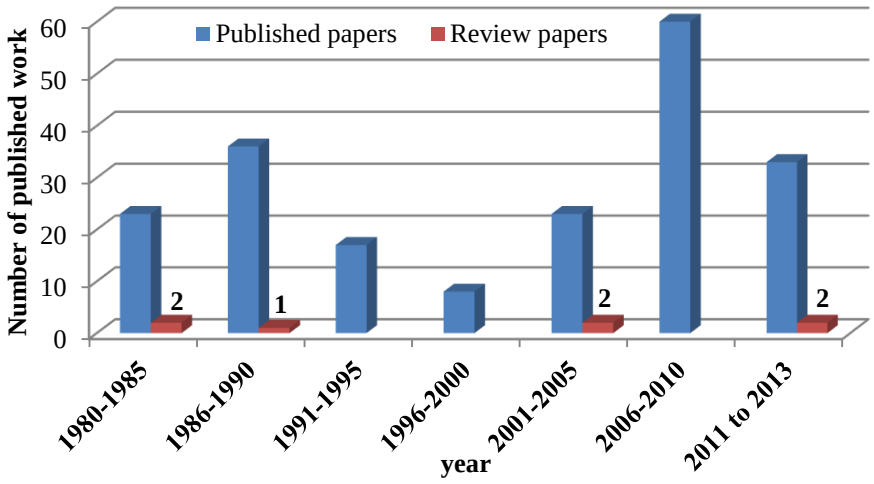

Figure 2.3. Distribution of the published work from 1980-2013 on frosting in heat/energy exchangers.

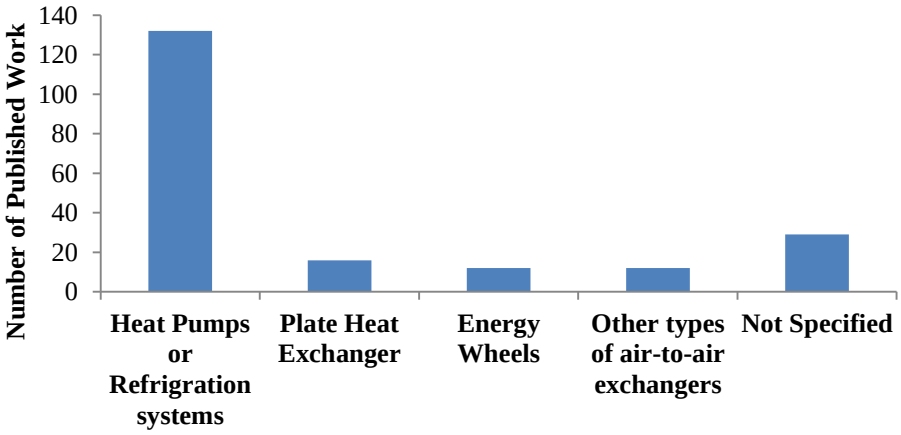

Figure 2.4. Distribution of the published work from 1980-2013 based on the type of heat/energy exchanger.

Since both heat and energy exchangers are considered in this review, it is also interesting to look at the distribution of papers by the type of energy transfer. As depicted in Figure 2.5, most of the

papers have included sensible heat transfer only, while a smaller amount have considered latent heat transfer or mass transfer in the exchangers as well. Figure 2.6 shows that the majority of the published works have reported frosting issues in exchangers, while a lower number have considered or investigated frost protection techniques and methods of defrosting the exchangers.

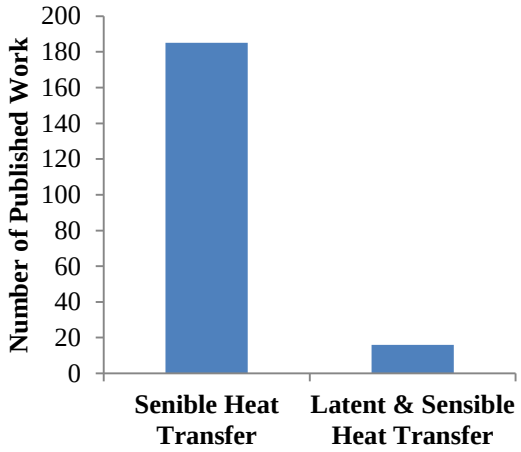

Figure 2.5. Distribution of the published work from 1980-2013 based on the energy transfer method.

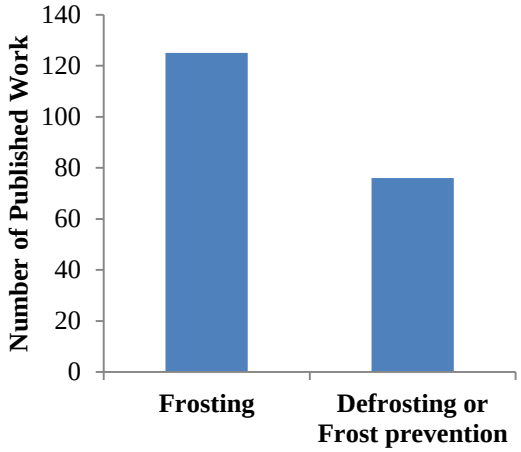

Figure 2.6. Distribution of the published work from 1980-2013 based on the content of the research.

Although, the concept of frost formation in exchangers has received increasing interest from researchers and industry over the past 30 years, this problem is still unresolved and specifically, more work is needed to study frost in exchangers which transfer latent heat as well as sensible heat. In addition, more research is required to find new defrosting techniques or frost prevention

methods. In recent years, new types of porous materials - called semi-permeable membranes- which can transfer moisture as well as heat have been developed and have applications in both air-to-air and air-to-liquid energy exchangers (Ge et al. 2013). However, the search for papers on frosting in energy exchangers produced no papers that studied frosting in membrane-based energy exchangers.

2.6 FROSTING IN EXCHANGERS

Frosting in heat and energy exchangers is observed when the outdoor temperature falls below the frosting threshold of the equipment at certain relative humidity (RH) levels (Phillips et al. 1992). In addition to the outside temperature and humidity ratio, the frosting limit (the lowest outdoor air temperature which does not lead to frosting in the exchanger) for each exchanger is strongly dependent on its design and the type of energy transfer (sensible or latent). Typically, frosting will be observed for outdoor temperatures below -5°C, if no frost protection techniques are implemented. In a mild climate, frost protection techniques have little impact on the performance of the exchangers, while in cold regions those techniques are important (Phillips et al. 1992). In the following subsections, the process of frost formation is explained and different studies on frosting in exchangers are described.

2.6.1 Physical process of frost formation in heat/energy exchangers

When warm moist air (exhaust air) passes over a surface with a low temperature, part of its energy in the form of sensible heat is transferred to the surface. If the temperature of the exhaust air goes below the dew point temperature, moisture will condense on the surface. If the surface temperature is lower than the freezing point of water, frosting will occur. This process is shown in Figure 2.7. From this figure, it can be seen that condensation and frosting may occur in the exhaust side of a heat exchanger.

In total energy exchangers, such as energy wheels or membrane exchangers, in which both latent and sensible heat can be transferred, a different process happens on the psychometric chart. As shown in Figure 2.8, the exhaust air temperature and humidity ratio decrease simultaneously. In this situation. Therefore, exhaust air can reach a temperature below the freezing point before frosting is observed. The addition of moisture transfer results in a decrease in the humidity ratio and dew point temperature of the exhaust air, as the air moves towards the outlet. A rule of thumb

predicts saturation conditions in an energy exchanger when a straight line connecting the inlet supply and exhaust conditions on the psychometric chart touches the saturation line (Holmberg 1989a). If the contacting point is below the freezing temperature (similar to Figure 2.8), frosting in the exchanger may occur.

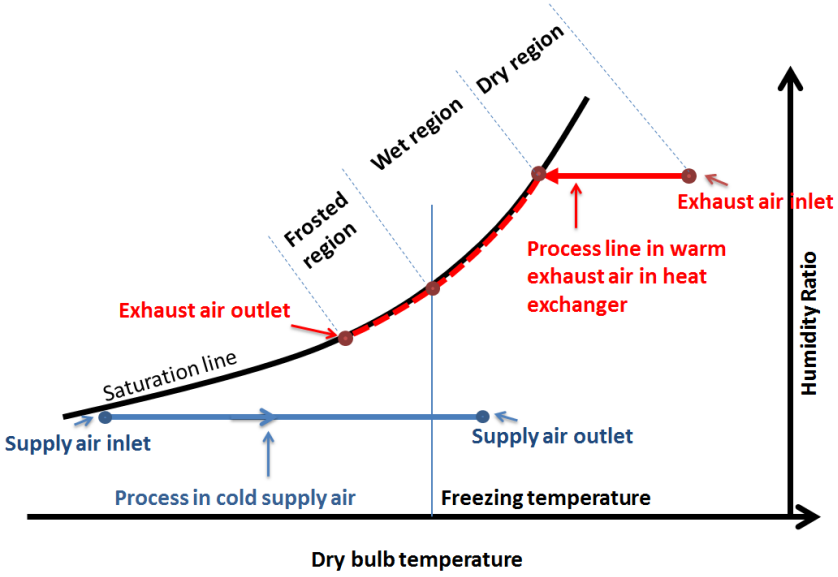

Figure 2.7. Psychometric chart showing the processes in the exhaust and supply air streams in heat exchangers.

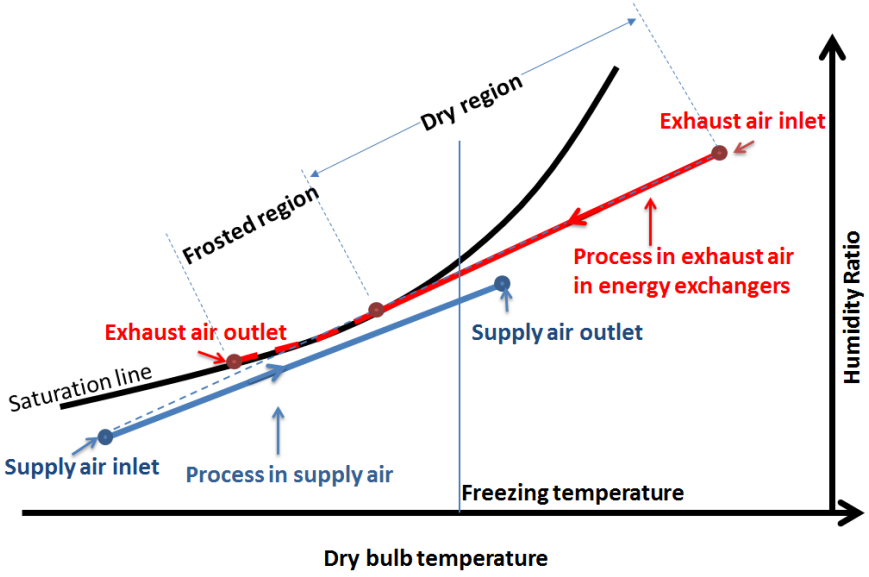

Figure 2.8. Psychometric chart showing the processes in the exhaust and supply air streams in energy exchangers.

Based on the description of the frosting process, it can be concluded that the main factors that lead to frosting are high air humidity ratios and low surface temperatures inside the exchanger. In addition to the type of exchanger, the rate of frost-buildup is dependent on the air conditions, the surface temperature and the water vapor permeability of the surface. The reviewed literature on frosting in heat/energy exchangers can be classified into three main categories:

- Measurement of frost properties such as density, porosity, growth rate, conductivity and thermal heat transfer coefficient,
- Frost formation on heat exchanger surfaces and the effect of frost on the performance of the equipment (exchanger effectiveness, pressure drop, and flow rate) without any defrost cycle and
- Development of defrosting techniques for heat exchangers and investigating the effects of those techniques on the performance of an exchanger.

2.7 RESEARCH ON FROST PROPERTIES

To be able to analyze the effects of frost formation on exchangers, the properties of frost should be taken into consideration. These properties include frost growth rate, structure, density, thermal conductivity, and roughness. Some review papers have been published in this area (Iragorry et al. 2004; Kondepudi & O'NEAL 1987). The aim of this section is to present key results of research on frost properties which will help the reader understand frost growth which is necessary to predict the effects of frosting in energy exchangers.

2.7.1 Frost formation, structure and location on simple geometries

Formation of frost is an unsteady process with different steps. The difference between each step is related to the structure of the frost. Iragory (Iragorry et al. 2004) defined these steps as: Dropwise Condensation Period (DWP) or Nucleation, Tip-Growth Period (TGP) or frost formation, and densification and Bulk-Growth (DBG) or frost layer which is shown in Figure 2.9. Mao (Mao 1991) experimentally monitored the process on a flat plate in which a laser beam was used to measure the frost thickness. Melting of the upper layer of frost and the penetration of liquid in to the lower layers changed the frost layer into ice. Important parameters affecting frost growth on

the surface of a heat exchanger were shown to be the air velocity and temperature, plate temperature, humidity ratio of the air, and properties of the surface(O'NEAL & Tree 1985).

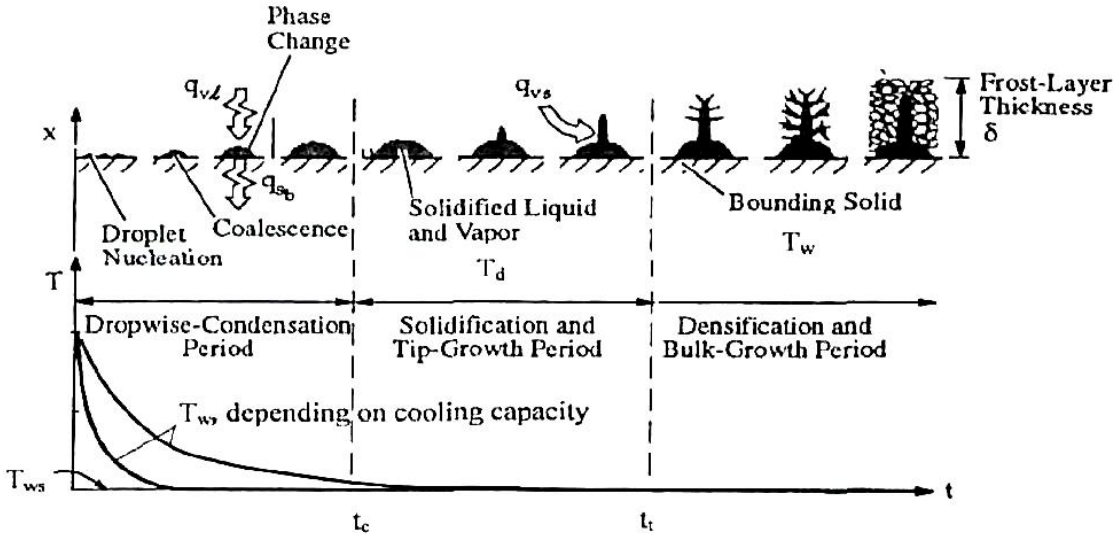

Figure 2.9. Frost growth process with time (Iragorry et al. 2004). t is time and T is the cold wall surface temperature.

Since frost formation is a transient process, the temperature of the frost layer in contact with the air varies with time, which results in different structures within the frost layer. This inhomogeneous structure makes it difficult to find a general equation or correlation to predict frost properties. Knowledge of the frost thickness on a flat plate is required to calculate the pressure drop or mean velocity over a surface. Frost thickness was found to be linearly related to the air humidity by O'Neal and Tree (O'NEAL & Tree 1985), while Fisk et al. (Fisk et al. 1984) found a non-linear relation between those frost thickness and humidity. Fisk et al. (Fisk et al. 1984) proposed that heat release during condensation in heat exchangers also played an important role on frost growth and caused the non-linear relationship. A comprehensive review of the studies on frost properties over the 50 years before 1985 is provided by O'Neal and Tree (O'NEAL & Tree 1985). They found that the structure of frost can be considerably different on a plate with a temperature of -5ºC compared to -30ºC. Also, the frost growth process on simple geometries such flat plate, cylinder, parallel plates, and annuli were compared together. The location of thick frost layer on a isothermal flat surface was found to be very dependent on the airflow rates, while in a

channel with parallel plates with constant temperature, frosting was observed to be independent of the air flow rate for air velocities higher than 8 to 10 m/s.

In addition to the experimental work, researchers have tried to create theoretical models to predict frost properties. Padki et al. (Padki et al. 1989) used a numerical method to find frost thickness, its rate of growth, and the temperature distribution along a frosted surface with a flat plate and cylindrical plate geometry. To simplify the model, they utilized correlations for the heat transfer coefficient on similar geometries without frosting. The results were in agreement with the experiments in the literature, however their model was one-dimensional and no-blockage or pressure drop were considered. Thus, their findings are not applicable in the geometries in which partial blockage by frost is considerable. The same problem was observed in numerical results by Chen (Chen 2000) on finned surfaces and Mercadier (Mercadier et al. 1993) for counter-flow heat exchangers. In (Chen et al. 2000) the effect of frost on pressure drop was found to be eight times higher than the effect on the heat transfer rate. Pressure drop was described to be more reliable than the measurement of the heat transfer coefficient in determining the effect of frosting on the performance of air finned coil. It is difficult to develop numerical models and correlations for frost growth on a surface due to:

- The change in frost properties with time and location on the surface,
- The continuous change in the frost-air interface temperature and
- Alternating melting and freezing processes in the frost layer when the frost-air interface temperature is changing.

2.7.2 Frost density, thermal conductivity and heat transfer coefficient

Iragorry et al. (Iragorry et al. 2004) categorized findings of the studies on frost properties into thermal conductivity, average density, frost thickness and the frost-to-air heat transfer coefficient. Frost density is in direct relation to conductivity. In addition to the frost density, the grain size and flow path length (or tortuosity) were also found to affect the conductivity. When the temperature difference between the air and the plate was large, the density of the frost was found to be lower than when the temperature difference was small. Thus, the density of the frost found in heat exchangers is expected to be low, since the temperature difference is usually high. Also, low

conductivity is a result of low density frost which has a large impact on effectiveness. The air velocity and the orientation of the plates are other factors that affect the density of the frost (Iragorry et al. 2004).

The roughness of a surface plays an important role in heat transfer from the surface, especially in transitional and turbulent flow regimes (Kondepudi & O'NEAL 1987). Due to the high surface roughness of a frost layer, the frost-to-air heat transfer coefficient (outside the laminar flow regime) is higher than under the same conditions for a surface without frost (O'NEAL & Tree 1985). It is difficult to measure the roughness of frost, and only very limited studies were reported in (Kondepudi & O'NEAL 1987). In most correlations found in the literature, the heat transfer coefficient of a frosted surface is assumed to be the same as a non-frosted surface. Although, in laminar and transitional flows this assumption may be correct, in turbulent flows the frost roughness will have an effect on the heat transfer coefficient.

2.7.3 Frost on extended surfaces

For exchangers with extended surfaces such as finned heat exchangers, more variables contribute to the performance of the exchanger. Kondepudi and O'Neal (Kondepudi & O'NEAL 1987) reviewed the research on extended surfaces (mostly theoretical), and categorized the research findings into four group: fin efficiency, total heat transfer coefficient, pressure drop, and surface roughness under frost formation. It was reported that 1 to 3 mm of frost reduced the fin efficiency up to 20%. However, fin efficiency increased at the initial stage of frosting due to an increase in the surface roughness and air velocity passing over the fins. The rate of frost growth on finned surfaces was measured using a laser beam by Thomas (Thomas 1999), and the results were used to validate a numerical model by Chen (Chen 2000; Chen et al. 2000). A one-dimensional porous structure was considered for the frost layer by Chen but the model lacked proper prediction of the pressure drop when the blockage by the frost was large. Indeed, a very small change in the frost thickness resulted in a high change in the pressure drop and that made the validation of the theoretical and numerical results difficult.

2.7.4 Frost deposition pattern

Frosting is inevitable in many systems. Thus, some researchers have tried to control the distribution of frost. An uneven temperature distribution along the fin surface in heat exchangers

can have some effect on frost growth. Wu et al. (Wu et al. 2001) investigated parameters that have more effects on the frost deposition pattern (FDP) to find a way to produce uniform frost formation on the air side surface of a plain-fin-tube evaporator to retard blockage of the airflow path. They found FDP was dependent on air velocity, humidity and surface temperature (dependent on air and refrigerant temperature and refrigerant flow rate), and concluded that equal FDP on all of the rows was possible. To explore more details of FDP, Gao and Gong (Gao & Gong 2011) tried to model frosting on the same type of exchanger. Their results confirmed that the temperature difference between the air and the surface has more effect on frosting than the humidity. Padhmanabhan et al. (Padhmanabhan et al. 2011) found that ignoring uneven frost growth resulted in 20% to 50% error in predicting frost thickness and 40% error in coil heat transfer capacity. They developed a semi-empirical frost model to simulate non-uniformities in FDP In addition to temperature, humidity and flow rate of air, Padhmanabhan et al. studied air flow patterns. They found that ignoring the flow pattern produced a large error in predicting the frost thickness and coil capacity. Although, some improvement is still required, their model is considered one of the most accurate models for predicting frosting in fin-tube heat exchangers.

2.7.5 Summary

In the literature presented in this section, the research has mainly focused on understanding the process of frost formation on simple geometries and calculating or predicting frost properties. The literature can be summarized as follows:

- The important frost properties are thermal conductivity, average density, thickness, and heat transfer coefficient.
- The surface and air temperature, air humidity, flow rate, and surface geometry affect the frosting rate.
- Frosting has a greater effect on pressure drop than on the heat transfer rate.
- Uneven frost deposition may cause considerable error in numerical results.
- The transient process of frosting (which contains freezing and melting), and its inhomogeneous structure make it difficult to develop accurate frosting models.

These findings are useful for prediction of heat transfer in more complicated geometries, where frost formation and direct measurement of its properties are not feasible. One of those conditions happens when frost is forming in heat or energy exchangers. In the following sections published work on the field of frosting in air-to-air heat and energy exchangers are reviewed.

2.8 AIR-TO-AIR HEAT EXCHANGERS

Because of their simplicity in design, heat exchangers are used more than energy exchangers in heating systems of buildings. Researchers have tried to measure different aspects of the effects of frosting in heat exchangers, such as the location of frost growth in exchangers, how frost affects the performance (including effectiveness, pressure drop and the rate of change in those parameters by time), and frosting thresholds for when frost occurs. This section will review the literature on frosting in air-to-air heat exchangers and the following section will review the literature on frosting in all other energy exchangers.

2.8.1 Frost deposition pattern in exchangers

Bantle et al. (Bantle et al. 1987; Bantle 1987) presented the first one-dimensional mathematical model for frost in a counter-flow plate heat exchanger by using empirical correlations. Although, the numerical and experimental heat transfer rate and temperature results had the same trend, differences between the values were considerable. Non-uniform frost formation inside the exhaust air channels was suspected to be the main reason for disagreement of the numerical results with the experiments. Figure 2.10 shows stream lines they calculated for the case of negligible entrance effect. Exhaust air particles on streamline $\psi 1$ follow a longer path (and time) compared to particles on other streamlines ($\psi 2$ & $\psi 3$), and are expected to experience a greater temperature reduction. Therefore, frosting in the particles on $\psi 1$ will happen sooner than on other streamlines resulting in non-uniform frost deposition. This non-uniformity and blockage of the air channels near the supply air inlet, turns the streamlines in to three dimensional patterns. One very difficult part in modeling exchangers under frosting is dealing with this non-uniformity.

Although counter-flow heat exchangers usually have a higher effectiveness compared to cross-flow exchangers, the construction and header design of the latter is simpler. In addition, full blockage of exhaust air due to frosting is less likely to happen in the cross-flow configuration. The typical distribution of different regions in these exchangers under frosting is shown in Figure 2.11.

The frosting threshold in cross-flow exchangers is typically at temperatures below -5°C (Ninomura & Bhargava 1995).

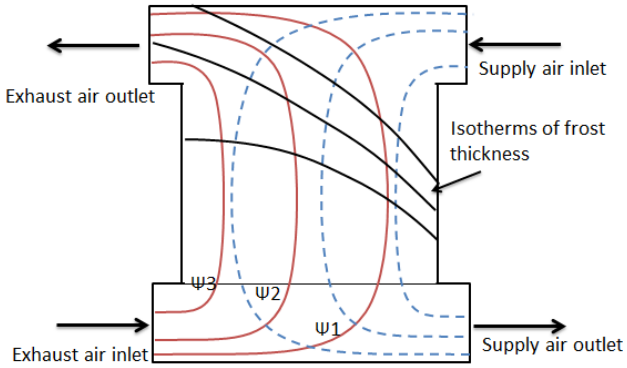

Figure 2.10. Streamlines of flow configuration in cross counter-flow heat exchanger under laminar flow regime (Bantle et al. 1987).

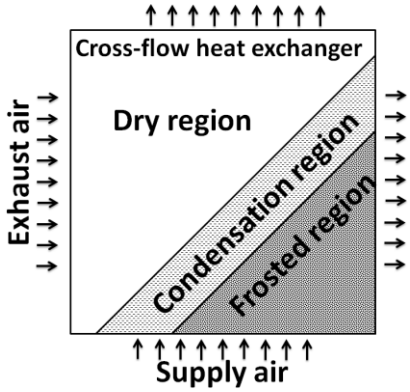

Figure 2.11. Different regions in a typical cross-flow heat exchanger under frosting (Mercadier et al. 1993).

2.8.2 Effectiveness of heat exchangers under frosting

If no condensation or frosting happens in an exchanger and the change in air properties are not significant, the effectiveness of an exchanger is independent of the inlet air properties (Besant & Simonson 2000). Otherwise, frosting affects the efficiency of the HRV or effectiveness of the exchanger. For example, an increase in the pressure drop or decrease in flow rate through an exchanger, caused by frosting, changes the working point of the fan delivering the airflow, which reduces the performance of the fan. Also, the layer of frost decreases heat transfer between two air streams by increasing the thermal resistance of the separating walls or reduces the heat transfer coefficient due to a reduction in the flow rate.

The change in the effectiveness with time, under frosting conditions, in a plate heat exchanger was calculated by Phillips et al. (Phillips, Chant, et al. 1989). Results showed that an exchanger with a high effectiveness frosted at a higher temperature than an exchanger with a lower effectiveness. But this conclusion was not in agreement for the results by Holmberg (Holmberg 1989b). He numerically modeled two types of cross-flow plate heat exchangers, single-pass and double-pass, under steady state conditions (Figure 2.12). As expected the sensible effectiveness was higher for the double-pass heat exchanger (Nyman & Simonson 2005). But, the frosting limit was lower for latter exchanger. Holmberg also found that the sensible effectiveness increased with RH or temperature of the warm air, or a reduction in the cold air temperature. Although, condensation increased the sensible effectiveness, higher condensation resulted in more frost eventually. Holmberg's steady state model didn't include frost growth or its effect on the exchanger's pressure drop and flow rate. Thus, the results of this study are relevant only when no frost is observed. A similar problem was observed in the numerical results by Mercadier et al. (Mercadier et al. 1993) compare to experiments when partial blockage happened in the exchanger. They modeled a plate heat exchanger considering unsteady conditions. After 40 minutes of operating under -25ºC, more than half of the channels near the exhaust inlet were blocked leading to a rapid drop in the effectiveness. They found that the rate of change in the effectiveness and the outlet temperatures were very high in the first five minutes of operating the exchanger and after that, the rate of change remained constant. These results were in agreement with experiments.

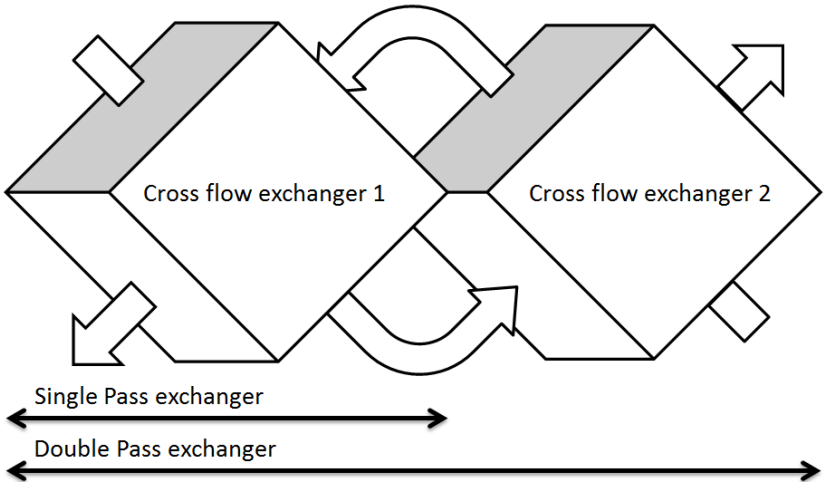

Figure 2.12. Double-pass heat exchanger (Holmberg 1989b).

Phillips et al. (Phillips, Chant, et al. 1989) used a computer program to model a counter-flow air-to-air plate heat exchanger under frosting conditions. Three similar exchangers with different effectivenesses, 50%, 65% and 85% were modeled under supply temperatures of -20ºC and -40ºC. Changes in effectiveness and air stream temperatures with time were calculated. Results showed that a higher effectiveness lead to faster frosting and channel blockage. For the exchanger with 50% effectiveness, steady state conditions were reached after a specific amount of reduction in the effectiveness due to frosting. In the exchanger with 65% effectiveness, steady state conditions were not met after 24 hours and for the exchanger with 85% effectiveness, complete blockage happened before 15 hours. Thus, exchangers with lower effectiveness will have less working problems under frosting conditions. A lack of empirical correlations for frosting and no experimental data to validate the results were the main limitations of this work.

2.8.3 Frost location

Condensation, frosting and melting in a counter-flow air-to-air heat exchanger was modeled numerically with Simulink and the results were compared with experimental data by Nielsen et al. (Nielsen et al. 2009). It was found that frost forms closer to the exhaust air outlet. This result was also found by Holmberg in cross-flow heat exchangers (Holmberg 1989b) and Simonson et al. (Simonson & Besant 1998) for energy wheels. Unlike in the work in (Holmberg 1989b; Nielsen et al. 2009; Simonson & Besant 1998) , Mercadier et al. (Mercadier et al. 1993) found that the rate of frost growth was higher near the exhaust air inlet than other parts of air channels, and partial air channel blockage was observed near the exhaust inlet. This difference shows the dependency of the frost location to the design and air properties, and no clear conclusion can be extracted.

2.8.4 Summary

Based on the literature reviewed in section 6, the following conclusions can be made:

- A lack of experimental data and non-uniformities in frost deposition patterns are the main challenges in presenting accurate numerical models,
- Three dimensional flow pattern in cross-flow heat exchangers make it more difficult to model frosting compared to counter-flow exchangers,

- Cross-flow heat exchangers are preferred for cold regions because they have less blockage problem,
- Exchangers with lower effectivenesses have a lower frosting limit,
- The location of frost growth in the exhaust side may vary depending on the test conditions.

2.9 AIR-TO-AIR ENERGY EXCHANGERS

As described in the introduction, heat and moisture are simultaneously transferred between two air streams in an energy exchanger. A review has been done by Alonso et al. (Alonso et al. 2012) for different types of air-to-air exchangers to be used in cold regions. Results showed that energy exchangers have less risk of frosting in cold climates. Considering both IAQ and frosting problem, the best recommendation for cold regions was to use recuperative energy exchangers. However, further investigation did not reveal more studies to consider recuperative energy exchangers such as membrane-based exchanger under frosting.

A design comparison of different types of energy exchangers has been provided in (Barringer & McGugan 1988; Barringer & McGugan 1989). In (Barringer & McGugan 1989) the effects of heat and moisture recovery on space conditioning load and indoor air quality of residential houses, for three different weather conditions (very cold and dry, cold and humid, and warm and humid) were modeled. It was found that heat and moisture recovery was required for very cold and dry regions, to reduce the conditioning load and keep the indoor air quality at suitable conditions, while moisture recovery was not recommended in warm and humid regions. From this study, it can be concluded that energy exchangers have two benefits over heat exchangers in very cold and dry regions; a reduction in conditioning load and a lower frosting limit.

2.9.1 Frosting limit

Two common types of energy exchangers are energy wheels and porous plate enthalpy exchangers. Porous plate enthalpy exchangers, as described in (Barringer & McGugan 1988) have a similar design to plate heat exchangers, but incorporate treated paper with a high moisture permeability instead of an impermeable plate. This type of paper core was not recommended when condensation occurred on the surface. The frosting limit, temperature at which frosting was observed, of plate enthalpy exchangers, using a treated paper core for moisture transfer was found to be

approximately 5˚C less than similar plate heat exchangers (Fisk et al. 1984; Barringer & McGugan 1988). However, this type of exchanger is not widely used.

One of the first comparisons between air-to-air heat and energy exchangers was reported by Fisk et al. (Fisk et al. 1984), in which three types of heat and energy exchangers were tested under equal cold supply air conditions to find the frosting limit of each exchanger. The three exchangers consisted of a cross-flow heat exchanger, a counter-flow heat exchanger, and a cross-flow enthalpy type (paper based) exchanger. This study was the only work found in which an enthalpy-type plate exchanger was tested under frosting conditions. The test was conducted for six hours. Fisk et al. used a visual technique to monitor frost formation and the pressure drop across the exchanger. The visual monitoring allowed for earlier frost detection than the pressure drop measurements. The frosting limit for the enthalpy exchanger was found to be lower than the frosting limit for the two heat exchangers (Figure 2.13), due to the moisture transfer from exhaust air to supply air. Interestingly, as the RH increased, the frosting limit first increased and then decreased in the cross-flow heat exchanger, while in the counter-flow heat exchanger, the frosting limit was independent of RH. The researchers related the trend in the cross-flow heat exchanger to the condensation heat release when the RH increased. The results of Fisk et al. (Fisk et al. 1984) were in agreement with Holmberg (Holmberg 1989b) who compared the frosting limits of one-core and double-core heat exchangers. Due to higher condensation in the double-core exchanger, the frosting limit was lower for the double-core exchanger.

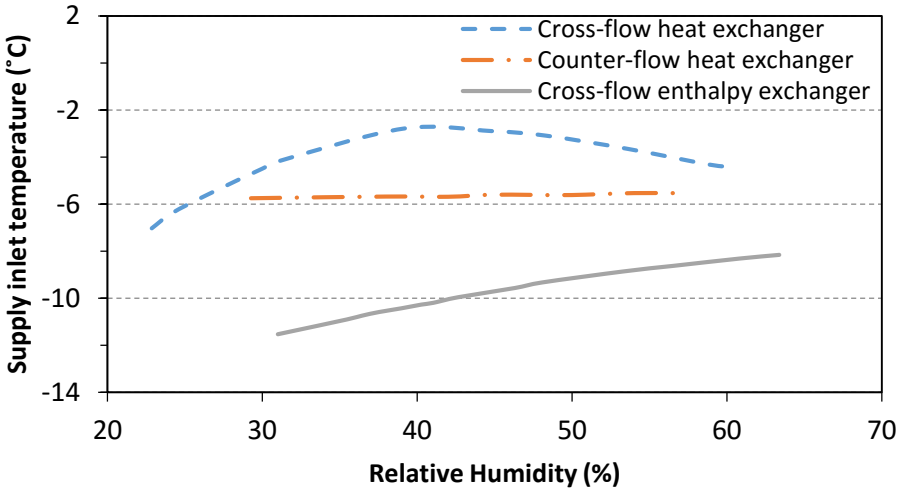

Figure 2.13. Experimental frosting limit for three types of exchangers (Fisk et al. 1984).

The frosting limit in energy wheels is dependent on air properties, design and material, so a typical value is difficult to find as it varies from one energy wheel to the next. It can be concluded from the literature, however, that the frosting limit in energy wheels is generally 5 to 15ºC lower than typical heat exchangers (Airxchange Inc. 2005; Ruth et al. 1975; Barringer & McGugan 1988; Barringer & McGugan 1989). For example in (Holmberg 1989a), the frosting limit of a hygroscopic wheel was found to be approximately 10ºC less than for a non-hygroscopic surface. Simonson and Besant (Simonson & Besant 1998) found that the frosting limit of an energy wheel is dependent on the type of desiccant coating used on the energy wheel surface. Under similar exhaust air conditions, condensation occurred at a higher temperature when a desiccant coating with a non-linear sorption isotherm was used, as compared to a desiccant coating with a linear sorption isotherm.

Bilodeau et al. (Bilodeau et al. 1999) determined the time for frosting to occur on an energy wheel, under different exhaust humidities and supply air temperatures, as shown in Figure 2.14. The results revealed that the frosting limit varies nonlinearly with temperature and RH. The dark region in this figure represents the conditions with no frosting. It can be concluded that frost control strategies based on fixed temperature and humidity values are not reliable (Bilodeau et al. 1999).

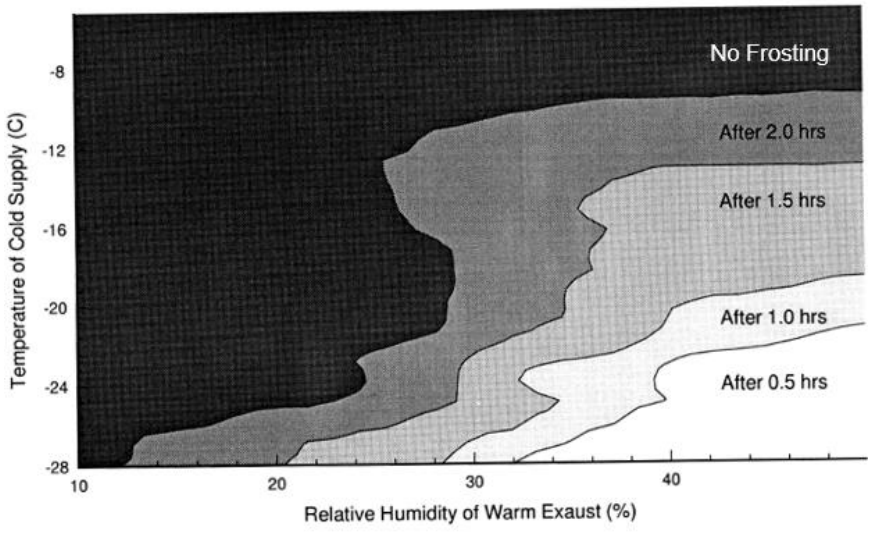

Figure 2.14. Frosting limit in an energy wheel with an exhaust air inlet of 22 °C and different humilities at different supply air temperature and a humidity ratio of $0.23 g_w/kg_a$ (Bilodeau et al. 1999).

Theoretical analysis of frosting in exchangers with acceptable uncertainty is very difficult and requires a great range of assumptions. Therefore, laboratory and field tests are required to find frosting limits and the possible change in the performance of an exchanger due to frosting (Shoukri 1979). Gazi and Simonson (Gazi & Simonson 2012) tested an energy wheel under supply temperatures of -20ºC to -40ºC when indoor conditions were 22ºC and 30% and 40%RH. For an indoor humidity of 30%RH and a supply air temperature of -29ºC frosting was observed, while with an indoor humidity of 40% RH, the onset of frosting was observed at -20ºC (Figure 2.15). This result was consistent with those in (Simonson & Besant 1998) where frosting was predicted for RH values higher than 35% RH with supply air temperatures below -20ºC. This shows the high dependence of the onset of frosting on the RH of the exhaust air stream. Thus, using energy exchangers with high latent effectivenesses would decrease the risk of frost formation considerably. It should be mentioned that using liquid nitrogen to provide the low supply air temperature in these tests made it difficult to perform the test for a long time.

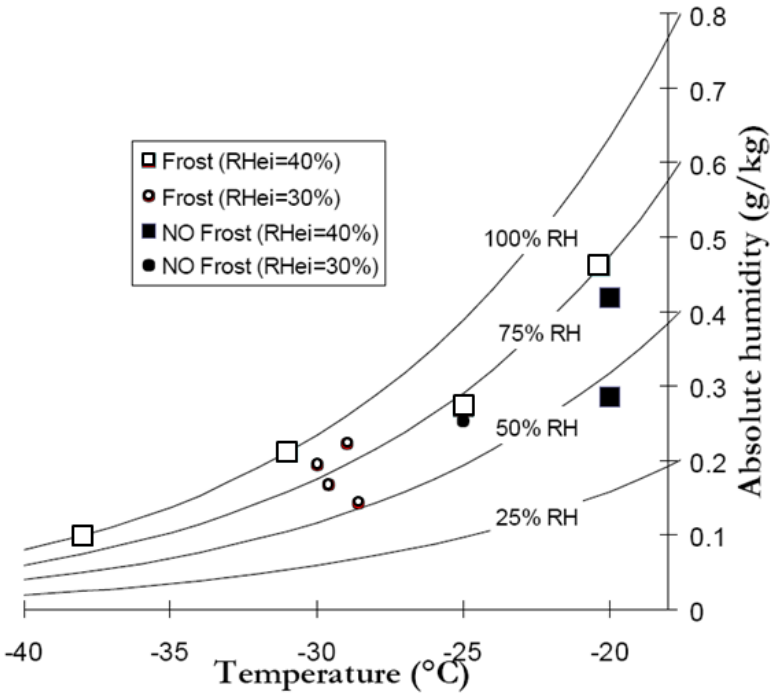

Figure 2.15. Results of frosting limits in an energy wheel for different exhaust air relative humidity(Gazi & Simonson 2012).

2.9.2 Frost type and location

Knowing the area in an energy exchanger where most of the frost may form is important as it helps engineers to develop or use efficient frost protection techniques. To predict the location of frost formation, the possible types of frost and required air conditions should be calculated. However, similar to what was found for heat exchangers, there is no general agreement for the location of frost formation in the literature. Ruth et al. (Ruth et al. 1975) described two types of frosting processes; direct vapor frosting, and vapor to liquid frosting. Observation of each of these processes was dependent on the matrix temperature and triple point of the vapor. If the matrix temperature is above the triple point, the vapor first condenses as liquid, while for temperatures lower than the triple point, the vapor would condense as a solid phase.

In addition to the frosting processes, two different types of frost were observed by Bilodeau et al. (Bilodeau et al. 1999); Rough frost and glazed frost. Rough frost occurs when the gradients of temperature and mass transfer are high. Rough frost grows rapidly and as a result, has a lower conductivity and density than the glazed frost. Experiments showed that the possibility of glazed frost forming in rotary exchangers in cold climates was less likely.

Holmberg (Holmberg 1989a) related the formation of frost to the temperature and showed the distribution of frosted and non-frosted regions as depicted in Figure 2.16. Similarly, Bilodeau (Bilodeau et al. 1999) mentioned that the formation of frost is more likely at the exhaust air outlet, where the matrix has the lowest temperature. However, as described previously, frosting is also dependent on the rate of condensation or adsorption, and the coldest point in the exchanger is not always the same as the point with highest condensation or adsorption rate. For this reason, other researchers found different frost distribution zones. In (Shang et al. 2005), it was observed that at the early stage, frost thickness increased faster in the middle of the wheel, and similar to what was found from the numerical model in (Simonson & Besant 1998) the frost thickness was higher in that area.

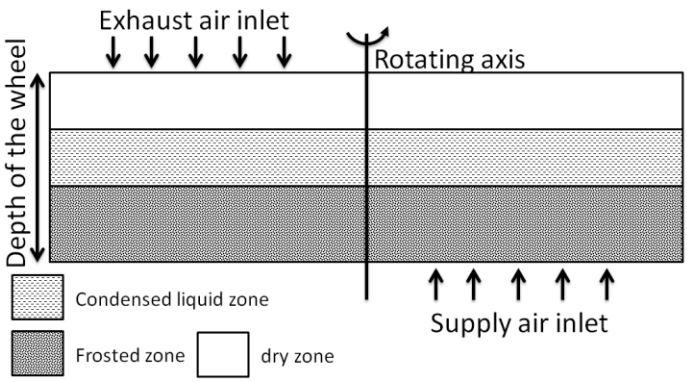

Figure 2.16. Regions in a cross view of the energy wheel with frosting (Holmberg 1989a).

In Figure 2.17, the matrix temperature at different rotational angles and radial locations are shown, to demonstrate at what locations condensation and frosting/melting are more likely. Matrix temperature and moisture content across the air channels at different angles is shown in the graph. At steady state conditions, the entire matrix tube would contain three zones, a frosted section, a section with liquid water and a section where condensation or adsorption-desorption happens periodically. However, in the extreme cold supply air, no steady conditions would be observed and frost accumulation in the tubes results in the full blockage of the air passage.

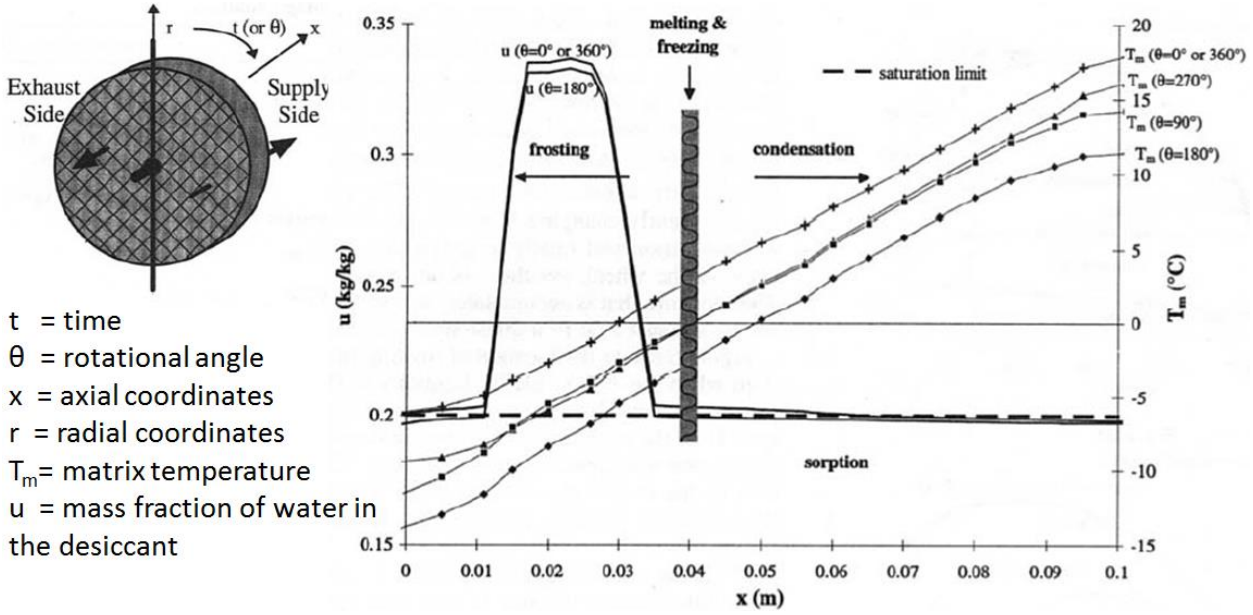

Figure 2.17. Moisture content and frost formation across air tubes in energy wheel (Simonson & Besant 1998).

2.9.3 Impact of frosting on effectiveness

In addition to experimental work, Bilodeau et al. (Bilodeau et al. 1999) also numerically modeled an energy wheel with frost formation using three-dimensional equations. They found that reducing the mass flow rate of the air or increasing the wheel thickness decreased the formation of frost, and gradually increase enthalpic effectiveness. The reason for this is that a thicker wheel augments heat transfer as well as mass transfer and reduces frost formation. Bilodeau et al. found that a high exhaust air RH increased the matrix temperature, which also reduced frost formation. Simulation results in (Simonson & Besant 1998) indicated that a desiccant with linear sorption isotherms provided higher total effectiveness and less condensation and frosting under similar conditions to that of a desiccant with type I isotherms described previously. As depicted in Figure 2.18 latent effectiveness changes non-linearly with RH for both types of desiccants. Due to higher effectiveness values and less sensitivity to the RH of the exhaust air, wheels with a desiccant coating that has a linear isotherm are more preferable for cold regions.

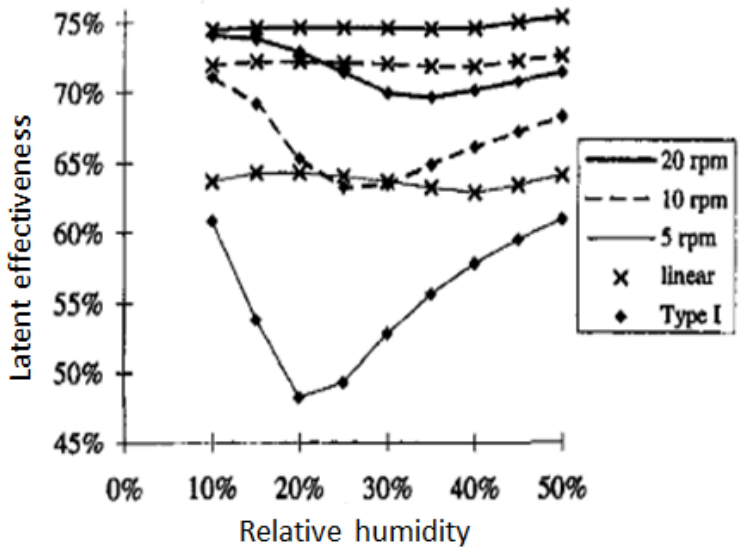

Figure 2.18. Latent effectiveness of an energy wheel for different relative humidity values with a supply air temperature of -20 °C for two different desiccant coatings(Simonson & Besant 1998).

Observation and measurement of frost properties inside the air channels of exchangers is difficult, so most researchers use numerical modeling to determine the properties of frost. Shang et al. (Shang et al. 2005) used one-dimensional equations for heat and mass transfer in porous media to develop a numerical model to predict the frost properties in an air channel of a desiccant coated

energy wheel when the supply air temperature was -40ºC. In Shang's model, just one air stream was solved, as shown in Figure 2.19. They reported variations in the pressure drop in 1-2 minute cycles due to frost formation and frost fracture by fatigue phenomena. The numerical results showed large variations in temperature at the frost-air interface. As the frost fracture was not modeled directly, frost formation was modeled in two separate cases; before the first fracture and after several fractures. Their results showed a gradual increase in the frost thickness and average density of the frost with time, which is in agreement with the literature. Shang et al. found that the sensible effectiveness of the energy wheel decreased with time when frosting occurred in the exchanger. The experiments done by Gazi and Simonson (Gazi & Simonson 2012), however, showed that the effectiveness of an energy wheel increased when frosting occurred. They related this increase in effectiveness to air leakage from the supply side to the exhaust side, due to the frost blocking the matrix. A schematic of the air leakage caused by frost blocking the matrix is shown in Figure 2.20.

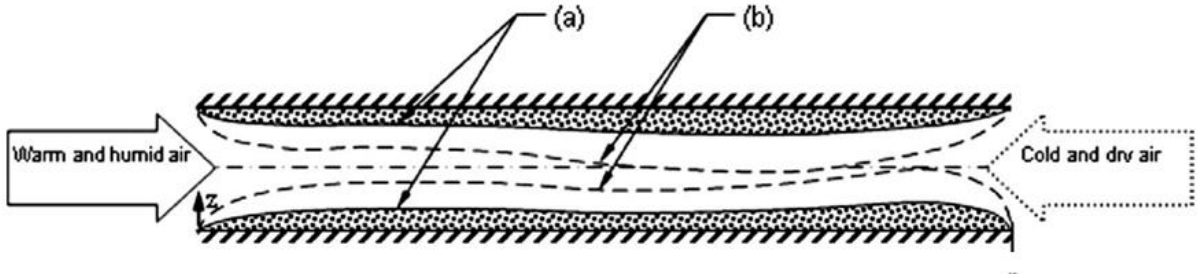

Figure 2.19. Schematic of frost thickness in the numerical model by Shang et al. (a) after first frost fracture, (b) just before the frost fracture (Shang et al. 2005).

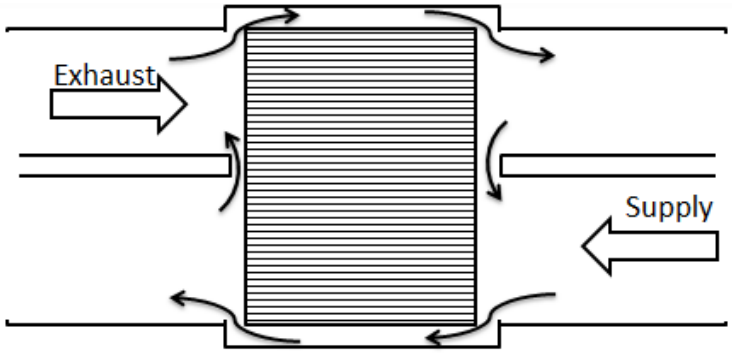

Figure 2.20. Cross-leakage in energy wheels with frost blocking the matrix.

2.9.4 Surface treatment effect

Different shapes of matrices constructed with aluminum, plastic or synthetic fibers are used in regenerative wheels. The matrix may or may not be coated with a desiccant. Coating of the matrix with a desiccant is required for moisture transfer. Without this coating, the equipment is called a heat wheel, as it can transfer only sensible heat if no condensation happens in the wheel.

Experimental testing and theoretical analysis on frost formation in energy wheels with hygroscopic surfaces by Ruth et al. (Ruth et al. 1975) is considered as the very first work in this topic. Moisture was transferred in the case of a non-hygroscopic matrix when condensation occurred in the exhaust air, while in the case of a hygroscopic surface, moisture was transferred even without condensation.

Surface treatment of energy wheels was investigated numerically by Holmberg (Holmberg 1989a), where two types of surfaces were considered, one hygroscopic and one non-hygroscopic. The non-hygroscopic surface was made of untreated aluminum, while in the hygroscopic case, an oxide layer was formed on the aluminum surface. He found that the time it took for a 50% increase in the pressure drop in hygroscopic wheels was twice that for non-hydroscopic wheels under similar inlet conditions. In addition, the results of Simonson and Besant (Simonson & Besant 1998) presented previously indicate a considerable effect of the desiccant type on the latent effectiveness and frosting limit.

2.9.5 Frost detection methods

One of the most accurate methods to find frosting in an exchanger is visual observation. Due to complexity of the designs, however, observation of frost is not usually practical in most exchangers. Thus, measurement of the air stream properties and performance of the exchanger are generally used to determine when frost forms inside the exchanger. The pressure drop across an exchanger has been suggested in the literature as a reliable factor in determining the presence of frost in exchangers, and in some cases the amount of frost as well(Shang et al. 2005). Ruth et al. (Ruth et al. 1975) suggested using a pressure activated switch as a simple and economical means of frost detection and control. Holmberg used pressure drop measurements to compare the performance of exchangers under very cold supply air. Measurement of the effectiveness of an exchanger is another parameter that can be used to determine when frosting occurs. Gazi and

Simonson (Gazi & Simonson 2012) used this method for energy wheels and compared the results with the pressure measurement technique. They found blockage of the air channels increased the leakage between the two air streams resulting in an increase in apparent effectiveness due to frosting where other researchers found that the effectiveness decreased with frosting. Gazi and Simonson concluded that pressure drop was a more reliable parameter in frost detection.

In the laboratory test on an energy wheel under frosting in (Shang et al. 2005) the average frost thickness was calculated from the pressure drop, as a function of time. Although the average pressure drop increased with time, high fluctuations in the instantaneous pressure drop were observed during 2 to 4 min cyclic periods, which was a consequence of frost growth and frost fracture. The magnitude and period of these fluctuations increased with time until a specific time. Although pressure monitoring is the best practical method for detection of frost, as described in (Fisk et al. 1984), it is not as accurate as visual techniques. Thus, new techniques or new correlations are required to accurately relate the change in pressure drop to the mass fraction of frost in an exchanger.

A comparison between sensible heat exchangers and energy exchangers is presented in Table 2.1. In this table, heat exchangers are considered as the reference energy exchangers are compared with the reference. Energy exchangers generally have higher capital costs, but have higher energy savings, which can result in lower life cycle costs.

Table 2.1. Qualitative comparison between heat and energy exchangers.

	Energy				Cost implication	Environment
	Frosting limit (temperature)	Sensible effectiveness	Latent Effectiveness	Defrosting time	Material & Construction	IAQ
Heat Exchanger	↔	↔	NA	↔	↔	↔
Energy Exchanger	↓	↔	↑	↓	↑	↑

↔ : Reference value ↑ : More than reference value ↓: less than reference value

2.10 DEFROSTING TECHNIQUES

Due to the transient nature of the frosting process, it is evident that control strategies for exchangers in cold climates based on a fixed freezing point or a fixed time are inappropriate and may be detrimental to the equipment. A life-cycle analysis of using heat exchangers in cold regions was reported by Nyman and Simonson (Nyman & Simonson 2005). They found that energy exchangers under frosting conditions have an optimal operating set point below which defrosting techniques should be activated. This set point should be calculated based on the weather conditions, energy source for heating (electricity or gas) and frost control strategy. One of the main goals in most studies on frosting in heat/energy exchangers is to find a suitable way to reduce the negative effects of frost-buildup. If frosting occurs in exchangers for a long period, use of the exchangers may not be economical. Methods for protecting exchangers against frost can be categorized as frost formation prevention or retardation, and frost removal or defrosting. Different defrost strategies in heat pumps have been presented in (Wang et al. 2011). However, not all those techniques are practical for air-to-air exchangers. Several defrosting techniques for air-to air exchangers are described by (Phillips, Bradley, et al. 1989; Airxchange Inc. 2005; Pfeiffer & Hubner n.d.). Phillips et al. (Phillips, Bradley, et al. 1989) claimed that in a region with mild weather (less than 4200 heating degree days), no considerable difference was observed between different frost control strategies; while in the very cold regions the differences were noticeable. In the following section, common methods of defrosting are described.

2.10.1 Preheating the inlet air

Preheating the supply or exhaust inlet is a simple technique to reduce or prevent frosting. Some heating elements are placed in the air ducts, before the entrance of the exchanger. When the outdoor temperature goes below the frosting threshold, the heating elements are activated. To prevent frost formation, the inlet (supply or exhaust) temperature should always be higher than the frosting limit. Another control strategy is to use a pressure drop across the exchanger core to activate the defrosting cycle (Fisk et al. 1985). In addition to air-to-air heat exchangers, preheating the air has been reported for heat pumps (Sisk 1980). The disadvantage of preheating the inlet air in very cold regions is that it reduces the energy recovered by the energy exchanger considerably (Kragh et al. 2005). A comparison of different frost protection strategies shows that preheating the

supply air is not economical in regions with long periods of cold temperatures (Phillips, Bradley, et al. 1989; Phillips et al. 1992).

2.10.2 Reducing the supply airflow rate

This technique is used to remove frost that has formed inside an exchanger. In this method, the supply airflow rate is decreased, while the exhaust airflow rate remains unchanged. Kragh et al. (Kragh et al. 2005) monitored the exhaust flow rate and effectiveness of a counter-flow plate heat exchanger with this technique for a single-family house and in a laboratory test. Frost protection was activated for exhaust air outlet temperatures below 3˚C and deactivated at 5˚C. In the field test, the flow rate started to decrease after 2 hours of the exchanger working with a supply temperature of -5 ˚C. The disadvantage of this technique is that it is not useful for long periods, since running the exchanger with an unbalanced flow rate would increase infiltration in the building. Tommerup (Tommerup & Svendsen 2005) found a similar problem when they used this method for a single family house.

A sensitivity study was done by Nyman and Simonson (Nyman & Simonson 2005) on the frost control system set point temperature. Closing the supply side, while the exhaust side remained open was selected as the defrosting technique. They considered three different set points for the exhaust outlet temperature, -30ºC (no frost control), 5ºC, and 10ºC. They found the difference in the recovered energy for the first two set points was 2-4%, but for 10ºC the recovered energy decreased by 12% compared to the two other set points. Therefore, they suggested 5ºC as optimum frost control temperature.

Preheating or reducing the supply air flow rate was used by Fisk et al. (Fisk et al. 1985) in testing a counter-flow and a cross flow heat exchanger. The defrosting time fraction (time required to defrost over total elapsed time) was found to be dependent on the duration of each cycle, as well as on the outside temperature and indoor air conditions. The average defrosting time fraction was found to be more for counter-flow exchangers compared to the cross-flow model. Therefore, from an energy savings point of view, using a counter-flow exchanger when frosting is likely to occur for a significant fraction of the year has no advantages over a cross-flow exchanger. In addition, full blockage of the air streams in cross-flow exchangers is less likely to occur, which was confirmed in experiments by Fisk et al. (Fisk et al. 1985).

2.10.3 Recirculating warm exhaust air

In this technique, ventilation is stopped temporarily, and indoor air is recirculated through the exchanger to melt the frost. This method is similar to the two previous methods; however, no outdoor air enters the building (through ventilation or by infiltration). A comparison of defrosting techniques by Phillips et al. (Phillips, Bradley, et al. 1989) showed that this technique is most suitable for extremely cold climates. Warm air recirculation was utilized in designing a residential building in an arctic area in (Ninomura & Bhargava 1995). It was recommended that the defrosting time should not exceed 20% of the total operational time. Their control system was activated when the supply air outlet temperature went below 1°C and deactivated when the temperature went back to 4°C. When recirculating the warm indoor air, increasing the fans speed causes more heat transfer from the fans into the circulated air, which enhances melting (Davis 1996).

Defrosting by recirculating warm exhaust air and shutting off the supply air was suggested by (Phillips, Chant, et al. 1989) as a defrost method in plate heat exchangers with supply air temperatures between -20ºC and -40°C. It was recommended to run a 4-5 minute defrosting cycle after every 40 minutes of working time. A lack of empirical correlations for frosting and no experimental data to validate the results are the main limitations of (Phillips, Chant, et al. 1989), on the other hand in (Fisk et al. 1985), experimental results were provided in which preheating or shutting off the supply airflow was suggested as the two main defrosting techniques. The difference between the two methods, in practical applications, is that with preheating, the operation of the exchanger is not interrupted. Fisk et al. found that 6% to 26% of the heat exchanger operational time was used for defrosting under supply air temperatures of -12 to -20ºC. A more detailed calculation for defrost time under a variety of outdoor temperatures was provided in (Ninomura & Bhargava 1995) along with a life-cycle cost analysis for a heat exchanger with warm air recirculation as the defrosting method in residential houses that showed a payback period of seven years. Ninomura and Bhargava (Ninomura & Bhargava 1995) recommended using frost protection technique for temperatures below -4°C. Defrost cycle duration was calculated around 13% for supply temperature below -4°C and 22% for temperatures below -25°C by warm exhaust air recirculation.

2.10.4 Bypassing the supply air

In this technique, all or part of the supply air is bypassed around the exchanger, into the supply outlet, while the exhaust airflow rate remains unchanged, as seen in Figure 2.21. In some cases, a moisture adsorbing system is incorporated when the exhaust air is passing thorough the exchanger to adsorb moisture and pass it into the supply air (Davis 1996). The amount of supply air that is bypassed around the core is controlled by the set point temperature or pressure drop in the exhaust side. Although no air leakage problems are observed, an unbalanced airflow through the exchanger would decrease the energy transfer rate of the exchanger considerably (Bantle et al. 1987).

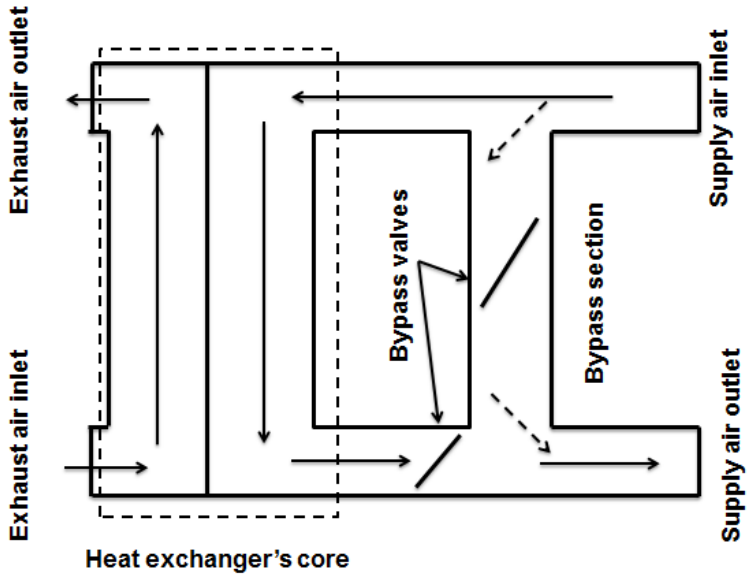

Figure 2.21. Schematic of a bypass system in an exchanger (Bantle et al. 1987).

Heat recovery units are typically equipped with a bypass, which is used to move the airflow around the heat exchanger. Because of its simplicity and high reliability (in removing frost), this technique is also used in the air-conditioning systems on airplanes (Chichindayev 2006). In these systems, one third of the cold air should be bypassed when the temperature goes below -8˚C.

2.10.5 Reducing the effectiveness of the exchanger

Reducing the effectiveness of an exchanger will decrease the risk of frost formation because the warm and humid exhaust air is not cooled as much. Effectiveness can be decreased by changing the working conditions of the exchanger. In heat pipes this can be done by tilting the pipes, and in

energy wheels this can be done by changing the wheel speed (ASHRAE 2012). This technique has been suggested by some companies (Airxchange Inc. 2005) and has been investigated by several researchers (Simonson & Besant 1998; Holmberg 1989a; Ruth et al. 1975). Holmberg (Holmberg 1989a) suggested reducing the exchanger effectiveness until the pressure drop returns back to preset values. Simonson and Besant (Simonson & Besant 1998) used this method for different desiccant types in energy wheels. To choose an economical defrosting technique, the time required for defrosting is important, because if the time is small it may be more economical to shut down the wheel completely, rather than reducing the speed. Ruth et al. (Ruth et al. 1975) found that with lower exchanger effectiveness or when the indoor RH was lower, frosting was less likely. Ruth et al. used a very simple model, but it was useful in the estimation of the frosting limit of energy wheels. By knowing the temperature limit, it was easy to estimate the total time before frosting would occur in an energy wheel in a cold season.

2.10.6 Auxiliary exchanger or double core heat exchanger

In this technique, two separate exchanger cores are considered as one system, as seen in Figure 2.22. When frost build up increases the pressure drop or decreases the flow rates from a set limit, a control system distributes the supply and exhaust air to the second core, while part of the exhaust air (10%) is used for melting the frost in the main core. The time between section switch was 30 to 60 minutes spending on the flow rate. Kragh et al. (Kragh et al. 2007) tested this system under -6ºC supply air temperature, and found that the increase in pressure drop deactivated the system after 23 hours when the defrosting cycle was off. On the other hand when the defrost cycle was activated no considerable change in the effectiveness and flow rate was observed during 24 hours test. Advantages of this system are that the pressure drop is low, and it has a simple construction, but a disadvantage is that its size is bigger than other exchangers with similar capacity. Numerical modeling of this system was presented by Nielsen et al. (Nielsen et al. 2009). Although, good agreement was observed for the frosting process, results deviated from the experiments during the defrosting cycle. Nielsen related the source of this difference to neglecting the effects of natural convection, and poor measurement methods in the experiments. Due to a lack of experimental results under very cold temperatures, the performance of the system in very cold climates is uncertain.

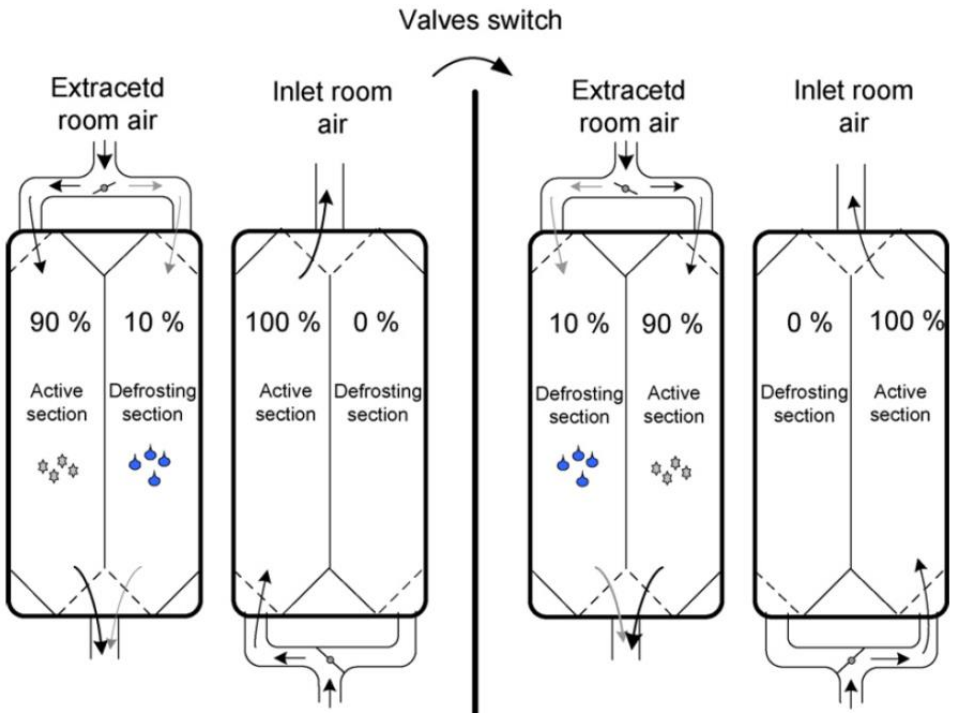

Figure 2.22.An auxiliary exchanger or double core heat exchangers (Kragh et al. 2007).

2.10.7 Coating on the surface of energy wheels

The use of different types of coating on the surface of energy wheels is being given more attention, since coating and desiccant technology is an important parameter in rotary energy exchangers. If the moisture adsorption capacity of the wheel is increased, less frosting will be observed (Simonson & Besant 1998; Moallem et al. 2012). A parametric study done by (Östin & Johannesson 1991) showed that a hydrophobic coating on the aluminum surface has no effect on frosting (rate of growth or location),while a hydrophilic coating can hinder the formation of frost. Frost free time, the time during which no frost was observed on the surface, was used to compare the effects of the different coatings. Parameters affecting the frost free time were temperature, RH and coating thickness. Although, the frosting limit did not change, experiments have shown that frost free time increased considerably as the coating thickness increased (Östin & Johannesson 1991). A drawback of using a hydrophilic coating is the disappearance of anti-frosting properties after three cycles of frosting-defrosting (Östin & Johannesson 1991). Liu et al. (Liu et al. 2010) studied effect of coating on frosting on fin-tube-heat exchangers surface. Similar to (Östin & Johannesson 1991), they found that the frosting limit did change with the type of coating, however

a thicker coating resulted in a higher pressure drop in the exchanger due to a reduction in active space for the airflow. Contrary to (Liu et al. 2010) and (Östin & Johannesson 1991), Wang et al. (Wang et al. 2007) found that hydrophobic surfaces can retard the frosting process. Although frost free time didn't change much in a horizontal orientation, no frost was observed in a vertical orientation when the surface temperature was -7^0C on super hydrophobic surface(Wang et al. 2007). One advantage of this surface over the hydrophilic surfaces was the stability of frost free properties of the surface when repeating the experiments.

2.10.8 Phase-change materials

Although much work has reported on modeling and measuring the performance of heat exchangers under frosting conditions, none of previously cited works considered the thermal capacity of the separating walls between the airstreams. Using phase-change materials (PCM) on the separating walls inside the exchanger was suggested by Qarnia et al. (Qarnia et al. 2001) A cross-flow heat exchanger with PCM on the separating walls is shown in Figure 2.23.

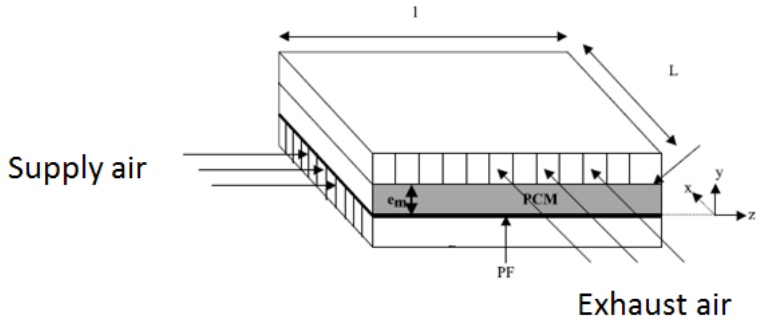

Figure 2.23. A cross flow heat exchanger with PCM (Qarnia et al. 2001).

In this technique, the exhaust air surface is kept above the freezing point by utilizing PCM and electrical heating elements. The effects of electrical load and Biot number (proportional to the ratio of PCM thickness over the PCM thermal conductivity) for the PCM layer were investigated numerically and experimentally for this type of exchanger. Qarnia et al. (Qarnia et al. 2001) found that increasing the electrical heating or Biot number improved the frosting limit of the exchanger, while increasing the heating energy decreased the efficiency of the exchanger (not effectiveness). A drawback for this system is the lack of experimental results to prove applicability of this system under very cold supply air.

2.10.9 Moving belt and rollers

This technique, which is designed to partially close the supply air channels of cross-flow plate heat exchangers, was invented by Hallgren (Hallgren 1981). In this system, a device consisting of a belt and rollers is mounted on a moving frame and is used to cover some of the supply air channels of the exchanger, as shown in Figure 2.24. The warm exhaust air continues to flow in the adjacent channels, causing the frost that has formed to melt. The advantages of this system are continuous defrosting without considerable change in effectiveness and pressure drop, and the possibility of removing frost in select channels. This is important, since frosting may occur in different areas of the core of cross-flow heat exchangers. However, unbalanced flow rates in the exchanger for long periods will depressurize the building, which will lead to an increase in infiltration.

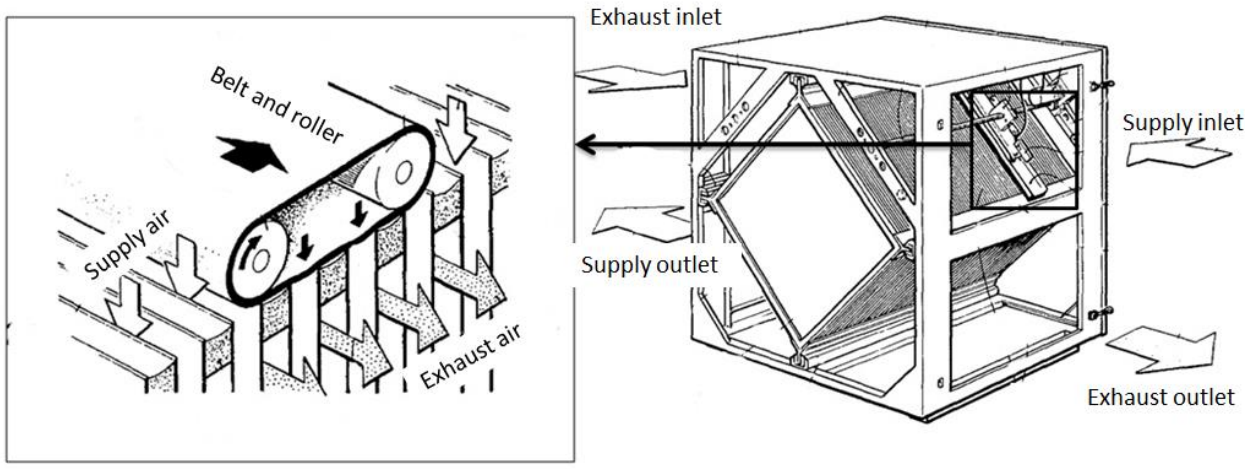

Figure 2.24. Defrosting system to partially block supply air channels (Hallgren 1981).

2.10.10Design and Installation of Exchangers

In addition to defrosting or frost protection techniques, which are important in order to keep the effectiveness of an exchanger high in cold climates, appropriate installation (location and orientation) of the exchangers is also important. Knowing that condensing water vapour is the main source of frost, exchangers should be designed in a way to remove the condensation before it freezes. Installing the exchangers so that the exhaust airflows upward, would help the condensation run off the warm side of the air channels. In addition, when frosting is a problem, installing the exchanger in a heated room (such as a utility room) is preferred to an unheated room

(such as an attic) (Tommerup & Svendsen 2005). Chichindayev (Chichindayev 2006) suggested some new modifications to the design of exchangers to keep the surface temperature above zero. To achieve this, Chichindayev tried to keep the thermal resistance of the cold air passage higher than that of the warm air. Two suggestions were to reduce the airflow velocity by increasing the number of air channels, and the second was to use a multiple-pass exchanger. Chichindayev found that increasing the number of passes lead to a more favorable temperature distribution on the exchanger's surface that kept the exhaust air channels above the freezing point. However, the effectiveness of this new design was not compared with typical design.

A summary of the frost control strategies discussed is presented in Table 2.2. Capital cost, operating cost, and IAQ for each technique were compared with the same exchanger without defrosting cycle. It should be noted that in most strategies the duration of the defrosting cycle depends on the inlet conditions.

Table 2.2. Frost control strategies or defrosting techniques in air-to-air heat/energy exchangers.

Technique	Control parameter	Capital cost	Operating cost	IAQ	Advantages	Disadvantages
Preheating the inlet air (Fisk et al. 1985; Kragh et al. 2005; Phillips et al. 1992; Phillips, Bradley, et al. 1989)	Air temperature	↔	↑	↔	Simple; Can be used as frost prevention	Not economical in regions with long cold seasons
Reducing or closing the supply air side (Nyman & Simonson 2005; Kragh et al. 2005; Tommerup & Svendsen 2005; Fisk et al. 1985)	Flow rate	↔	↔	↓	Simple	May decrease IAQ. Increases infiltration to building;
Recirculating warm exhaust air (Davis 1996; Ninomura & Bhargava 1995; Phillips, Bradley, et al. 1989)	Flow rate	↔	↔	↓	Simple; Melting process can be enhanced by increasing flow rate; suitable for extremely cold climates.	No outdoor ventilation air during defrosting
Bypassing the supply air partially or fully (Bantle et al. 1987; Chichindayev 2006; Davis 1996)	Flow rate	↔	↑	↔	Simple	Reduced energy recovery during defrosting
Reducing the effectiveness (Airxchange Inc. 2005; Ruth et al. 1975; Simonson & Besant 1998; Holmberg 1989a)	Rotational speed of wheel, Tilting angles in heat pipes	↔	↑	↔	Simple; Can be used as frost prevention	Longer defrosting time than other techniques; Not applicable in plate heat/energy exchangers; reduced energy recovery during defrosting
Auxiliary exchanger or double core heat exchanger (Nielsen et al. 2009; Kragh et al. 2007)	Flow rate	↑	↔	↔	one exchanger provides energy recovery while other exchanger is defrosted	increased capital cost for large or redundant exchanger; Not enough experimental results are available under very cold temperature
Changing surface properties (Östin & Johannesson 1991; Simonson & Besant 1998; Moallem et al. 2012; Liu et al. 2010; Wang et al. 2007)	Coating type and thickness, Membrane permeability	↑	↔	↔	appropriate materials may significantly reduce the frosting limit	Depend on many parameters each design is different; Uncertainty in material long-term performance and durability
Use of Phase-change materials (Qarnia et al. 2001)	Surface temperature	↑	↔	↔	Continues high performance running	Not enough experimental results are available under very cold temperature; Difficult design and control system
Partial blockage of supply inlet (Hallgren 1981)	Flow rate	↔	↔	↔	Continues high performance running	The amount of the blockage or moving speed of belt & roller depend on operating conditions.

↔ : No considerable change ↑ : Increase ↓ : Decrease

2.11 CONCLUSIONS

This paper reviews open literature in the field of frosting in air-to-air heat/energy exchangers. The concept of frost formation in exchangers has received increasing interest from researchers and industry over the past 30 years. Several papers were described that studied formation of the frost layer and measured the frost properties such as density, thermal conductivity and roughness. The unsteady process of frosting makes it difficult to get a general conclusion about these properties or develop a specific correlation to accurately predict frost properties. Based on the literature review in this paper, the following conclusion on frosting in air-to-air heat/energy exchanger can be made:

- Blockage of the air channels by frost decreases the exchanger's effectiveness considerably. Providing an equal frost deposition pattern would delay blockage,
- Moisture transfer in energy exchangers decreases the frosting limit,
- Most of the available results for energy exchangers are presented for energy wheels.
- Energy wheels with hydroscopic surfaces have lower frosting limit compare to non-hydroscopic wheels,
- Of the different method available to detect frost (temperature and effectiveness monitoring, pressure drop measurement, visual inspection) pressure drop monitoring is the most reliable technique, if no visual technique is possible,
- One advantage of hydrophobic surfaces over the hydrophilic surfaces was its stability to retain frost free properties after repeated testing,
- Although, the frosting limit did not change, experiments have shown that hydrophobic can retard the frosting process. In some other cases hydrophilic surfaces was suggested to improve frosting limit. Thus, no general conclusion can be drawn thorough the literature for the effect of coating on frosting
- Defrosting or frost protection techniques were described. However, with all of these techniques, a portion of the recovered energy would be sacrificed or the capital cost would be increased, which makes the techniques impractical in certain cold conditions,

- It can be reported that few innovative techniques for frost protection have been presented in the last fifteen years, such as exchangers with PCM , or auxiliary exchangers,

Important topics that have not been covered in the literature, based on the presented statistics and the literature review are:

- No work (numerical or experimental) has been reported on frosting in membrane-based energy exchangers,
- Few numerical models were reported that considered the effect of frost accumulation on the airflow rate in energy wheels and plate heat exchangers,
- Very few new defrosting techniques for air-to-air heat/energy exchangers have been presented in the last 15 years and
- Very few studies have considered supply air temperatures less than -20 ºC.

In general, the problem of frosting in air-to-air heat/energy exchangers is still unresolved, and specifically, more work is needed to study frost in exchangers which transfer latent heat as well as sensible heat. Some discrepancies in results, new surface materials, and different cooling and heating techniques would suggest new interesting areas for future work for researchers. In addition, more research is required to find new defrosting techniques or frost prevention methods to improve the performance of heat/energy exchangers under all outdoor conditions.

Also, most of the literature focused on changes in effectiveness, pressure drop or time of defrosting. However, the effect of frosting on energy consumption would depend on the exchanger design, working condition and defrosting technique. This effect is one area that is lacking in the literature and an area of future work.

2.12 ACKNOWLEDGEMENT

The authors acknowledge the financial support of Natural Sciences and Engineering Research Council of Canada (NSERC) through Smart Net-Zero Energy Building Strategic Research Network (SNEBRN).

CHAPTER 3:

EXPERIMENTAL METHODS

3.1 OVERVIEW

In this chapter, the test facility for testing cross-flow air-to-air exchangers along with an uncertainty analysis are presented. When testing exchangers under frosting conditions, it is very important to use a reliable method to detect frosting in the exchangers. The existing frosting detection methods in the literature are analyzed in this chapter and compared to a new method which is introduced and evaluated for the first time in the literature.

The manuscript presented in this chapter was published in the Journal of Experimental Thermal and Fluid Science in April 2016. A fellow PhD student, Mr. Fathieh participated in experimental planning, sensor installation and calibration, and in proof reading the paper. Mr. Kadylak and Mr. Huizing from dPoint Technologies Inc. are industry partners for a portion of this project. They contributed in providing the test section and the prototype heat and energy exchangers, commenting on the data analysis, and proof reading the paper. Mr. Rafati's contributions to the manuscript are preparing the facility (including sensor calibration and installation), planning and conducting all experiments, analyzing the data (including uncertainty analysis), writing the manuscript, and incorporating co-authors' comments.

The experimental data presented in the following chapters in this thesis (Chapters 4, 5, and 6) have been measured with the facility and the methods described in this chapter. In some of the chapters, there are minor modifications in the test methodology and these are described in the included chapters.

Experimental methods for detecting frosting in cross-flow air-to-air energy exchangers

(Experimental Thermal and Fluid Science 77 (2016) 100–115)

Mohammad Rafati Nasr, Farhad Fathieh, David Kadylak, Ryan Huizing, Robert W. Besant, Carey J. Simonson

3.2 ABSTRACT

Frost formation in air-to-air heat/energy exchangers is a challenging problem in regions with very cold weather conditions, when energy recovery is most needed. Membrane-based energy exchangers may assist in overcoming frosting. In this paper, an experimental facility was developed to enable researchers to test air-to-air exchangers under frosting conditions. The test setup, sensors and data acquisition system, uncertainty bounds for major parameters, and experimental procedure are described. Two geometrically identical plate exchangers: one with a water vapor permeable membrane (energy exchanger), and one with an impermeable plate (heat exchanger) were tested under frosting conditions. The first step in frosting experiments is to find a reliable and cost-efficient method to detect frosting in the exchangers. Four methods were used to determine the onset of frost growth: visual inspection, change in the effectiveness ($\Delta\varepsilon$), change in the pressure drop across the exchanger (Δp), and change in the outlet temperature (ΔT). The main contributions of the paper are the detailed comparison of these methods and the introduction of a new frost detection method based on temperature measurements only (ΔT method).

It is concluded that the Δp and ΔT methods were more reliable and practical than the other methods for both heat and energy exchangers. The ΔT method detected frosting sooner and with lower uncertainties than the other methods. Furthermore, the ΔT method was least affected by the operating conditions. On the other hand, the ΔP method gave a better indication of the severity of frosting in the exchanger as more frost resulted in a higher pressure drop across the exchanger.

3.3 INTRODUCTION

Air-to-air energy/heat exchangers are used in heating, ventilation and air-conditioning (HVAC) systems to reduce the energy used to condition the buildings. In these HVAC systems, fresh outdoor air (supply air) and the stale indoor air (exhaust air) pass through channels in the exchanger. Depending on the exchanger design, sensible energy (heat), or sensible and latent energy (heat + moisture) are transferred between the two air streams (Alonso et al. 2015; Reay 1980; Mardiana-Idayu & Riffat 2012). The energy transfer rate depends on the exchanger design and operating conditions (ASHRAE 2012; Zhang 2008). However, in cold outdoor weather, frosting inside the exchanger negatively impacts the performance of the exchanger (Rafati Nasr, Fauchoux, Besant, et al. 2014; Rafati Nasr, Fauchoux, Kadylak, et al. 2014). Frosting in exchangers can reduce the energy recovery by reducing the air flow, increasing the power consumption of fans, decreasing effectiveness, or deflecting the exchanger plates (creating flow maldistribution and possible physical damage). Protecting heat and energy exchangers from frosting has remained a challenge for decades (Rafati Nasr, Fauchoux, Besant, et al. 2014). This problem is more critical for the regions with arctic weather conditions such as Canada and Northern Europe, especially during the winter when the need and potential to recover energy from the indoor air is at its maximum.

Despite a large number of publications on frosting in energy exchangers, frost properties and models are limited to some specific surface geometries and temperatures (Iragorry et al. 2004; Padki et al. 1989; Chen et al. 2000). There is a gap to understand the functional dependency of the frost-air interface temperature, which plays an important role in heat transfer analysis, makes it difficult to theoretically predict the behavior of an exchanger under frosting (Bantle et al. 1987; Phillips, Chant, et al. 1989; Phillips et al. 1992; Phillips, Bradley, et al. 1989; Liu et al. 2013; Liu et al. 2014). As a result, an experimental approach is necessary to study frosting in exchangers.

During frosting, warm and humid air (indoor air) that is flowing through the exchanger is cooled below the dew point temperature and the dew point temperature must below freezing. The conditions at which frost begins to grow in an exchanger is called the frosting limit. In this paper frosting limit is defined as the combination of outdoor air temperature and indoor air relative humidity. There are only a few works in the literature which determined the frosting limit in air-to-air exchangers. Kragh et al. (Kragh et al. 2005) measured frosting limit of $-5℃$ for typical

counter-flow heat exchangers when the relative humidity was 42%. Fisk et al. (Fisk et al. 1984) compared different cross-flow and counter-flow exchangers experimentally and concluded that a paper based cross-flow energy exchanger has a lower frosting limit temperature than the counter-flow and cross-flow heat exchangers. In another study, Holmberg (Holmberg 1989a) found that the frosting limit is approximately 5 to 10℃ lower in desiccant coated energy wheels than in heat wheels. Gazi (Gazi & Simonson 2012) reported the frosting limit for an energy wheel between -20℃ and-25℃ through experiments. In general, energy wheels are more frost resistant than plate exchangers, however, the carryover of air from one stream to the other in wheels is undesirable in some applications. In contrast, carryover is insignificant in membrane energy exchangers compared to wheels.

In recent years, employing water vapor permeable membranes in the design of plate exchangers (called energy exchangers) has extended application of membranes (Zhang 2012; Zhang 2008). In these exchangers, heat and moisture are transferred between two air streams simultaneously. The exchange of water vapor between the supply and exhaust air reduces the exhaust air dew point as it flows though the exchanger and as a result less frost is formed in the membrane-based exchangers (Rafati Nasr, Fauchoux, Kadylak, et al. 2014). Through a field test for a house in Ontario, Canada, Zhang et al. (Zhang & Fung 2015a) found that the performance of an energy exchanger did not change until the supply temperature reached -16℃. They also showed that defrosting cycle is needed 3.5 times more for a heat exchanger than for an energy exchanger (Zhang & Fung 2015b). In another field test (Garber-Slaght et al. 2014), eight different energy exchangers were monitored during the winter, in Alaska, USA, without one frosting failure. However, the average outdoor temperature during monitoring time did not go below -16℃ and in some cases the exchangers were in defrosting cycle for 80% of their operating time. Overall, the data on frosting in membrane energy exchanger is very limited (Rafati Nasr, Fauchoux, Besant, et al. 2014).

Frost growth and frost structure are time dependent, even when the test conditions are constant. Dealing with this transient process is the main challenge in frosting research. In addition, maintaining fully steady-state test conditions in experiments is very difficult since many parameters/equipment are involved in the tests. For example, the continuous change of the frost layer inside the exchangers directly affects the test conditions, such as the hydrodynamics of the

airflow or flow rate. Therefore, it is not easy to apply the results in the literature on frosting limit in exchangers to exchangers with different operating conditions and surface properties. The main goals of this paper are listed as follows:

- Develop a test facility to investigate frosting in energy exchangers, and
- Study frosting in cross-flow air-to-air energy exchangers to
    - Evaluate different frost detection methods and their uncertainty, and
    - Compare the conditions at which frosting occurs (frosting limit) in energy exchangers and heat exchangers.

3.4 EXPERIMENTAL METHODOLOGY AND UNCERTAINTY ANALYSIS

A test facility (Figure 3.1) is built to test cross-flow air-to-air exchangers under frosting conditions. The layout of the test facility is an open loop which consists of two environmental chambers, four fans, a test section, connecting pipes, measurement devices, and a data acquisition system (DAQ). There are two air streams: one simulates indoor (exhaust) air conditions and one outdoor delivered to the test section (supply) air conditions. Air is drawn from each chamber and passes through an exchanger in two separate ducts. Two fans are used in each air stream; one before and one after the test section. The separate fans allow control of the pressure within the exchanger core. Two fans are used in each air stream to minimize air leakage to/from the ambient, and to produce balanced mass flow rates (balanced flow) in the two streams. Flow rates are adjusted by voltage regulators connected to each fan. The preliminary experiments also show that the test facility can produce supply air flow with temperatures as low as $-32℃$ and an exhaust air flow with a relative humidity between laboratory conditions (as low as 10% RH in the winter) and 90% RH.

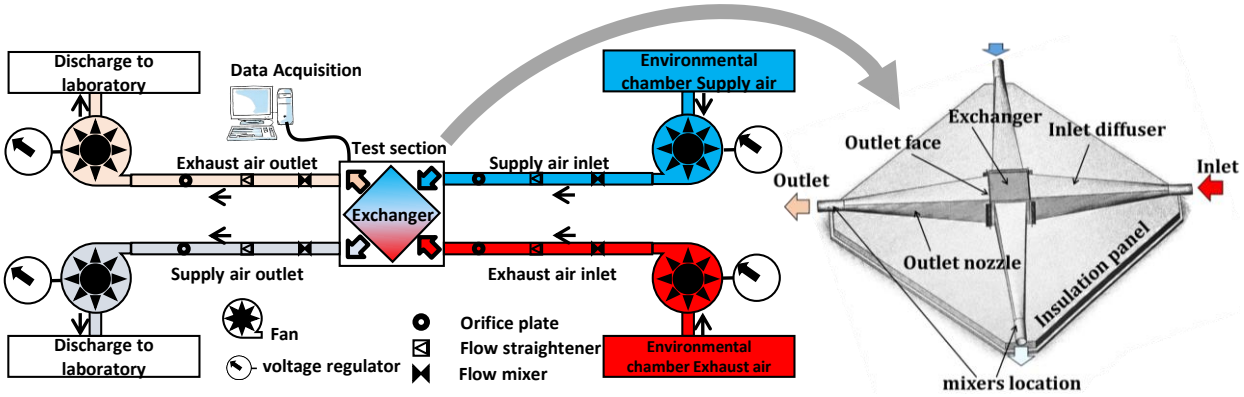

Figure 3.1. Schematic of the experimental setup for air-to-air cross-flow exchangers.

An exchanger core is located in the test section (Figure 3.1). Pipes with 50.8 mm inner diameter are connected to the exchanger with inlet expansions and outlet reduction diffusers. These headers are designed to produce uniform flow fields at the core inlet faces. Velocity measurements, with a TSI velocity meter TA410, confirm uniform velocity profiles for the air streams entering the exchanger. The design of the test section makes it possible to remove and replace the exchanger core easily. This feature facilitates testing different core designs with similar geometry. This also allows for measurement of the mass of frost in the exchanger after the frosting tests are complete by measuring the mass of the exchanger as a function of time.

An energy exchanger and a heat exchanger with identical geometries are tested in this paper. In the energy exchanger, the separating plate between the two air streams is a polymer membrane which is permeable to water vapor. For the heat exchanger, the plates are made with an impermeable polymer film with the same thickness as the permeable membrane (Figure 3.2).

In both exchangers aluminum fins (corrugated arrangement) are used between the plates to enhance heat and mass transfer and support the plates. The physical properties of the exchangers are presented in Table 3.1.

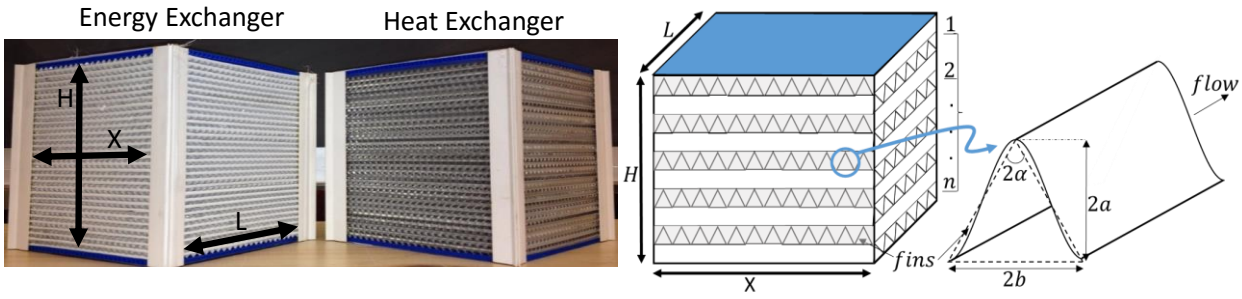

Figure 3.2. Exchanger design and dimensions

Table 3.1. Physical specifications of the heat and energy exchangers tested.

Parameter	Value	Reference
Number of channels for each flow, n	31	Lab measurement
Half duct height, a	$1.33 \pm 0.07\ mm$	Lab measurement
Half duct width, b	$3.75 \pm 0.07\ mm$	Lab measurement
Apex angle, α	$54° \pm 2°$	Lab measurement
Hydrodynamic diameter, D_h	$2.39\ \pm 0.16\ mm$	Lab measurement
Exchanger width X, height H, depth L	$165 \pm 2\ mm$	Lab measurement
Membrane thickness, δ	$100 \pm\ 0.02\ \mu m$	Lab measurement
Membrane water vapor diffusivity, D_{wp}	$2.0 \times 10^{-6} \pm 3 \times 10^{-7}\ m^2/s$	Lab measurement
Thermal conductivity of membrane, k_p	$0.44\ W/(m.K)$	(Zhang 2008)
Thermal conductivity of fin, k_f	$237\ W/(m.K)$	(ASHRAE 2009)
Thermal conductivity of air, k_a	$0.0258\ W/(m.K)$	(ASHRAE 2009)

First the environmental chambers run for 30 to 60 minutes to provide the desired conditions. The exchanger is placed in the test section and the fans are activated. After a transient period the operating conditions at the exchanger reach steady state. Tests are continued for few hours and data is recorded every minute into the tests. Each exchanger is tested separately at different operating conditions with and without frosting to evaluate its performance.

3.4.1 Instrumentation and uncertainty analysis

There are different standards available for testing air-to-air exchangers (ASHRAE 2013; CSA 2009; ASME 1991) as discussed in (Ciepliski 1997) and (Ciepliski et al. 1998), but these mainly

deal with test conditions without frosting. In this paper, ASHRAE Standard 84 (ASHRAE 2013) is used. This standard focuses on performance parameters, reporting procedure and necessary equipment for testing air-to-air energy exchangers. In addition, the following references are used during the measurement and performance evaluation: AMSE PTC 19.1 (ASME 2005), to conduct an uncertainty analysis for the experimental data, ISO 5167-1 (ISO 2003), to measure the flow rate with orifice plates, and AHRI 1061 (AHRI 2011) to choose the operating conditions for performance evaluation.

Data are measured in both air streams at different locations before and after the exchanger. Temperature, relative humidity, flow rate, and pressure are measured with thermocouples, RH sensors, orifice plates, and pressure transducers, respectively. Data acquisition is accomplished with a set of hardware (data modules and chassis) connected to a computer. The commercially available LabVIEW 2008 software program is used to record signals from the sensors which are connected to different NI-SCXI modules mounted on a NI-SCXI chassis (National Instruments, Austin TX).

Temperature: The air temperature is measured using T-type thermocouples (copper-constantan). Calibration of the thermocouples is done with a Hart Scientific 9107 Dry Well Calibrator (Fluke Corporation, Washington) at temperatures between -30°C and 30°C with 5℃ increments. During calibration, signals from the sensors are recorded for each temperature increment, for one hour after steady-state has been reached. This process is repeated twice to include the hysteresis effects. The bias uncertainty in the transfer standard is 0.1℃. Maximum precision error in the sensors (P≈0.03 ℃) is taken into account.

Pressure: Pressure is measured using two types of pressure transducers, depending on the range of Δp. The pressure drop across the orifice plate (for flow rate measurements) is measured with a general purpose diaphragm pressure transducer P305D (Validyne Engineering, CA), while low pressure transducers, Validyne DP103, are used to capture changes in the pressure drop across the exchanger. The low pressure transducers are attached to static pitot tubes which are placed just before and after the exchangers adjacent to the inlet and outlet faces.

The low pressure transducers are calibrated for the range of 0 to 220 Pa, while the other pressure transducers are calibrated for 0 to 800 Pa. Both types of transducers are calibrated with the

combination of Druck DPI 605 Pressure Calibrator (General Electric, USA) and a micro manometer, 34FB2TM (Meriam Process Technologies, OH). This calibration technique reduces the uncertainty in the transfer standard to 1 Pa. The precision uncertainty for each transducer is 0.25% of the full scale.

Relative humidity: Humidity and temperature transducers, type HMP 233 (Vaisala Oyj, Helsinki), are used to measure both the relative humidity and temperature of the air. These sensors are calibrated with a Thunder Scientific Model 1200 humidity generator which has a bias uncertainty of 0.5% RH. Calibration of the humidity sensors is a really sensitive and time consuming process, because the calibration curve changes with temperature. A calibration curve is created for each sensor using a temperature that is close to temperature that the sensor would experience during the frosting test. Due to limitations of the humidity generator to calibrate the RH sensors at temperatures below 0℃, a chilled mirror dew point sensor, model General Eastern 1211H (General Electric, USA) is used in the cold air stream (supply inlet). This sensor is expensive and bulky, but very accurate for a wide range of temperatures especially (± 0.2℃ standard accuracy) at very low temperatures (-35℃ for dew/frost point).

Flow rate: Flow rates are measured using four orifice plates (ISO 2003) which are economical and accurate enough for the experiments in this paper. The pressure drop across the orifice plates are measured by general purpose pressure transducers and the flow rate is monitored continuously through each test (uncertainty in Table 3.3).

Membrane properties: A Permatran-W® 101K device (Mocon, Minneapolis, MN) is used to measure the water vapor diffusivity of the membrane (in Table 3.1). The experimental procedure and uncertainty analysis for this test are presented in (Ge et al. 2014) in more detail.

To determine the uncertainty of each sensor, according to ASME PTC 19.1 (ASME 2005), pre-test calibrations for the required test range are conducted. Once the data is collected, the precision uncertainty (at 95% confidence level) and the bias uncertainty are calculated for each sensor and combined according to equation (3-1). In this paper, the bias uncertainties in the transfer standards are obtained from manufacturer's reference data. Data acquisition errors are assumed to be negligible, and data reduction errors are calculated from Standard Error of Estimate (SEE) for linear regression. For parameters that are calculated from measured values such as flow rate or

effectiveness, the uncertainty is propagated using equation (3-2). Based on this methodology, the uncertainty of a calculated parameter, U_R, is a function of the measured parameters, φ_j. Table 3.2 and Table 3.3 present a summary of the uncertainties in measured and calculated parameters.

$$U = \left[P^2 + \sum_j B_j^2\right] \tag{3-1}$$

$$R = f(\varphi_1, \varphi_2, \ldots, \varphi_j) \Rightarrow U_R = \sqrt{\sum_{j=1}^{j_{max}} \left(\frac{\partial R}{\partial \varphi_j} U_{\varphi_j}\right)^2} \tag{3-2}$$

Table 3.2. Uncertainties in measured values.

Parameter	Symbol	Bias±	Precision±	U±
Temperature (°C)	T	0.22	0.03	0.2-0.3
Relative humidity Vaisala (% RH)	RH	1.2-1.5	1.0	1.6-2
Relative humidity chilled mirror (% RH)	RH	2.3	1.0	2.5
Pressure (general purpose transducer) (Pa)	p	2.2-5.1	2.0-3.5	3-6
Pressure (low pressure transducer) (Pa)	p	2.8	0.6	3

Table 3.3. Total uncertainties in calculated values.

Parameter	Symbol	Uncertainty(%)
Humidity ratio	w	2-6
Mass flow rate of air	$\dot{m}$	2
Sensible effectiveness	ε_s	2
Latent effectiveness	ε_l	2-6

3.4.2 Mass and energy balance

According to ASHRAE Standard 84 (ASHRAE 2013), in each experiment, mass and energy inequalities (equations (3-3) to (3-6)) should be satisfied for the operating conditions without condensation and frosting. Equation (3-5) is for energy exchangers, and equation (3-6) is for sensible exchangers only.

Dry air: $$\left|\frac{\dot{m}_{SI} - \dot{m}_{SO} + \dot{m}_{EI} - \dot{m}_{EO}}{\dot{m}_{min(SI,EI)}}\right| < 0.05 \quad (3\text{-}3)$$

Water vapor: $$\left|\frac{\dot{m}_{SI}\mathrm{w}_{SI} - \dot{m}_{SO}\mathrm{w}_{SO} + \dot{m}_{EI}\mathrm{w}_{EI} - \dot{m}_{EO}\mathrm{w}_{EO}}{\dot{m}_{min(SI,EI)}(\mathrm{w}_{SI} - \mathrm{w}_{EI})}\right| < 0.2 \quad (3\text{-}4)$$

Total energy: $$\left|\frac{\dot{m}_{SI}\mathrm{h}_{SI} - \dot{m}_{SO}\mathrm{h}_{SO} + \dot{m}_{EI}\mathrm{h}_{EI} - \dot{m}_{EO}\mathrm{h}_{EO}}{\dot{m}_{min(SI,EI)}(\mathrm{h}_{SI} - \mathrm{h}_{EI})}\right| < 0.2 \quad (3\text{-}5)$$

Sensible heat: $$\left|\frac{\dot{m}_{SI}c_p\mathrm{T}_{SI} - \dot{m}_{SO}c_p\mathrm{T}_{SO} + \dot{m}_{EI}c_p\mathrm{T}_{EI} - \dot{m}_{EO}c_p\mathrm{T}_{EO}}{(\dot{m}c_p)_{\min(SI,EI)}(\mathrm{T}_{SI} - \mathrm{T}_{EI})}\right| < 0.2 \quad (3\text{-}6)$$

where $\dot{m}$: mass flow rate of the dry air (kg/s)

w: Moisture content of the air (kg_{water}/kg_{air})

h: Enthalpy of the air (kJ/kg),

T: Temperature of the air (℃),

and the subscripts $SI, SO, EI,$ and EO represent Supply Inlet, Supply Outlet, Exhaust Inlet, and Exhaust Outlet, respectively.

These equations are used to calculate the rate of mass or energy loss compared to the maximum potential mass or energy transfer rate under steady state conditions. According to ASHRAE Standard 84 (ASHRAE 2013), tests with frosting or condensation may not meet the criteria for mass and energy inequalities. Equations (3-4) to (3-6) are modified to include such effects by adding an extra term into the numerator. These extra terms represent the condensation rate in equation (3-7), and energy storage rate in the condensed water or frost layer ($q_{f/s}$), in equations (3-8) and (3-9). To find the condensation or frosting rate ($\dot{m}_{f/s}$) the mass of exchanger is measured by removing the exchanger from a test section before and after the test. Due to experimental limitations, the average condensation or frosting rate for the entire experiments are used instead of the instantaneous values. The enthalpy of the condensed water or frost layer depends on its temperature, however it is not practical to find the temperature inside the air channels. To simplify the calculation process, the condensed water or frost layer is assumed to be at the temperature of the air at the exhaust outlet.

$$\left|\frac{\dot{m}_{SI}\mathrm{w}_{SI}-\dot{m}_{SO}\mathrm{w}_{SO}+\dot{m}_{EI}\mathrm{w}_{EI}-\dot{m}_{EO}\mathrm{w}_{EO}-\dot{m}_{f/s}}{\dot{m}_{min(SI,EI)}(\mathrm{w}_{SI}-\mathrm{w}_{EI})}\right|<0.2 \quad (3\text{-}7)$$

$$\left|\frac{\dot{m}_{SI}\mathrm{h}_{SI}-\dot{m}_{SO}\mathrm{h}_{SO}+\dot{m}_{EI}\mathrm{h}_{EI}-\dot{m}_{EO}\mathrm{h}_{EO}-q_{f/s}}{\dot{m}_{min(SI,EI)}(\mathrm{h}_{SI}-\mathrm{h}_{EI})}\right|<0.2 \quad (3\text{-}8)$$

$$\left|\frac{\dot{m}_{SI}c_p\mathrm{T}_{SI}-\dot{m}_{SO}c_p\mathrm{T}_{SO}+\dot{m}_{EI}c_p\mathrm{T}_{EI}-\dot{m}_{EO}c_p\mathrm{T}_{EO}-q_{f/s}}{\left(\dot{m}C_p\right)_{min(SI,EI)}(\mathrm{T}_{SI}-\mathrm{T}_{EI})}\right|<0.2 \quad (3\text{-}9)$$

$$q_{f/s}=\dot{m}_{f/s}h_{fg/sf} \quad (3\text{-}10)$$

where subscripts f and s refer to the liquid and solid phase of water (frost) due to condensation or frosting and $h_{fg/sf}$ the enthalpy of the liquid or solid water.

In this paper, one more step is taken to compare the mass or energy losses to their uncertainties. The ratio of mass loss (numerator in equations ((3-3), (3-4), (3-7)) or energy loss (numerator in equations ((3-5) to (3-6), (3-8) to (3-9)) to their respective uncertainties $\Delta\varphi/U_{\Delta\varphi}$ are calculated and presented for the experiments in the results section.

3.4.3 Methods to detect the onset of frosting

As was mentioned earlier, the main objective of this paper is to propose and evaluate methods of detecting the onset of frosting in exchangers. Possible methods of frosting detection in the literature have been reviewed and summarized by Rafati Nasr et al (Rafati Nasr, Fauchoux, Besant, et al. 2014). However, no comprehensive evaluation and comparison of the different frosting detection methods are found in the literature. In this paper, possible methods of frosting detection are introduced and experimentally evaluated. In addition, a new method of frost detection through temperature measurements is proposed in this study. In this section each method is described along with its procedure.

3.4.3.1 Visual Inspection

The easiest way to recognize frosting on any surface is to visually observe the surface provided the surface is visible. In heat/energy exchangers, ideally, it is preferred to see inside the air channels to determine when frost begins to form. However, it is not always practical to use visual equipment inside the channels or at the face of the exchanger because of size limitations and

damage to the electronics due to low temperatures and frosting. To overcome these challenges, two CIC-3 wireless inspection cameras (R.P. Electronic Components Ltd., Vancouver) are used to monitor the core during the experiments. These endoscopes are installed at the two outlet faces, one in the exhaust side and one in the supply side. In addition to the endoscopes, further inspections by eye are performed and photographs are taken with a digital camera once the exchanger is removed from the test section.

3.4.3.2 Pressure difference

Measurement of the pressure difference across the exchanger is the most common method to detect frosting in the literature. In this method, an increase in the static pressure drop across the exchanger is considered as an indicator of frosting, due to partial blockage of the channels by frost. The pressure drop on both the supply and exhaust sides of the exchanger are monitored continuously during the experiments, while the air flow rates are kept constant by adjusting the speed of the fans.

3.4.3.3 Effectiveness

During frosting, the frost acts as a fouling layer which reduces the energy transfer rate in the exchanger. Therefore, changes in the energy transfer effectiveness of the exchanger can indicate frosting. The effectiveness (ε) of an exchanger is calculated using equations (3-11) to (3-13) for steady state conditions without phase change (ASHRAE 2013).

$$\varepsilon = \frac{q}{q_{max}} \tag{3-11}$$

$$q = \begin{cases} C_{SO}(\varphi_{SI} - \varphi_{SO}) & \text{supply side} \\ C_{EI}(\varphi_{EO} - \varphi_{EI}) & \text{exhaust side} \end{cases} \tag{3-12}$$

$$q_{max} = C_{min}(\varphi_{SI} - \varphi_{EI}) \tag{3-13}$$

Where ε effectiveness,

q sensible, latent, or total energy transfer rate,

φ dry-bulb temperature for sensible effectiveness, humidity ratio for latent effectiveness or enthalpy for total effectiveness,

C $\dot{m}c_p$ for sensible, $\dot{m}h_{fg}$ for latent or $\dot{m}$ for total effectiveness,

$\dot{m}$ mass flow rate of dry air ,

c_p specific heat capacity of dry air, and

h_{fg} heat of vaporization of water.

In these equations, the energy transfer rate (q) represents the heat, moisture, or enthalpy transfer rate for the sensible, latent, and total effectiveness, respectively. Two values are obtained for the effectiveness, based on the calculations for the supply and exhaust side. These two values are very similar when the mass flow rates of air are equal and there is no condensation or frosting in the exchanger. In this paper, both the supply and exhaust side effectivenesses are calculated to see how they are different during frosting. Moreover, the difference between the supply and exhaust side effectivenesses, $\Delta\varepsilon = |\varepsilon_E - \varepsilon_S|$, is calculated over time.

In addition to experimental measurements, a theoretical approach is also used to calculate the effectivenesses of the exchanger (Zhang 2008) and these values are compared with the experimental values. When the dry air flow rates in the supply and exhaust side are equal, the effectiveness is calculated by equation (3-14) for a flat plate cross-flow exchanger. The physical properties of the exchangers from Table 3.1 and the operating conditions (e.g. flow rate) are used to calculate the Number of Transfer Unit for sensible (NTU_s) and latent (NTU_l) heat transfer. The exchanger performance parameters calculated from the theory are presented in Table 3.4. Air mean velocity in each channel and Reynolds number are calculated with equation (3-15) and (3-16).

$$\varepsilon_{s/l} = 1 - exp\left[\frac{exp\left(-NTU_{s/l}^{0.78}\right) - 1}{NTU_{s/l}^{-0.22}}\right] \quad (3\text{-}14)$$

$$u_a = \frac{Q}{n\,(2a)\,X} \quad (3\text{-}15)$$

$$Re = \frac{u_a D_h}{\nu_a} \quad (3\text{-}16)$$

Table 3.4. Theoretical performance parameters.

Definition	Symbol	Value	Uncertainty $\frac{U_\varphi}{\varphi}$	Reference
Volumetric flow rate	Q	20.8 L/s	0.02	Lab measurement
face velocity of air	u_a	1.5 m/s	0.07	Lab measurement
Reynolds Number	Re	235	0.1	Lab measurement
Convective heat transfer coefficient	h	20.3 (W / (m^2 · K))	0.08	(Zhang 2008)
Convective mass transfer coefficient	h_m	8.17×10^{-3}(m/s)	0.05	
Overall heat transfer coefficient	$(UA)_{tot_s}$	37.89 (W/K)	0.09	
Overall mass transfer coefficient	$(UA)_{tot_l}$	10.34×10^{-3} (m^3 / s)	0.14	
Number of Transfer Unit (sensible)	NTU_s	1.6	0.10	
Number of Transfer Unit (latent)	NTU_l	0.5	0.14	
Sensible effectiveness	ε_s	58%	0.06	
Latent effectiveness	ε_l	32%	0.11	

In these equations, $u_a$is the face velocity of the air at the exchanger and $D_h$is the hydrodynamic diameter of the air channels in the exchangers. The low Reynolds number indicates that the air is laminar inside the channels of the exchangers.

3.4.3.4 Temperature difference

The cross-flow configuration of the air streams in the exchanger creates non-uniform temperature profiles at the outlets of the exchanger (Zhang 2008). To capture these profiles, twelve thermocouples are used at each outlet. These thermocouples are arranged in three rows of four as shown in Figure 3.3. This figure also shows the locations of the pitot tubes and endoscopes discussed previously. The thermocouples are placed very close to the outlet face to measure the temperature of air streams close to the thermocouples before mixing with the air streams from other channels (≈2cm from the outlet face). The three rows will indicate if there is any stratification in the exhaust air due to buoyancy effects and the four columns show the temperature gradients in each row from one side to the other side.

Assuming that the air flow is uniform at the outlets of the exchanger, the bulk air temperature can be calculated simply by averaging the twelve thermocouples at the outlet face (T_{ave}). Nevertheless, when frosting occurs in the core, the assumption of uniform flow at the outlet is no longer valid. Therefore, simply averaging the twelve thermocouples does not give the bulk temperature. To solve this problem, the air temperature is measured further downstream after the header and a mixer to determine the bulk mean temperature at the outlet of the exchanger (T_{mix}). Using the

mixed air properties is preferred in performance evaluation of cross flow exchangers. The difference between the two temperatures, ($\Delta T = |T_{mix} - T_{ave}|$), should be constant and close to zero when heat losses are negligible and there is no frosting in the exchanger. When frost begins to form in the exchanger, the air flow will not be uniform at the outlet (on the exhaust side) and ΔT will deviate from the value before frosting occurred (ΔT_0). Therefore, it is proposed for the first time in the literature, that this temperature measurement can be used in a cross-flow energy exchanger to detect frosting. Therefore, ΔT is monitored during experiments to verify this new frost detection technique.

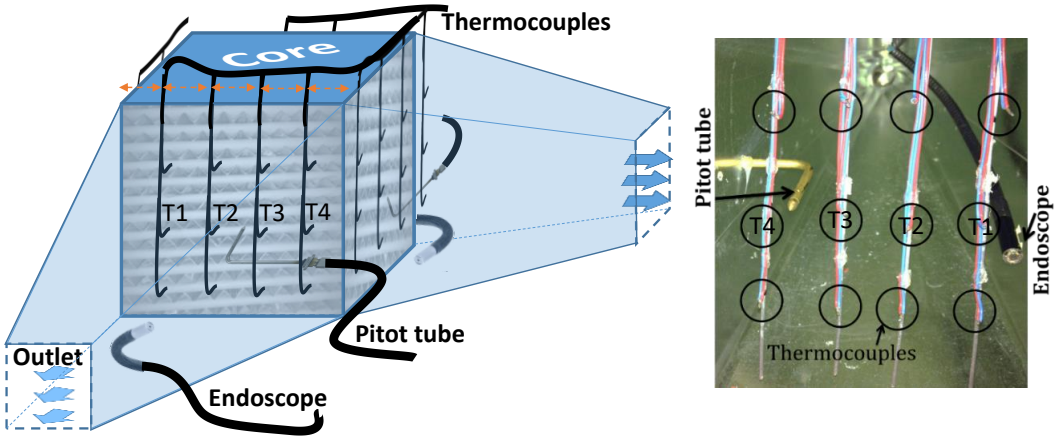

Figure 3.3. Locations of the thermocouples, pitot tubes, and endoscopes at the outlet of the exchanger.

3.4.4 Time to detect frosting

Among the methods used to detect frosting, the pressure drop, effectiveness, and temperature methods can be applied continuously. Although the change in these measured parameters may be due to frosting, changes may be due to random variations and within the uncertainty bounds of the measurements. To confirm frosting, the change in the parameters compared to their initial values should be greater than their uncertainty (equation (3-17)). Therefore the time it takes to detect frosting, t_f, is defined as the time it takes for the inequality (3-17) to be satisfied. In this inequality, φ represents any of the measured parameters (pressure, p, effectiveness, ε, effectiveness difference between the supply and exhaust sides, $\Delta\varepsilon$, or temperature difference, ΔT). Subscript 0 refers to the initial value at the beginning of the experiments.

$$\left|\frac{\varphi-\varphi_0}{U_{\varphi-\varphi_0}}\right| \geq 1 \qquad (3\text{-}17)$$

3.5 RESULTS

3.5.1 Verification of experiments

Preliminary experiments are conducted to find the performance parameters for each exchanger when there is no condensation or frosting at AHRI winter test conditions (AHRI 2011). The flow rate is set according to the recommendation of the manufacturer (Table 3.4). The experiments are run for approximately one hour under steady-state conditions. The summary of the results for both exchangers are presented in Table 3.5. It is found that the sensible effectiveness of both exchangers are equal within experimental uncertainty. The effectiveness on both the supply and exhaust sides are also equal within experimental uncertainty but are not presented in Table 3.5. The experimental effectiveness values (Table 3.5) also agree with theoretical values (Table 3.4) within the uncertainty bounds. These tests at AHRI conditions are repeated after the frosting experiments (almost one year later) and the results are found to agree within the uncertainty limits as well.

The mass and energy inequalities (equations (3-3) to (3-6)) for the preliminary experiments are satisfied for both exchangers, as shown in Figure 3.4. In addition, the mass and energy loss ratios, are less than one for the entire experiments ($\Delta\varphi/U_{\Delta\varphi} \leq 1$). The results in these two sets of graphs for each exchanger confirm that the test facility is well sealed, there is minimal heat and mass transfer with the surroundings, the test procedure is correct, and the sensors' uncertainties are correctly quantified, and there in no condensation or frosting in the exchangers.

Table 3.5. Experimental effectiveness for both the HRV and ERV at AHRI test conditions (i.e., with no frosting before and after the frosting experiments).

Date	Type	T_{EI} (°C)	RH_{EI} (%RH)	T_{SI} (°C)	RH_{SI} (%RH)	$\dot{m}$ (g/s)	ε_s%	ε_l%	ε_t%	Δp (Pa)
2014	HRV	21.3±0.2	47±2	2.2±0.2	44±2	23.6±0.4	58±2	-	-	22±3
	ERV	21.3±0.2	46±2	2.2±0.2	44±2	23.6±0.4	57±2	32±4	46±4	24±3
2015	HRV	21.6±0.2	47±2	2.2±0.2	55±2	24.1±0.4	58±2			23±3
	ERV	21.6±0.2	47±2	2.1±0.2	56±2	23.8±0.4	58±2	35±4	48±4	26±3

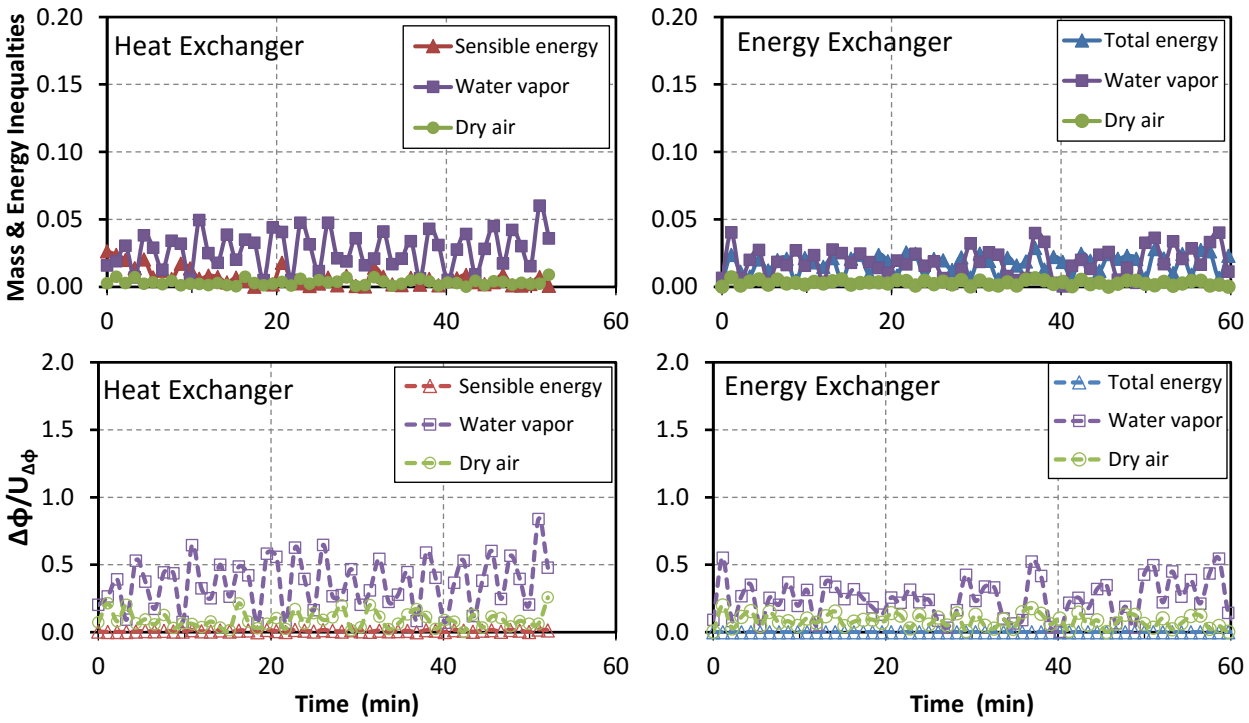

Figure 3.4. Mass and energy inequalities for the heat and energy exchangers under AHRI winter test conditions (no frosting).

Through preliminary frosting experiments, it is found that it takes one hour or more from the time the equipment starts running to when the inlet operating conditions in the test section reach the set points under steady state conditions. During this transient period frost may begin to form in the exchanger. To reduce the effect of this transient period on the final results, the equipment is run with an auxiliary (or dummy) exchanger in the test section until the steady state conditions are reached. This auxiliary exchanger is geometrically identical to the exchanger being tested. During the transient test period with the auxiliary exchanger in the test section, the flow rate and test conditions can be freely adjusted to the desired set points without the concern of biasing the frosting limit by accidently initiating frosting in the auxiliary exchanger. No data is recorded at this initial stage. The auxiliary exchanger is replaced with the main exchanger once the operating conditions reach steady state. It takes one to two minutes to replace the core. The length of the experiments with frosting are planned to be three hours to allow enough time to capture the gradual changes in measured parameters.

3.5.2 Frosting detection methods

The literature shows that many factors affect frosting in energy exchangers including, flow rate, inlet temperatures and moisture content, and the exchanger type (Rafati Nasr, Fauchoux, Besant, et al. 2014; Fisk et al. 1984; Gazi & Simonson 2012; Shang et al. 2005). However, to evaluate and compare the proposed frosting detection methods, experiments are conducted under low supply temperature, the control variables in setting the operating conditions are limited to the supply inlet temperature (T_{SI}) and the exhaust inlet relative humidity (RH_{EI}). The flow rate is maintained at $20.8\ L/s$, and the exhaust air inlet temperature (T_{EI}) is $\sim$22℃ for all experiments. Both the heat and energy exchangers are tested separately with a similar procedure. The range of operating conditions are shown in Table 3.6.

Table 3.6. Range of operating condition used to compare the different frost detection methods.

T_{EI}(°C)	RH_{EI}(%RH)	T_{SI}(°C)	RH_{SI}(%RH)	$Q(L/s)$
21 to 23	5 to 55	0 to -32	35 to 45	20.8

In the following subsections, the results for the experiments on both exchangers when $T_{SI} = -20$℃ and $RH_{EI} = 20\%\ RH$ are presented as an example. Under these operating conditions both exchangers experienced frosting. The mass measurement of the exchanger core before and after the three hour long experiments show 185 g and 56 g of frost gain for the heat exchanger and energy exchanger, respectively. The heat exchanger experiences 3.5 times more frost accumulation than the energy exchanger for the same experiment. The modified energy and mass inequalities which include frosting effects (equations (3-7) to (3-9)) are shown in Figure 3.5. The graphs show that the criteria are satisfied for both exchangers, however, the normalized water vapor loss in the heat exchanger is higher than 1.0 at some points which indicates some water vapor loss during experiment. It is believed that using the average condensation rate instead of instantaneous condensation rate in equation (3-7) is the main reason that the normalized vapor loss exceeds 1 as the condensation rate may change during test. For the energy exchanger, the total energy loss is more than the uncertainty throughout the test. This means there is an energy loss between the test section and the environment. Considering the fact that the supply air is much colder than the environment this heat loss is inevitable and the results are acceptable since the values are smaller

than the limit specified by ASHRAE Standard 84. In the following subsections the results from each frost detection method are described.

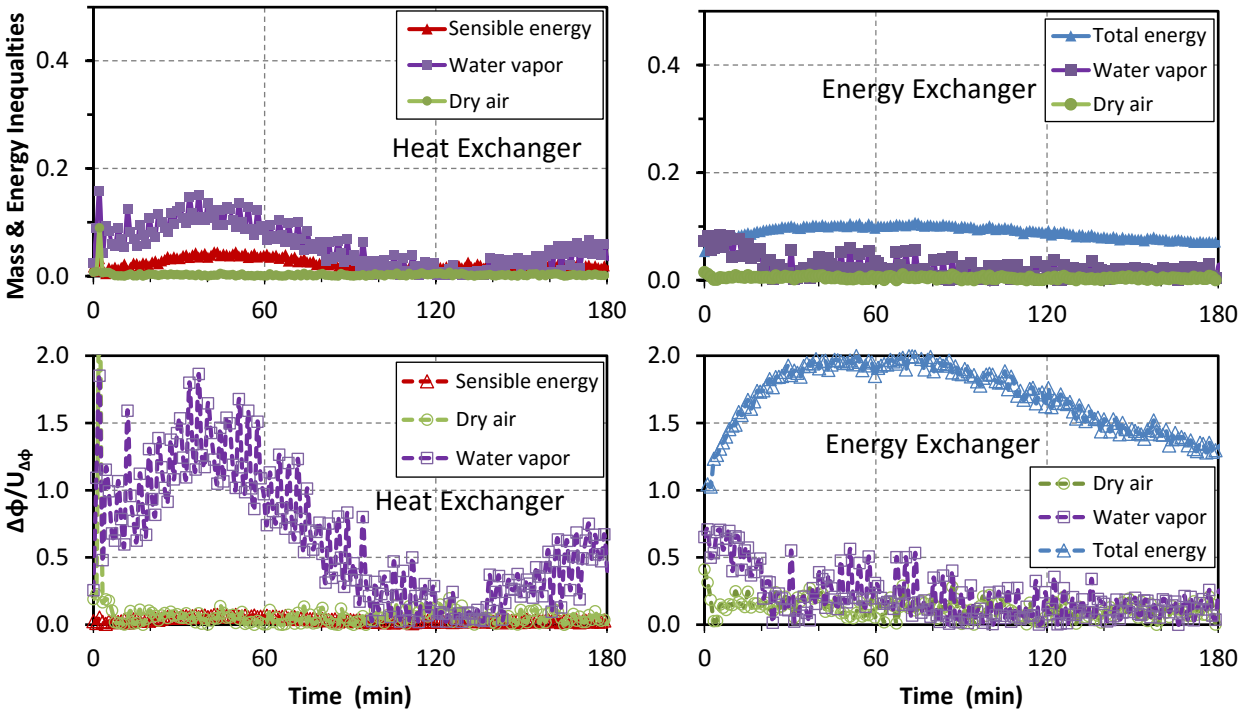

Figure 3.5. Mass and energy inequalities for the heat and energy exchangers ($T_{SI} = -20$℃ and $RH_{EI} = 20\%$RH).

3.5.2.1 Visual

Photographs from the exhaust outlet side of the heat and energy exchangers are shown in Figure 3.6 and Figure 3.7, respectively. The photographs with the higher resolutions are taken with a digital camera before and just after the experiments when the exchangers are removed from the test section. Through these photos it can be seen that frost (white spots) is observed in the first few minutes of the experiment. However, these frosted areas do not change significantly throughout the experiments. Comparing the photographs at 45 min and 180 min in Figure 3.7, it can be seen that the white spots in some channels (see lighter colored circles), diminish with time during the experiments. This frost disappearance could be due to frost growth further upstream in the air channels obstructing the flow resulting in no more frost growth near the outlet. This shows the unsteady behavior of frost growth and removal. The frost appears to be slowly melting due to small heat gain through the duct since these channels are closer to the duct wall. At the same time, the

air flow rate in the non-blocked air channels increases which causes more condensation and eventually frosting in those channels. Therefore, it is expected to see the visualized frosting spots at the outlet move slowly from the coldest corner to the warmer side during the experiments. This observation is in agreement with the results presented by (Mercadier et al. 1993) who showed a gradual change in the maximum frosting location in a cross-flow exchanger. They reported that the maximum frosting thickness is moving towards the exhaust inlet with time which causes more blockage in the exhaust outlet.

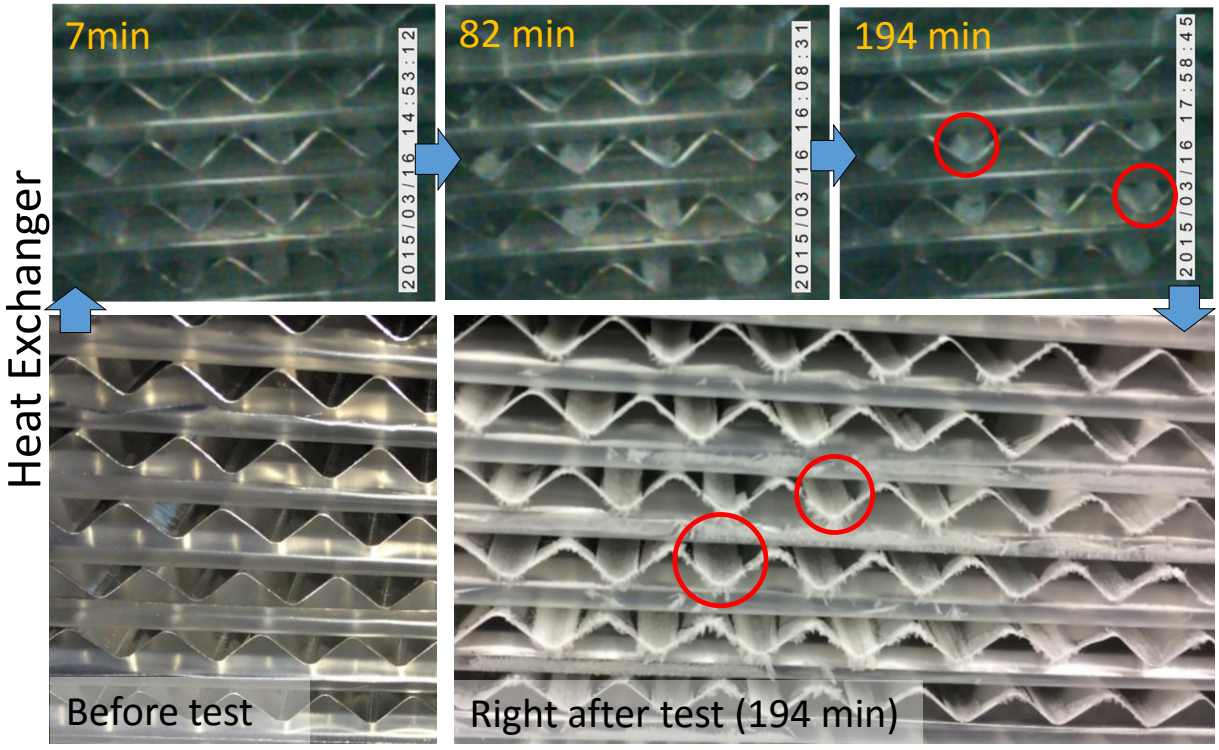

Figure 3.6. Photographs of the exhaust side outlet of the heat exchanger at different times during the experiment ($T_{SI} = -20$℃ and $RH_{EI} = 20$%RH).

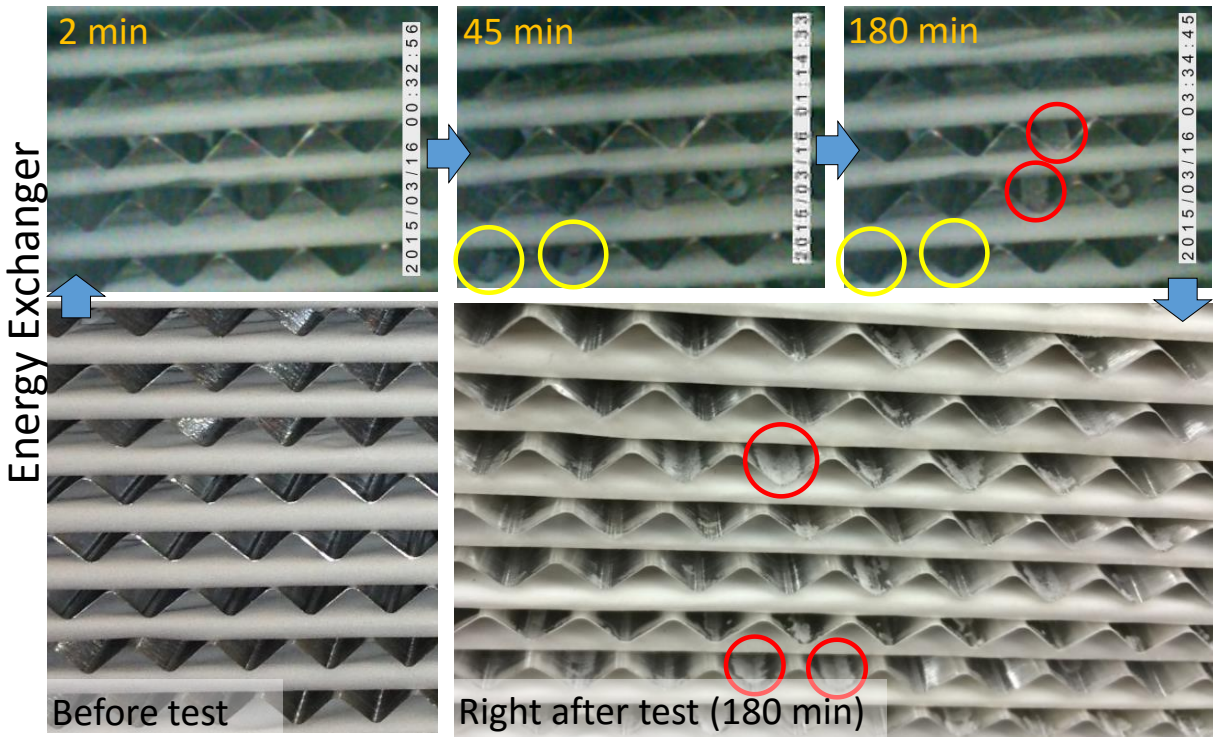

Figure 3.7. Photographs of the exhaust side outlet of the energy exchanger at different times during the experiment ($T_{SI} = -20$℃ and $RH_{EI} = 20$%RH).

Although the "after test" photos in Figure 3.6 and Figure 3.7 show differences between the heat exchanger and energy exchanger, it is hard to see considerable differences between the two exchangers in the endoscope photographs. This may be due to the fact that endoscope photographs do not cover the entire outlet face or that the resolution of the photographs are not as high as the resolution of the regular camera.

Overall, the following observations are found from the visual frosting detection method:

1. Frost (white spots) is observed at the very beginning of the experiments. In most of experiments with frosting it is noticed that the frost is observed in the first 10 minutes.

2. The amount of frost in the photos increases very little with time after the initial observation of frost, sometimes even a reduction of the frost is noticed.

3. No frost is observed in the supply side for both exchangers. This observation is based on the photographs from the outlet face of the exchanger during and after the experiments.

Since it is not feasible to visualize inside the air channels, the exchangers are left at room conditions after the frosting tests for a while to allow all the frost to melt. Later, the exchangers are positioned in a way to let the water leave the core. Visual observation proves that all the frost is in the exhaust side only. Therefore, it can be concluded that the condensed water in the energy exchanger stays on the membrane surface on the exhaust side.

4. Comparison of the visual results for both exchangers does not show considerable differences in the frost areas, whereas the amount of frost measured by weight is 3.5 times higher in the heat exchanger than in the energy exchanger.

These observations indicate that the visual method is reliable in detecting frosting but not a good indicator of the amount of frost. It should be kept in mind that the visual method is a qualitative method which makes it hard to apply in frosting protection systems; however, it is a good reference to validate the other frosting detection methods.

3.5.2.2 Pressure drop

Results for the change in pressure drop (Δp) across the exchanger (Figure 3.8) show a gradual increase in Δp on the exhaust side, while Δp is constant on the supply side. These results confirm the supply air channels are frost free. At the end of the experiment, Δp is 6 times higher and 2.5 times higher than the initial value for the heat exchanger and energy exchanger, respectively. This indicates that there is considerably more frost in the heat exchanger. Frost accumulation reduces air flow in the passage and increases the surface roughness, both of which increase the pressure drop through the exchangers.

Another observation in this figure is the change in the slope of the Δp graph over time. This change may be related to the frost thickness growth, however due to the complexity of relation between ΔP and frost thickness this is difficult to prove. It can be seen in Figure 3.8 that the energy exchanger is more frost resistant than the heat exchanger, which means there is less frost in the energy exchanger. This is because of the water vapor transfer through the membrane between the two air streams in the energy exchanger which reduces the amount of condensation and frosting on the exhaust side (Rafati Nasr, Fauchoux, Besant, et al. 2014).

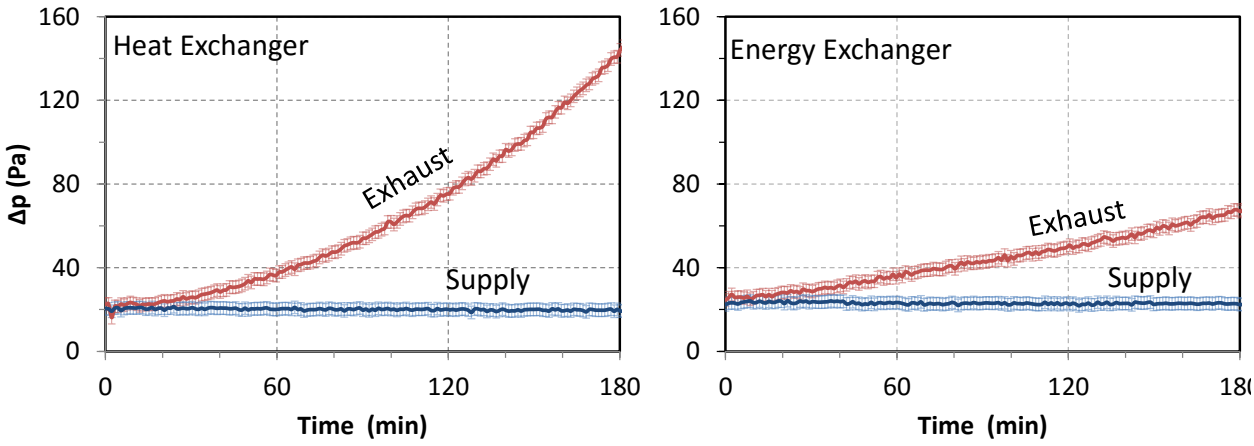

Figure 3.8. Change in pressure drop across the exchangers ($T_{SI} = -20$℃ and $RH_{EI} = 20\%$RH).

Despite the fact that Δp increases during frosting, the high sensitivity of the low pressure transducers and continuous fluctuations in pressure readings (which are within the uncertainty range) make it difficult to accurately determine the onset of frosting. As described in 3.4.4, the amount of change in pressure drop compare to its uncertainty is calculated and is shown in Figure 3.9. The horizontal axis represents the time from beginning of the test (i.e., the time when the auxiliary exchanger is removed and the tested exchanger is sealed in the test section as described in section 3.1). It can be seen that it takes more than 30 minutes into the test to confirm frosting with the Δp method. Frosting is confirmed when the change in Δp is greater than its uncertainty in both the heat and energy exchangers. The time when frosting is detected is shown by t_f. The uncertainty in t_f is defined as the difference between t_f and the time it takes for $\Delta p - \Delta p_0$ to increase to twice its uncertainty value. The uncertainty in $t_f$is lower for the heat exchanger since the rate of change of pressure in the heat exchanger is higher. Also, for the first ~30 minutes the pressure drop is not affected considerably by frosting while the image of the exchanger face shows evidence of frosting within 10 minutes from the beginning of the test.

Other experiments where only condensation forms in the exchangers (no frost) show negligible change in Δp, which means that the frost formation is the main source of the Δp change in Figure 3.9. Therefore, Δp is a reliable method to detect the presence of frosting, but it is somewhat slow in detecting the onset of frosting. Since the Δp method is a quantitative method, it is likely preferred over the visualizing technique. However, due to relatively small values of pressure drop

across the exchangers and the high cost of precise pressure sensors it might be a costly method in practice.

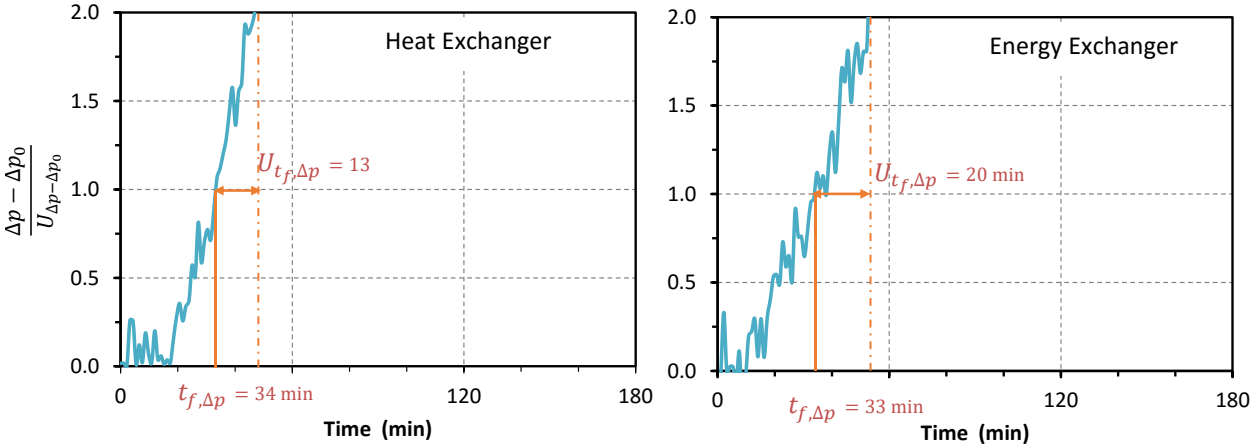

Figure 3.9. Change in Δp during the test (normalized with the uncertainty) showing the time to detect frosting, t_f, and the uncertainty in the frosting time (U_{t_f}) with the Δp method ($T_{SI} = -20$℃ and $RH_{EI} = 20$%RH).

3.5.2.3 Effectiveness

As another method of detecting frost, effectiveness is calculated for both the supply and exhaust sides of the heat and energy exchangers. The results are shown in Figure 3.10.

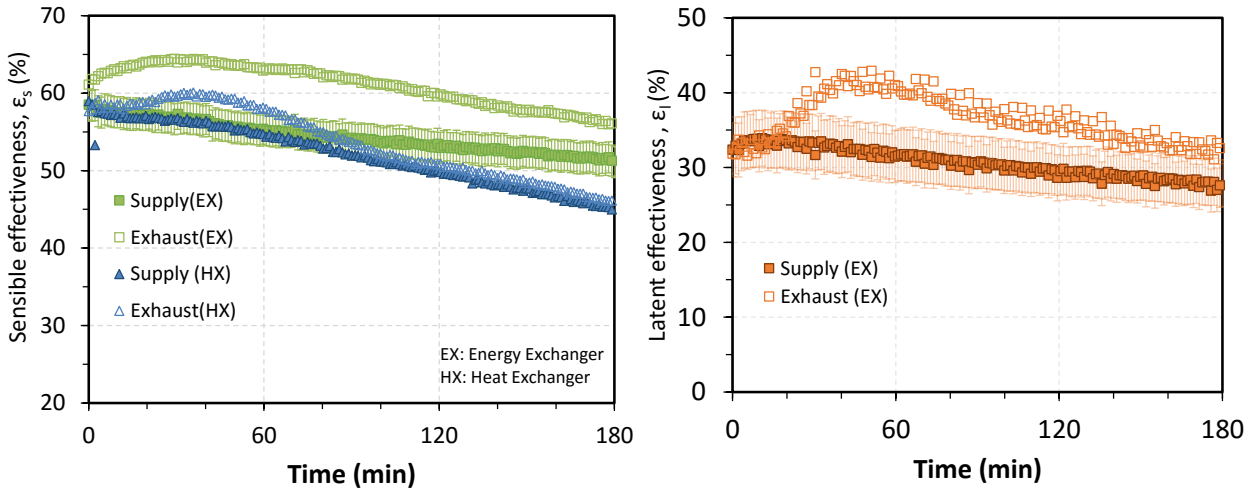

Figure 3.10. The sensible and latent effectivenesses of the supply and exhaust streams. ($T_{SI} = -20$℃ and $RH_{EI} = 20$% RH). The error bars represent the 95% uncertainty bounds of each measurement.

The following observations are found from the results in Figure 3.10:

1. All effectiveness values eventually decrease with time. The rate of change in sensible effectiveness is greatest for the heat exchanger. For the energy exchanger, the changes in both the sensible and latent effectivenesses during the test are within the uncertainty range in this example which makes it difficult to recognize frosting by the effectiveness measurement alone. At the same time, the results in Figure 3.9 show high pressure drop across the exchangers. Therefore, the effectiveness method has more delay in detecting frosting compared to visual and Δp methods.

2. The supply side effectiveness continuously decreases due to frost growth, while the exhaust side effectiveness initially increases and then decreases. This trend can be explained by the fact that the initial frost layer enhances the convective heat and mass transfer between the air stream and surface resulting in higher sensible and latent effectiveness in the exhaust side. As a result, the temperature of the warm exhaust air temperature decreases more in the case of frosting than in the case of no frost and thus the condensation rate in the exhaust side increases initially due to frosting.

3. Condensation could possibly increase the supply side ε_l due to wicking of water through the membrane, but this is not observed for the exchangers in this research. The previously described frosting detection methods also did not show any sign of condensation and frosting in the supply side. On the other hand, the condensation heat release, if it is significant, should reduce the exhaust side ε_s and increase the supply side ε_s. Since none of these changes are captured it is concluded that the heat of phase change is negligible in these experiments. Later in the test, the frost thickness grows to the point where the increased heat and mass transfer resistance of the frosted membrane exceeds the increase in convective transfer coefficients and ε begins to decrease continuously with time. Similar phenomena of increased heat transfer followed by decreased heat transfer is evident in the crystallization fouling of a heat exchanger(Pääkkönen et al. 2015).

The difference between the supply and exhaust side effectivenesses ($\Delta\varepsilon$), which is usually greater for the heat exchanger, can possibly be used to detect the onset of frosting. The change in $\Delta\varepsilon$ during the test (normalized by the uncertainty) are presented in Figure 3.11. This difference for both

sensible and latent effectivenesses, $\Delta\varepsilon$ (as described in 2.3.3), are calculated and compared with the initial values in Figure 3.11. These values are compared with their uncertainty to confirm frosting and to calculate t_f. To confirm frosting, the difference should be more than the uncertainty in the difference in effectivenesses.

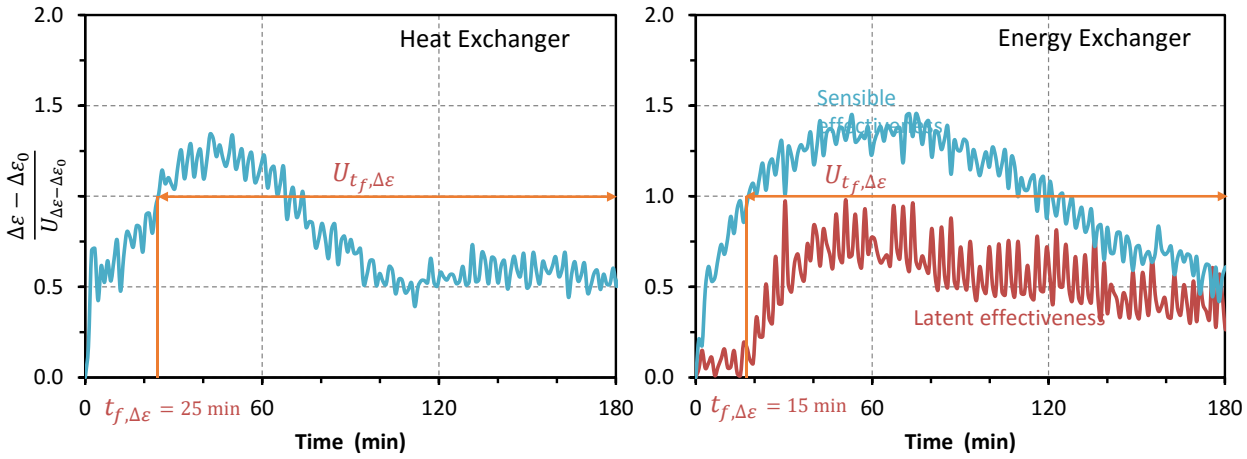

Figure 3.11. Normalized $\Delta\varepsilon$ as a function of time showing the time to detect frosting, t_f, for the heat and energy exchangers ($T_{SI} = -20$℃ and $RH_{EI} = 20$%RH).

The $\Delta\varepsilon$ results confirm frosting and show t_f = 25 min and 15 min for the heat exchanger and energy exchanger, respectively. However, the graphs do not reach to a value of two which means that the uncertainty in $t_f$is very high. Moreover, after a rapid initial jump in the ratio, the values increase slowly and then decrease below one at some point. Therefore, it is not possible to recognize frosting by this method over the entire test. The difference in latent effectiveness does not indicate frosting at all. It can be concluded that both ε and $\Delta\varepsilon$ methods are not very reliable in detecting the onset of frosting.

3.5.2.4 Temperature difference

In this method, the temperature of the mixed air after mixer which is downstream of the exchanger (T_{mix}) is compared with the average temperature from the twelve thermocouple readings (T_{ave}) at the outlet face of the exchanger. The temperature difference ($\Delta T = T_{mix} - T_{ave}$) is shown in Figure 3.12 as a function of time. During frosting, ΔT in the exhaust side gradually increases in both exchangers due to air flow maldistribution in the exchanger which is caused by non-uniform

frost growth in the different air channels. On the other hand, ΔT on the supply side stays constant in all experiments, which once again indicates no frosting in the air channels on the supply side of the exchanger.

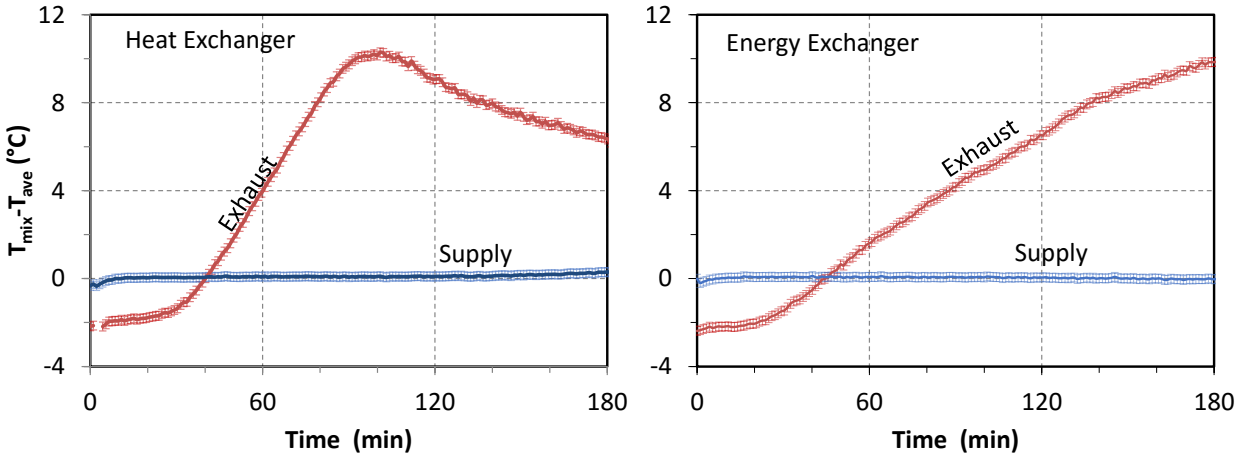

Figure 3.12. Difference between exhaust outlet temperature measured after a mixer (T_{mix}) and average of the 12 thermocouples at the face of the exchanger (T_{ave}) during a frosting test ($T_{SI} = -20$°C and $RH_{EI} = 20$%RH).

A comparison between the heat and energy exchanger shows a more rapid change in ΔT in the heat exchanger. To find the frosting detection time, the change in ΔT with respect to its uncertainty is shown in Figure 3.13. The results show that $t_f = 11\ min$ and 17 min for the heat and energy exchanger, respectively. It can be seen that the rate of change in ΔT is much higher than Δp and $\Delta \varepsilon$ methods which results in faster frosting detection and lower uncertainty in t_f. The uncertainty in $t_f$is calculated the same way as Δp method in section 3.2.2 and the values are $U_{t_f} = 14\ min$ and 8 min for the heat and energy exchanger respectively.

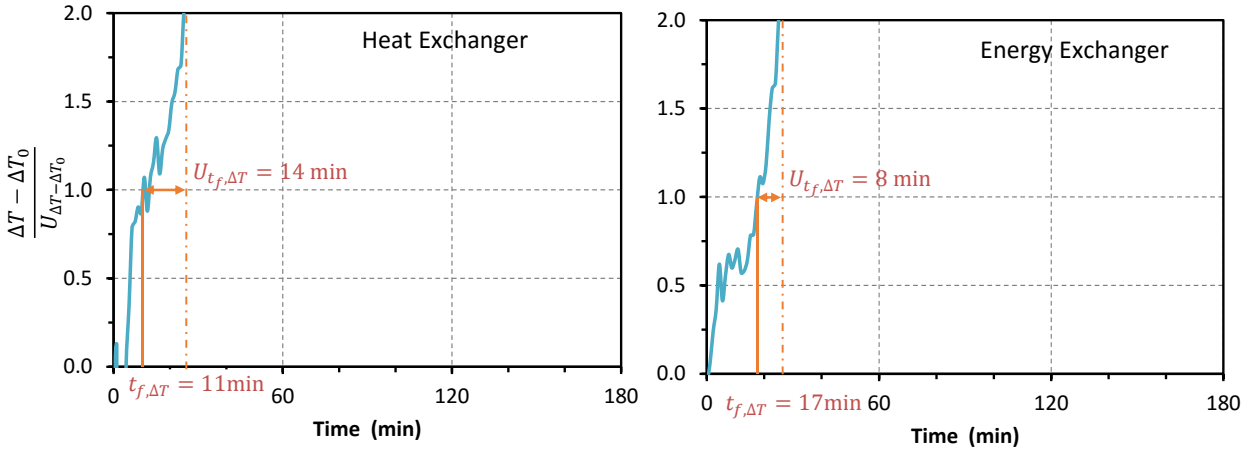

Figure 3.13. Normalized ΔT as a function of time showing the time to detect frosting, t_f, for the heat and energy exchangers ($T_{SI} = -20$℃ and $RH_{EI} = 20$%RH).

For different experiments with no frosting, the results show constant values of ΔT (or a difference very close to 0℃) over the entire experiments which means that $T_{ave}$and T_{mix} are very close when there is no frosting. The main source of small differences between these two values is the heat loss between the measurement station in the test facility.

Another interesting point in Figure 3.12, is that the maximum value for ΔT does not necessarily occur at the end of the test even though the frost is expected to continuously grow during the test. To understand the reason for this, the temperature from each of the four columns of thermocouples (Figure 3.3) as well as T_{mix} and T_{ave} are shown in Figure 3.14. It can be seen that T_{mix} gradually increases because of the reduced heat transfer between the airstreams, due to frost growth. The other temperatures (T_{ave} and T_1 to T_4), however decrease and then increase. The column of thermocouples in the corner closest to the supply inlet (T_1), are the first to decrease, followed by T_2, T_3 and T_4 (in order). The temperatures decrease due to lower local air flow rates in these areas caused by partial blockage of the exhaust air channels by frost. Since the total heat transfer rate in the exchanger is nearly constant (as shown by nearly constant ε_s values over the first 40 minutes in Figure 3.10), the reduced mass flow rate results in a lower outlet air temperature.

The increase in the temperatures, along with fluctuations, which is seen after 80 min in Figure 3.14 is likely due to a reduced total heat transfer rate as the frost grows in the air channels and stationary air around the thermocouples ($T_1 - T_4$). At this advanced frost stage, most of the exhaust air is

only passing through the very corner of exchanger furthest from the supply inlet (furthest from the "cold corner") where no thermocouples are located. Further investigation into how frost is forming in the exchanger is left for future studies

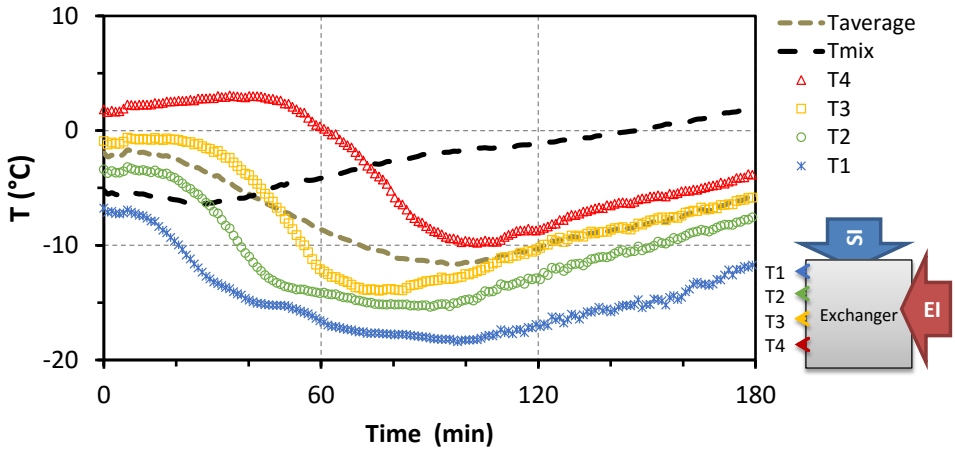

Figure 3.14. Temperature distribution at the exhaust outlet in heat exchanger ($T_{SI} = -20$℃ and $RH_{EI} = 20\%$RH).

The results from the visual inspection method, as well as Figure 3.14 , indicate that the air channels closer to the supply inlet are the first to experience frosting. However, in the test facility, thermocouples are not located completely at the corner of the exchanger where the frosting is initiated (Figure 3.3). If the thermocouples are placed closer to this corner, the ΔT change will be captured sooner. This idea can be evaluated by recalculating ΔT for different thermocouples at different locations as presented in Figure 3.3 (Equation (3-18)).

$$\Delta T_j = T_{mix} - T_j \quad j = 1,2,3,4 \tag{3-18}$$

These different ΔT_js are calculated and presented in Figure 3.15 for both exchangers. It can be seen that the results from the thermocouple closest to the supply inlet (ΔT_1), increase sooner than the thermocouples at the other locations. This finding can be used to develop a very quick and economical way to detect frosting since only one thermocouple at the corner of the exchanger can be used instead of twelve thermocouples.

Overall, the ΔT method is able to detect frosting in cross-flow exchangers and with a small uncertainty in frosting time. Thus this paper proves that temperature measurements can be used as a new method to detect frosting which has not been discussed previously in the literature.

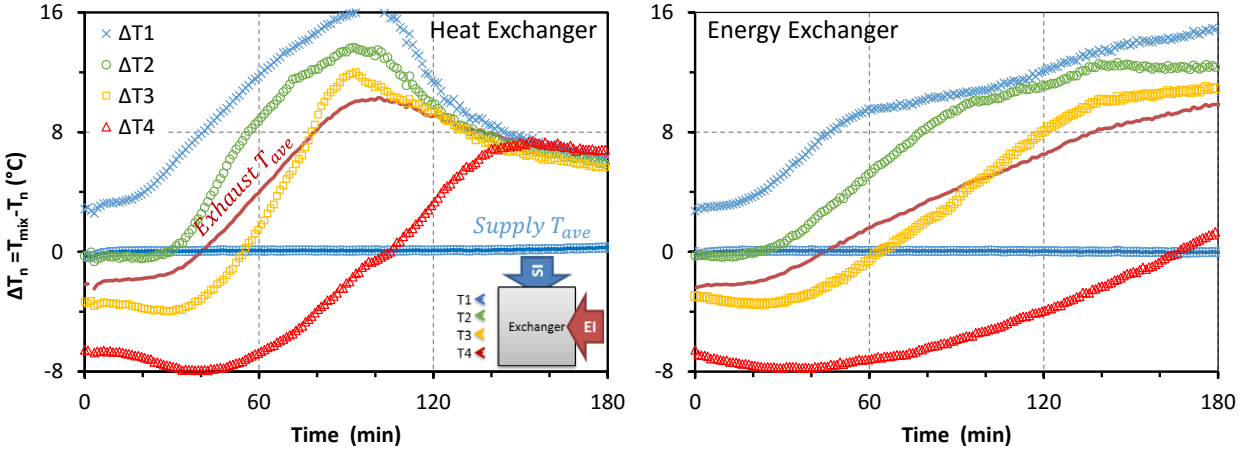

Figure 3.15. ΔT using thermocouples at different locations ($T_{SI} = -20$°C and $RH_{EI} = 20\%$ RH).

3.5.3 Time to detect the onset of frosting

The time it takes to detect frosting, t_f, for the four methods discussed, is summarized in Figure 3.16. It appears that the visual and ΔT methods require the least time to identify frosting in the exchangers and the Δp method requires the longest time to identify frosting. The results for t_f from heat and energy exchanger are within the uncertainty for all of these three methods; however, the high uncertainty in the $\Delta \varepsilon$ method can also lead to high values of t_f. Therefore, effectiveness monitoring is the least desirable method to detect frosting.

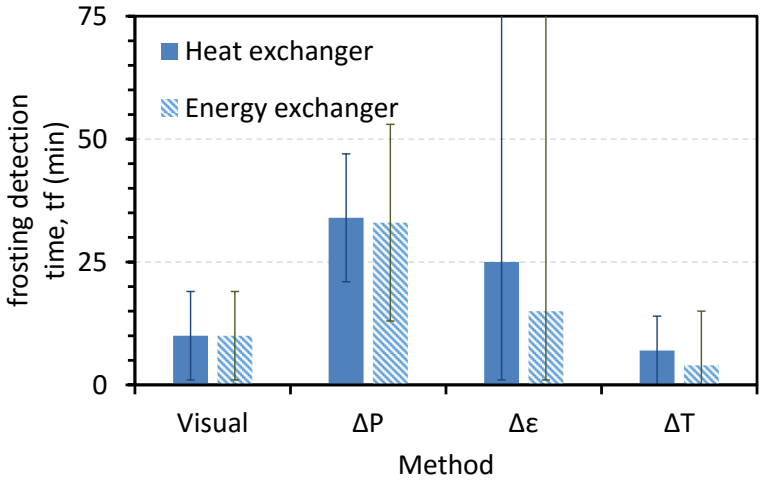

Figure 3.16. Time to detect frosting by different methods for $T_{SI} = -20℃$ and $RH_{EI} = 20\%RH$.

3.5.4 Comparison of frosting detection methods

To be able to clearly understand how the frosting detection time changes with operating conditions, the values of t_f based on different methods and operating conditions are summarized in Figure 3.17. The results from the Δp method indicate that a higher indoor humidity or lower outdoor temperature lead to faster frosting detection. In the $\Delta\varepsilon$ method, a similar trend is observed with the exception of one point. However, the high uncertainty in the results for $\Delta\varepsilon$ is still observed. For the ΔT method, the change in t_f with operating conditions and the type of exchanger is much lower than the other two methods. Therefore, it can be concluded that of the methods studied in the paper, the ΔT method is the first to detect frost and has the lowest uncertainty. There are still some exceptions in the graphs which may be due to a small inevitable difference between the experimental procedure and other operating conditions involved in the tests.

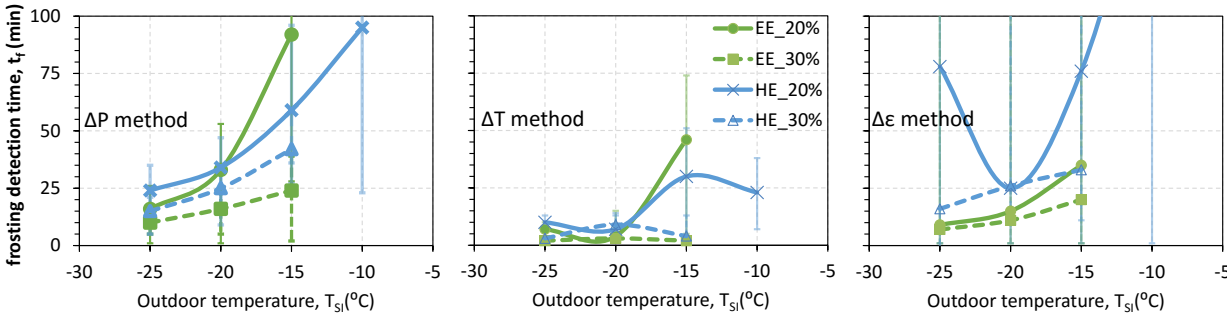

Figure 3.17. Frosting detection time, with different methods at different operating conditions.

Evaluation of the suggested frost detection methods has shown that ΔP and ΔT techniques are more reliable and practical. A parametric study on these two methods based on $T_{outdoor}$ and RH_{indoor} is conducted to evaluate their validity, reliability, and utility under different operating conditions. The results are summarized in Figure 3.18. It should be noted that both exchangers experienced frosting in all operating conditions presented in this figure. In a few cases, the experiments are stopped sooner to prevent any damage to the exchangers or sensors due to a thick frost layer forming. The frosting detection time based on ΔT and Δp for each test is shown in the figure as well. The following points are found:

1. The ΔT method clearly indicates frosting in all experiments, while the ΔP method does not always clearly indicate frosting due to higher relative uncertainty.

2. In the ΔP method, the severity of the frosting can be identified by the magnitude of ΔP, while in the ΔT method it is not feasible to estimate the amount of frost that is formed in the exchanger.

3. The rate of change in ΔP increases by reducing $T_{outdoor}$ or by increasingRH_{indoor}. For example, it is found that 10% increase in RH_{indoor} or 5°C decrease in $T_{outdoor}$ have similar effect on the trend of Δp versus time.

4. ΔT always reached a maximum value, between 16 to 18℃, in both exchangers. Thus, this maximum is independent of membrane or separator properties.

5. Measurement of the mass of the exchangers shows that a similar ΔP or ΔT for an exchanger under different operating conditions does not necessarily represent the same amount of frost. This means that the average density of frost (and as a result the structure of frost) changes with operating conditions. However, this point needs more in depth research which was out of the scope of this paper.

6. The value of ΔT at the beginning of each test is different. This temperature comes from the heat loss between the inlet and outlet of the headers which depends on the operating conditions.

7. Generally, the time to detect frosting in the ΔT method is much shorter than the Δp method. This lower detection time is partly due to the lower relative uncertainty in the temperature measurements compared to the pressure drop measurement.

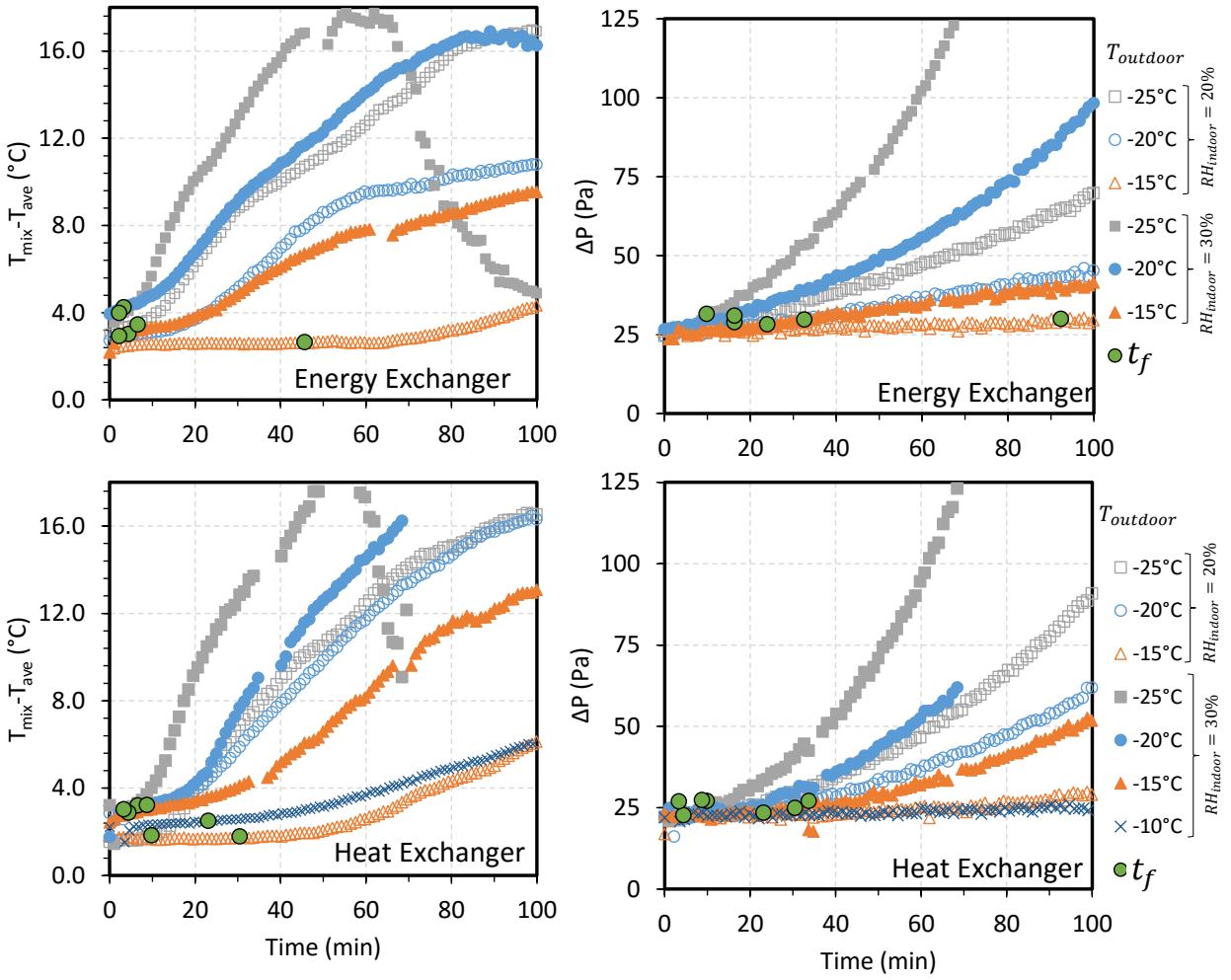

Figure 3.18. ΔT and ΔP at different operating conditions. The green dots in the figure represents the time (according to the method in figures 3.12 and 3.13) where the frost detection method is able to conclude that frosting is occurring in the exchanger.

In conclusion, the ΔT and ΔP methods are reliable methods to detect the onset of frosting in exchangers. In other words, if frost is forming in an exchanger, under a specific operating condition, these two methods are able to quickly and clearly indicate frosting. The ΔT method, which is introduced for the first time in this paper, is consistent with the ΔP method and can be used as an alternative and economical technique to detect frosting in cross flow air-to-air

exchangers. The ΔP method may be more useful for the laboratory tests since it gives more information about the frosting conditions, while the ΔT method is recommended for practical applications where the cost and reliability of the method are both important.

The four frosting detections methods are compared in Table 3.7.

Table 3.7. Comparison between the frosting detection methods used in this paper.

Method	**Advantages**	**Disadvantages**
Visual	-Easy to use -Quickly detects frosting -Low uncertainty in t_f -Relatively inexpensive	-Does not show the amount of frost inside the exchanger -Not practical in frost protection systems because it is a qualitative method -Frequent maintenance required
ε &$\Delta\varepsilon$	-Shows the effect of frosting on heat and mass transfer -Quantitative method	-Not reliable in practical applications due to high uncertainty in t_f -Complex in terms of installation of different sensors and measurement
Δp	-Easy to use -Responds relatively quickly to the presence of frost -Quantitative method -Good indicator of the amount of frost	-Relatively expensive -Frequent calibration is needed -Sensitive to flow rate
ΔT	-Easy to use -Responds quickly to the presence of frost -Low uncertainty in t_f -Relatively independent of the operating conditions and exchanger type -Inexpensive and stable sensors -Low maintenance cost -Quantitative method -Frequent calibration is not needed	-Does not indicate the amount of frost

3.6 CONCLUSIONS

An experimental facility was developed to test small air-to-air energy exchangers under winter operating conditions. Two exchangers, one with a permeable membrane (energy exchanger), and one with an impermeable membrane (heat exchanger), were tested under frosting conditions. Different techniques to detect frosting in the exchangers (visual inspection, change in pressure drop, change in effectiveness, and change in temperature difference) were evaluated by comparing their accuracy and the time required to detect frosting. Among these methods, the difference in temperatures is a novel method which is proposed in this study. The results showed that mass and energy inequalities are satisfied for the operating conditions with and without condensation and frosting. Based on the results in the paper which are summarized in Table 3.7, the change in pressure drop and the temperature difference methods are preferred over the other methods because they are quicker and quantitative methods and are very sensitive to frosting (i.e. they quickly detect frost with low uncertainties). Although the operating conditions and the type of exchanger have some effects on the results by both methods, the temperature change method is less affected by these factors.

3.7 ACKNOWLEDGMENT

This research was financially supported by the Natural Sciences and Engineering Research Council of Canada (NSERC) through the Smart Net-Zero Energy Building Strategic Research Network (SNEBRN), ASHRAE through a grant-in-aid to Mr. Rafati Nasr, dPoint Technologies Inc. through in-kind support for a NSERC Engage project, and the University of Saskatchewan. The authors also express their gratitude to Dr. Fauchoux, and Mr. Liu for their assistance in designing the experiments and discussing the results in this paper.

CHAPTER 4:

THEORETICAL MODEL

4.1 OVERVIEW

Based on the information presented in the previous chapter, it can be seen that the experimental approach to find the frosting threshold operating conditions in an exchanger is very complicated, time consuming, and expensive. One of the objectives of this PhD work is to develop a theoretical model to predict the frosting limit for exchangers, based on the exchanger design parameters and operating conditions.

The model in this chapter is the result of a joint collaboration between researchers at the Norwegian University of Science and Technology (NTNU) and the University of Saskatchewan (U of S). The model is validated with the experiments done at the U of S. A series of assumptions is defined in the model, some of which are based on the experimental observations presented in Chapter 3. The model and the exchangers' physical properties such as dimensions, channel spacing and water vapor permeability are used to find the frosting limit of the exchangers. In addition, the frosting limit for the same conditions in the model are obtained through experiments. Finally, a parametric study of the design parameters on the frosting limit is conducted.

During our joint collaboration, Mr. Liu, a PhD student from NTNU, visited the U of S for five months and worked with the researchers at the U of S. Mr. Liu and Mr. Rafati Nasr contributed to the manuscript equally. Both were deeply involved in the theoretical model development, preparation, planning and conducting of the experiments, analyzing the experimental data, performing the parametric study using the model, preparing the manuscript, and incorporating co-authors' comments. Dr. Mathisen and Dr. Alonso are Mr. Liu's supervisor and mentor, respectively. Mr. Fathieh, helped in experimental preparations and sensor calibration, as well as data analysis. Due to significant contribution of Mr. Liu to this paper, he is presenting this paper as a part of his PhD thesis as well.

This chapter has been published in Energy and Buildings in November 2015. In addition, section 4.6.2.1 in this chapter is added from a technical paper accepted for presentation in ASHRAE winter conference in Las Vegas, USA in January 2017.

A Theoretical Model to Predict Frosting Limits in Cross-Flow Air-to-Air Flat Plate Heat/Energy Exchangers

Energy and Building, November 2015

Peng Liu, Mohammad Rafati Nasr, Gaoming Ge, Maria Justo Alonso, Hans Martin Mathisen, Farhad Fathieh, Carey Simonson

4.2 ABSTRACT

In cold climates, the water vapor in the warm and moist exhaust air may condense on the designed high efficiency heat/energy exchanger surfaces in mechanical ventilations. The ice or frost, which degrades the performance of exchangers, will occur when the surface temperatures are below the freezing point. In this study, a simplified theoretical model to predict the inlet conditions under which frost will form in the flat plate heat/energy exchangers is developed. The model uses the exchanger design parameters and operating conditions to determine the frosting limit. Exhaust air inlet humidity and supply air inlet temperature are regarded as the operating variables of the frosting limits while other design and operating parameters are kept as constants. Experiments are conducted to validate the model. The results show that the predicted frosting limits have consistent agreement with experiments, and energy exchangers have a lower risk of frosting than the heat exchangers. Furthermore, a parametric analysis using the theoretical model is performed to estimate the impact of number of heat and moisture transfer units (NTU_s and NTU_m), aspect ratio of aluminum spacer channel, air flow rate, and membrane permeability on frosting limits of heat/energy exchangers. It is found that air flow rate has significant impact on frosting limits. The combination of sensible and latent effectiveness ensuring no frost inside energy exchanger are also studied theoretically. The developed frosting limits model is new to the literature and simpler than CFD modeling and can be applied to improve the design of exchangers to reduce or avoid frosting in cold climates.

4.3 INTRODUCTION

Air-to-air heat/energy recovery ventilators (HRVs/ERVs) have been widely used in heating, ventilation and air-conditioning (HVAC) systems to reduce energy consumption for ventilation and the green-house gas emission, especially in hot and humid climates or cold climates. In these

systems outdoor fresh air and the indoor stale air enter the exchangers by separated sides. Sensible heat, latent heat, or both are transferred from one air stream to another, depending on the temperature and moisture gradients. When warm and moist exhaust air passes over the cold plate surface of an exchanger, water vapor condenses and frost forms on the surface if the plate temperature is lower than both the air dew point and water freezing point. In cold climates defined by international climatic zones with thermal criteria (ASHRAE 2007) such as Canada and northern Europe, frost often forms inside the HRVs/ERVs and would negatively impact the performance of the exchangers in winter (Rafati Nasr, Fauchoux, Besant, et al. 2014). This frosting issue is more critical when the outdoor temperature is extremely low.

Defrosting or protecting heat and energy exchangers from frosting has remained as an important issue for decades. A recent numerical simulation for a residential house under Canadian winter condition by (Zhang & Fung 2015a) showed that the yearly demand of defrosting cycle for a heat exchanger is 3.5 times higher than an ERV. The reason is that ERVs transfer both heat and moisture simultaneously between supply and exhaust air streams, which encounter frosting at a lower temperature compared to HRVs in cold climates. (Fisk et al. 1984) and (Ruth et al. 1975) indicated that the frost occurred approximately 5 to 10℃ lower in a desiccant wheel (ERV) than conventional HRVs. Another study by Rafati (Rafati Nasr, Kassai, et al. 2015) indicated that the ERV is more efficient than the HRV under frosting conditions. It also concluded that preheating the supply air to prevent frosting is more efficient than bypassing the supply air method to defrost the exchangers, and the prediction of the frosting limits is critical for the exchangers in practical applications. The recent literature reviews on the use of heat/energy exchangers in cold climates, frost and frosting control strategies for air-to-air exchangers found that the flat plat (membrane) energy exchanger has a promising future in reducing or avoiding the frost instead of conventional heat exchanger. (Alonso et al. 2015; Rafati Nasr, Fauchoux, Besant, et al. 2014)

The research work in frosting of flat plate heat/energy exchangers can be divided in two categories. The first type is dealing with predicting the properties of a frost layer such as density, heat conductivity and surface roughness as a function of time and temperature. Most of these models are correlations or combination of theoretical and experimental results on frost properties. Detailed reviews in frost properties and models were published (Iragorry et al. 2004; Padki et al. 1989; Chen et al. 2000). However, most of these models are limited to some specific geometries and a

range of temperature of the cold surface. Therefore, it is not easy to apply those results to other air-to-air exchangers with different exchanger configurations and operating conditions. In addition, there is a lack of quantitative dependency analysis of the frost-air interface temperature which plays a very important role in heat transfer analysis.

In the second category, effect of frosting in the performance of the heat or energy exchangers was described. Bantle (Bantle et al. 1987) used an empirical heat transfer coefficient for a frosted surfaces to predict the performance of a counter-flow exchanger. Philips et al. (Phillips, Chant, et al. 1989) used a numerical method to determine changes in effectiveness in a counter-flow exchanger under frosting condition. He calculated the frost thickness and evaluated its effect on the effectiveness. In other works (Phillips et al. 1992; Phillips, Bradley, et al. 1989), Phillips assumed the frosting limit as a known parameter and based on that he theoretically calculated the energy impact of different defrosting strategies for a counter-flow exchanger using weather data.

The frosting limit in this study refers to the specific combinations of supply (outdoor) air temperature and exhaust (indoor) air relative humidity which initiate frosting in different flat plate heat/energy exchangers. There are only few works which investigated the effects of operating conditions on frosting and frosting limits. Ruth (Ruth et al. 1975) conducted tests on an aluminum heat-wheel and found that occurrence of frosting was greatly dependent on the exhaust air humidity. Frosting was observed at outdoor temperature ranged from -26℃ to -16℃ when the relative humidity of exhaust air was between 25%RH and 30%RH. Fisk (Fisk et al. 1984) compared frosting limits for different cross-flow exchangers experimentally. He used an analytical model to predict the frosting limit for a counter-flow exchanger as a reference in the work. In his model, the influence of the heat released from condensation on temperature of the plat was considered. He further investigated the indoor and outdoor environmental conditions that initiated freezing with experiments for cross- and counter-flow flat plate heat exchangers and a cross-flow energy exchanger. The frosting limits of the three exchangers were plotted in the research (Fisk et al. 1985). However, the theoretical frosting limit model was not given in the research. Tests were conducted to determine the frosting limits for a "counter-flow pure-plate" heat exchanger (Sauer et al. 1981). The frosting limits ranged linearly from -23℃ to -9℃ of outdoor air temperature with exhaust air RH from 58%RH to 32%RH when the exhaust air temperature was 24°C. The criterion of determining the limits was not presented. Holmberg(Holmberg 1989b) used CFD method to

solve coupled heat and mass transfer equations in a two dimensional space to predict temperature distribution in a single and double pass cross-flow heat exchanger under steady state conditions. In another work, Holmberg (Holmberg 1989a) theoretically calculated the frosting limits for energy wheels. In his model two types of wheels with constant effectivenesses for fixed inlet conditions were presented. Through a field test for a house in Ontario (Canada), Zhang (Zhang & Fung 2015a) found energy exchanger performance was not deteriorated until supply air temperature reached $-16℃$. In recent years, Liu et al. (Liu et al. 2013; Liu et al. 2014) developed a theoretical one-dimensional model to determine frosting limits for counter flow heat and energy exchangers. Liu applied this model with weather data of Norway to predict frosting operation conditions throughout the daily coldest outdoor temperature of a year for a counter-flow energy exchanger. In his model, two conditions to cause frosting formation are subzero surface temperature and condensation over the surface.

In general, following shortcomings are noticed in the literature:

- Previous researche were mainly based on experiments that were limited to specific design or operating conditions.
- The proposed models were limited to counter-flow heat/energy exchangers.
- Most of theoretical works were validated with experiments only for a specific design or operating condition.
- The main type of energy transfer was sensible heat. Very few studies have considered latent heat in the form of mass transfer.
- The authors did not find the specific theoretical model in the literature which predicted the theoretical frosting limit for cross-flow air-to-air flat plate heat/energy exchangers.

In this study, a theoretical model to predict the critical operating conditions for frosting in cross-flow heat/energy exchangers is developed. The frosting limits of heat/energy exchangers for a residential use are theoretically and experimentally studied. The effects of design parameters are also evaluated which may guide the free-free air-to-air cross-flow flat plate heat/energy exchangers design.

4.4 MATHEMATICAL MODEL

The main goal of this study is to develop a theoretical model to predict the critical operating conditions in which the onset of frosting occurs in cross-flow exchangers. It is important to include the exchanger physical and design parameters (such as air channel spacing, thermal conductivity and water vapor diffusivity of the plates) and operating conditions (such as air-flow rate, temperature and relative humidity). Due to two-dimensional nature of heat and mass transfer in cross-flow flat plat exchangers, modeling is more complex than the counter-flow arrangement.

Two necessary conditions to trigger frosting are condensation formation and subzero temperature of the plate surface at the same spots. These two conditions are used to derive frosting limits for different exchangers in this study. If the design parameters and air flow rate keep unchanged then supply air (outdoor) temperature and exhaust inlet (indoor) relative humidity play more important roles in the frosting limit (Rafati Nasr, Fauchoux, Kadylak, et al. 2014).

4.4.1 Assumptions

In cold climate regions condensation and frosting are potential to take place in the exhaust side in HRVs/ERVs (Rafati Nasr, Fauchoux, Besant, et al. 2014). The temperature and humidity distributions across a cross-flow exchanger are not uniform (Zhang, 2008), therefore the possibility of frosting at some locations is higher than other parts. According to experiments (Mercadier et al. 1993) and numerical modeling (Holmberg, 1989; Zhang, 2008), frosting more likely first appears at the exhaust air outlet in the flow channels closest to the supply air inlet which is known as “cold corner” for the cross-flow exchangers. (Figure 4.1). In this study, the outlets of first exhaust channels at the corner are regarded as the most likely positions of frost emerging. (Figure 4.1(b)).

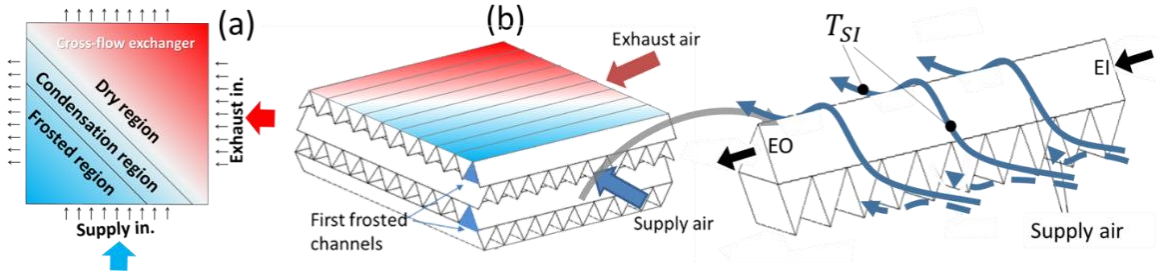

Figure 4.1. (a) Qualitative temperature distribution and frosting location in a cross-flow exchanger, (b) The channels with highest risk of frosting in a corrugated cross-flow air-to-air exchanger.

The following assumptions are used in this research:

1. Frosting initially forms in the outlets of exhaust air channels that are closest to the supply inlet in both heat and energy exchangers (Figure 4.1(b));
2. The supply air temperature which passes over the first channels is equal to T_{SI}(Figure 4.1(b));
3. Air flows through all channels are homogeneous and incompressible;
4. The air mass flow rates between each plate are identical;
5. Thermal and mass entrance effects in the air channels are negligible;
6. The convective heat transfer coefficients and specific heat capacity of both air streams are equal and constant throughout the air channels of exchangers;
7. No air leakage occurs from/to the exchangers or between two air streams;
8. The thermal resistance of the exchanger plates is negligible due to the thin thickness;
9. Condensation occurs only on the exhaust side;
10. Condensation heat has a negligible impact on frosting in energy exchanger. The effect on plate heat exchangers can also be omitted when the indoor air relative humidity is below 30%RH (Fisk et al. 1984);
11. The thermal properties of both fluids and exchanger walls do not vary with temperature;
12. The velocity, temperature, and humidity distributions of the fluids are uniform at the inlets of the exchanger;
13. There is no heat sources and heat sinks in the air stream;
14. The exchangers are well insulated and no heat is transferred between the exchanger and surrounding.

4.4.2 Critical supply (outdoor) air temperature

A critical outdoor air temperature is defined as the lowest outdoor air temperature to maintain the membrane temperate at the most likely positions of frosting occurring over the freezing point. The heat transferring through the first exhaust channels to supply air side is calculated by equation (4-1).

$$q = U_1 A_1 \Delta T_{lm} \tag{4-1}$$

$\Delta T_{lm}$is the log mean temperature differences which is defined in equation (4-2). Heat gain by air from inlet to outlet in the first channel is computed by equation (4-3).

$$\Delta T_{lm} = \frac{\Delta T_1 - \Delta T_2}{ln\left(\frac{\Delta T_1}{\Delta T_2}\right)}, \qquad \Delta T_1 = T_{EI} - T_{SI} \ \& \Delta T_2 = T_{EO} - T_{SI} \tag{4-2}$$

$$q = \dot{m}_1 c_p (T_{EI} - T_{EO}) \tag{4-3}$$

T_{EO} can be calculated as a function of $U_1, A_1, T_{EI}\ and\ T_{SI}$. To meet frosting condition, the plate temperature (T_p) should be equal to or lower than freezing point. The plate temperature T_p is the arithmetic average of the supply and exhaust air temperature at the corresponding positions when the thermal resistance of plate is negligible due to the thin thickness. Thereafter, the plate temperature at exhaust outlets for the first channels can be expressed in equation (4-4).

$$T_p\big|_{@EO} = \frac{\mathrm{T}_{SI} + \mathrm{T}_{\mathrm{EO}}}{2} = \frac{T_{EI} - T_{SI}}{2\ exp(NTU_{h1})} + T_{SI} \tag{4-4}$$

Where the number of heat transfer unit (NTU_{h1}) is given by equation (4-5).

$$NTU_{h_1} = \frac{(U_1 A_1)_s}{\dot{m}_1 c_p} \tag{4-5}$$

The critical supply air temperature$T_{SI_{cr}}$ is expressed in equation (4-6) when $T_p\big|_{@EO} = 0$. This temperature shows the value at which the plate temperature reaches freezing point at the most likely position of frosting.

$$T_{SI_{cr}} = \frac{T_{EI}}{1 - 2\exp(NTU_{h1})} \quad (4\text{-}6)$$

4.4.3 Condensation limit

The condensation limit is a combination of indoor relative humidity and outdoor air temperature resulting in the exhaust air at most likely frosting positions starting to condensate.

Using heat and mass transfer analogy, the moisture content of the exhaust outlet air close to most likely frosting position can be expressed as equation (4-7). The moisture content of exhaust inlet (indoor) air is presented with equation (4-8) through rearranging equation (4-7). Number of moisture transfer unit (NTU_m) is given in equation (4-9).

$$w_{EO} = \frac{w_{EI} - w_{SI}}{exp(NTU_{m1})} + w_{SI} \quad (4\text{-}7)$$

$$w_{EI} = w_{EO}(exp(NTU_{m1})) + w_{SI}(1 - exp(NTU_{m1})) \quad (4\text{-}8)$$

$$NTU_{m_1} = \frac{(U_1 A_1)_l}{\dot{m}_1} \quad (4\text{-}9)$$

W_{SI} is the moisture content of supply (outdoor) air and regarded as known values which are usually very low for cold climates. The relationship between moisture content and relative humidity is described using Clapeyron equation as shown in equation (4-10). The water vapor starts to condense when the exhaust air close to the surface reaches saturation namely relative humidity of exhaust air at outlet being 100%RH. The condensation limits can be described through equation (4-7) to (4-10). The limits can be expressed as a function of the inlet temperature and moisture parameters.

$$w = \frac{10^6 RH}{e^{5294/(T+273)} - 1.61RH\ 10^6} \quad (4\text{-}10)$$

4.4.4 Frosting limits

The frosting limits consist of the critical outdoor temperature and the condensation limit which are addressed above. Frosting starts when the outdoor temperature is lower than the critical outdoor air temperature and the indoor RH exceeds the condensation limits.

The NTU_h and NTU_m used in the model can be computed for specific exchangers through the numerical modeling in the literature. The NTU_h and NTU_m of plate exchangers with cross-corrugated triangular spacer are calculated and validated in this paper. The frosting limits of heat exchanger can be calculated with this model by substituting $\mathrm{NTU_m} = 0$ due to no moisture transfer.

4.5 EXPERIMENTAL VALIDATION

4.5.1 Test facility

A test facility was built up to test full size cross-flow air-to-air exchangers. This facility enables researchers to test different exchangers under non-frosting and frosting conditions. The layout of the test facility is shown in Figure 4.2. The test rig consists of two environmental chambers, four fans, a test section, and connecting pipes.

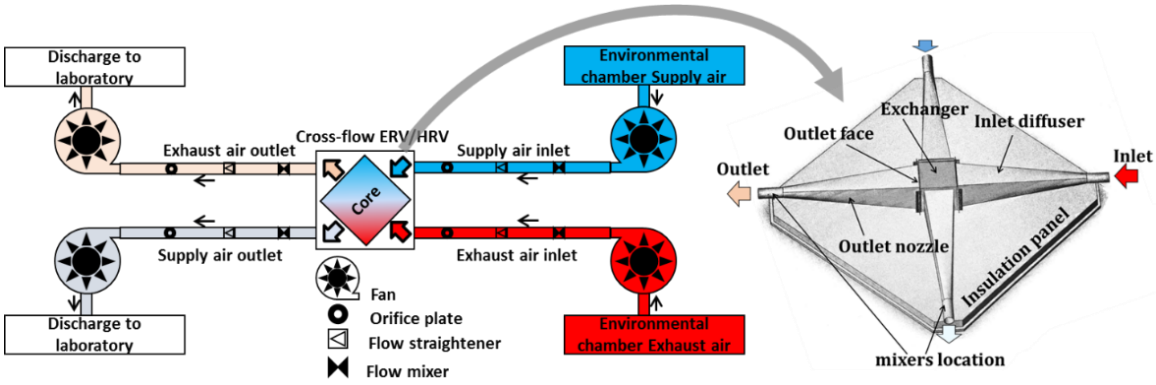

Figure 4.2. Schematic of the experimental setup for air-to-air cross-flow exchangers.

This test setup is designed as an open loop with two fans in each air stream. Air is drawn from each chamber in a separate air stream using two fans; one before and one after the test section, in each air stream. Flow rates are adjusted by voltage regulator connected to each fan. Presence of two fans at each air stream allows to control the pressure at the exchanger to minimize the air leakage to or from the ambient, and to produce balanced flow rate. The exchanger can be tested at any temperature between -30°C to 30°C, while relative humidity can be 10%RH to 90%RH for the flow rate equal to $20.8\ \mathrm{L/s}$. In the test section the exchanger is located in an insulated test box (Figure 4.2). Pipes are connected to the exchanger with inlet expansion and outlet contraction diffusers. These headers are designed to produce uniform flow fields at the exchanger inlet face.

Velocity measurement at the face of the exchanger confirmed uniform profile for the inlet air. Moreover, heat loss in the headers is negligible.

Different parameters such as temperature, relative humidity, flow rate and pressure drop are measured or calculated in experiments. Temperature of air is measured using T-type thermocouples (copper constantan). Vaisala humidity and temperature sensors are used to measure both relative humidity and temperature. Air flow rate is measured by employing an orifice plate according to standard (ISO 2003). Pressure drop is measured by two types of pressure transducers. Pressure drops across the orifice plates (for flow rate measurement) are gained by general purpose diaphragm pressure transducers, while low pressure transducers are used to capture changes in pressure drop across the exchanger. Performance of the exchanger is evaluated by effectiveness which is the ratio of the actual energy transfer over the maximum possible energy transfer (ASHRAE 2013).

Uncertainty of sensors are determined according to ASME PTC 19.1 (ASME 2005). Each sensor is calibrated with a calibrator where its signals are recorded by a data acquisition system (DAQ). Once the data are collected, precision and bias are calculated for the sensor. Then calibration curves are developed where they are applied to raw data from experiments.

4.5.2 Frosting detection methods

During the design of the test facility, possible methods of frost detection were reviewed (Rafati Nasr, Fauchoux, Besant, et al. 2014). The visual technique and pressure drop method are used in this study, since they are more accurate in detecting the frosting limit. In the visual technique, two endoscope cameras are used to view the exchanger during the experiments. These endoscopes are installed just after the outlet face, one in the exhaust side and one in the supply side. The endoscopes are 9 mm in diameter which is larger than the channel spacing, therefore, it is not possible to insert the endoscope inside the channels. Static pressure drop across the exchanger is also monitored during the entire experiment. An increase in pressure drop across the exchanger is a sign of frosting due to partial blockage of the channels by frost. More details for these methods were presented in (Rafati Nasr, Fauchoux, Kadylak, et al. 2014).

In all experiments, the pressure drop across the exchanger and the photographs are analyzed to detect frosting. It takes approximately 3 hours for each experimental test. Figure 4.3 (a) shows a comparison of the pressure drop in two experiments for heat and energy exchangers. It is clear that pressure drop in the exhaust side where the risk of frosting is higher, increased, while no change in the supply side was captured. This means there is no frost in the supply side and that was in agreement with visual method. Figure 4.3 (b) shows partial frost formation at the exhaust outlet of the energy exchanger by visual method in the energy exchanger experiment. It can be seen that the channels at the exhaust outlet are covered with frost. Such situation was observed for heat exchanger under the similar working conditions. Thus, in this example the working conditions were considered in the frosting zone.

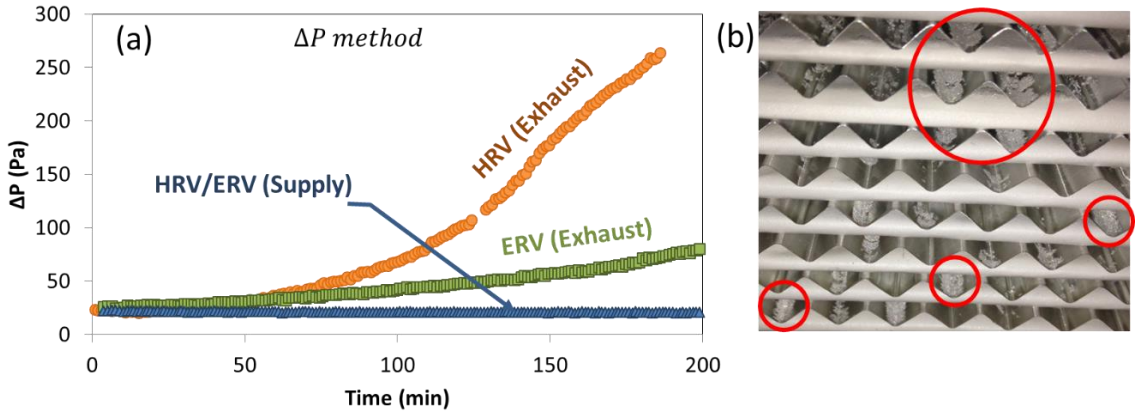

Figure 4.3. Frosting detection method when:
$T_{SI} \sim -15℃$, $T_{EI} \sim 22$, $RH_{SI} \sim 45\%$RH, $RH_{EI} \sim 37\%$RH (a) Pressure drop method, (b) View of the energy exchanger at the end of experiment.

To find the frosting limit experimentally, each exchanger is tested at different T_{SI} and RH_{EI} while the rest of operating conditions are fixed. The lowest RH_{EI} at each T_{SI} or in another word, the highest T_{SI} at each RH_{EI} with frosting that is captured with either by pressure drop or visual method defines the experimental frosting limit. To check the repeatability and accuracy of the results, exchangers are tested twice at some of the frosting limit points.

4.6 RESULTS AND DISCUSSION

4.6.1 Model validation: NTU_h and NTU_m of heat/energy exchanger

The numbers of transfer units of heat and moisture heat are indispensable to compute the frosting limits using the developed model in this study. This section will illustrate the method to model the performance of the exchangers with aluminum cross-corrugated triangular spacers. Two geometrically identical exchangers are tested in the study. The energy exchanger is made with polymer membranes to separate the supply and exhaust air streams, which are permeable to water vapor, while the heat exchanger is made with impermeable polymer films with the same thickness (Figure 4.4).

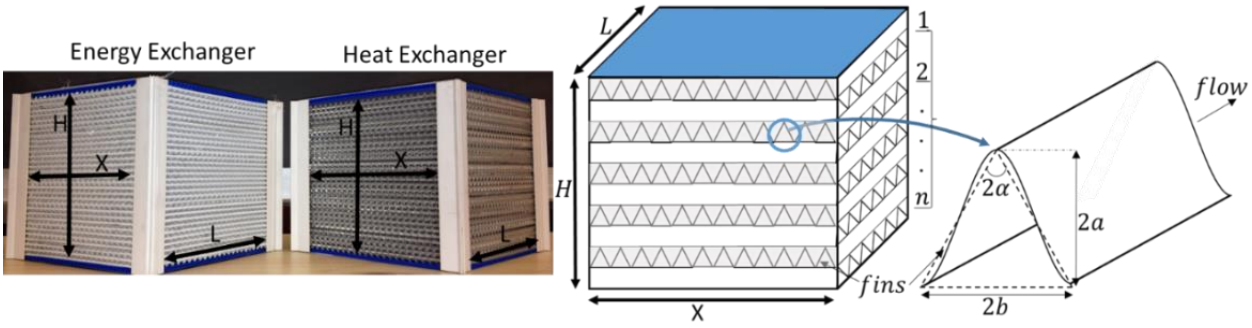

Figure 4.4. Tested exchangers and their geometrical parameters.

NTU calculation for air-to-air cross-flow exchangers using design and physical properties of the exchanger is available in detail in (Zhang, 2008). The physical dimensions of the exchangers and properties of the membranes are presented in Table 4.1and Figure 4.4. A key parameter is the water vapor diffusivity of the membrane, provided by the manufacturer, which was measured to be $2 \times 10^{-6}\, m^2/s$ according to the method of (Ge et al. 2014).

Table 4.1. Physical specification of the heat and energy exchangers tested.

Parameter	Value	Reference
Number of channels for each flow, n	31	Lab measurement
Half duct height, a	$1.52 \pm 0.07mm$	Lab measurement
Half duct width, b	$3.61 \pm 0.07\ mm$	Lab measurement
Apex angle, α	$49° \pm 2°$	Lab measurement
Hydrodynamic diameter, D_h	$2.63\ \pm 0.16mm$	Lab measurement
Exchanger width X, height H, depth L	$165 \pm 2\ mm$	Lab measurement
Membrane thickness, δ	$100 \pm\ 0.02\ \mu m$	Lab measurement
Membrane water vapor diffusivity, D_{wp}	$2.0 \times 10^{-6} \pm 3 \times 10^{-7}\ m^2/s$	Lab measurement
Thermal conductivity of membrane, k_p	$0.44\ W/(m\ K)$	(Zhang 2008)
Thermal conductivity of fin, k_f	$237\ W/(m\ K)$	(Zhang 2008)
Thermal conductivity of air, k_a	$0.0258\ W/(m\ K)$	(ASHRAE 2009)
Density of air, ρ_a	$1.12\ kg/m^3$	(ASHRAE 2009)
Water vapor diffusivity in the air, D_{va}	$2.82 \times 10^{-5}\ m^2/s$	(Zhang 2008)
Kinetic viscosity of air, ν_a	$15.52 \times 10^{-6}\ m^2/s$	(ASHRAE 2009)
Volumetric air flow rates, Q	$20.8\ \pm 0.5\ L/s$	Lab measurement
Face velocity, u_a	$1.5 + 0.1\ m/s$	Lab measurement
Reynolds Number, Re	228+22	Lab measurement

The Reynolds number indicates laminar flow regime inside the air ducts. Using equations in (Zhang 2008) the pressure drop, ΔP, across the exchanger was calculated as 20.3 Pa. The theoretical ΔP is in agreement with the experimental value, $23\ \pm 3\ Pa$. According to the procedure which is presented in (Zhang 2008) heat and mass transfer coefficients (h and h_m respectively), the total heat and mass transfer coefficients ($U_{tot_s}\ and\ U_{tot_l}$), NTU, and effectivenesses are obtained from Equations (4-5), (4-9), (4-11) to (4-13). The calculated exchanger performance parameters for the design condition are shown in Table 4.2.

$$(UA)_{tot_s} = \left[{(hA)_s}^{-1} + \left(\frac{A_p k_p}{\delta}\right)^{-1} + {(hA)_E}^{-1} \right]^{-1} \tag{4-11}$$

$$(UA)_{tot_l} = \left[{(h_m A)_s}^{-1} + \left(\frac{A_p D_{wp}}{\delta}\right)^{-1} + {(h_m A)_E}^{-1} \right]^{-1} \tag{4-12}$$

$$\varepsilon_{s/l} = 1 - exp\left[\frac{exp\left(-NTU_{h/m}^{0.78}\right) - 1}{NTU_{h/m}^{-0.22}}\right] \tag{4-13}$$

To verify the NTU calculated from the theory, both exchangers were tested at AHRI winter test condition (AHRI 2011). A full uncertainty analysis was conducted to account for propagation

uncertainty through the measurements bias and precision error. The results from repeated experiments were within the uncertainty range. Experimental and theoretical results are summarized in Table 4.3and shows good agreements. It can be concluded that the theory is reliable in predicting the NTU_h and NTU_m. This theoretical model will be used to conduct a parametric study on the frosting limits in this paper.

Table 4.2. Theoretical performance parameters.

Parameter	Parameter	Value	uncertainty $\frac{U_\varphi}{\varphi}$
Nusselt Number	Nu	1.9	0.04
Sherwood Number	Sh	0.69	0.02
Heat Transfer Coefficients	h	20.3 (W/m^2K)	0.08
Mass Transfer Coefficients	h_m	$8.17 \times 10^{-3}(m/s)$	0.07
Total Heat Transfer Coefficients	$(UA)_{tot_s}$	37.89 (W/K)	0.09
Total Mass Transfer Coefficients	$(UA)_{tot_l}$	$1.05 \times 10^{-2}(m^3)$	0.14
Number of Heat Transfer Unit	NTU_h	1.6	0.10
Number of Moisture Transfer Unit	NTU_m	0.5	0.14

Table 4.3. Comparison between the experimental and theoretical effectivenesses.

Exchanger type	ε_s		ε_l	
	Theoretical	Experimental	Theoretical	Experimental
HRV	$58\% \pm 3\%$	$58\% \pm 2\%$	$-$	$-$
ERV	$58\% \pm 3\%$	$58\% \pm 2\%$	$32\% \pm 3\%$	$32\% \pm 4\%$

4.6.2 Model Validation: Frosting limit

To determine the experimental frosting limit, each exchanger is tested under the conditions near the theoretical frosting limit. The theoretical model is used to select the test conditions for the experiments. In the validation experiments, the exhaust inlet temperature and supply inlet relative humidity are approximately constant ($T_{EI} \approx 22$ ℃, $RH_{SI} \approx 45\% RH$), while RH_{EI} and T_{SI} change between 5%RH to 50%RH and -5 to -33℃, respectively. Results of these experiments lead to a map for frosting limit. In total more than 80 tests were conducted, and each was run for 2 to 3 hours.

4.6.2.1 Experimental Frosting Limit

The summary of the experiments and the frosting limit results are presented in Figure 4.5. In this figure, the operating conditions in which exchangers have frost are shown with solid circles. The test conditions with no frosting are shown with the X symbol. The criteria used to define "frosting" and "no frosting" points is based on the observation from the methods (Δp and ΔT method) in Chapter 3. Figure 4.5 shows that a lower indoor relative humidity leads to a lower frosting limit temperature for both the heat and energy exchanger. This finding is explained by the fact that lower moisture content in the air reduces the dew point temperature in the exhaust air side and thus a lower surface temperature is required to produce condensation and frosting.

Results in Figure 4.5 are used to develop a frosting limit graph for each exchanger. These graphs are shown in Figure 4.6. Comparing the results between the heat and energy exchanger confirms that the energy exchanger is more frost resistant. In other words, at the same outdoor temperature, the heat exchanger experiences frosting at a lower indoor moisture content than the energy exchanger. For example, when the outdoor temperature is -10℃, the indoor humidity should be below 20%RH and 30%RH to have the frost free heat and energy exchanger, respectively. As another example, when the indoor RH is 30%RH, the heat exchanger experiences frosting at - 5℃, whereas for the energy exchanger first experiences frosting at - 10℃. The results shows that in both exchangers frosting is nearly inevitable for all prospective indoor condition when the outdoor temperature is less than -25℃. In Table 4.4 a summary of the uncertainties in measured and calculated parameters are presented. It should be noted that all these values are an approximate, since these may change for each test.

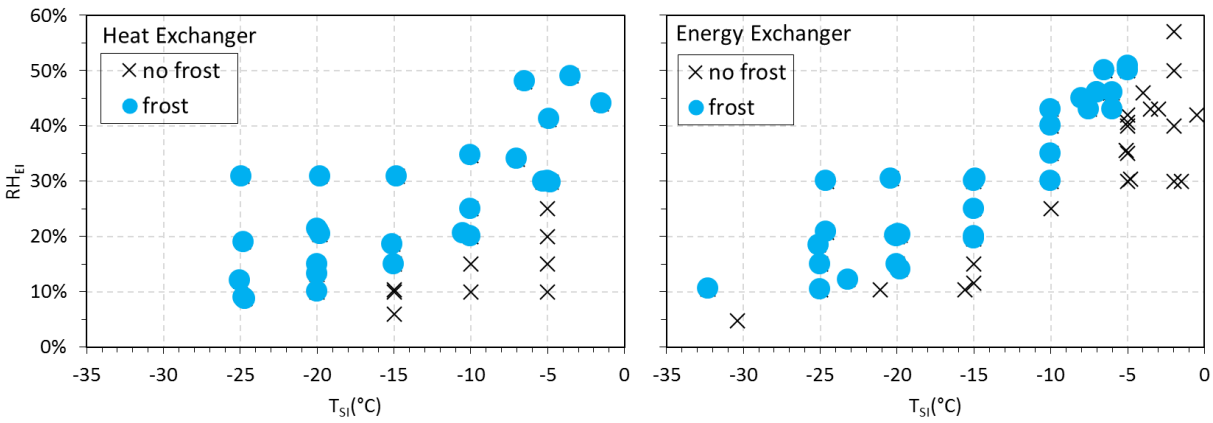

Figure 4.5. Experimental test points showing conditions with and without frosting in the heat exchanger and energy exchanger.

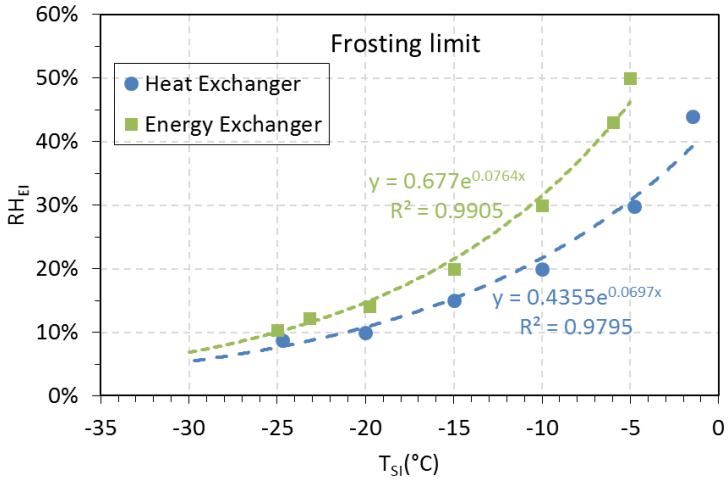

Figure 4.6. Experimental frosting limit for heat and energy exchanger.

Table 4.4. Uncertainties in measured and calculated values with 95% confidence interval.

Parameter		Uncertainty
Temperature (°C)	T	0.2-0.25
Relative humidity Vaisala (% RH)	RH	1.5-2
Pressure drop (Pa)	Δp	3-7
Mass flow rate (%)	$\dot{m}$	2
Sensible effectiveness (%)	ε_s	2
Latent effectiveness (%)	ε_l	2-6
Humidity ratio (%)	w	2-6

4.6.2.2 Theoretical model verification

Comparison between theoretical model and experiments are shown in Figure 4.7 (a) and (b). In this figure only the lowest RH_{EI} at each T_{SI} in which frosting captured is presented. The RH discrepancies between theoretical and experimental frosting limits, ΔRH, are shown in Figure 4.7 (a) and (b) as well. The dashed line indicates the critical supply inlet (outdoor) air temperature. The plate temperature at the most likely frosting positions is below the freezing point if the outdoor temperature is lower than the critical temperature (the left area of the dashed line). The experimental and theoretical results have same trends as shown in Figure 4.7 (a) and (b). The lower the supply inlet air temperature is, the less moisture can be carried by the exhaust air without occurring frost in exchangers. The trend is obviously consistent with the engineering experience. Overall, very good agreement between experiments and theoretical predictions are obtained for both heat and energy exchangers. To verify the model at $T_{SI} \leq -25$°C, RH_{EI} should be less than 10%RH. These conditions were not obtained in the experiments due to high humidity level in the lab.

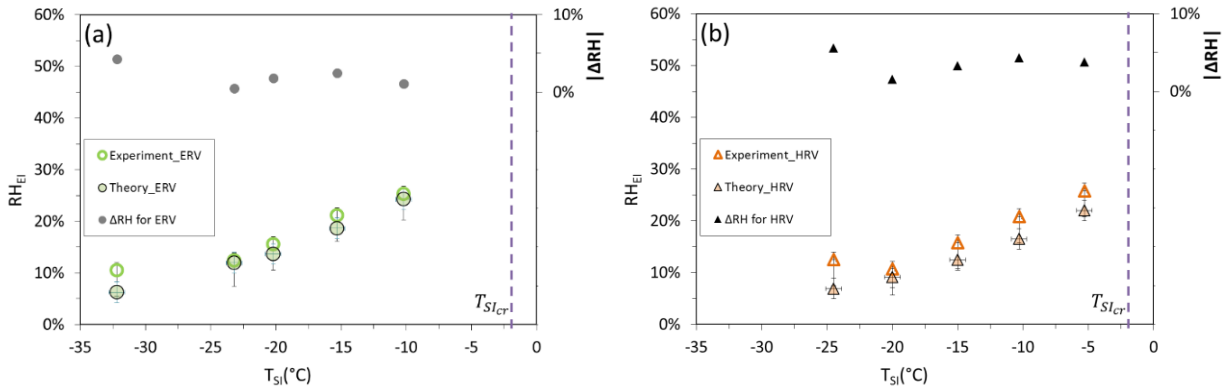

Figure 4.7. Experimental and theoretical frosting limits for the (a) energy exchanger and (b) heat exchanger.

All the theoretical results slightly over predict the frosting limits compared to the experiments. Theoretical model assumes frost emerging once the frosting conditions are met. However, the amount of the frost is too small to be detected by the pressure or visualization methods when the operating conditions are close to the limits, especially for the low RH of exhaust air (the points closer to the left axis in Figure 4.7 (a) and (b)). As a result, the theoretical model is more sensitive

compared to the experimental tests to detect frosting limits. The researchers or engineers have to be aware of over predicting when they employ the frosting limit model to evaluate or design an exchanger.

Comparison between heat exchanger and energy exchanger shows that the energy exchanger has a lower risk of frosting as expected. A bigger gap between heat and energy exchangers frosting limits is observed at a higher RH_{ei}. It results from the significant effect of moisture transfer in energy exchanger on frosting. Therefore, any parameter that affects the moisture transfer such as membrane permeability, membrane thickness, exchanger design and operation conditions, may play an important role in the frosting limit.

Considering the results in Figure 4.7 (a) and (b), these specific exchangers still have frost problem inside the exhaust channels in the general recommended comfort zone of indoor relative humidity (30%RH-60%RH) (ASHRAE 2009) and at any $T_{SI} < -2.3℃$ when the exchanger is running at nominal air flow rate. However, it should be noted that in most cold climate regions the actual indoor relative humidity is usually much lower than the recommended level which somehow results in lower risk of frosting in exchangers. (Kumaran & Sanders 2008; Alonso et al. 2015) (Kumaran & Sanders 2008)

4.7 PARAMETRIC ANALYSIS

A parametric study is conducted to identify important factors for the frosting limit. In this regard, a two-steps process is adopted; the effects of NTU_h and NTU_m on the frosting limit, and the effects of design parameters on NTU_h and NTU_m. The results in the parametric analysis are presented for the energy exchanger. The analysis for heat exchanger can refer to the parameters only related to heat transfer.

4.7.1 Effect of NTU on the frosting limit

The effects of NTU_h and NTU_m on the frosting limit of the cross-flow energy exchanger are shown in Figure 4.8 and Figure 4.10. In both figures, the region on the left hand side of critical outdoor temperature ($T_{SI_{cr}}$) represents that the plate/membrane surface temperature at the most likely frosting position is below freezing point. The condensation occurs in the upper area of the condensation limit ($RH_{EI_{cr}}$). Consequently, the upper-left overlapping area shows the operating

conditions with frosting according to the theoretical model. The lower-right boundary of this overlapping area is then the frosting limit. In Figure 4.8 and Figure 4.10, the solid lines represent the base case presented in Table 4.2. Rest of the lines are developed through changing NTU_h (in Figure 4.8) and NTU_m (Figure 4.10).

In Figure 4.8 the frosting limit change considerably when NTU_h varies from 1 to 5.The changing rate is not proportional with NTU_h. Increasing NTU_h can only slightly affect the frosting limit after the NTU_h value reaches 3. Decreasing NTU_h could narrow-down the frosting region in the map; however, this measure will in turn reduce the effectiveness (Figure 4.9) and energy recovery rate in practice. The final counteracted consequence is difficult to estimate only from this research. The design parameters that could affect NTU_h will be investigated in the next part of parametric analysis.

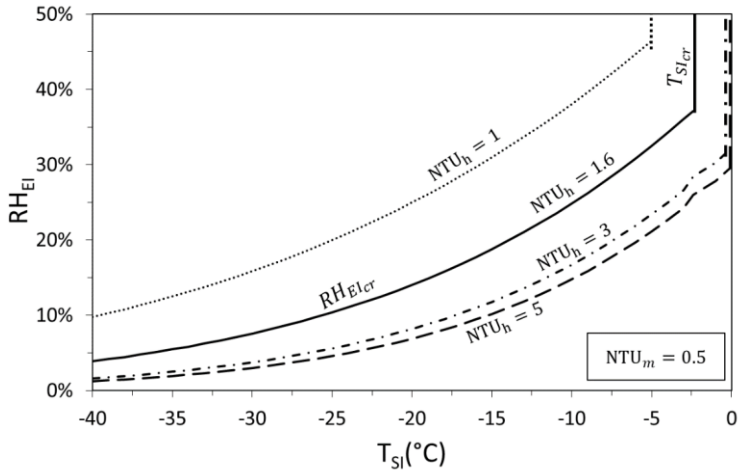

Figure 4.8. Effect of NTU_h on frosting limit of the energy exchanger. Upper-left area represents the frost zone.

Figure 4.10 indicates that if the NTU_m is raised from 0.5 to 3 while NTU_h stays constant (1.6), the frosting region will be greatly reduced, especially at higher NTU_m. The significantly increased latent effectiveness could be the reason for the greatly reduced frosting region. Figure 4.9 which is developed from Equation (4-13) shows that at lower NTU the variation rate of effectiveness is higher. The triangular points in the figure represent the sensible and latent effectiveness of the energy exchanger used in this research.

The frost will be completely avoided for typical indoor air moisture levels ($RH_{EI} < 40\%RH$) when the NTU_m reaches to 3. The results agree with previous findings that the energy exchangers with higher latent effectiveness undergo less frost in cold regions.

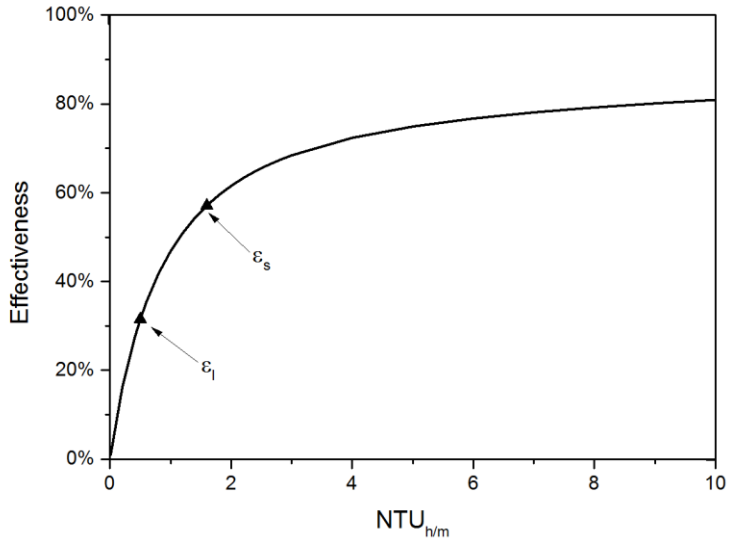

Figure 4.9. Effectiveness VS NTU for both sensible and latent heat.

One of the manners to raise NTU_m without changing NTU_h is to reduce the moisture transfer resistance of the membrane. The membrane moisture diffusion and convection resistance will be discussed in the following analysis.

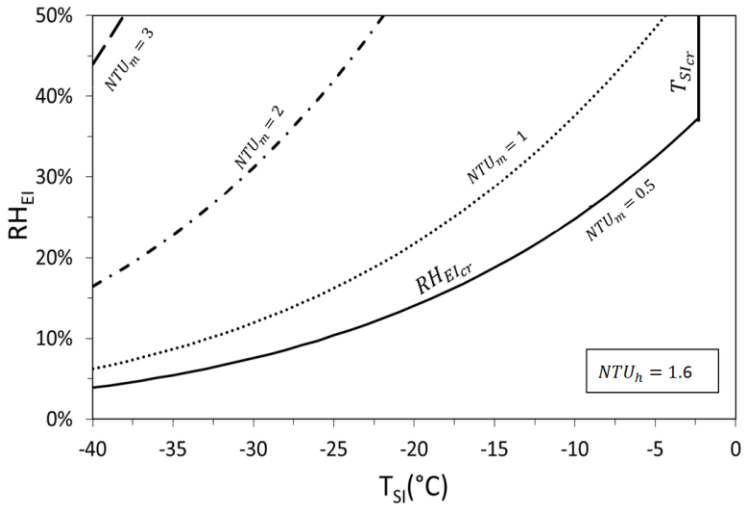

Figure 4.10. Effect of NTU_m on frosting limit of the energy exchanger. Upper-left area represents the frosting zone.

The developed frosting limit model can also be used to guide the design of heat/energy exchangers to avoid frosting. In the model, the specific combinations of sensible and latent NTU can be applied to predict if the exchanger is under frosting condition for the known operating condition. The process of computing the combinations is similar to determine frosting limits by changing variables and knowns. The sensible and latent effectiveness is only the function of NTU_s and NTU_l respectively as shown in Figure 4.9 for mass balanced air-to-air flat plat heat/energy exchangers. The minimum ε_l required to prevent frosting at different values of ε_s and T_{SI} are shown in Figure 4.11 when the indoor RH is a constant (30%RH). The more widely used and straightforward combinations of sensible and latent effectiveness which can theoretically ensure frost free design are given in Figure 4.11. It can be seen that an exchanger with a higher sensible effectiveness requires a higher latent effectiveness to prevent frosting. The required lowest latent effectiveness is slightly lower than sensible effectiveness to completely prevent frosting under the designated operating conditions.

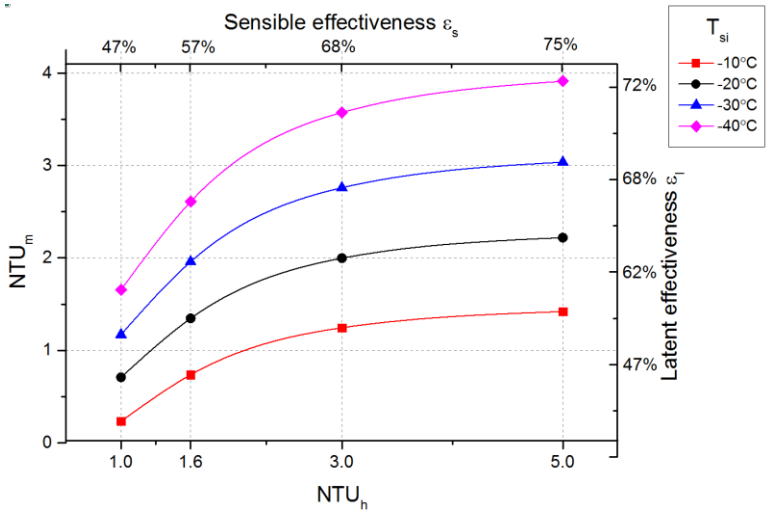

Figure 4.11. Minimum latent effectiveness for frost free energy exchanger versus sensible effectiveness at different T_{SI}

4.7.2 Parametric study on NTU

After understanding the role of NTU_h and NTU_m in frosting limit, a parametric study on the design parameters of exchanger is performed in this section. Among those air channel aspect ratio, air-flow rate, membrane permeability are selected. Each of these parameters is changed by a factor

between 0.25 to 4.00 and the resulting NTU is recorded. Their influence on NTU_h and NTU_m is depicted in Figure 4.12 and Figure 4.13 respectively.

As it can be seen in Figure 4.12 and Figure 4.13, decreasing air-flow rate can significantly increase NTU_h and NTU_m which have counteracting impacts on frosting limit indicated in Figure 4.8 and Figure 4.10. The eventual consequence of changing air-flow rate on frosting limit can be somehow indicated by Figure 4.11 in respect with different NTU_h and NTU_m. For instance, if the air flow is halved in comparison with experiment condition, the NTU_h and NTU_m become 3.3 and 1.0 respectively which can be found in Figure 4.12 and Figure 4.13. The influences of these NTU_h and NTU_m can then be addressed by using Figure 4.11. The aspect ratio greatly affects heat transfer while it has negligible influence on moisture transfer. Higher aspect ratio enlarges the frosting area concluded from Figure 4.10, Figure 4.12 and Figure 4.13. Meanwhile the high aspect ratio also increases the pressure drop through the intensive spacer. On the other side, a lower aspect ratio means a wider supporting aluminum spacer at a fixed channel spacing in which case the elastic membrane tends to deform. The deformation probably cause frosting as well which was found with the experiments (Aarnes 2012). An optimal aspect ratio of aluminum spacer air channels can be determined based on these criteria.

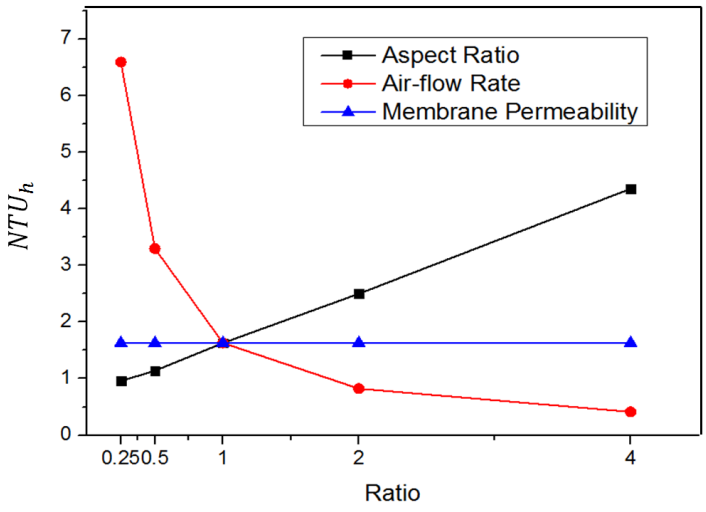

Figure 4.12. Effects of different design parameters on NTU_h. The horizontal axis shows the ratio of the values over base value used in this paper.

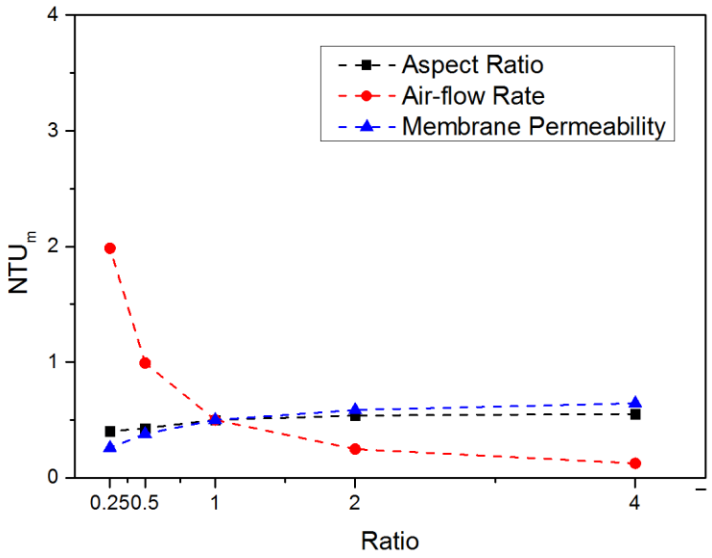

Figure 4.13. Effects of different design parameters on NTU_m. The horizontal axis shows the ratio of the values over base value used in this paper.

The NTU_h is independent on membrane permeability, since the membrane moisture permeability has no effect on heat transfer. The influence of membrane permeability on NTU_m can also be negligible in the tested energy exchanger. The reason is that the diffusion resistance of membrane merely accounts for a small proportion of total moisture transfer resistance and convective resistance dominates in the total moisture transfer resistance. The effective means to improve moisture transfer is to enhance moisture convection in the exchanger.

4.8 SUMMARY AND CONCLUSIONS

A theoretical model is developed to predict frosting limits for cross-flow air-to-air heat /energy exchangers in cold climates. The model involves the exchanger's design parameters and operating conditions which include air flow rate, supply and exhaust inlet temperature and relative humidity. The frosting limits of these two types of exchangers are plotted in a coordinate with supply (outdoor) air temperature versus exhaust (indoor) air relative humidity using the mathematical model. The theoretical limits are validated with experiments and relatively consistent with experimental results. It is found that the energy exchanger is considerably more frost resistant than the heat exchanger. The critical temperature (frosting limit) of the energy exchanger is 5℃ to10℃ lower than the heat exchanger under the same air flow rate Q and exhaust air relative humidity RH_{EI}, which is in agreement with other research.

The parametric analysis of theoretical frosting limit is conducted for the flat plate (membrane) energy exchanger with respect to NTU_h and NTU_m and exchanger design parameters. Changing NTU_h merely affects frosting limit in a narrow range while increasing NTU_m with fixed NTU_h can significantly reduce the frosting zone.

The influence of air-flow rate needs to be further investigated due to the counteracting effects on frosting limit. An optimal air channels aspect ratio can be determined in considering the criterion of frosting.

The combinations of sensible and latent effectivenesses ensuring no frost are theoretically evaluated for the cross-flow flat plate energy exchanger at different supply (outdoor) air temperatures.

The model is applicable to estimate frosting limits of all flat plate air-to-air heat/energy exchangers as long as the physical properties and performance parameters are available. In a more practical level, this model can be used in programing a HRV/ERV control system to activate a frost protection cycle only based on the inlet conditions. However, to get to that level, much more studies and a detailed model validation for different design are recommended.

4.9 ACKNOWLEDGEMENTS

This research was financially supported by the Research Council of Norway through the Norwegian University of Science and Technology, the Research Centre on Zero Emission Buildings (ZEB) and collaboration between the University of Saskatchewan and the Norwegian University of Science and Technology (NTNU). The authors gratefully acknowledge the support from dPoint Technologies Inc. for its in-kind support. The authors also express their gratitude to Mr. David Kadylak and Mr. Ryan Huizing for their tremendous help in preparing the paper and experimental setup preparation.

CHAPTER 5:

FROSTING-DEFROSTING AND REQUIRED DEFROSTING TIME

5.1 OVERVIEW

In this chapter, an experimental approach is taken to monitor the performance of the exchanger under frosting and defrosting cycles. The objectives in this chapter are: to measure frost accumulation and frost removal during frosting and defrosting phases, to investigate the effect of operating conditions on the frost accumulation/removal, and to compare the frost accumulation and frost removal for heat and energy exchangers. In addition, two methods to calculate the required defrosting time are assessed in this chapter; the first method is to use the mass of the exchanger as a reference to determine when defrosting is complete, and the second method is to use the change in moisture content of the air between the inlet and outlet of the exchanger. Although the experiments presented in this chapter are for conditions where gravity has no effect on frost (or water) removal, the methodology introduced can also be used for configurations where the effect of gravity is incorporated into the tests.

As the lead author, Mr. Rafati conducted the experiments, analyzed the data, and wrote the manuscript and incorporated my supervisor’s comments.

Measurement of required defrosting time for air-to-air heat and energy exchangers

Mohammad Rafati Nasr, Carey J. Simonson

5.2 ABSTRACT

Heat and energy recovery ventilators have the potential to significantly reduce the energy consumption for heating, during the cold season, in buildings. However, in regions with very cold climate condition, this equipment become inefficient due to frost formation exactly when the potential to recover energy is the greatest. The current frost protection control strategies that are used in HRV/ERV units are usually not adjusted for the operating conditions. An in-depth experimental investigation is conducted in this paper on two geometrically identical prototype cross-flow air-to-air heat and energy exchangers, to study the effect of operating conditions on frost accumulation, frost removal, and exchanger performance. In each test, the exchangers are tested in two steps: a frosting phase followed by a defrosting phase. Defrosting of the exchangers is simulated by shutting off the supply air, and the frost removal rate and required defrosting time are measured. It was found that the operating conditions (mainly supply air temperature and exhaust inlet air moisture content) have significant effect on the frost accumulation and frost removal rate. The results indicate the frost accumulation rate stays almost constant during the frosting phase in both heat exchangers and energy exchangers for fixed inlet operating conditions, while the heat exchanger has an almost three times higher frost accumulation rate than the energy exchanger. The change in pressure drop across the exchanger follows an exponential trend during these tests. In the defrosting phase, the frost removal rate decreases with time. Also, the required defrosting time for the energy exchanger is found to be much lower than for the heat exchanger. This paper introduces a new method to evaluate exchangers under frosting and defrosting phases and presents an in-depth performance analysis (frosting and defrosting data) of these equipment. The experiments in this paper are for the conditions where gravity has no effect on frost (or water)

removal, however the methodology introduced in this paper can be used for configurations where the effect of gravity is incorporated into the tests.

5.3 INTRODUCTION

In Canadian weather conditions, the potential to recover energy is the greatest in the winter when the difference between the indoor and outdoor air temperatures is large; however, during these very cold conditions, as categorized by (ASHRAE 2007), frost often forms in HRV/ERV units, drastically reducing the heat/energy recovery. Frost formation in HRVs/ERVs decreases the energy recovery by reducing the air flow through the exchanger, increasing the power consumption of fans, decreasing the exchanger effectiveness, and deflecting the exchanger plates. When warm and humid air passes over a cold surface inside the exchanger, the air is cooled, and if the surface temperature is below the dew point temperature of the air, condensation forms on the surface. If the surface temperature is also lower than the freezing point of water, frosting will occur. Frosting is a transient and complex process which depends on the operating conditions, as well the surface properties (Iragorry et al. 2004).

The different methods which are used to protect exchangers from frost can be categorized into two groups: frost prevention, and frost removal or defrosting methods. One common technique to maintain a frost free exchanger is to preheat the supply inlet air. In this method (shown in Figure 5.1), the inlet supply air temperature for the exchanger is always maintained above the frosting limit of the exchanger. In previous studies, the authors have introduced a methodology to find the frosting limit for cross-flow heat and energy exchangers using experiments (Rafati Nasr, Fathieh, et al. 2015; Rafati Nasr & Simonson 2016) and a theoretical model (Liu et al. 2016). The main drawback of the preheating method is that operation of the preheater may be costly, especially if an electrical heater is used. In addition, the amount of heat/energy recovery is reduced by preheating the supply air.

In the second group, a mechanism is designed to remove the accumulated frost. One example is shutting off the supply fan for a period of time, while the exhaust fan is still operating, to help to remove the frost. This method is simple, however there is no heat/energy recovery, and the unbalanced flow during the defrost cycle can depressurize the building. To prevent the depressurizing problem, some units are equipped with a bypass system to bring outdoor air to the

building during defrosting (shown in Figure 5.2). In practice, the amount of defrosting time is usually fixed for a range of supply inlet temperatures or for all operating conditions below the frosting temperature threshold. However, in previous studies (Rafati Nasr & Simonson 2016; Liu et al. 2016), it is found that the indoor air moisture content has a great impact on the frosting limit. Therefore, the defrosting time requirement is believed to be a function of both the supply air temperature and exhaust air moisture content. The authors did not find any work to address the dependency of defrosting time on these parameters. In addition, no method is found in the literature to measure the required defrosting time. It should be mentioned that other operating conditions, such as indoor air temperature, air flow rate, and outdoor air moisture content are of less importance since they stay almost constant for a specific application in the cold season.

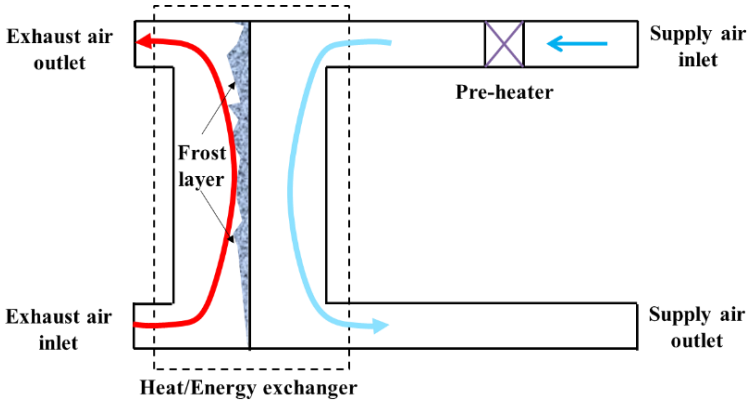

Figure 5.1. Protecting an air-to-air exchanger by preheating the supply air.

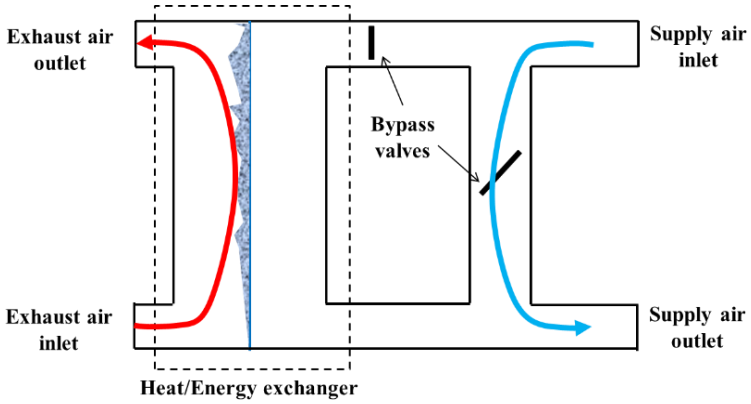

Figure 5.2. Defrosting an air-to-air exchanger by shutting off the supply air.

The main objective of this paper is to experimentally evaluate methods to measure the required defrosting time of one cross-flow heat exchanger and one cross-flow energy exchanger. In this regard, the following sub-objectives are defined in this paper:

- To measure frost accumulation and frost removal during frosting and defrosting phases,
- To investigate the effect of operating conditions on frost accumulation/removal, and
- To compare the frost accumulation and frost removal for a heat and energy exchanger.

5.4 METHODOLOGY

An experimental approach is adopted to achieve the objectives in this paper. A heat exchanger and an energy exchanger are investigated under frosting and defrosting conditions. Performance parameters of the exchanger, such as pressure drop and effectivenesses (ASHRAE 2013) as well as change in mass of the exchanger are monitored during frosting and defrosting.

5.4.1 Test facility

Two cross-flow air-to-air heat and energy exchangers are tested at various operating conditions with frosting, using the test facility shown in Figure 5.3. The exchangers are placed horizontally in an insulated test box which is equipped with sensors to measure air properties before and after the exchanger. Simulated indoor and outdoor air are produced in two environmental chambers located upstream of the exchanger. Air is forced through the air ducts using two fans in each stream; one upstream and one downstream of the test box. To create uniform flow through the exchanger, the air streams enter and leave the test section through expansion and reduction diffusers, which are embedded in the test box. The air temperatures are measured with T-type thermocouples, air relative humidities (RH) are measured with capacitance type RH sensors, air flow rates are measured using orifice plates and pressure transducers, and low pressure transducers are used to measure the pressure drop across the exchangers. In addition to the sensors, an endoscope camera is installed at the exhaust outlet of the exchanger for visual inspection during the tests.

Calibration of instrumentation used to take measurement are conducted before and after the experiments to account for the uncertainty in each measurement. Mass and energy balances for the

experiments are done with reference to (ASHRAE 2013). Details of the sensors specifications, calibration, data acquisition system (DAQ), and mass and energy balance verifications are presented in (Rafati Nasr, Fathieh, et al. 2015). The uncertainties in the measured and calculated parameters are summarized in Table 5.1.

The heat exchanger and the energy exchanger studied are geometrically identical. The separating plates in the heat exchanger are made with a water vapor impermeable polymer film, while the energy exchanger uses a permeable membrane with the same thickness as the impermeable film. Aluminum fins are placed between the plates in both exchangers to enhance mixing and heat and mass transfer and to support the membrane. The physical specifications of the exchangers are presented in Table 5.2.

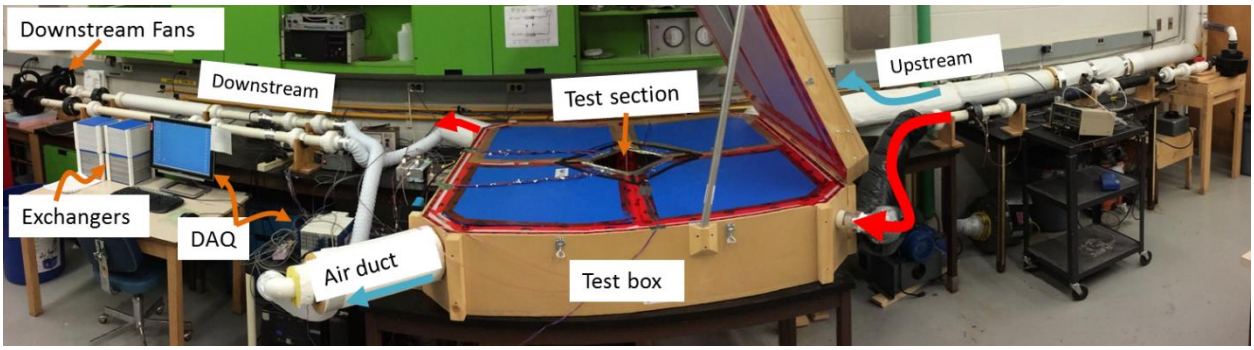

Figure 5.3. Photograph of the test facility used for frosting and defrosting tests.

Table 5.1. Uncertainties in the Measured and Calculated Values.

Parameter	Symbol	U
Temperature (°C)	T	0.2-0.3
Relative humidity Vaisala (%RH)	RH	1.6-2.5
Pressure (general purpose transducer) (Pa)	P	3-6
Pressure (low pressure transducer) (Pa)	P	3
Humidity ratio (%)	w	2-6
Mass flow rate (%)	m	2
Sensible effectiveness (%)	ε_s	2
Latent effectiveness (%)	ε_l	2-6

Table 5.2. Physical Specifications of the Heat and Energy Exchangers.

Parameter	Value	Reference
Number of channels for each flow, n	31	Lab measurement
Half duct height, a	1.52±0.07 mm	Lab measurement
Half duct width, b	3.61±0.07 mm	Lab measurement
Apex angle, α	49°±2°	Lab measurement
Hydrodynamic diameter, D_h	2.63 ±0.16 mm	Lab measurement
Exchanger width X, height H, depth L	165±2 mm	Lab measurement
Membrane thickness, δ	100± 0.02 μm	Lab measurement
Membrane water vapor diffusivity, Dwp	2.0×10-6±3×10-7 m2/s	Lab measurement
Thermal conductivity of membrane, kp	0.44 W/(m.K)	(Zhang 2008)
Thermal conductivity of fin, kf	237 W/(m.K)	(ASHRAE 2009)

In each test, the equipment is run for one to two hours initially with an auxiliary exchanger in the test section, until the desired operating conditions are achieved. Then, the auxiliary exchanger is replaced with the main exchanger and data recording is started. The exchanger stays in these operating conditions for a set time (varies between 1 hr to 3 hrs) and frost accumulates in the exchanger during this phase of the test (the frosting phase). After the frosting phase, the exchanger is defrosted. To defrost the exchanger, the supply air fans are turned off while the exhaust air continues to flow with the same inlet operating conditions as during the frosting phase. During this defrosting phase, the frost is melted and evaporation of the liquid water into the exhaust air makes the exchanger dry. Depending on the operating conditions, the defrosting phase can last as long as 6 hrs.

5.4.2 Measurement of frost mass

It is very useful to measure the frost accumulation (m_f) during the frosting phase, and frost removal rate during the defrosting phase. Ideally, this can be achieved by measuring the moisture content at the inlets and outlets of the exchanger and the assumption of conservation of water vapor (equation (5-1)). However, during long experiments, a small uncertainty in the w measurement eventually leads to a large deviation between the actual m_f (measured with a mass balance, which is described later in this section) and m_f calculated from the humidity measurements.

$$m_f = \text{moisture removed from exhaust air} - \text{moisture transfered to supply}$$
$$m_f = \sum \dot{m}_a(w_{EI} - w_{EO}) - \sum \dot{m}_a(w_{SO} - w_{SI}) \quad (5\text{-}1)$$

Where m_f is mass of frost or condensed water

$\dot{m}_a$ is the mass flow rate of the dry air (the same for the supply and exhaust side)

w is the moisture content

EI, EO,SI, and *SO* indicate: exhaust inlet, exhaust outlet, supply inlet, and supply outlet.

A more accurate method to measure the mass of the frost is to measure the change in the mass of the exchanger during the entire test. In this paper, the mass measurement is done manually several times during a test, by using a high precision mass balance. Before a test, the mass of the exchanger is measured. During the test, the exchanger is removed periodically from the test section to measure the mass. This measurement is done with caution for a duration of almost one minute after which the exchanger is returned to the test section. During this short period, the air flow continues without interruption and the presence of sufficient insulation around the test section prevents any major deviation in the test conditions. To minimize the effect of exchanger displacement, the mass measurement is performed only once per hour.

Once the time for the frosting phase is complete, the mass measurement followed by a defrosting phase is carried out. During the defrosting phase, the same methodology as for the frosting phase is adopted, to measure the mass of the remaining frost/water in the exchanger. Defrosting conditions are maintained until the mass measurement indicates a negligible amount of remaining water (<5 g) in the exchanger.

In real applications, exchanger plates are usually arranged vertically to allow the excess water or melted frost to drain faster during the defrosting phase. This is different than the horizontal orientation in this paper. This change in orientation may have little impact on the frost mass accumulation results, since gravity does not overcome the bounding force between a frost layer and a surface. However, during defrosting, gravity influences removal of the liquid water (melted frost). In this paper, the focus is mainly on evaluating the methods to find the required defrosting time. Therefore, the effect of gravity is eliminated by conducting these experiments with the exchanger plates oriented on a horizontal plane. It is believed that values would be different when the orientation changes, however the method is still valid.

5.4.3 Criteria to measure the defrosting time

Defrosting can be considered complete when all the liquid water or accumulated frost is removed from the exchanger. In practice, making the exchanger fully dry takes a very long time and in many cases it is unnecessary to remove all the condensed water from the exchanger. On the other hand, if the exchanger is exposed to a cold temperature when it contains considerable liquid water, icing will occur in the exchanger, which is more damaging to the exchanger than frosting. Therefore, two different methods are introduced to measure the required defrosting time.

In the first method (called $m_f$criteria), defrosting is considered complete when the mass of the remaining water is less than a limit ($m_{f\ limit}$) where the risk of icing is negligible. No information in the open literature was found to consider mass of frost as an indication to measure required defrosting time. Therefore the value for $m_{f\ limit}$ is defined based on the observation in the experiments for the exchanger used in this paper.

One simple method is to define $m_{f\ limit}$ is by monitoring the Δp during frosting which is increasing gradually. The amount of frost (based on mass of frost) in the exchanger which causes 10% or more increase in pressure is used as a reference. For example if during a frosting experiment, Δp increases by 10% when the mass of frost is 10g, then $m_{f\ limit} = 10\text{g}$. However, under extreme operating conditions with very low temperature and high humidity the condensation rate (and as result the frosting rate) is very high, and the Δp may not show a rapid change. According to the preliminary experiments, defrosting phase can be considered complete when the remaining water in the exchanger is less than 10-15 gr which is equivalent to 2% of the mass of dry exchangers. Criteria (5-2) is defined to find $m_{f\ limit}$. According to this criteria, when the mass of the liquid water in the exchanger is less than 2% of the exchanger mass (≈10 g) or the amount frost causing 10% increase in pressure drop across the exchanger, whichever is less, the defrosting phase is finished.

$$m_{f\ limit} = \min \quad (2\%\ \text{of exchanger mass}, \quad m_f\ \text{causes}\ 10\%\ \text{increase in}\ \Delta p\ ) \qquad (5\text{-}2)$$

For equation (5-2), by measuring Δp and mass of frost (m_f) with time during experiments, a correlation between and Δp and m_f is developed. To calculate the amount of frost for 10% increase in Δp, the value of Δp in the beginning of experiment is used as reference. At the end, $m_{f\ limit}$ for 10% in Δp increase is calculated.

Since measuring the mass of the exchanger during operation is not always practical, in the second approach (called Δw criteria), the difference between the inlet and outlet air moisture content in the exhaust side ($\Delta w = |w_{EI} - w_{EO}|$) is monitored to find the defrosting duration. Theoretically, when the exchanger is dry and there is no supply air flow, $w_{EI} = w_{EO}$, therefore, $\Delta w = 0$. To account for the uncertainty associated with the measured data, defrosting is considered complete when equation (5-3) is satisfied. This equation indicates that defrosting is complete when the difference between w_{EI} and w_{EO} is within the uncertainty.

$$\Delta w \leq U_{\Delta w} \implies \frac{\Delta w}{U_{\Delta w}} \leq 1, \ \ \Delta w = |w_{EI} - w_{EO}| \tag{5-3}$$

5.4.4 Operating conditions

Previous experiments on the same exchangers showed that the chance of frosting is greater when the supply air temperature is low and the indoor air relative humidity is high (Rafati Nasr & Simonson 2016). For this paper, the experiments are designed to cover different supply temperatures and exhaust relative humidities (detailed in Table 5.3) to help understand the frost mass accumulation and frost removal rate as functions of these two parameters. Great care is taken to keep the operating conditions at the set points throughout each test, however due to the transient nature of frosting, some variations in the test conditions are inevitable. To ensure that the results are reliable some of the tests are repeated.

Table 5.3. Test plan (highlighted boxes show test that was carried out under these conditions).

Flow Rate (L/s)	Exhaust inlet relative humidity, RH_{EI} (% RH)	Supply inlet temperature, T_{SI}						
		Heat Exchanger (HX)				Energy Exchanger (EX)		
		-10°C	-15°C	-20°C	-25°C	-15°C	-20°C	-25°C
Q_0 = 20.8	20							
	30							
1.25Q_0	20							

The shaded boxes indicate the experiments performed. The dark shade is for the experiments with $RH_{EI} = 30\%\ RH$ and the light shade is for the $RH_{EI} = 20\%\ RH$ tests.

5.4.5 Parameter definitions

The dimensionless parameters used in this paper are defined in equations (5-4) to (5-6). The frosting time, t_f, refers to actual time from when the frosting test begins until the presence frost is identified. The defrosting time, t_{df}, is the time from when the defrosting phase starts until defrosting is finished, as defined by the criteria presented in Section 5.4.3.

$$\text{Normalized defrosting time } t_{df}^* = \frac{\text{Defrosting time}}{\text{Frosting duration}} = \frac{t_{df}}{t_{f\_final}} \tag{5-4}$$

$$\text{Required defrosting time ratio } DTR = \frac{\text{Defrosting duration}}{\text{Frosting duration}} = \frac{t_{df\_final}}{t_{f\_final}} \tag{5-5}$$

$$\text{Normalized frost (water) mass } m_f^* = \frac{frost\ (water)\ mass}{frost\ mass|_{@t_{df}=0}} = \frac{m_f}{m_f|_{@t_{df}=0}} \tag{5-6}$$

5.5 RESULTS AND DISCUSSION

Prior to the main frosting and defrosting tests presented in this paper, experiments are conducted at standard winter test conditions without frosting (AHRI 2014). The results in Table 5.4 show that both the heat exchanger and energy exchanger have similar sensible effectivenesses. This finding is in agreement with the literature that the material of the plate has a negligible effect on sensible effectiveness (Liu et al. 2016).

Table 5.4. Experimental effectiveness for both heat and energy exchangers at AHRI test conditions (no frosting) (Rafati Nasr, Fathieh, et al. 2015).

Type	T_{EI} (°C)	RH_{EI} (%RH)	T_{SI} (°C)	RH_{SI} (%RH)	$\dot{m}_a$ (g/s)	ε_s%	ε_l%	ε_t%	NTU_s	NTU_m	ΔP (Pa)
HRV	21.3±0.2	47±2	2.2±0.2	44±2	23.5±0.4	58±2	-	-	1.6	-	23±3
ERV	21.3±0.2	46±2	2.2±0.2	44±2	23.5±0.4	57±2	32±4	46±4	1.6	0.5	25±3

Afterwards, experiments at various operating conditions are conducted which include a frosting phase (normal operation) followed by a defrosting phase. During the defrosting phase, there is no air flow in the supply side. The range of operating conditions tested during the frosting and defrosting experiments are shown in Table 5.5. Experiments are initially designed with a frosting phase of three hours at steady inlet conditions, however when the frosting growth rate is high, the duration of the frosting phase is reduced to prevent any serious damage to the exchanger and sensors.

Table 5.5. Operating condition for frosting and defrosting tests.

T_{EI}(°C)	RH_{EI}(%RH)	T_{SI}(°C)	RH_{SI}(%RH)	Q(L/s)
21 to 23	20 to 30	-5 to -25	35 to 45	21 to 26

5.5.1 Frosting

A summary of the average operating conditions for all experiments discussed in this paper is presented in Table 5.6. It can be seen that the test conditions are very close to the test plan presented in Table 5.3. The test names, which are used in the graphs in this paper, represent major factors in the experiment including the type of exchanger (EX for energy exchanger and HX for heat exchanger), supply inlet temperature, and exhaust inlet relative humidity. If the flow rate is different than 20.8 L/s (40 cfm), the last part of the test name also reflects this flow rate, in cfm.

Table 5.6. Summary of the operating conditions for each test.

#	Test name	Exchanger type	Operating condition				
			T_{SI} (°C)	RH_{SI}	T_{EI} (°C)	RH_{EI}	Q (L/s)
1	EX_-25C_20%RH_trial 2	EX	-25.1	39%	22.0	19%	20.8
2	EX_-25C_20%RH	EX	-24.6	39%	22.0	21%	20.8
3	EX_-25C_30%RH	EX	-24.6	38%	22.2	30%	20.8
4	EX_-20C_20%RH_trial 2	EX	-20.1	38%	22.0	20%	20.8
5	EX_-20C_20%RH	EX	-19.8	39%	22.0	20%	20.8
6	EX_-20C_20%RH_50 cfm	EX	-19.9	39%	22.1	21%	26
7	EX_-20C_30%RH	EX	-20.4	39%	22.0	31%	20.8
8	EX_-15C_20%RH	EX	-15.0	48%	22.6	20%	20.8
9	EX_-15C_30%RH	EX	-14.9	45%	22.1	31%	20.8
10	HX_-25C_20%RH	HX	-24.8	40%	22.2	19%	20.8
11	HX_-25C_30%RH	HX	-24.9	36%	22.0	31%	20.8
12	HX_-20C_20%RH_trial 2	HX	-19.9	40%	22.2	21%	20.8
13	HX_-20C_20%RH	HX	-19.8	37%	22.0	20%	20.8
14	HX_-20C_20%RH_50 cfm	HX	-20.0	39%	22.2	21%	26
15	HX_-20C_30%RH	HX	-19.8	40%	22.1	31%	20.8
16	HX_-15C_20%RH	HX	-15.1	44%	21.9	19%	20.8
17	HX_-15C_30%RH	HX	-14.8	41%	22.0	31%	20.8
18	HX_-10C_20%RH	HX	-10.5	45%	22.2	21%	20.8
19	HX_-5C_30%RH	HX	-4.8	56%	22.2	30%	20.8

Before conducting these experiments, the tests at one operating condition for the heat exchanger and energy exchanger are repeated, to determine the repeatability of the measurements. The performance of the exchangers such as effectiveness, pressure drop across the exchanger, and mass of the frost are measured. The effectiveness and pressure drop values are found to be repeatable within their respective uncertainties. Additionally, the measurement of the mass of frost for the repeated experiments, presented in Figure 5.4, shows an agreement between the results. Also, it is found that removing the exchanger from the test box for a short period (1-2 minutes) has negligible effect on the experimental results. For example, in a repeated experiment the exchanger was removed from the test section during the frosting for a minute to measure the frost accumulation rate and was placed back to the test box. Frost accumulation rate in both exchangers changed between 3% to 6% between two experiments. Part of these changes are from minor variations in

the operating conditions in the repeated tests which are unavoidable in practice. These variations are believed as primary reasons for a slight increase in the mass of frost in trial 2, as seen in Figure 5.4.

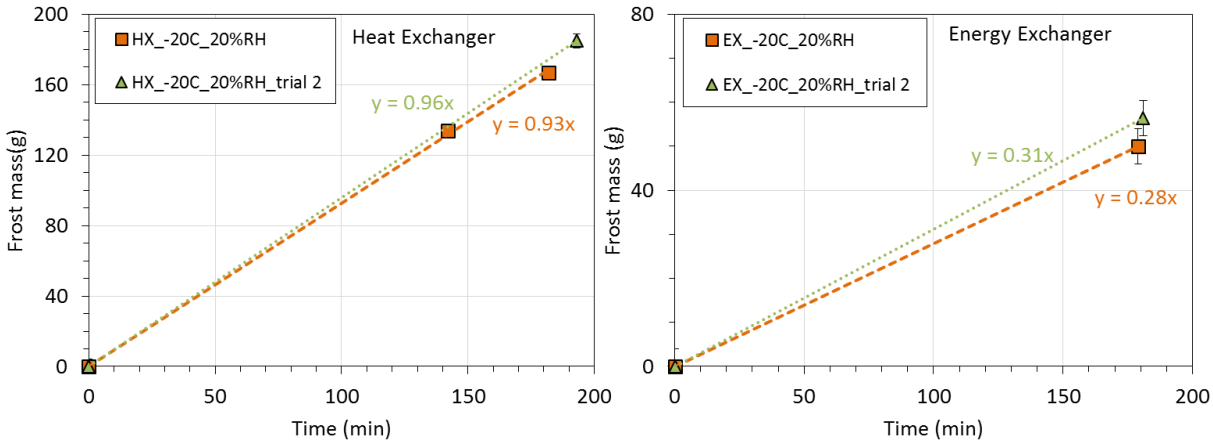

Figure 5.4. Mass of frost in the heat exchanger and energy exchanger as a function of time for repeated tests.

Figure 5.4 shows that the frost accumulation rate in the heat exchanger is almost three times that in the energy exchanger. In addition, the frost accumulation rate appears to be constant during each experiment in this figure. To verify this finding, a comparison is conducted under other operating conditions.

Figure 5.5 compares the mass of frost for the heat exchanger and energy exchanger under different operating conditions. In these tests, the mass of frost is measured multiple times during the frosting phase. The results show that the rate of frost growth is almost constant during each frosting test. With this finding it is concluded that the driving force for frost formation does not change significantly during each test. The important parameters in defining this driving force are; temperature and moisture differences between the two air streams ($\Delta T, \Delta w$), total heat or mass transfer surface area (A), and the overall heat and mass transfer coefficients (U, U_m). There is no clear correlation between the frosting rate and these governing parameters, due to the complexity of the transient frosting process and the two dimensional heat and mass transfer in the cross-flow exchanger. However, it is known that a higher heat transfer rate or smaller mass transfer rate will result in a higher condensation and frosting rate (equation(5-7)). For example, Figure 5.5 shows

that a lower T_{SI} (equal to a larger ΔT) or higher RH_{EI}(equal to a larger Δw) increases the frosting rate.

$$\text{In a heat exchanger:} \quad \dot{m}_f \propto U, A, \Delta T, w_{EI}$$
$$\text{In an energy exchanger:} \quad \dot{m}_f \propto U, \frac{1}{U_m}, A, \Delta T, \Delta w \tag{5-7}$$

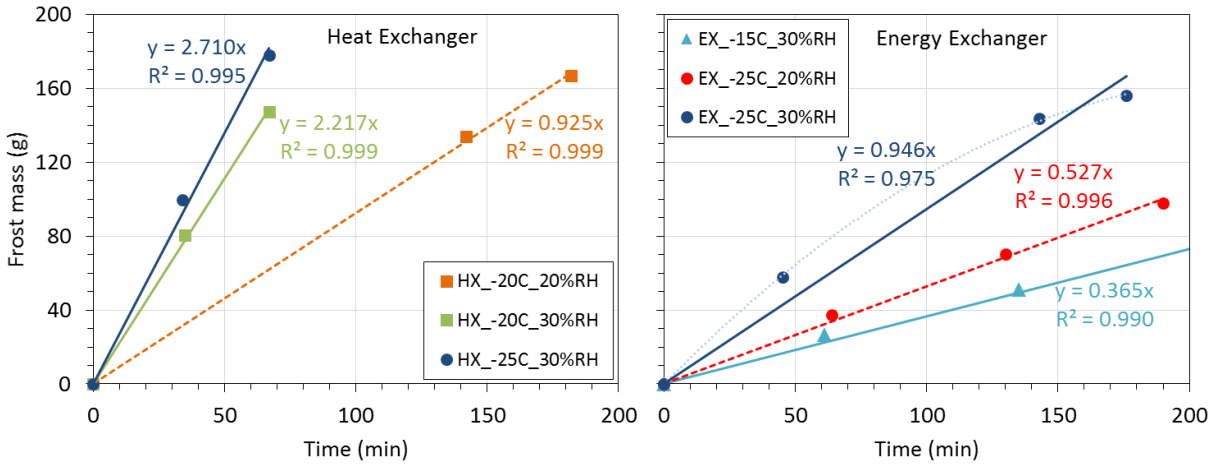

Figure 5.5. Mass of frost in the heat exchanger and energy exchanger as a function of time under different operating conditions.

According to Zhang (Zhang 2008), the Nusselt number (Nu in equation (5-8)) is almost constant in the air channels in the laminar regime in cross-flow exchangers. During frost formation in exchangers, the hydraulic diameter of the channels (D_h) decreases. Therefore, the heat transfer coefficient (h) is expected to increase. k_a in equation (5-8) is thermal conductivity of air. An enhancement in the heat transfer coefficient by the frost layer is accompanied by an increase in the condensation heat release rate and a lower surface area, due to partial blockage of the channels by frost. Therefore, the sensible heat transfer, as well as the frosting rate, remains unchanged. In extreme conditions (operating conditions with lower supply temperatures, greater RH_{EI}, or longer a frosting phase), when most of the channels are blocked, the negative effect of frost on heat transfer dominates, therefore the frosting rate is reduced. A slight deviation from a straight line in Figure 5.5 for EX_-25C_30%RH is explained by this fact.

$$Nu = \frac{hD_h}{k_a} \tag{5-8}$$

In real applications, the air flow rate may change. Thus, the effect of flow rate on the frosting rate is studied. In theory (equations (5-9)and (5-10)), an increase in the air flow rate ($\dot{m}_a$) (in the laminar region) reduces the number of transfer units (NTU) and effectiveness (ε_s) (Liu et al. 2016). However, a higher flow rate, means higher condensation rates. In these equations $\dot{m}_a$represents mass flow rate of dry air and c_p is the specific heat capacity of air.

$$\uparrow \dot{m}_a \Rightarrow\downarrow NTU \Rightarrow\downarrow \varepsilon_s \Rightarrow\downarrow \dot{m}_f \tag{5-9}$$

$$NTU_s = \frac{(UA)_s}{\dot{m}_a c_p} \tag{5-10}$$

Figure 5.6 compares the results for the two tests presented in Figure 5.4 with a third test, at a 25% higher flow rate. It can be seen that the mass accumulation rate increases by about ≈15%. However, part of this 15% increase is due to the slight difference in operating conditions (T and RH are presented in Table 5.6). Therefore, it is concluded that a slight variation in flow rate has a negligible effect on the frosting rate. However, when the flow rate variation is significant, the frost accumulation rate can be large, even for the same operating conditions. This figure again shows that the frost accumulation rate in the heat exchanger is three times that of the energy exchanger.

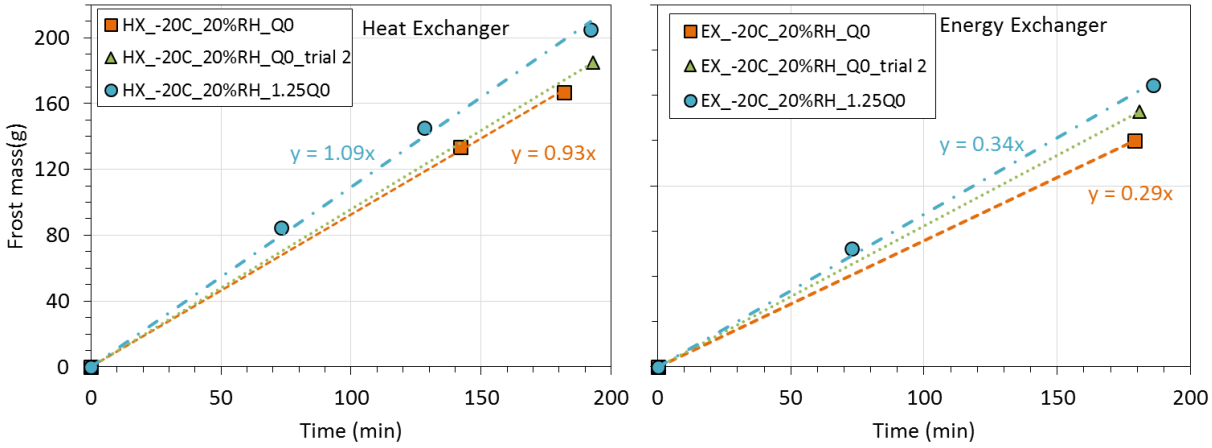

Figure 5.6. Effect of flow rate on frost growth for the heat and energy exchangers.

A summary of the results for the frosting phase of all the experiments is provided in Table 5.7 At first glance, the change in pressure drop does not seem to have any relation with to the operating conditions. The change in Δp, for experiment 2, is shown in Figure 5.7. It can be seen that the

increase in the pressure drop follows an exponential trend. Frost growth narrows down the air flow passage and increases the surface roughness, both of which increase the pressure drop through the exchanger.

Table 5.7. Summary of the results of the frosting tests.

#	Test name	Frosting specification			$m_{f\ limit}$ (for 10% Δp change) (g)	Change during frosting test	
		Duration (min)	mass (g)	growth rate (g/min)		Δp (Pa)	$\Delta\varepsilon_s$ (%)
1	EX_-25C_20%RH_trial 2	157	67	0.43	7	86	-10
2	EX_-25C_20%RH	190	98	0.53	7	185	-13
3	EX_-25C_30%RH	176	156	0.95	11	>364	-30
4	EX_-20C_20%RH_trial 2	181	56	0.31	7	42	-7
5	EX_-20C_20%RH	179	50	0.28	8	32	-6
6	EX_-20C_20%RH_50 cfm	186	62	0.34	8	62	-7
7	EX_-20C_30%RH	182	127	0.70	9	214	-15
8	EX_-15C_20%RH	183	21	0.11	9	9	-3
9	EX_-15C_30%RH	210	74	0.37	11	41	-6
10	HX_-25C_20%RH	189	203	1.07	22	245	-8
11	HX_-25C_30%RH	67	178	2.71	34	101	-9
12	HX_-20C_20%RH_trial 2	193	185	0.96	26	140	-15
13	HX_-20C_20%RH	182	167	0.93	24	103	-14
14	HX_-20C_20%RH_50 cfm	192	205	1.09	30	202	-16
15	HX_-20C_30%RH	67	147	2.22	56	39	-6
16	HX_-15C_20%RH	317	143	0.45	27	57	-9
17	HX_-15C_30%RH	99	158	1.62	49	31	-6
18	HX_-10C_20%RH	199	59	0.30	31	9	-2
19	HX_-5C_30%RH	205	78	0.38	NA	6	-1

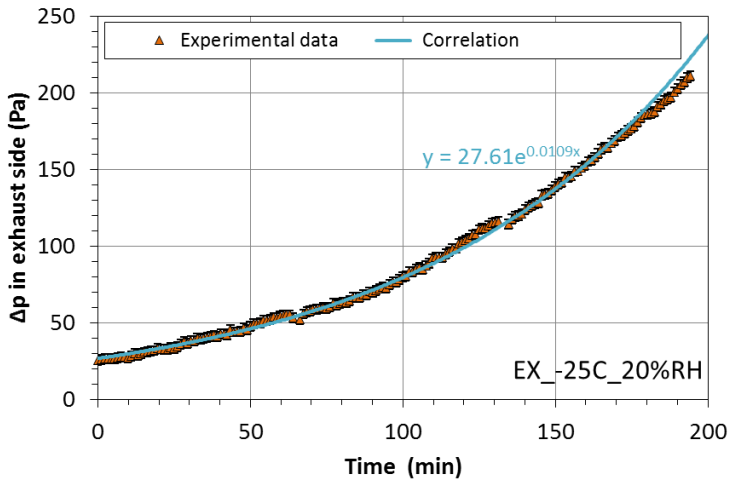

Figure 5.7. The change in the pressure drop across the energy exchanger during one test.

Table 5.7 contains the frost accumulation rate, which is measured with the mass measurement technique, as well as the change in pressure drop (Δp) and the change in sensible effectiveness (ε_s) of the exchanger. In addition, the amount of frost that increases the pressure drop by 10% (equation (5-2)) for each test is presented in Table 5.7. The following items are observed from the results in Table 5.7:

- Increase in RH_{EI} or decrease in T_{SI} will results in increase in mass of frost or frost accumulation rate

- In the heat exchanger, the frosting rate is almost three times higher than in the energy exchanger, under similar operating conditions.

- The reduction in ε_s for the heat exchanger is two to three times higher than the reduction for the energy exchanger, under similar operating conditions and frosting durations.

- The changes in the pressure drop and effectiveness for tests 8, 18 and 19, are negligible, even though the mass of frost is significant. It is believed that a large portion of the measured mass is from condensed water inside the exchangers instead of frost. Under these operating conditions, the change in the performance of the exchangers are anticipated to be insignificant, however longer tests are needed to confirm that.

- Regardless of the operating conditions, nearly 10 g of frost leads to a 10% increase in the pressure drop across the energy exchanger. However, in the heat exchanger, depending on the operating conditions, 22 g to 56 g of frost is accumulated before Δp increases more than 10%. This amount of frost is 2 to 5 times of what is observed in the energy exchanger under any conditions. Rapid condensation in the heat exchanger and possibly the presence of more liquid water in the heat exchanger (which is not affecting the pressure drop) is the main reason for the difference in $m_{f\ limit}$ between the heat exchanger and the energy exchanger.

Based on these observations, there is a need to find the frost growth patterns on the surfaces separating the airflows in the heat exchanger and energy exchanger. This can be done theoretically by conducting 3D modeling of the exchanger or by designing and conducting experiments to monitor the frost inside the exchanger in the future.

With a constant change in the frost thickness and exponential change in Δp, it can be concluded that the pressure drop is a non-linear function of the hydraulic diameter (D_h) of the air channel. To evaluate this finding a simplified theoretical analysis is conducted. From the Darcy-Weisbach equation in fluid mechanics (White 2011), the pressure drop in a circular channel with laminar flow is defined by equations (5-11)and (5-12). Based on the information presented in Table 5.2 and Table 5.5, the flow is in laminar regime in the channels in the exchangers.

$$\Delta p = \frac{8fLQ^2}{\pi^2 D_h^5} \Rightarrow \Delta p = \phi.\frac{fQ^2}{D_h^5} \tag{5-11}$$

$$f = \frac{\phi}{Re} \Rightarrow f = \phi.\frac{D_h}{Q} \tag{5-12}$$

$$\text{(5-11) and (5-12)} \Rightarrow \Delta p = \phi.\frac{Q}{D_h^4} \xrightarrow{Q \text{ is constant}} \Delta p = \frac{\phi}{D_h^4} \Rightarrow \frac{\partial \Delta p}{\partial D_h} \propto D_h^{-5} \tag{5-13}$$

f is the roughness factor of the air channel, Q is the flow rate, D_h is the hydrodynamic diameter of the air channel, L is the length of the channel, Re is the Reynolds number and ϕ represents any constant value. Equation (5-12) is developed with the assumption of a constant flow rate. For the exchangers studied in this paper, the air channels are triangular, however by using the equivalent hydraulic diameter, similar result to (5-13) is achieved. Based on this equation, even when the frost

thickness is changing at a constant rate, Δp increases with D_h to the power of five, which indicates that the pressure drop is going to have a fifth order trend as, the correlation shows in Figure 5.7. It was found that Δp follows a power trend as well in all frosting tests, but it is not possible to confirm by visual inspection that D_h is changing linearly with time. Indeed, Shang (Shang et al. 2005), when studying experimental frosting in an energy wheel, found that the frost thickness is not uniformly distributed along the flow channel.

To evaluate the effects of the operating conditions on Δp, a summary of the predicted trends and their standard error of estimate (SEE), for all experiments, is provide in Table 5.8. It was found that exponential functions to correlate the change in pressure drop with time are more applicable. The presence of two variables in the exponential equations make it easier to relate these factors to the operating conditions. It is seen that factor "a" in this table represents the pressure drop in the early experiment (with no frost), while factor "b" is proportional to the rate of change in Δp during the frosting phase. Therefore, by comparing the "b" factor for different experiments, it can be understood that a higher air moisture content or lower air temperature results in a faster change in pressure drop (greater "b").

In experiments 6 and 14, in which the air flow rate is 25% higher than the others, factor "a" increases proportionally by about 25%. These results are in agreement with equation (5-13) which shows a linear relation between flow rate and pressure drop. On the other hand, factor "b" changes much less (~7%). Therefore, air flow rate has an insignificant effect on the rate of change in Δp for a small variation in flow rate. However, when flow rate variation is significant, rate of change in Δp can be large. In practice, HRV/ERV units are designed for a specific range of flow rates which can be used as a reference for experiments in the lab.

Table 5.8. Summary of the frosting experiments and pressure change during frosting phase.

#	Test name	$\Delta p = a.e^{b\,t_f}$ (Pa)		
		a	b	SEE
1	EX_-25C_20%RH_trial 2	26.03	0.0097	1.445
2	EX_-25C_20%RH	28.08	0.0105	2.544
3	EX_-25C_30%RH	26.31	0.0234	2.913
4	EX_-20C_20%RH_trial 2	25.77	0.0054	0.933
5	EX_-20C_20%RH	25.56	0.0047	0.897
6	EX_-20C_20%RH_50 cfm	32.58	0.0058	1.404
7	EX_-20C_30%RH	26.00	0.0139	1.121
8	EX_-15C_20%RH	25.50	0.0017	0.720
9	EX_-15C_30%RH	26.42	0.0044	1.151
10	HX_-25C_20%RH	22.83	0.0136	0.877
11	HX_-25C_30%RH	17.49	0.0293	1.657
12	HX_-20C_20%RH_trial 2	19.88	0.0110	0.344
13	HX_-20C_20%RH	18.96	0.0106	0.446
14	HX_-20C_30%RH_50 cfm	25.52	0.0118	0.632
15	HX_-20C_30%RH	18.03	0.0177	1.105
16	HX_-15C_20%RH	19.15	0.0046	0.146
17	HX_-15C_30%RH	18.00	0.0107	1.816
18	HX_-10C_20%RH	20.46	0.0021	0.775
19	HX_-5C_30%RH	23.42	0.0009	0.112

5.5.2 Defrosting

During each test, the exchangers enter the defrosting phase right after the frosting phase is complete. In this phase, the exhaust inlet operating conditions remain constant while the supply air fans are turned off.

To check the repeatability of the tests during the defrosting phase, the same operating conditions are used for experiments 4 and 5 with the energy exchanger, and 12 and 13 with the heat exchanger (from Table 5.6). Results from the measurements of the mass of frost in the exchangers are shown in Figure 5.8. It is shown that the measurements for repeated tests are almost the same for each exchanger. It other words the results shows repeatability of the tests. Another important observation from Figure 5.8 is that the mass asymptotically approaches zero as time increases. This means the frost removal rate decreases with time in the defrosting phase. This trend can be approximated by an exponential function.

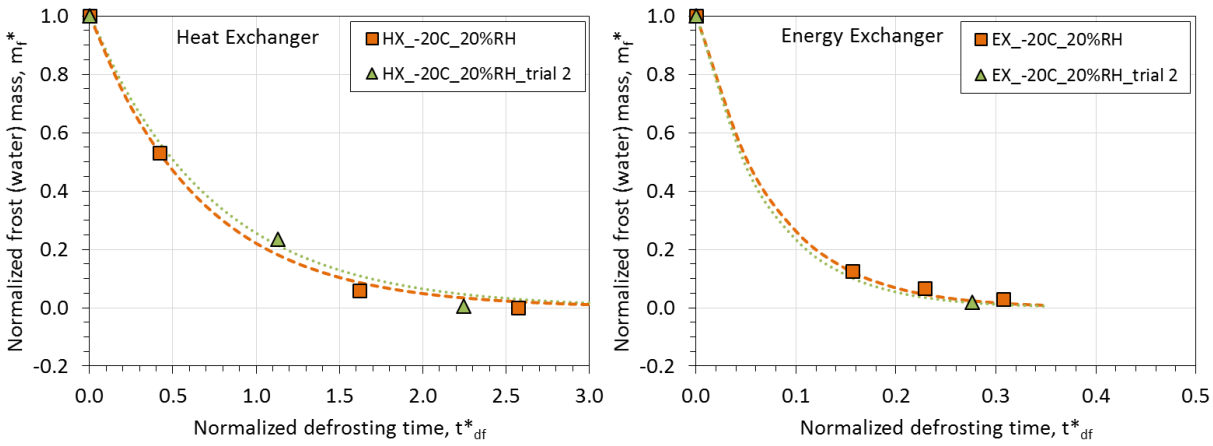

Figure 5.8. Mass of frost with time for the heat and energy exchangers for repeated experiments.

To investigate the effect of operating conditions on defrosting, a parametric study is conducted for different operating conditions, which is shown in Figure 5.9. In this figure, the mass of the frost follows an asymptotic trend for all operating conditions, which means that the frost removal rate decreases with time. This trend is different than what is observed in the frosting phase, where the mass increases linearly with time. To explain this asymptotic trend, the frost accumulation pattern and governing parameters in water removal should be considered. As it was found previously, frost growth is not uniform in a cross-flow exchanger (Rafati Nasr, Fathieh, et al. 2015). In some areas of the exchanger, the frost is thicker than in other areas. Therefore, when the exchanger enters the defrosting phase, the melted frost is not distributed evenly on the plates. Equation (5-14) shows the mass transfer from a wet channel surface to air flowing through the channel. During the defrosting phase, the surface with a smaller amount of frost dries faster, therefore the wet surface area (A in equation (5-14)) reduces with time and thus the frost removal rate decreases with time. Therefore, more surface coverage by frost during the frosting phase increases the frost removal rate.

$$\Delta m_f = h_m \, \rho_a A \, \Delta w_{lm} \tag{5-14}$$

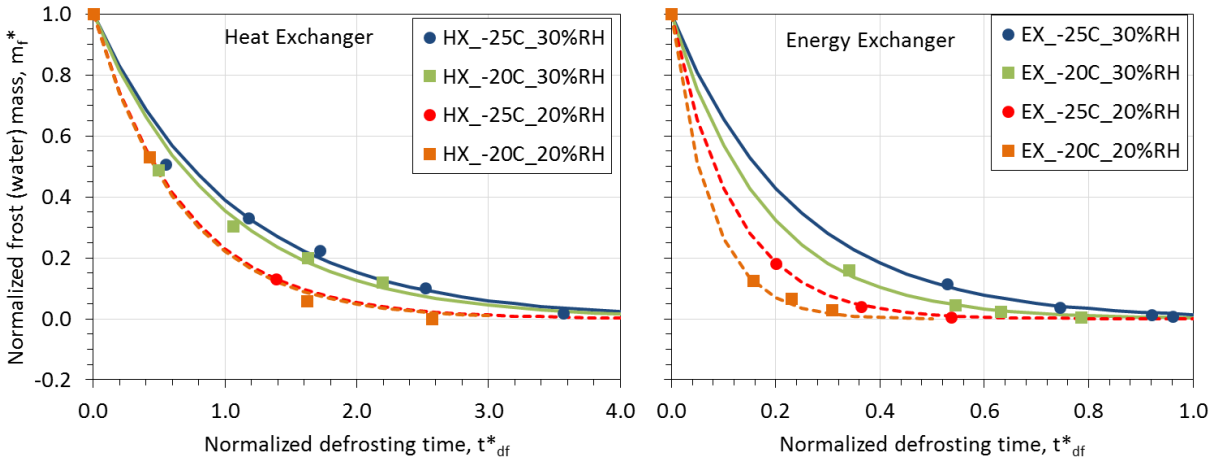

Figure 5.9. Mass of water/frost in the heat and energy exchangers as a function of time during the defrosting phase.

Figure 5.9 indicates that the energy exchanger has a much shorter defrosting time and higher frost removal rate. Due to the complex heat and mass transfer processes in a cross-flow exchanger, it is difficult to find the exact reason for this observation, however analyzing the main differences between heat exchangers and energy exchangers will explain the trend. The trend is mostly due to the vapor permeability of the membrane in energy exchanger. During the defrosting phase, the permeability of the membrane does not have much influence on the evaporation rate since there is no air flow on the supply side of the exchanger. However, during frosting, moisture transfer through the membrane changes the dew point of the exhaust air stream. As a result, there is a different frosting pattern and accumulation rate in the energy exchanger than the heat exchanger. Based on equation (5-14) and the discussion in the previous paragraph, it is believed that the frost pattern in an energy exchanger is formed in a way that the frost covers more surface area, thus there is more wet surface (A in equation (5-14)) during defrosting. However, in these experiments it is not feasible to visualize inside the exchanger to verify or reject this theory.

Another finding in Figure 5.9 is that frost removal trends in the heat exchanger are similar for similar values of RH_{EI}, independent of T_{SI}. Exhaust air at 30% RH has a lower frost removal rate compared to air at 20% RH. This means that the potential to evaporate accumulated frost (water) is mainly affected by RH_{EI}. Therefore, it can be concluded that the frost removal trend is independent of the amount of frost accumulated in the heat exchanger. For the energy exchanger

there is still some differences between the tests, which could be due to the difference in frost formation surface coverage which was discussed in the two earlier paragraph.

Visual observation of the outlet of the exchangers, during the frosting and defrosting phases, indicates that the melting process happens at much higher rate than the evaporation of water. In Figure 5.10, the exhaust outlet face of the heat exchanger is shown during the frosting and defrosting phases for one experiment. The figure shows that 25 minutes into the defrosting phase, all of the visible frost had turned into liquid water. However, the liquid water was still observed after 270 minutes from the activation of the defrosting phase. Therefore, an effective method to drain the condensed water out of the core would reduce the required defrost time considerably. In some experiments the visible frost is in liquid form less than 10 minutes into the defrosting phase, however the visual inspection at the early stages of defrosting was not conducted for all of the experiments presented in this paper.

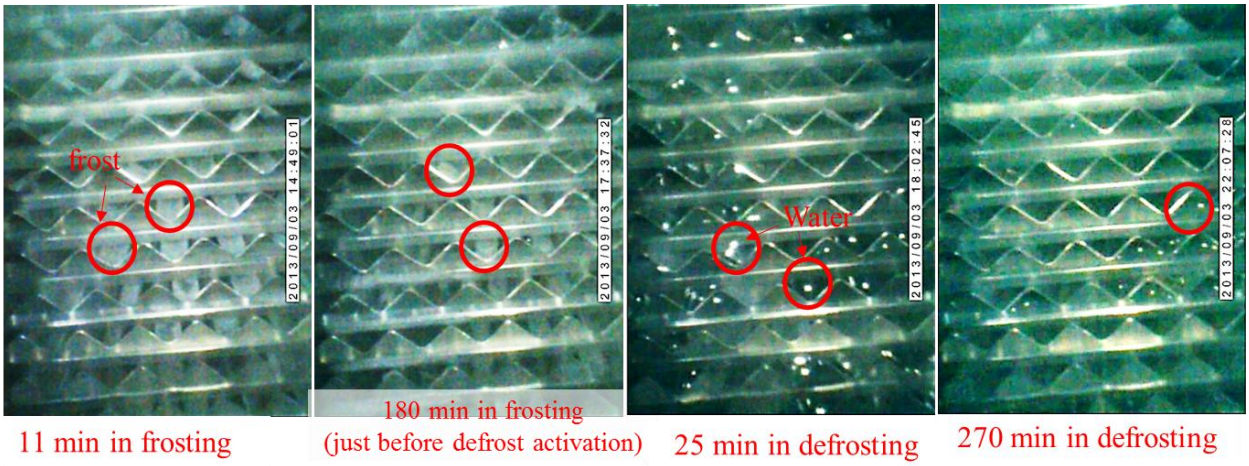

Figure 5.10. Photographs from the heat exchanger exhaust outlet for the test with $T_{SI} = -16^{\circ}C$ and $RH_{EI} = 34\%RH$.

The effect of the air flow rate on the frost removal rate during defrosting is presented in Figure 5.11. It can be seen that the mass of frost for the experiment with a greater flow rate follows the same trend as the tests at a lower flow rate. This is because the mass transfer coefficient (h_m) in equation (5-14) is nearly constant with flow rate in the laminar regime. It can be concluded that the required defrosting time is independent of flow rate for the range of flow rates measured in this paper.

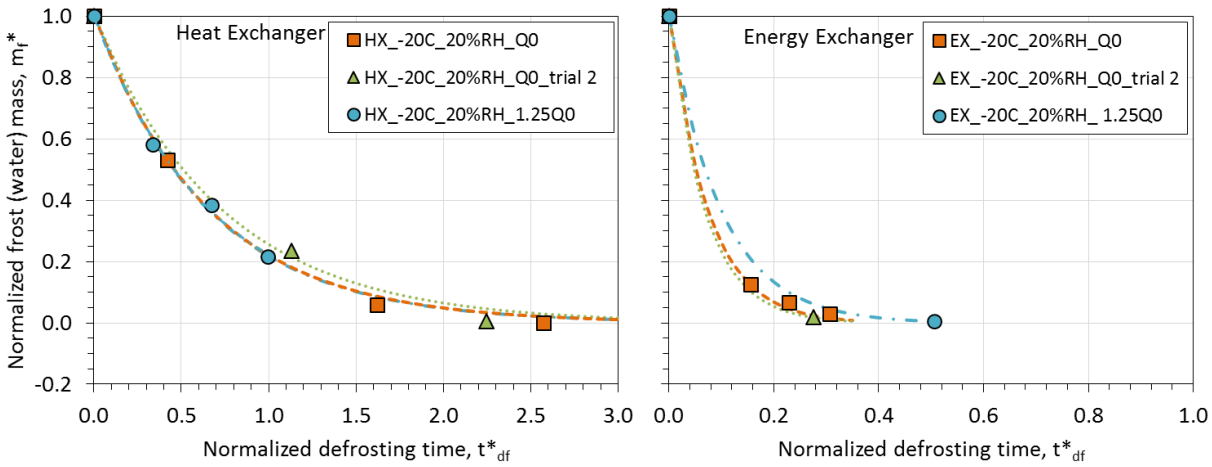

Figure 5.11. Effect of flow rate on defrosting for the heat and energy exchangers.

The change in mass measurement results for different operating conditions are correlated with an exponential curve fit using MATLAB. The factors of the curve fit, with respective standard error of estimate, are presented in Table 5.9. Factor "b" in this table is related to the evaporation rate. It can be seen that the heat exchanger tests with the same RH_{EI} have similar "b" values. In the energy exchanger, there is some variation in this factor. The absolute "b" factor is much greater for the heat exchanger.

Table 5.9. Summary of the experiments during the defrosting phase.

#	Test name	Defrosting equation $m_f^* = a\, e^{bt_{df}^*}$		
		a	b	SEE
1	EX_-25C_20%RH_trial 2	1.0	-11.1	NA
2	EX_-25C_20%RH	1.0	-8.5	0.01
3	EX_-25C_30%RH	1.0	-4.2	0.01
4	EX_-20C_20%RH_trial 2	1.0	-14.6	0.01
5	EX_-20C_20%RH	1.0	-13.4	0.02
6	EX_-20C_20%RH_50 cfm	1.0	-12.1	0.02
7	EX_-20C_30%RH	1.0	-5.7	0.01
8	EX_-15C_20%RH	1.0	-23.4	NA
9	EX_-15C_30%RH	1.0	-7.9	0.01
10	HX_-25C_20%RH	1.0	-1.5	0.00
11	HX_-25C_30%RH	1.0	-0.9	0.02
12	HX_-20C_20%RH_trial 2	1.0	-1.4	0.04
13	HX_-20C_20%RH	1.0	-1.5	0.02
14	HX_-20C_20%RH_50 cfm	1.0	-1.5	0.02
15	HX_-20C_30%RH	1.0	-1.1	0.05
16	HX_-15C_20%RH	NA	NA	NA
17	HX_-15C_30%RH	1.0	-1.1	0.05
18	HX_-10C_20%RH	1.0	-2.7	0.04
19	HX_-5C_30%RH	NA	NA	NA

5.5.2.1 Methods to measure the required defrosting time

In real applications, when an exchanger experiences frosting, a defrosting phase is activated periodically to remove the frost. Usually the duration of the defrosting periods are fixed, however the results of frosting presented earlier in this paper showed that the frosting rate changes with operating conditions. Therefore, it is necessary to measure the exact duration required for the defrosting phase under different operating conditions. In this regard, the dimensionless defrosting time ratio (DTR) which was defined in equation (5-5) is calculated for each operating condition. DTR represents the required defrosting time with respect to the frosting phase operation in the exchanger to remove the frost, based on the two criteria that are explained in section 5.4.2. In the first (m_f) criteria, when the mass of water is less than $m_{f\ limit}$ the defrosting is considered complete. In the second (Δw) criteria, when the difference between the exhaust inlet and the exhaust outlet moisture content ($|w_{EI} - w_{EO}|$) is within the uncertainty bound, the defrosting is

said to be complete. Figure 5.12 shows a comparison between the m_f and Δw criteria in the heat exchanger and energy exchanger using experiment 15 and 7, respectively. In this figure, the horizontal axis is dimensionless time (defined in equation (5-4)), the left axis represents the ratio of the moisture content difference between the inlet and outlet to its uncertainty, and the right axis shows the mass of frost. The time at which the Δw and m_f criteria are satisfied are defined as the DTR and are shown on the graph with the larger markers. Figure 5.12 shows that the defrosting time requirement for the heat exchanger is much longer than the energy exchanger. Also, it is observed that DTR based on the Δw criteria is similar to DTR based on the m_f criteria for these experiments. In the next step, a comprehensive study is conducted to find the effect of operating conditions on DTR.

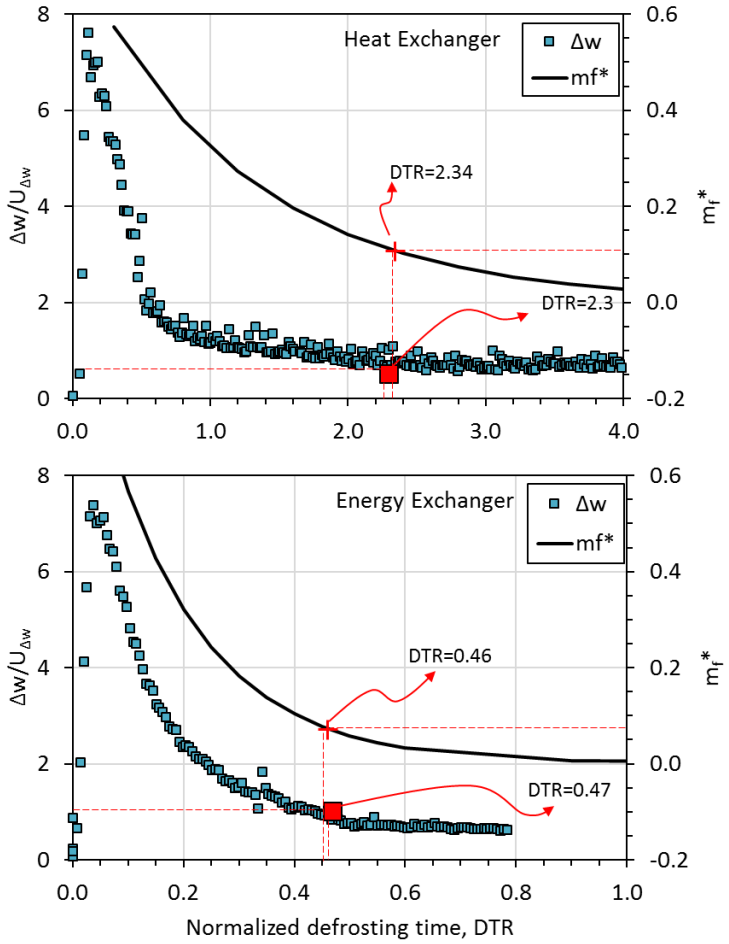

Figure 5.12. Comparison of required defrosting time for test 15 (HX) and test 7 (EX) using two different criteria. Dashed lines show the time when defrosting is complete.

The effect of the operating conditions and the type of exchanger on DTR is summarized in Figure 5.13. In this figure, the results are shown for two values of RH_{EI} and T_{SI} between -10 to -25℃. A very important finding in this figure is that DTR can be very different depending on the operating conditions and exchanger type. In general, a greater value of RH_{EI} or a smaller T_{SI} , results in a greater DTR. In the heat exchanger, there is a relatively large gap between DTR values for the m_f criteria and Δw criteria. The main reason for this difference is in the definition of $m_{f\ limit}$ (see equation (5-2)). Also, relatively high fluctuations in Δw during the tests with the heat exchanger increases the uncertainty in DTR with Δw method.

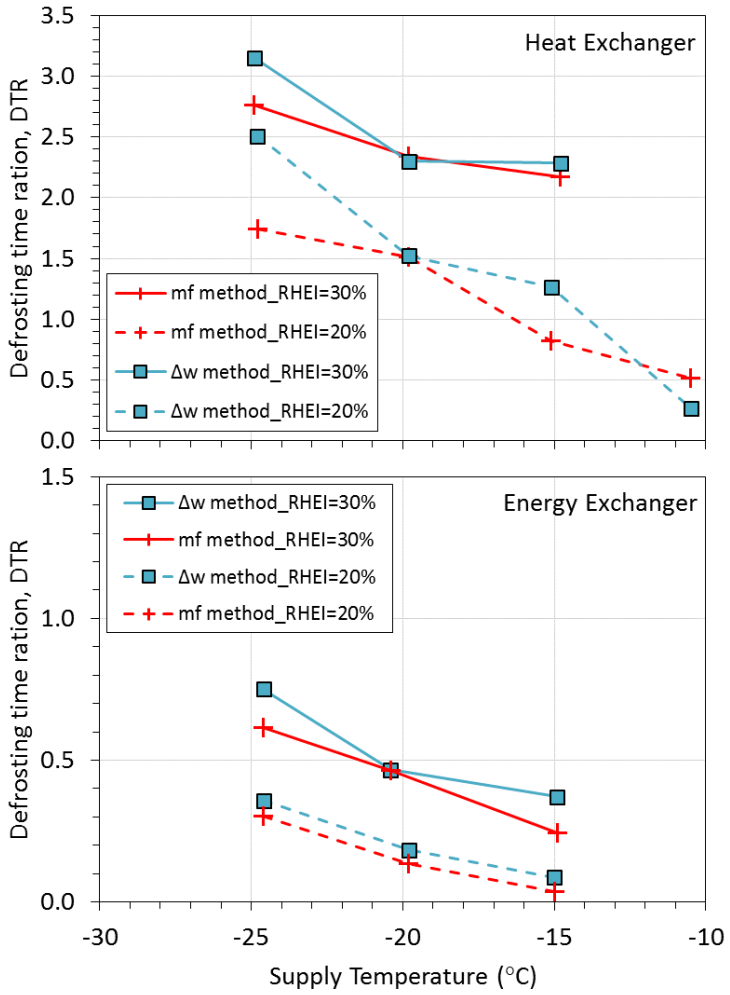

Figure 5.13. Required defrosting time ratio calculated from water mass measurement (m_f) and moisture content change (Δw) methods.

The results show that DTR>1 in the heat exchanger under some conditions. This means that the required defrosting time is longer than the frosting phase. However, as it was mentioned in the methodology section, the membranes in the exchangers in this paper are oriented horizontally. In real applications, if the exchangers are placed in a vertical direction to allow the water to drain from the exchanger by gravity, then lower DTR values are expected. However, gravity cannot remove all the water and the exchanger should be dried enough before it goes back to normal operation (frosting phase). With some modifications in the orientation of the test section, the methodologies introduced in this paper can be used to find the defrosting time for exchangers with membranes oriented vertically but that is out of the scope of this paper.

5.5.3 Summary and Conclusion

An in-depth experimental investigation is conducted in this paper on two cross-flow air-to-air heat and energy exchangers to study the effect of operating conditions on frost accumulation, frost removal, and exchanger performance. In each experiment, the exchangers are tested in frosting and defrosting phases. Measurement of the mass of the exchanger is used as the primary method to measure the amount of frost or condensed water in the exchanger. It was found that the operating conditions (mainly supply air temperature and exhaust air relative humidity) have significant effect on the frost accumulation and frost removal rates. Moreover, the heat exchanger has an almost three times higher frost accumulation rate than the energy exchanger, and the required defrosting duration for the energy exchanger is found to be much lower than for the heat exchanger.

The results indicate that the frost accumulation rate is almost constant at constant inlet conditions, while the frost removal rate changes with time during the defrosting phase. Therefore, DTR may not be the same if the duration of the frosting phase changes considerably. In real applications, there are some specific design factors according to which DTR can be measured. For example, many exchanger manufacturers define a specific defrosting cycle (e.g. $t_f = 1hr$) when the operating conditions are in the frosting region, or building design may not allow the HRV/ERV units to be deactiviated for more than a certain period. DTR can be measured with the methods described in this paper to satisfy the design or operating requirements.

Two different methods are proposed and evaluated in calculating the required defrosting time for exchangers. These methods lead to similar trends but slightly different values in the time

requirement for defrosting. Measurement of the mass of the exchanger (m_f criteria) can be considered as the most reliable method to calculate the defrosting time requirement, but this methods is a non-continuous and labor-intensive method that may not be possible in all experimental facilities, in which case the Δw method can be used. However, more in depth analysis is needed to verify the feasibility and accuracy of Δw method for commercial HRV/ERV units.

The experiments in this paper are for conditions where gravity has no effect on frost (or water) removal, however the methodology introduced in this paper can be used for configurations where the effect of gravity is incorporated into the tests. The method presented in this paper can be utilized to other types of air-to-air exchangers such counter-flow exchangers or heat/energy wheels.

5.6 ACKNOWLEDGMENT

This research was financially supported by the Natural Sciences and Engineering Research Council of Canada (NSERC) through the Smart Net-Zero Energy Building Strategic Research Network (SNEBRN), ASHRAE through a grant-in-aid to Mr. Rafati Nasr, dPoint Technologies Inc. through in-kind support for a NSERC Engage project, and the University of Saskatchewan. The authors also express their gratitude to Dr. Gaoming Ge, Mr. Farhad Fathieh, Dr. Melanie Fauchoux, Mr. David Kadylak and Mr. Ryan Huizing for their assistance in setting up the experimental facility, conducting experiments and analyzing the results.

CHAPTER 6:

ENERGY IMPACT OF FROSTING

6.1 OVERVIEW

In this chapter, a theoretical approach is introduced to estimate the energy impact of frosting-defrosting on the total energy recovered by the exchangers. A model of a single family house is used as a reference, with fixed indoor conditions, in three different locations with cold winter climates. The weather data for each location is used to calculate the total energy required to heat the ventilation air for the buildings. The frosting limit results from the experiments (Chapter 4) and the defrosting time required based on the operating conditions (from Chapter 5) are used to calculate the net energy recovery by the exchangers.

The manuscript presented in this chapter is published in Applied Energy. It should be mentioned that there are some differences between the frosting limit and defrosting time that are used in this chapter than those presented in Chapters 4 and 5. The main reason for these differences is that this chapter was published as a paper before the papers in Chapter 3, 4, and 5 were finalized. Improvement in the setup during the course of this PhD research resulted in minor changes in the results. For example, the frosting limit used in this chapter is slightly different by relatively 5 C than what was reported in chapter 4. Also, defrosting time values in this chapter have some differences with measured values presented in chapter 5. This chapter mainly shows the importance of including the frosting limit and defrosting time in energy calculations and introduces a methodology on how to address these parameters in energy calculations.

A visiting researcher, Dr. Miklos Kassai, and a post-doctoral fellow, Dr. Gaoming Ge, contributed to this manuscript by writing the non-experimental sections of the paper, proofreading, and providing guidance to clarify the discussions and energy analysis. Dr. Kassai, also contributed in the energy calculations based on the weather data and helped with the experiments. As the lead author, Mr. Rafati conducted the experiments, analyzed the data, developed the energy estimation model, wrote the experimental section of the manuscript, incorporated co-authors comments and addressed the reviewers' comments.

Evaluation of defrosting methods for air-to-air heat/energy exchangers on energy consumption of ventilation

Applied Energy Volume 151, 1 August 2015, Pages 32–40

Mohammad Rafati, Miklos Kassai, Gaoming Ge, Carey J. Simonson

6.2 ABSTRACT

Energy consumption for ventilation is extensive in cold climates. Air-to-air heat/energy recovery is a well-known and effective method to reduce the energy consumption. However, frosting commonly occurs inside heat/energy exchangers in cold climates, which would significantly degrade the performance of the exchangers. Preheating the outdoor air and bypassing the outdoor airflow are two effective methods for frosting prevention or defrosting. In this study, the performance of two cross-flow heat/energy exchangers at frosting and defrosting periods are experimentally tested under different operating conditions and the values of frosting limit and defrosting time ratio are presented. As well, the effects of these two defrosting methods on energy consumption of ventilation in three cold cities (i.e. Saskatoon, Anchorage and Chicago) are evaluated. The results show the outdoor air preheating method performs better than the outdoor air bypassing method. In addition, the heat/energy recovery potential in Saskatoon undergoes the largest reduction under frosting, and the cold weather conditions have less impact on energy exchangers than heat exchangers for heat/energy recovery.

6.3 INTRODUCTION

Outdoor air ventilation is necessary for modern commercial and residential buildings in order to maintain acceptable indoor air quality and provide a healthy indoor environment for occupants. The required energy consumption for conditioning outdoor air is extensive, which accounts for 20-40% of the overall energy consumed by air-conditioning systems in buildings (Zhang & Xiao 2008). The ratio can be even higher in hot and humid climates or cold climates, due to larger difference between outdoor and indoor air conditions. Air-to-air heat/energy recovery is a well-known and effective method to improve energy efficiency of air-conditioning systems because the

heat/energy exchangers can precondition outdoor air through transferring heat (or moisture) between outdoor supply air and indoor exhaust air (Besant & Simonson 2003; Rasouli et al. 2013; Rasouli et al. 2010; Xiao et al. 2011; Abdel-Salam & Simonson 2014). Besant and Simonson (Besant & Simonson 2003) reported that the annual energy consumption can be reduced between 31% to 64% by using an energy wheel and a heat wheel in a Chicago building air-conditioning system. Rasouli et al. (Rasouli et al. 2010) found that a run-around membrane energy exchanger (RAMEE) provided up to 40% annual heating energy saving and up to 20% annual cooling energy saving in an office building, depending on the climate and exchanger effectiveness. Moreover, the air-to-air heat/energy exchangers can significantly downsize the heating/cooling equipment, such as boilers and chillers, in new buildings (Besant & Simonson 2003; Rasouli et al. 2013).

Frosting is a significant challenge for the heat/energy exchangers when they are used in cold climates. Frost may form in the exhaust air side of heat/energy exchangers if the exchanger surface temperature is lower than both the air dew-point and the freezing temperature (Rafati Nasr, Fauchoux, Besant, et al. 2014). The frosting would partially or fully block the air flow channels (Wu et al. 2011), increase the pressure drop (Fisk et al. 1985; Gong et al. 2013), decrease the air flow rate (Fisk et al. 1985), degrade the heat/energy recovery effectiveness (Phillips, Chant, et al. 1989), and decrease the total heat (or moisture) transfer rate (Rafati Nasr, Fauchoux, Besant, et al. 2014; Fisk et al. 1985). If frosting occurs in exchangers for a long period, using the exchangers for energy recovery would be not economical and the frost may damage the exchangers. The frosting formations in heat/energy exchangers strongly depend on some factors, i.e. the outdoor air temperature, exhaust air humidity ratio and the type of exchanger (sensible heat only or energy recovery). Generally, the frosting limit (the operating conditions at which frost first begins in an exchanger) of energy exchangers is 5-10 °C lower than of typical heat exchangers (Rafati Nasr, Fauchoux, Besant, et al. 2014; Gazi & Simonson 2012; Rafati Nasr, Fauchoux, Kadylak, et al. 2014).

In order to maintain high energy recovery effectiveness and minimize the reduction of total recovered energy by heat/energy exchangers, numerous frost protection techniques and defrosting methods for the air-to-air heat/energy exchangers have been proposed and investigated over the past 30 years (Rafati Nasr, Fauchoux, Besant, et al. 2014; Fisk et al. 1985; Phillips, Chant, et al. 1989; Phillips et al. 1992; Airxchange Inc. 2005; Jang et al. 2013). Preheating the outdoor air,

bypassing the outdoor airflow, reducing the supply airflow rate, recirculating warm exhaust air, reducing the effectiveness of the exchanger, etc. are effective methods to protect exchangers against frost or remove frost (defrost) (Rafati Nasr, Fauchoux, Besant, et al. 2014; Phillips, Chant, et al. 1989). Phillips et al. (Phillips et al. 1992) compared different frost protection strategies for counter-flow heat recovery ventilators under different climatic conditions, and found that outdoor air preheating strategy achieved lower heat recovery rate, since preheating reduced the heat available for recovery.

In general, using energy recovery ventilators (ERV), such as energy wheels or membrane-based energy exchangers, instead of heat recovery ventilators (HRV) will reduce risk of frosting in the exchanger core. However, if the temperature of outdoor air goes very low the energy exchangers will experience frosting as well. Most of the open literature focused on the study of frosting limit and changes in effectiveness due to frosting in heat/energy exchangers. However, little has been conducted to investigate the energy performance of exchangers under frosting and defrosting conditions, especially for the energy (both sensible heat and moisture) exchangers. The recovered energy by exchangers and required energy consumption for ventilation strongly depend on the defrosting methods and operating conditions. In this study, the performance of two air-to-air cross-flow heat/energy exchangers at frosting and defrosting periods are experimentally tested under different operating conditions (i.e. different outdoor air temperatures) and the values of frosting limit and defrosting time ratio (DTR) are presented. Moreover, the influences of two simple and widely used defrosting methods, preheating the outdoor supply air and bypassing the supply airflow, for the heat/energy exchangers on energy consumption of ventilation in three cold cities (i.e. Saskatoon, Anchorage and Chicago) are evaluated.

6.4 DEFROSTING METHODS

6.4.1 Preheating the outdoor supply air

A common frost-protection technique for heat/energy exchangers is to preheat the outdoor supply air above the frosting limit before the air enters to the exchangers' cores (Figure 6.1). When the outdoor air temperature goes below the frosting limit, the heating elements are activated. Preheating the cold outdoor air consumes auxiliary energy (i.e. electricity or gas), but the

exchangers' operation is not interrupted by the frost-prevention system. The actual effectiveness of heat/energy exchangers is essentially equal to the nominal effectiveness without frosting.

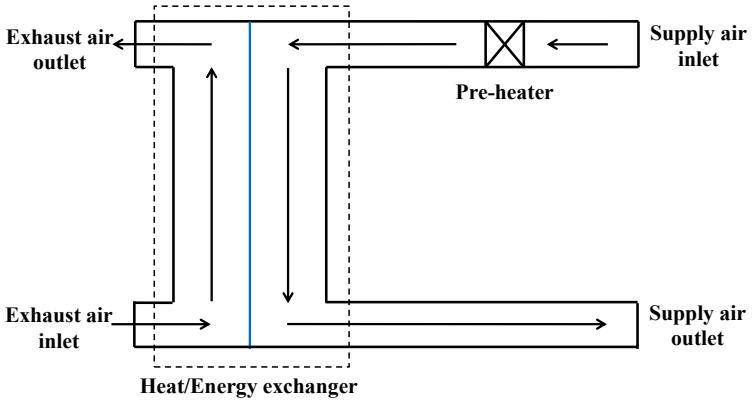

Figure 6.1. The schematic of a heat/energy recovery system with preheating.

6.4.2 Bypassing the outdoor airflow

Another common method to defrost the exchangers is bypassing the outdoor supply air periodically, as shown in Figure 6.2. In general, this is accomplished by fully closing the supply airstream in the exchanger, while the exhaust airstream continues to flow through the exchanger, warms up the core, and melts the accumulated frost or ice. After a period of time, the bypassing is turned off and normal operation of the exchanger (i.e. heat/energy recovery) resumes. During the defrosting period, an auxiliary re-heater (and a humidifier) should be turned on to heat/condition the outdoor air before supplied into a building.

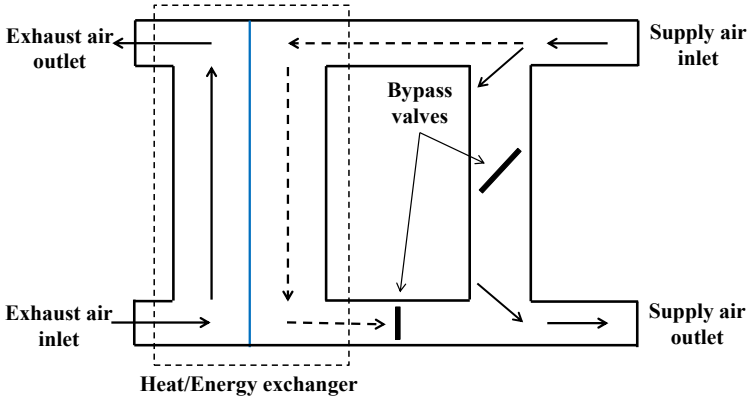

Figure 6.2. The schematic of a heat/energy recovery system with outdoor air bypassing.

6.5 METHODOLOGY

The methodology for calculating the heat/energy consumption for ventilation and recovered energy by heat/energy exchanger is presented in this section. Some important design parameters, such as the air flow rate and supply and exhaust (indoor) air conditions, are listed in Table 6.1 for the energy estimation of ventilation. For the energy performance parameters of the heat/energy exchanger (i.e. the effectiveness and frosting limit), they are measured by experimental tests and will be presented in the Section 6.6

Table 6.1. Design parameters for the energy estimation of ventilation.

Parameter	Flow rate (m^3/hr)	T_{Sup} (°C)	RH_{Sup} (%RH)	T_{EI} (°C)	RH_{EI} (%RH)
Value	75	20	35	22	40

6.5.1 Heat/energy consumption without energy recovery

In the case of no heat/energy recovery in the air-conditioning systems, the required energy consumption for ventilation is maximum, which depends on the ambient air conditions and the desired supply air conditions to indoor.

If only the supply air temperature is of concern for the ventilation air conditioning, the heating requirement is determined by the outdoor supply air inlet (T_{SI}) and the supply air temperature setpoint (T_{Sup}). An area can be plotted based on the ambient temperature duration curve (Kajtár et al. 2012) to represent the auxiliary sensible energy required to condition the air to the comfort level (Figure 6.3). Since this study focuses on the heating energy consumption for ventilation during periods with frosting risk in a year, auxiliary energy is only calculated for the outdoor air temperatures below 0ºC ($T_{SI} \leq 0$℃). The recommended supply air temperature to the indoor (T_{Sup}) is 20˚C in this study. Figure 6.3 shows the weather data of Saskatoon, Canada, and the heating requirement for ventilation as a case study. The heating requirement for ventilation (q_{aux_s}) can be calculated by Equation (6-1).

$$q_{aux\_s} = c_{Pair}\dot{m}_{air}\sum_{i}(T_{Sup} - T_{SI})\Delta t_i \quad (6\text{-}1)$$

Where c_{Pair} is the specific heat capacity of air, $\dot{m}_{air}$ is the air mass flow rate, T_{SI} represents the outdoor air temperature and Δt_i is the time span in the analyzed period which is 1 hr in the study.

In the case of both the supply air temperature and humidity are of concerns for the ventilation air conditioning, the required energy consumption for ventilation is different. It is dependent on the enthalpy difference between the designed supply air (h_{Sup}) and the outdoor air (h_{SI}). In order to compare the energy consumption results in this case with the results for the sensible heating case, energy consumption is only calculated for the period with outdoor air temperature below 0ºC. A graph of enthalpy versus outdoor air temperature from the weather data, as shown in Figure 6.4, is plotted and used to calculate the energy consumption for ventilation air.

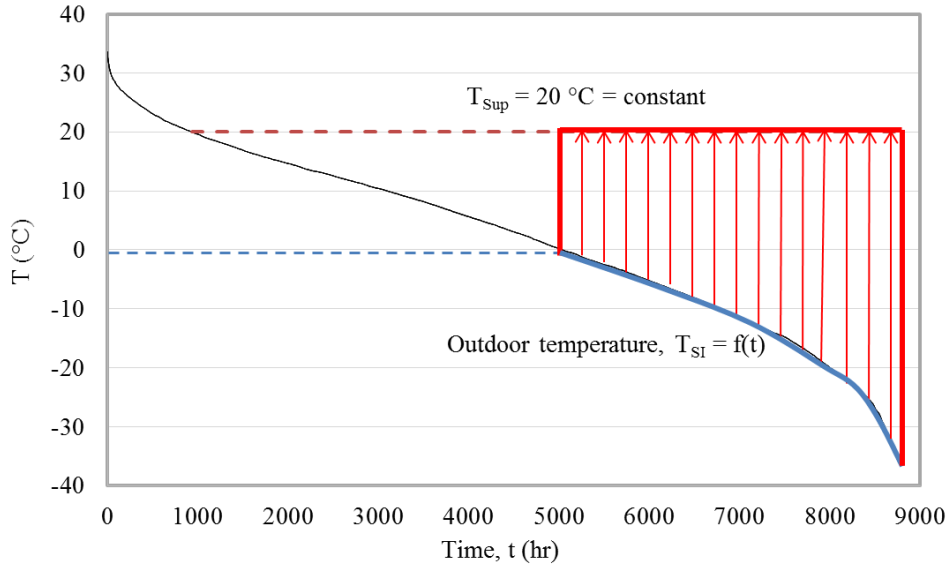

Figure 6.3. The ambient temperature duration curve of Saskatoon and the required heating for ventilation.

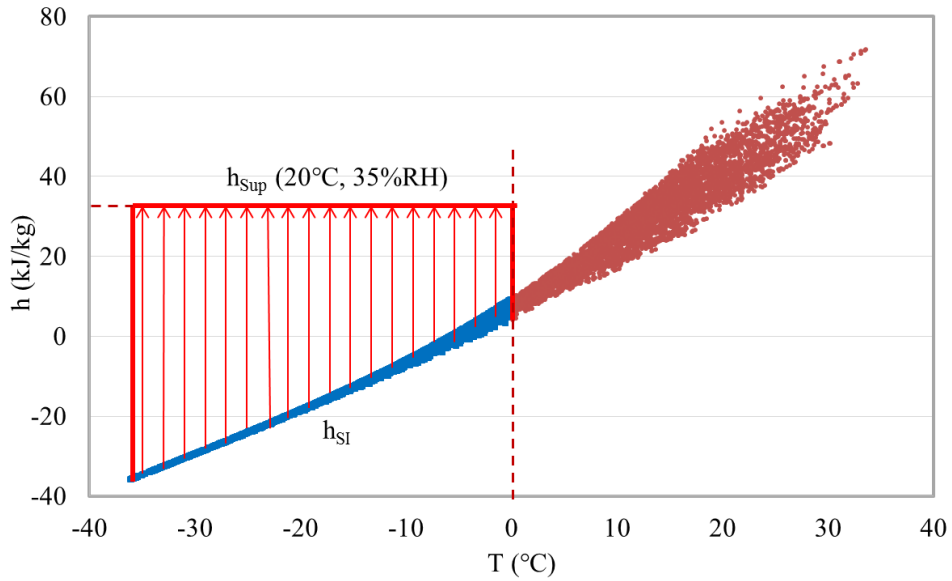

Figure 6.4. The ambient temperature-enthalpy curve of Saskatoon and the required energy for ventilation.

The designed supply air conditions are assumed to be 20°C and 35%RH during the winter. By having outdoor air enthalpy values and desired supply air enthalpy, the required total energy consumption for ventilation (q_{aux_t}) is calculated by Equation (6-2).

$$q_{aux\_t} = \dot{m}_{air} \sum_{i} (h_{sup} - h_{SI}) \Delta t_i \tag{6-2}$$

6.5.2 Heat/energy consumption when ignoring frosting effect

By integrating heat/energy recovery exchangers into the air-conditioning systems, the total required auxiliary heat/energy consumption for conditioning the outdoor air will decrease significantly. The maximum heat/energy recovery rates would be achieved when the heat/energy exchangers do not experience any frosting even at very low outdoor temperature. This condition is not practical, but it gives an estimation of the maximum possible heat/energy to be recovered.

6.5.2.1 Sensible heat recovery

In an ideal case using a constant sensible effectiveness ($\varepsilon_s = 0.62$ in this study) for the heat recovery exchanger, and assuming the exhaust indoor temperature (T_{EI}) to be 22°C (which is

relatively higher than T_{Sup} due to heat gain in the conditioned space), the ventilation air temperature after heat exchanger (T_{SO}) can be calculated with Equation (6-3).

$$T_{SO} = T_{SI} + \varepsilon_s(T_{EI} - T_{SI}) \tag{6-3}$$

The sensible heat recovered by the heat exchanger (Q_{rec_s}) and additional heating requirement of the re-heater (Q_{rh_s}) can be determined through Equations (6-4) and (6-5) based on the ambient temperature duration curve, as shown in Figure 6.5.

$$q_{rec\_s} = c_{Pair}\dot{m}_{air}\sum_i (T_{SO} - T_{SI})\Delta t_i \tag{6-4}$$

$$q_{rh\_s} = q_{aux\_s} - q_{rec\_s} \tag{6-5}$$

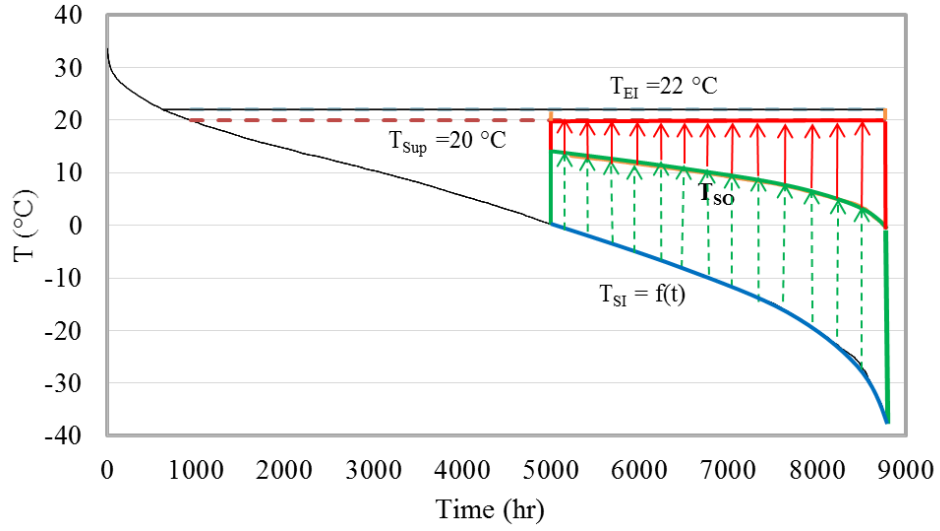

Figure 6.5. The sensible heat recovered by heat exchanger and required heating energy by the re-heater when ignoring frosting effect.

6.5.2.2 Total energy recovery

In the case of both the supply air temperature and humidity are of concerns for the ventilation air conditioning, both a re-heater and a humidifier would be needed to condition the air. When an energy recovery exchanger with constant effectiveness values ($\varepsilon_s = 0.57$ and $\varepsilon_t = 0.47$ in this study) is used in the air conditioning system and assuming a constant indoor (or exhaust) air conditions ($T_{EI} = 22°C$; $RH_{EI} = 40\%RH$), the enthalpy of ventilation air after energy exchanger (h_{SO}) can be calculated:

$$h_{SO} = h_{SI} + \varepsilon_t(h_{EI} - h_{SI}) \tag{6-6}$$

Based on Equations (6-6) and a desired supply air conditions ($T_{Sup} = 20°C; RH_{Sup} = 35\%RH$), the areas that represent the energy recovered by energy exchanger (Q_{rec_t}) and energy consumption by the re-heater and humidifier (Q_{rh_t}) can be plotted on the correlated ambient temperature-enthalpy diagram (Figure 6.6). They can be calculated by Equations (6-7) and (6-8), respectively, when ignoring the frosting effect.

$$q_{rec\_t} = \dot{m}_{air} \sum_i (h_{SO} - h_{SI})\Delta t_i \tag{6-7}$$

$$q_{rh\_t} = \dot{m}_{air} \sum_i (h_{Sup} - h_{SO})\Delta t_i = q_{aux\_t} - q_{rec\_t} \tag{6-8}$$

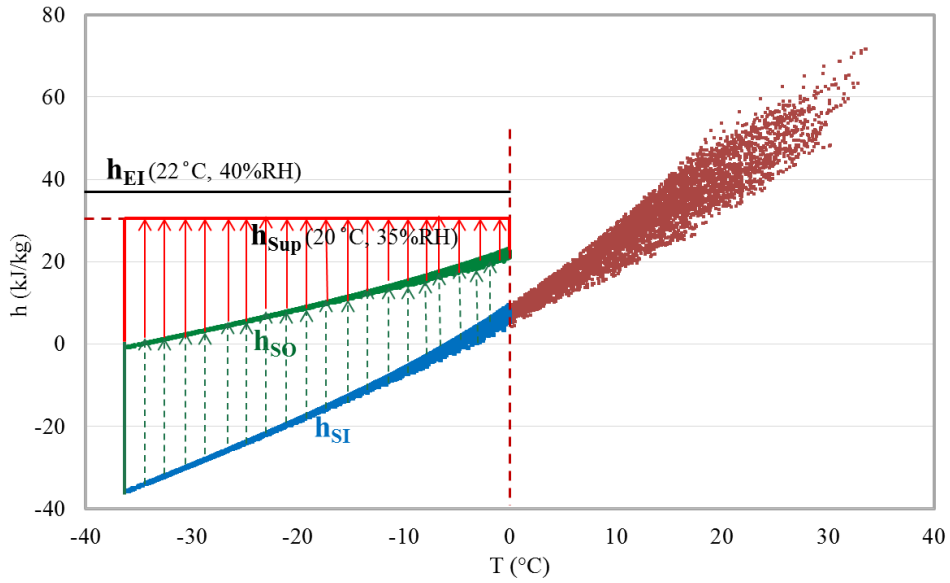

Figure 6.6. The energy recovered by energy exchanger and required energy for ventilation air when ignoring frosting effect.

6.5.3 Heat/energy consumption using pre-heating method

In practical applications, in order to protect the heat/energy recovery exchangers against frosting, a pre-heater can be installed to preheat the outdoor air above the frosting limit (T_{frost}). In this case, the recovery effectiveness of heat/energy exchangers is equal to their nominal effectiveness under

no frosting. In this study, the frosting limit temperature is assumed to be -1 °C for heat exchangers and -6 °C for energy exchangers based on experimental tests.

6.5.3.1 Sensible energy recovery

When the pre-heater is used to heat the outdoor ventilation air above the frosting limit temperature, the supply outlet temperature (T'_{SO}) is calculated through Equation (6-9).

$$T'_{SO} = T_{frost} + \varepsilon_s(T_{EI} - T_{frost}) \tag{6-9}$$

The areas that represent the heat recovered by heat exchanger (q'_{rec_s}) and heating requirement by the preheater and re-heater (q'_{aux_s}) are shown in Figure 6.7. They are calculated by Equations (6-10) and (6-11).

$$q'_{rec\_s} = c_{Pair}\dot{m}_{air}\sum_i (T'_{SO} - T_{frost})\Delta t_i \tag{6-10}$$

$$q'_{aux\_s} = q_{aux\_s} - q'_{rec\_s} \tag{6-11}$$

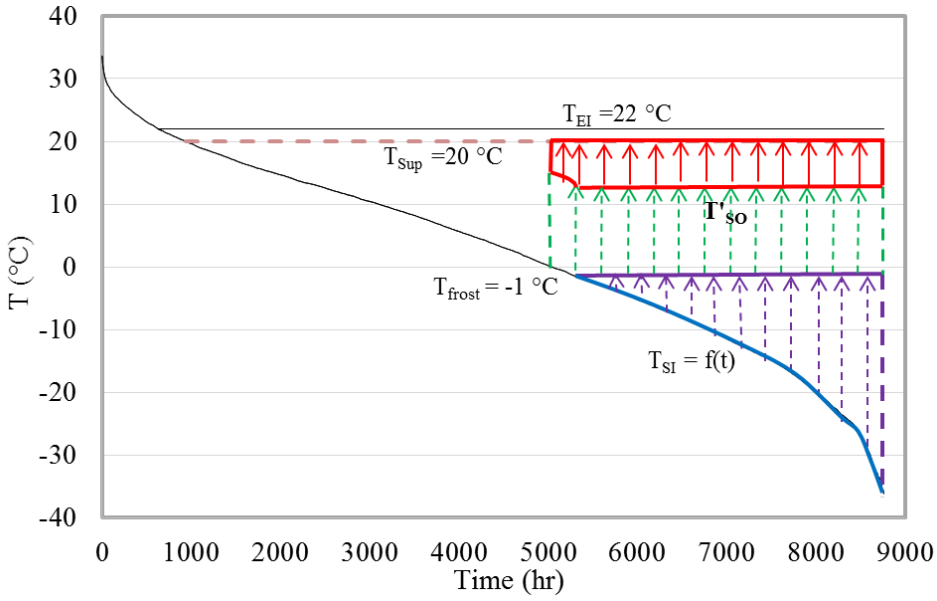

Figure 6.7. The recovered heat by heat exchanger and heating requirement by the pre-heater and re-heater when using pre-heating method.

6.5.3.2 Total energy recovery

The enthalpies of the supply air after the pre-heater (h_{frost}) and after the energy recovery exchanger (h'_{SO}) are calculated by Equations (6-12) and (6-13), respectively. It should be noted that only the temperature of the outdoor supply air changes in the pre-heating process, while the humidity ratio of air keeps constant.

$$h_{frost} = 1.006\, T_{frost} + w_{SI}\left(2501 + 1.86\, T_{frost}\right) \quad (6\text{-}12)$$

$$h'_{SO} = h_{frost} + \varepsilon_t\left(h_{EI} - h_{frost}\right) \quad (6\text{-}13)$$

Similarly, the areas that represent the energy recovered by energy exchanger (Equation (6-14)) and energy consumption by the preheater, re-heater and humidifier are plotted in Figure 6.8.

$$q'_{rec\_t} = \dot{m}_{air} \sum_i \left(h'_{SO} - h_{frost}\right)\Delta t_i \quad (6\text{-}14)$$

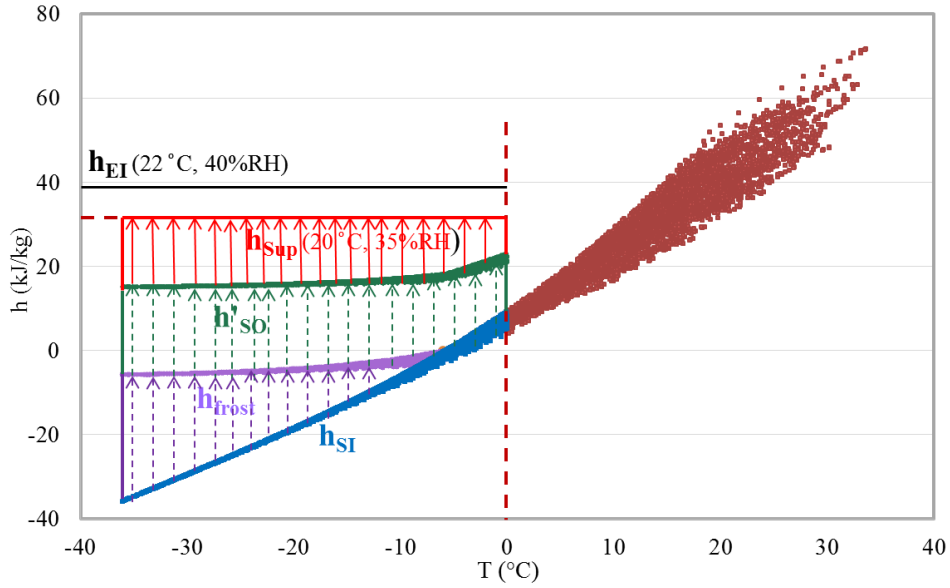

Figure 6.8. The recovered energy by energy exchanger and energy requirement by the pre-heater and re-heater and humidifier when using pre-heating method.

6.5.4 Heat/energy consumption using outdoor air bypassing method

In this method, outdoor ventilation air is bypassed from the supply side of the heat/energy exchangers periodically and indoor exhaust air is recirculated through the exchangers to melt or

remove the frost. The frequency of defrosting is important for the heat/energy recovery rates, since no heat/energy is recovered during the defrosting period and the effectiveness of heat/energy exchangers is assumed to be zero in this period. A defrosting time ratio (DTR) is proposed to show the frequency of defrosting for heat/energy exchangers, as shown in Figure 6.9. This ratio can be calculated by Equation (6-15). The DTR values of heat/energy exchangers were experimentally tested in this study and are presented in Section 6.6.

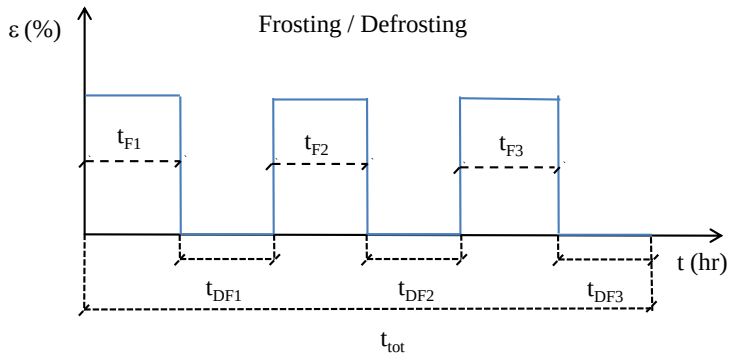

Figure 6.9. Schematic of the frosting and defrosting periods for heat/energy exchangers.

$$DTR = \frac{(t_{DF1} + t_{DF2} + t_{DF3})}{t_{tot}} \tag{6-15}$$

Where t_{DF} and $t_f$represent defrosting time and frosting time, respectively. Using the DTR value, the average sensible and total effectiveness of heat and energy exchangers during the whole operating period (t_{tot}) can be calculated by Equation (6-16), which takes the frosting effect into consideration.

$$\varepsilon_{avg} = \varepsilon \frac{(t_{F1} + t_{F2} + t_{F3})}{t_{tot}} = \varepsilon\,(1 - DTR) \tag{6-16}$$

6.5.4.1 Sensible energy recovery

Two separated areas could be determined on the ambient temperature duration curve to show the recovered heat by the heat recovery exchanger and the required heating consumption by the re-heater, as shown in Figure 6.10, when the outdoor air bypassing method is used for defrosting.

The average supply air temperature at the outlet of the heat exchanger (T''_{SO}) can be calculated using the average effectiveness with the same method described in 3.2.1, and the recovered energy (q''_{rec_s}) is calculated by Equation (6-17).

$$q''_{rec\_s} = c_{Pair}\dot{m}_{air}\sum_{i}(T''_{SO} - T_{SI})\Delta t_i \tag{6-17}$$

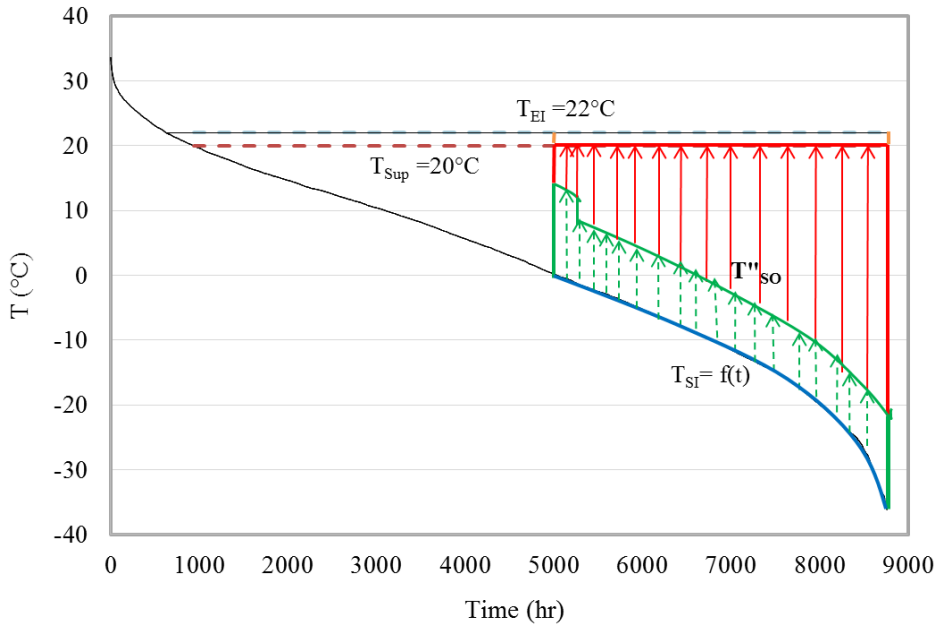

Figure 6.10. The recovered heat by the heat exchanger and the required heating by the re-heater when using outdoor air bypassing.

Compared with Figure 6.5, it is obvious that the amount of heat recovered by the heat exchanger reduces significantly when the frosting effect is taken into consideration. Correspondingly, the required heating by the re-heater increases.

6.5.4.2 Total energy recovery

The areas that represent the total energy recovered by energy exchanger and additional energy consumption for conditioning the ventilation air are shown in Figure 6.11. The average enthalpy of ventilation air after energy exchanger (h''_{SO}) can be calculated by average total effectiveness.

The recovered energy by the energy exchanger (Q''_{rec_t}) when using the outdoor air bypassing method can be calculated by Equation (6-18).

$$q''_{rec\_t} = \dot{m}_{air} \sum_i (h''_{SO} - h_{SI}) \Delta t_i \qquad (6\text{-}18)$$

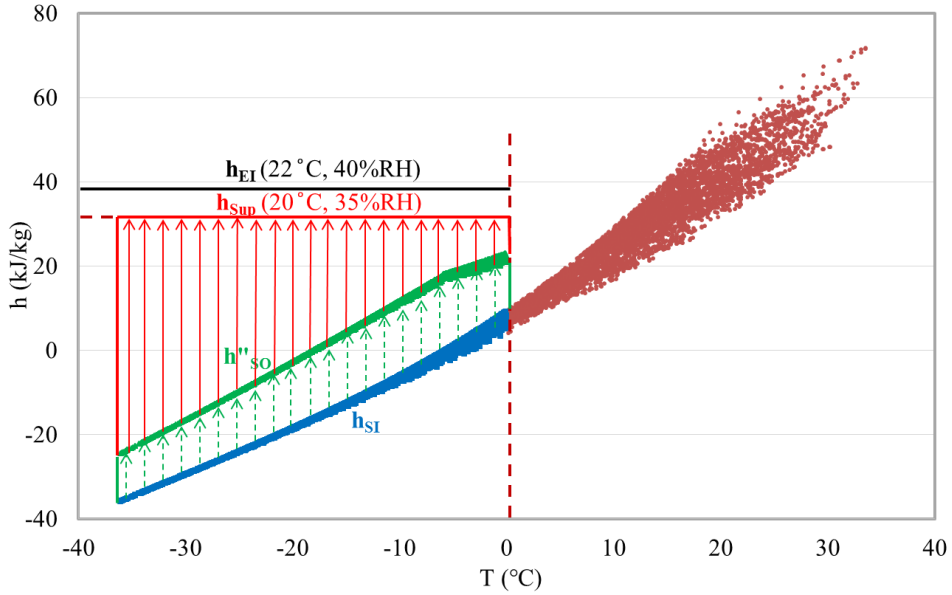

Figure 6.11. The total energy recovered by energy exchanger and additional energy consumption for conditioning the ventilation air when using the outdoor air bypassing.

6.6 EXPERIMENTAL FROSTING LIMIT AND DTR OF EXCHANGERS

Two types of air-to-air cross-flow exchangers, one sensible heat exchanger and one membrane-based energy exchanger, are investigated in this study. A series of experimental tests were conducted first to measure the effectiveness and frosting limit temperature for each core using the test facility (Figure 6.12) in the Energy Exchanger Research and Test Lab at the University of Saskatchewan. In all tests, the T_{EI} and RH_{EI} kept constant, but the supply inlet temperature (T_{SI}) was decreased gradually to get the frosting limit. It should be mentioned that visual techniques were employed to monitor the frosting in the experiments, which resulted in higher frosting limit found compared to the commonly used frosting detection methods, such as the pressure drop and effectiveness methods. A detail of the experimental procedure was presented in our previous publication (Rafati Nasr, Fauchoux, Kadylak, et al. 2014). The results on the effectiveness and frosting limit temperature of the heat/energy exchangers are shown in Table 6.2.

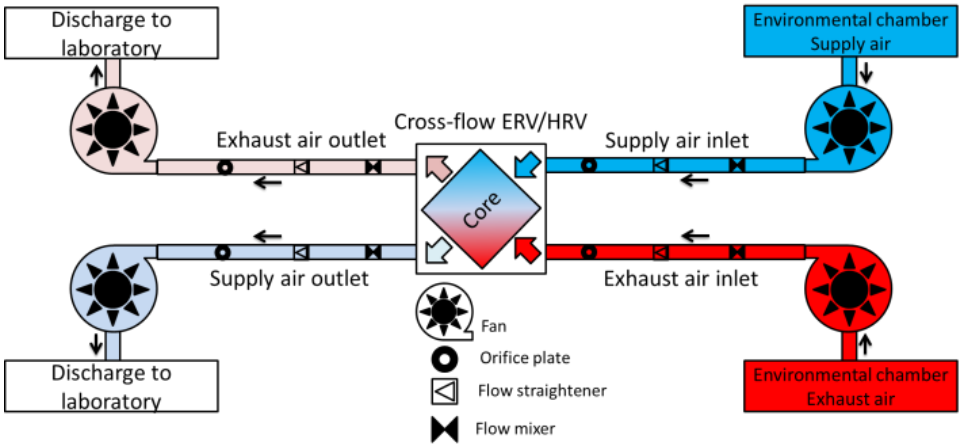

Figure 6.12. Schematic of the test facility for frosting/defrosting tests of heat/energy exchangers.

Table 6.2. Tested effectiveness and frost limit of the heat/energy exchanger.

Type	Flow rate (m^3/hr)	T_{EI} (°C)	RH_{EI} (%RH)	T_{frost} (°C)	ε_s (-)	ε_t (-)
HRV	75	22	40	-1	0.62	-
ERV				-6	0.57	0.47

The defrosting time ratio (DTR) strongly depends on the outdoor air temperature, exhaust indoor air temperature and humidity, and the type of exchanger (sensible heat exchanger or energy recovery exchanger). Experiments were also conducted by changing the supply inlet temperature while keeping the rest of inlet conditions. During the tests, both the heat and energy exchangers experienced a frosting period (i.e. $t_F \approx$ 4 hr) first at a certain condition with low outdoor air temperature (i.e. -5.3°C or -10.2°C). The pressure drop of the exhaust air stream across the exchanger increased gradually. Then the defrosting phase as shown in Figure 6.2 and Figure 6.9 was activated until the humidity ratio difference of the inlet and outlet of the exhaust air stream (frosted side) reached to zero and the pressure drop reduced to the normal value (i.e. 24 Pa) under no frosting. The defrosting time (t_{DF}) is recorded and used to calculate the DTR value at that operating condition. The experimental results for a heat exchanger and an energy exchanger are listed in Table 6.3 and 4. It is obvious that the DTR values of heat/energy exchangers increase as the outdoor air temperature (T_{SI}) decreases. Correspondingly, the average effectiveness values of the heat/energy exchangers decrease as the outdoor air temperature decreases.

Table 6.3. Defrosting tests for a heat exchanger using outdoor air bypassing.

T_{SI} (°C)	DTR (-)	ε_s (-)	$\varepsilon_{s\_avg} = (1\text{-DTR})\cdot\varepsilon_s$ (-)
-5.3	0.58	0.62	0.26
-10.5	0.64		0.22
-16.3	0.70		0.19

Table 6.4. Defrosting tests for an energy exchanger using outdoor air bypassing.

T_{SI} (°C)	DTR (-)	ε_s (-)	ε_t (-)	$\varepsilon_{s\_avg} = (1\text{-DTR})\cdot\varepsilon_s$ (-)	$\varepsilon_{t\_avg} = (1\text{-DTR})\cdot\varepsilon_t$ (-)
-10.2	0.18	0.57	0.47	0.47	0.39
-15.1	0.30			0.40	0.33
-18.7	0.38			0.35	0.29

Based on the tested average effectiveness values and the measured outdoor air temperatures, exponential equations (Figure 6.13) could be simply fitted to evaluate the average effectiveness of heat/energy exchangers at different outdoor air temperatures when they are lower than the frosting limits of the exchangers.

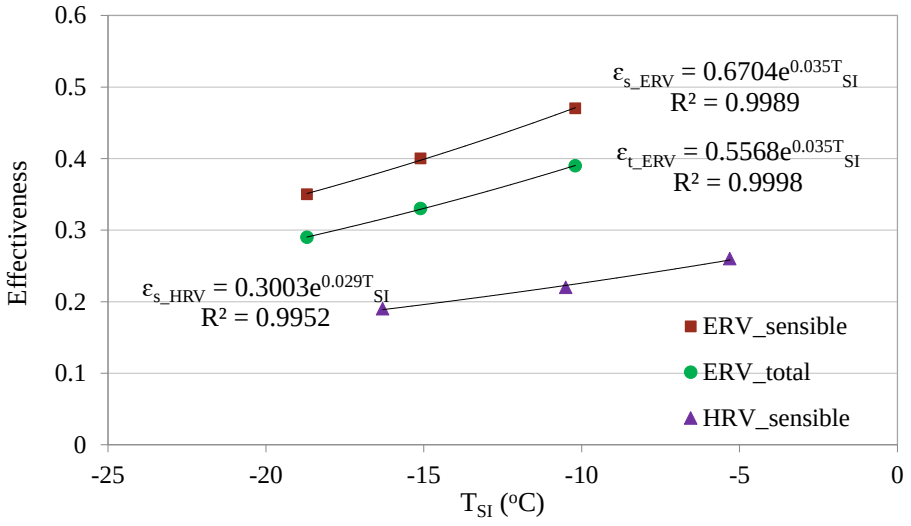

Figure 6.13. The fitted average effectiveness of heat/energy exchangers at different outdoor temperatures.

As shown in Figure 6.13, the average sensible effectiveness of the heat exchanger is much lower than the average effectiveness of energy exchanger. The main reason is that the heat exchanger is vulnerable to frosting under cold outdoor air conditions and would take longer time for defrosting (higher DTR value), as shown in Table 6.3.

6.7 RESULTS AND DISCUSSIONS

In this section, case studies are conducted to calculate the energy consumption for ventilation in three cold cities (Saskatoon, Anchorage and Chicago). Each of these cities represents a different type of cold region with respect to outdoor temperature and humidity level. Effectiveness values obtained from experimental tests (Section 6.6) are implemented to calculate the heat/energy recovered by exchangers. Figure 6.14 shows the energy requirement to condition the outdoor air before it enters to the building for three locations. Only the period that outdoor temperature is below 0^{o}C is considered for the energy estimation. It is obvious that longer cold season and lower outdoor moisture content resulted in greater amount of both sensible and total energy requirements for Saskatoon.

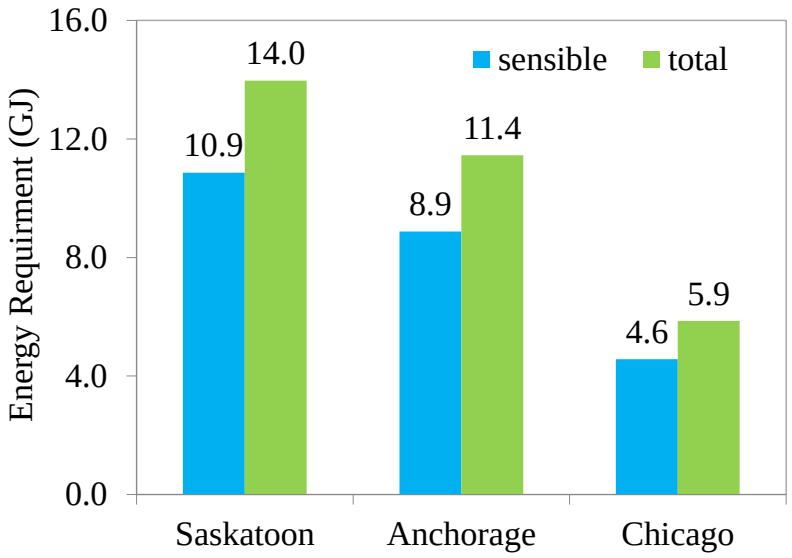

Figure 6.14. The energy requirement to condition the outdoor air when the outdoor temperature is less than 0^{o}C.

Figure 6.15 shows the amount of heat recovery by heat exchanger and energy recovery by energy exchanger as well as the auxiliary energy consumption for ventilation in Saskatoon, Canada, using

different defrosting strategies. In the figures, the symbol 'Pre-' represents the heat/energy consumed for preheating outdoor ventilation air before entering the exchangers, the symbol 'HRV' or 'ERV' represents the heat/energy recovered by the heat/energy exchangers, while the symbol 'Post-' represents the heat/energy consumed for further conditioning (reheating or reheating and humidifying) the ventilation air after the exchangers to obtain the desired supply air conditions. The saving percentage by heat/energy exchangers is also calculated by the amount of heat/energy recovered to total energy requirement as represented by the green lines in the figures. It is obvious that the heat/energy exchangers can recover most heat/energy from the exhaust air flow when ignoring the effect of frosting, which is in the range of 54% to 66%. When considering the frosting effect, the recovered heat/energy reduces significantly, especially for the heat exchanger.

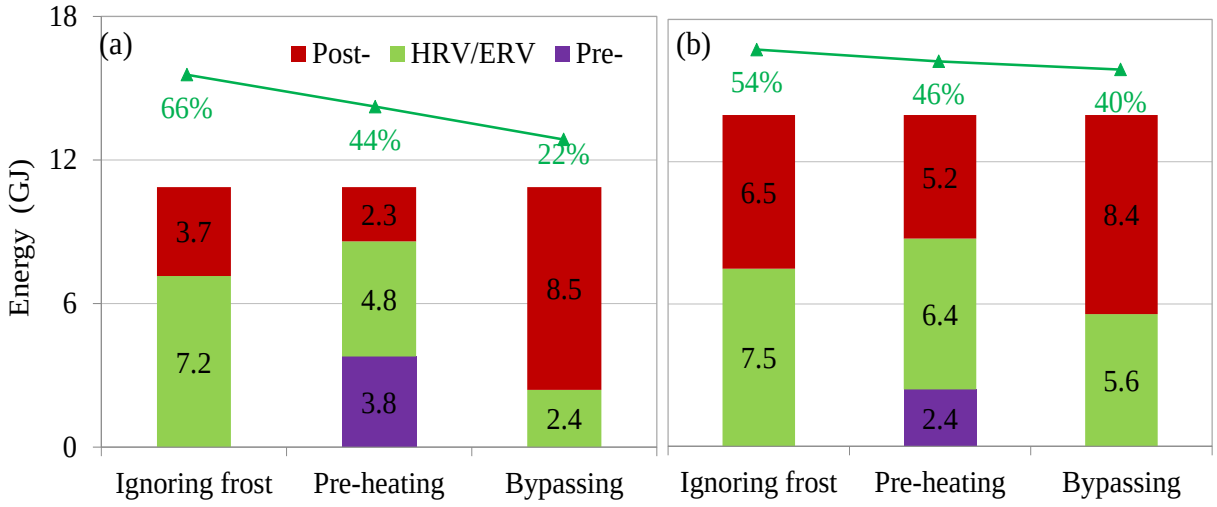

Figure 6.15. The amounts of energy recovery and auxiliary energy requirement for ventilation by (a) heat exchanger (sensible), (b) energy exchanger (total) using different defrosting methods (Saskatoon, Canada).

According to the results shown in Figure 6.15, it is found the outdoor air preheating method performs better than the outdoor air bypassing method, especially for the heat recovery by heat exchanger. As shown in Figure 6.15(a), the saving percentage by the heat exchanger using preheating method is 44%, which is twice of the saving using the bypassing method (22%). There are two main reasons causing this result. Firstly, preheating the outdoor air above the frosting limit makes the actual recovery effectiveness of exchangers be equal to the nominal effectiveness values (i.e. 62%) under no frosting condition, although the actual heat recovery rate by the heat exchanger

reduces significantly due to the decrease of temperature differences between exhaust air and the ventilation air after preheating. Secondly, the heat exchanger is vulnerable to frosting and its average effectiveness value is very low using the bypassing method (i.e. < 26% in Table 6.3), which considerably degrades the heat recovery performance of the heat exchanger. For the energy exchanger, the preheating method still has better performance than the bypassing method, but the energy saving difference between these two methods (i.e. 6%) is much lower than that of heat exchanger (i.e. 22%). It is because the energy exchanger has much lower possibility to undergo frost and hence lower DTR values compared to the heat exchanger, which slightly impacts the average energy recovery effectiveness as shown in Table 6.4.

Figure 6.16 compares the heat/energy saving potentials by heat/energy exchangers using different defrosting methods in three cold cities (Chicago, Anchorage and Saskatoon). There are almost the same saving percentages for each type of heat/energy exchanger in different cities when the frosting effect is ignored. For instance, the saving percentage of heat exchanger is around 66% under ignoring frost condition. The results also show that the heat/energy saving potential in Saskatoon has the largest reduction under frosting conditions, while there is a smallest reduction in Chicago. The reason is that the outdoor weather condition in Saskatoon is coldest among the three cities, and the freezing period (i.e. outdoor air temperature lower than 0°C) is longest (3713 hr) in a whole year, which makes the frosting effect be maximum in Saskatoon. Moreover, the weather condition has less impact on the energy exchanger than the heat exchanger for heat/energy recovery since the energy exchanger can effectively reduce the frosting possibility in cold climates.

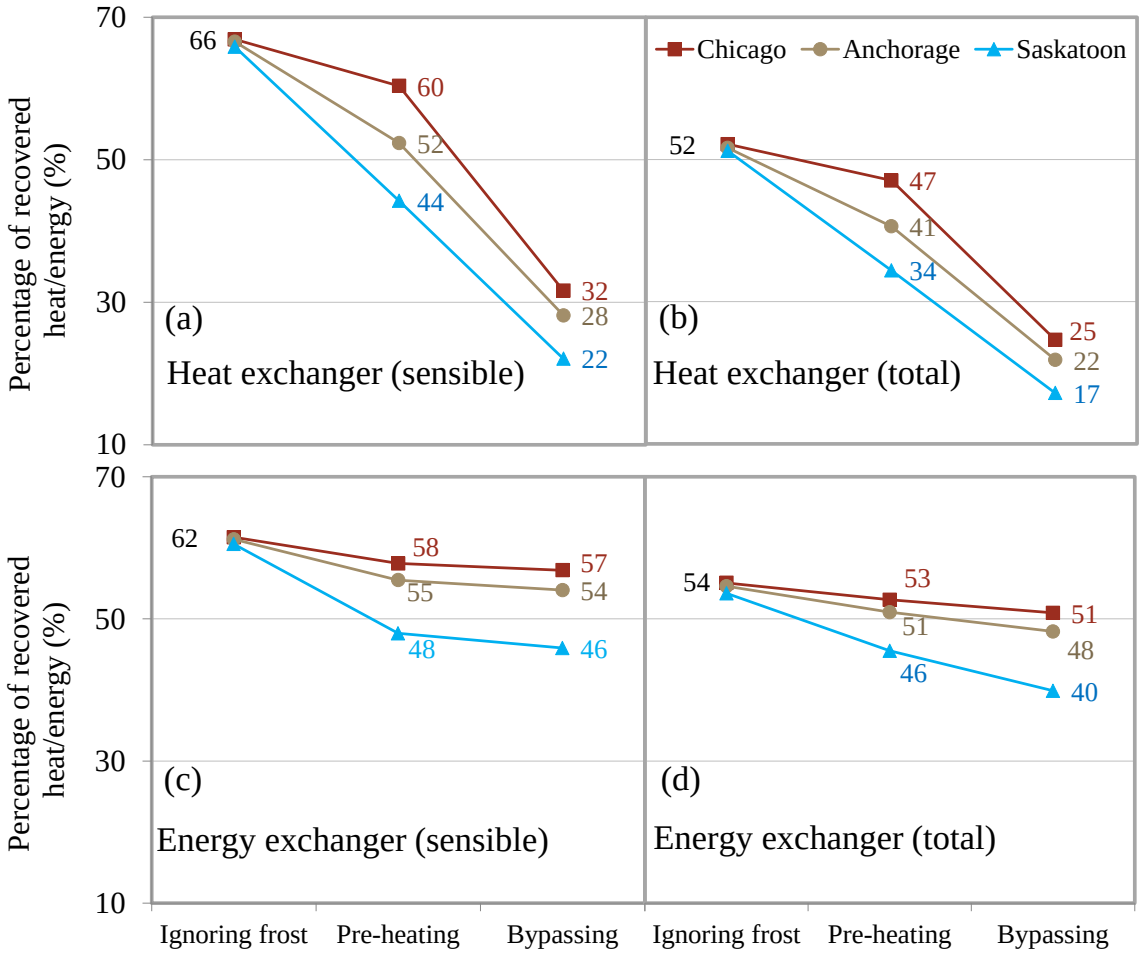

Figure 6.16. The saving percentages by heat/energy exchangers using different defrosting methods in three cold cities.

6.8 CONCLUSIONS

Frosting commonly occurs inside heat/energy exchangers in cold climates. In this study, the performance of heat/energy exchangers at frosting and defrosting periods are experimentally tested under different outdoor air temperatures. It is found that the values of defrosting time ratio (DTR) of heat/energy exchangers increase as the outdoor air temperature decreases. Correspondingly, the average effectiveness values of the heat/energy exchangers in the whole operating period decrease as the outdoor air temperature decreases. In addition, the average sensible effectiveness of the heat exchanger is much lower than the average effectiveness of energy exchanger.

The influences of two defrosting methods for air-to-air heat/energy exchangers, outdoor air preheating and outdoor airflow bypassing methods, on energy consumption of ventilation are evaluated in three cold cities (i.e. Saskatoon, Anchorage and Chicago). The results show that the outdoor air preheating method performs much better than the outdoor air bypassing method, especially for the heat recovery exchanger. The saving percentage using preheating method is 44%, which is twice of the saving using the bypassing method (22%) for the heat exchanger in Saskatoon. Based on this finding, the frosting limit detection of heat/energy exchangers is important and more research is needed in future work.

The results also show that the heat/energy saving potential in Saskatoon has the largest reduction under frosting conditions, while there is a smallest reduction in Chicago. The reason is that Saskatoon is coldest among the three cities and the freezing period is longest. The outdoor weather conditions play important roles for the frosting in exchangers and energy consumption for ventilation. Compared with the heat exchanger, the energy exchanger is less impacted by the weather condition for energy recovery since the energy exchanger can effectively reduce the frosting possibility in cold climates.

6.9 ACKNOWLEDGEMENTS

This research was financially supported by the Natural Sciences and Engineering Research Council of Canada (NSERC) through the Smart Net-Zero Energy Building Strategic Research Network (SNEBRN), ASHRAE through a grant-in-aid to Mr. Rafati Nasr, dPoint Technologies Inc. through in-kind support for a NSERC Engage project, the University of Saskatchewan and Hungarian Scholarship Board, Balassi Institute-Hungarian Scholarship Board Office, Budapest, Hungary.

CHAPTER 7:

SUMMARY AND CONCLUSIONS

7.1 SUMMARY AND CONCLUSIONS

This PhD thesis focused on frosting of membrane energy exchangers and heat exchangers through experiments and theoretical modeling. The following objectives are set to investigate frosting in air-to-air cross-flow heat/energy exchangers:

1. Develop a test facility to investigate frosting in exchangers,
2. Quantify the frosting limit for heat and energy exchangers,
3. Develop a theoretical model to predict the frosting limit for heat and energy exchangers,
4. Evaluate the energy impact of frosting and defrosting phases.

The thesis contains many comparisons between a membrane energy exchanger and a heat exchanger with identical geometries. The measured sensible effectiveness of these exchangers agreed with each other and theoretical values (58%) within experimental uncertainty (±2%).

A test setup was prepared for testing the prototype exchangers under frosting conditions. Four different methods to detect frosting in the exchangers were employed: (1) visual observing the frost growth, (2) monitoring the change in the effectiveness, (3) monitoring the pressure drop across the exchanger, and (4) measuring the temperature profile at the exhaust outlet. Using the temperature profile to detect frosting is a new method that was first introduced in this PhD study and was found to be an effective method for frost detection. The pressure drop and temperature profile methods were found to be the most practical, because they had much shorter response times and were more sensitive to the frosting conditions (i.e. they could quickly detect frost with low uncertainties).

The energy exchanger was found to be more frost resistant than the heat exchanger. The frosting limit of the energy exchanger was 5℃ to10℃ lower than the heat exchanger under the same air flow rate and exhaust air relative humidity, RH_{EI}. For example, when RH_{EI}=30%RH RH, the heat exchanger experienced frosting at a supply air temperature of -5℃, whereas the energy exchanger first experienced frosting at -10℃. In both exchangers, frosting was nearly inevitable for all indoor conditions when the supply air temperature was below -25℃.

A theoretical frosting limit model was developed and validated with experiments during this PhD study. The parametric analysis of the theoretical model showed that changing the number of heat transfer units (NTU_h) (similar to change the sensible effectiveness) had a small effect on frosting limit, while increasing the amount of mass transfer units (NTU_m) (similar to change latent effectiveness) with fixed NTU_h had a large effect on the frosting limit. The model can be applied to different types of flat plate air-to-air heat/energy exchangers to estimate the frosting limit of the exchangers, as long as the physical properties and performance parameters of the exchangers are known.

An in-depth experimental investigation, which was new to the literature, was conducted in this thesis to evaluate the effect of operating conditions on frost accumulation, frost removal, and exchanger performance. The exchangers were tested in two steps: a frosting phase followed by a defrosting phase. Measurement of the mass of the exchanger was introduced as an accurate method to measure frost accumulation and removal rates. The results indicated that the frost accumulation rate stayed almost constant during the frosting phase in both the heat exchanger and energy exchanger, for fixed inlet operating conditions. The heat exchanger had a frost accumulation rate almost three times higher than the energy exchanger. The pressure drop across the exchanger over time followed a power trend, which is influenced mainly by indoor humidity (RH_{EI}) and the outdoor temperature (T_{SI}). In the defrosting mode, the frost removal rate decreased exponentially with time. In general, the frost removal rate was much higher in the energy exchanger than in the heat exchanger. As a result, the time required to defrost the energy exchanger was found to be much lower than for the heat exchanger. Also, the results indicated that the required defrosting time for each exchanger changed considerably with RH_{EI} and T_{SI} and this finding can be used in practice in frost protection systems for HRV/ERV units.

The overall impact of frosting in heat and energy recovery in buildings was calculated with a method presented in Chapter 6. In this chapter two commonly-used methods of frost protection in exchangers were adopted; (a) avoid frost by preheating the supply air and (b) allow frost to build up and then remove frost by shutting off or bypassing the supply air periodically. The results indicated that the energy recovery can be significantly reduced due to frosting in regions with a cold climate. Compared with the heat exchanger, the energy recovery of the energy exchanger was less impacted by the weather conditions, since the energy exchanger has a lower frosting limit temperature and therefore can effectively reduce the possibility of frost in cold climates. The method of avoiding frost entirely was better in terms of energy recovery; however, the data for defrosting the exchangers were obtained from experiments in the lab which are different than in practice because the exchanger plates were horizontal which meant that run off of liquid water was neglected compared to practical installation with vertical plates. The methodologies used in this thesis can be applied for the configurations where the effect of gravity is incorporated into the tests.

7.2 CHALLENGES/LIMITATIONS

7.2.1 Transient Nature of Frosting Tests

Measurement of the mass of the exchanger is a non-continuous and labor-intensive method that may not be practical in long-term research. Each experiment took approximately one working day to be completed. During some experiments, the operating conditions fluctuated due to changes in the relative humidity level in the lab, defrosting of the evaporators in the environmental chamber, or a flow rate change due to a high pressure drop caused by frost in the exchanger. To reduce these fluctuations in the operating conditions, it is recommended to develop a smart control system for the environmental chambers, fans and steam generators, so the test setup runs automatically to provide consistent set point conditions at the test section.

7.2.2 Heat Loss

Due to the very low temperature of the supply air used, extra care must be taken to ensure that the heat gained by air stream are low. One of the main sources of heat gain is the supply fan. Changing the location of the fan or using thermal insulation around the casing for the fans could be a solution

to reduce this heat gain. During this PhD work, placing the upstream fan inside the cold chamber was found to be very useful.

7.2.3 Calibration

Instrumentation such as common humidity sensors or pressure transducers may not be rated for very low temperatures or may have unknown or large uncertainties at low temperatures. Great care should be taken into account to recalibrate the sensors for low temperatures or chose sensors with low uncertainty at low temperatures.

7.3 CONTRIBUTIONS

This thesis contains the following contributions to the scientific literature and practical applications of air-to-air energy exchangers.

- provided a comprehensive review on the works on frosting in air-to-air heat and energy exchangers and identifies different technologies to protect the exchangers from frosting,
- presented a comparison between different techniques to detect frosting in exchangers and identified a new practical method (ΔT method) to detect frosting in cross-flow air-to-air exchangers,
- quantified the frosting limit operating conditions in membrane energy exchangers,
- presented in-depth comparisons between performance of heat and energy exchangers under frosting and defrosting phases,
- developed and verified a theoretical model to predict the frosting limit in cross-flow heat and energy exchangers,
- presented a reliable method to measure the required defrosting time for exchanger, and
- introduced a theoretical method to calculate the overall impact of frosting in the total energy recovery in buildings in different climates.

7.4 FUTURE WORK

The following recommendations are made for future work on this project:

1. investigate the frost formation process on a membrane surface and compare the process with an impermeable plate,

2. develop a theoretical model or conduct numerical modeling on frosting on the surface of a membrane to predict the heat and mass transfer through the frosted surface,

3. conduct 3D numerical modeling of a cross-flow energy exchanger with the presence of frosting and compare the results with experiments in this thesis,

4. apply the findings in Chapter 3 of this thesis to develop a new frost detection system for commercial HRV/ERV units,

5. in chapter 3, measurement of the mass of the exchangers shows that a similar ΔP or ΔT for an exchanger under different operating conditions does not necessarily represent the same amount of frost. This means that the average density of frost (and as a result the structure of frost) changes with operating conditions. However, this point needs more in depth research which was out of the scope of this thesis.

6. improve the theoretical model for frosting limit presented in Chapter 4 to include exchangers with different spacing designs and different flow configurations (e.g. counter-flow, counter-cross-flow, energy wheel),

7. continue the experiments on frosting-defrosting cycles presented in Chapter 4 for different orientations, to include the effect of gravity in frost accumulation and frost removal,

8. investigate the effect of test duration on required defrosting duration,

9. improve the model in Chapter 6 to include energy impact of frosting based on yearly energy demand for different climate zones and building designs, and

10. develop a code or subroutine function for commercial energy modeling software, such as TRNSYS.

REFERENCES

Aarnes, S.M., 2012. *Membrane Based Heat Exchanger, M.Sc. Thesis*. Norwegian University of Science and Technology. Available at: http://www.diva-portal.org/smash/get/diva2:566164/FULLTEXT01.pdf.

Abdel-Salam, A.H. & Simonson, C.J., 2014. Annual evaluation of energy, environmental and economic performances of a membrane liquid desiccant air conditioning system with/without ERV. *Applied Energy*, 116, pp.134–148. Available at: http://dx.doi.org/10.1016/j.apenergy.2013.11.047.

AHRI, 2011. *AHRI Standard 1061, 2011 standard for Performance Rating of Air-to-Air Heat Exchangers for Energy Recovery Ventilation Equipment*, Arlington, USA.

AHRI, 2014. *AHRI Standard 1061, 2014 Performance Rating of Air- to-Air Exchangers for Energy Recovery Ventilation Equipment*, Arlington, USA.

Airxchange Inc., 2005. *Frost control strategies for for airxchange enthalpy wheels*, Available at: http://www.airxchange.com/Collateral/Documents/English-US/Frost Control Strategies for Airxchange Wheels.pdf.

Alonso, M.J. et al., 2012. Review of air-to-air heat / energy exchangers for use in NZEBs in the Nordic countries. In *Proceedings of the Second International conference on Building Energy and Environment, Boulder, Colorado*. pp. 536–543.

Alonso, M.J. et al., 2015. Review of heat/energy recovery exchangers for use in ZEBs in cold climate countries. *Building and Environment*, 84, pp.228–237. Available at: http://linkinghub.elsevier.com/retrieve/pii/S0360132314003679.

ASHRAE, 2009. *2009 ASHRAE Handbook Fundamentals*, Atlanta, USA: ASHRAE.

ASHRAE, 2012. *2012 ASHRAE handbook-HVAC Systems and Equipment Handbook*, Atlanta, USA: ASHRAE.

ASHRAE, 2013. *ANSI/ AHRAE Standard 84-2013 Method of Testing Air-to-Air Heat/Energy Exchangers*, Atlanta, USA: ASHRAE.

ASHRAE, 2007. *ANSI/ASHRAE/IESNA Standard 90.1-2007, Energy Standard for Buildings Except Low-Rise Residential Buildings*, Atlanta, USA: ASHRAE.

ASME, 2005. ASME PTC 19.1 test uncertainty. In New York, NY, USA: ASME.

ASME, 1991. PTC 30, Air-Cooled Heat Exchangers. In New York, NY, USA: ASME, p. 82.

Bantle, M., Barber, E. & Besant, R.W., 1987. A mathematical model of a plate type air-to-air heat exchanger operating under frost forming conditions. In K. C. Cheng, V. J. Lunardini, & N. Seki, eds. *Proceedings of the 1987 International Symposium on Cold Regions Heat Transfer*. New York, NY, USA: ASME, pp. 195–205.

Bantle, M.R.L., 1987. *Frost formation in an air to air heat exchanger, M.Sc. thesis*. University of Saskatchewan.

Barringer, C.G. & McGugan, C.A., 1989. Effect of residential air-to-air heat and moisture exchangers on indoor humidity. *ASHRAE Transactions*, 2, pp.461–474. Available at:

http://www.osti.gov/energycitations/product.biblio.jsp?osti_id=5783867 [Accessed January 31, 2013].

Barringer, C.G. & McGugan, C.A., 1988. *Investigation of enthalpy residential air-to-air heat exchangers, ASHRAE, Technical Committee 5.5, Air-to-Air Energy Recovery*, Atlanta, USA.

Besant, R.W. & Simonson, C.J., 2000. Air-to-air energy recovery. *ASHRAE journal*, 42, pp.31–42.

Besant, R.W. & Simonson, C.J., 2003. Air-to-air exchangers. *ASHRAE journal*, 45(4), pp.42–54. Available at: http://cat.inist.fr/?aModele=afficheN&cpsidt=14746904 [Accessed January 19, 2013].

Bilodeau, S. et al., 1999. Frost formation in rotary heat and moisture exchangers. *International Journal of Heat and Mass Transfer*, 42(14), pp.2605–2619. Available at: http://www.sciencedirect.com/science/article/pii/S0017931098003238.

Caltech, 1999. SNOWCrystal.com. Available at: http://www.its.caltech.edu/~atomic/snowcrystals/frost/frost.htm.

Charneux, R., 2012. CH-12-C052-Toward Net-Zero Energy Labs in Northern ClimateMontreal Examples. *ASHRAE Transactions*, 118, pp.42–54.

Chen, H., 2000. *Modeling and measurement of frost characteristics on heat exchanger surfaces*. PhD thesis,University of Saskatchewan.

Chen, H., Thomas, L. & Besant, R., 2000. Modeling Frost Characteristics on Heat Exchanger Fins: Part II, Model Validation and Limitations. *ASHRAE transactions*, 106(2), pp.368–376.

Chichindayev, A. V., 2006. Flight vehicle design: special features of optimizing a heat exchanger-condenser equipped with an antiicing system. *Russian Aeronautics*, 49(1), pp.1–6.

Ciepliski, D.L., 1997. *Testing an air-to-air rotary energy recovery device using performance test standards*. M.Sc. thesis, University of Saskatchewan.

Ciepliski, D.L., Besant, R.W. & Simonson, C.J., 1998. Some recommendations for improvements to ASHRAE Standard 84-1991. *ASHRAE transactions*, 104(1B), pp.1651–1665.

CSA, 2009. CAN/CSA-C439-09 (R2014) - Standard laboratory methods of test for rating the performance of heat/energy-recovery ventilators. In CSA, p. 54.

Davis, G.B., 1996. Energy recovery ventilator: means for defrosting heat exchanger medium and damper motor actuation means. *US Patent 5,497,823*.

Fisk, W.J. et al., 1984. Onset of freezing in residential air-to-air heat exchangers. *ASHRAE transactions*, 91, pp.145–158.

Fisk, W.J. et al., 1985. Performance of Residential Air-to-Air Heat Exchangers during Operation with Freezing and Periodic Defrosts. *ASHRAE transactions*, 91(2), pp.159–172.

Gao, T. & Gong, J., 2011. Modeling the airside dynamic behavior of a heat exchanger under frosting conditions. *Journal of Mechanical Science and Technology*, 25(10), pp.2719–2728.

Available at: http://www.springerlink.com/index/10.1007/s12206-011-0615-5.

Garber-Slaght, R., Stevens, V. & Madden, D., 2014. *Energy Recovery Ventilators in Cold Climates*, Fairbanks, AK, USA. Available at: www.cchrc.org.

Gazi, I.M. & Simonson, C.J., 2012. Frosting Conditions for an Energy Wheel in Laboratory Simulated Extreme Cold Weather. In *7th International Cold Climate HVAC Conference November 12-14, 2012 Calgary, Alberta, Canada*. p. 9.

Ge, G. et al., 2014. Material properties and measurements for semi-permeable membranes used in energy exchangers. *Journal of Membrane Science*, 453, pp.328–336. Available at: http://linkinghub.elsevier.com/retrieve/pii/S0376738813008983.

Ge, G. et al., 2013. Research and applications of liquid-to-air membrane energy exchangers in building HVAC systems at University of Saskatchewan: A review. *Renewable and Sustainable Energy Reviews*, 26, pp.464–479.

Gong, G. et al., 2013. Research on frost formation in air source heat pump at cold-moist conditions in central-south China. *Applied Energy*, 102, pp.571–581. Available at: http://dx.doi.org/10.1016/j.apenergy.2012.08.001.

Hallgren, K., 1981. Method and device for defrosting heat exchanger without impairment of its heat exchange efficiency. *US Patent 4,244,422*, (741).

Holmberg, R.B., 1989a. Prediction of condensation and frosting limits in rotary wheels for heat recovery in buildings. *ASHRAE transactions*, 95(32), pp.64–69.

Holmberg, R.B., 1989b. Sensible and latent heat transfer in cross-counterflow gas-to-gas heat exchangers. *Journal of Heat Transfer*, 111(February), pp.173–177. Available at: http://www.osti.gov/energycitations/product.biblio.jsp?osti_id=7002486.

Iragorry, J., Tao, Y.X. & Jia, S., 2004. Review article: A critical review of properties and models for frost formation analysis. *HVAC&R Research*, 10(4), pp.393–420.

ISO, 2003. *ISO 5167-1: 2003, Measurement of fluid flow by means of pressure differential devices inserted in circular cross-section conduits running full -- Part 1: General principles and requirements*, Geneva, Switzerland: International Standards Organization.

Jang, J.Y. et al., 2013. Continuous heating of an air-source heat pump during defrosting and improvement of energy efficiency. *Applied Energy*, 110, pp.9–16. Available at: http://dx.doi.org/10.1016/j.apenergy.2013.04.030.

Kajtár, L., Kassai, M. & Bánhidi, L., 2012. Computerised simulation of the energy consumption of air handling units. *Energy and Buildings*, 45, pp.54–59. Available at: http://dx.doi.org/10.1016/j.enbuild.2011.10.013.

Kondepudi, S.N. & O'NEAL, D.L., 1987. The effects of frost growth on extended surface heat exchanger performance : a review. *ASHRAE transactions*, pp.258–269.

Kragh, J. et al., 2007. New counter flow heat exchanger designed for ventilation systems in cold climates. *Energy and Buildings*, 39(11), pp.1151–1158. Available at: http://linkinghub.elsevier.com/retrieve/pii/S0378778807000059.

Kragh, J., Rose, J. & Svendsen, S., 2005. Mechanical ventilation with heat recovery in cold climates. In *Proceeding of the Seventh Nordic Symposium on Building Physics in Nordic*

Countries. Technical University of Denmark, pp. 1–8.

Kumaran, K. & Sanders, C., 2008. *Annex 41 MOST-ENG Subtask 3: Boundary Conditions and Whole Building HAM Analysis* 1st ed., International Energy Agency (Exco ECBCS). Available at: http://www.iea-ebc.org/projects/completed-projects/ebc-annex-41/.

Liu, P. et al., 2016. A Theoretical Model to Predict Frosting Limits in Cross-Flow Air-to-Air Flat Plate Heat / Energy Exchangers. *Energy and Buildings*, 110, pp.404–414.

Liu, P. et al., 2014. Frosting Limits for Counter-flow Membrane Energy Exchanger (MEE) in Cold Climates. In *13th International Conference on Indoor Air Quality and Climate,Hong Kong*.

Liu, P., Mathisen, H.M. & Alonso, M.J., 2013. Critical Sensible and Latent Effectiveness for Membrane Type Energy Recovery Ventilator (ERV) in Cold Climates. In *IAQ 2013 Environmental Health in Low Energy Buildings Conference*. Vancouver, Canada: ASHRAE.

Liu, Z. et al., 2010. Experimental investigations of frost release by hydrophilic surfaces. *Frontiers of Energy and Power Engineering in China*, 4(4), pp.475–487. Available at: http://www.springerlink.com/index/10.1007/s11708-010-0114-x.

Mao, Y., 1991. *The Measurement and analysis of frost accumulation on a flat plate with forced convection, M.Sc. thesis*. University of Saskatchewan.

Mardiana-Idayu, A. & Riffat, S.B., 2012. Review on heat recovery technologies for building applications. *Renewable and Sustainable Energy Reviews*, 16(2), pp.1241–1255. Available at: http://linkinghub.elsevier.com/retrieve/pii/S136403211100476X.

Mercadier, Y., Duong, T. & Lagace, F., 1993. Dynamic performance of a cross flow heat recovery ventilator operating under frost conditions. In *Proceedings of the Fourth International Symposium on Thermal Engineering and Science for Cold Regions*. Hanover, NH, pp. 113–121.

Moallem, E. et al., 2012. Experimental measurements of the surface coating and water retention effects on frosting performance of microchannel heat exchangers for heat pump systems. *Experimental Thermal and Fluid Science*, 39, pp.176–188. Available at: http://linkinghub.elsevier.com/retrieve/pii/S0894177712000337.

Namvar, R. et al., 2012. Transient characteristics of a liquid-to-air membrane energy exchanger (LAMEE) experimental data with correlations. *International Journal of Heat and Mass Transfer*, 55(23-24), pp.6682–6694. Available at: http://linkinghub.elsevier.com/retrieve/pii/S001793101200508X [Accessed November 18, 2012].

Nielsen, T.R., Rose, J. & Kragh, J., 2009. Dynamic model of counter flow air to air heat exchanger for comfort ventilation with condensation and frost formation. *Applied Thermal Engineering*, 29(2-3), pp.462–468. Available at: http://linkinghub.elsevier.com/retrieve/pii/S1359431108001385 [Accessed November 11, 2012].

Ninomura, P.T. & Bhargava, R., 1995. Heat recovery ventilators in multifamily residences in the arctic. *ASHRAE Transactions*, 101, pp.961–966. Available at:

http://www.inive.org/Ibase_search/search-detail-airbase-001.asp?ID=9142.

NRC, 2011. *Energy Efficiency Trends in Canada 1990 to 2009*, Ottawa, ON, Canada. Available at: http://oee.nrcan.gc.ca/publications/statistics/trends11/pdf/trends.pdf.

Nyman, M. & Simonson, C.J., 2005. Life cycle assessment of residential ventilation units in a cold climate. *Building and Environment*, 40(1), pp.15–27. Available at: http://linkinghub.elsevier.com/retrieve/pii/S0360132304001532 [Accessed February 2, 2013].

O'NEAL, D.L. & Tree, D.R.D., 1985. A review of frost formation in simple geometries. *ASHRAE Transactions*, pp.267–281. Available at: http://cat.inist.fr/?aModele=afficheN&cpsidt=8388371.

Östin, R. & Johannesson, G., 1991. A polymeric approach to counteract frosting in air-to-air heat exchangers. *Heat Recovery Systems and CHP*, 11(5), pp.415–421. Available at: http://www.sciencedirect.com/science/article/pii/089043329190009S.

Pääkkönen, T.M. et al., 2015. Modeling CaCO3 crystallization fouling on a heat exchanger surface – Definition of fouling layer properties and model parameters. *International Journal of Heat and Mass Transfer*, 83, pp.84–98. Available at: http://www.sciencedirect.com/science/article/pii/S0017931014010692.

Padhmanabhan, S.K. et al., 2011. Modeling non-uniform frost growth on a fin-and-tube heat exchanger. *International Journal of Refrigeration*, 34(8), pp.2018–2030. Available at: http://linkinghub.elsevier.com/retrieve/pii/S0140700711001459.

Padki, M.M., Sherif, S.A. & Nelson, R.M., 1989. A simple method for modeling the frost formation phenomenon in different geometries. *ASHRAE Transactions*, (1972), pp.1127–1137.

Pfeiffer, S. & Hubner, H., Untersuchungen zum Einfrieren von Regenerativ-Wärmeübertragern. *Klima, Kälte, Heizung*, 15(10), pp.449–452. Available at: http://cat.inist.fr/?aModele=afficheN&cpsidt=7721009.

Pfluger, R., Bräunlich, K. & Elisabeth, S., 2015. Ventilation for residential buildings workshop. In *19th International Passive House Conference*. Leipzig, Germany, p. 87.

Phillips, E.G., Chant, R.E., et al., 1989. A model to compare freezing control strategies for residential air-to-air Heat Recovery Ventilators. *ASHRAE transactions*, 95(2), pp.475–483.

Phillips, E.G., Bradley, L.C., et al., 1989. Comparison of freezing control strategies for residential air-to-air heat recovery ventilators. *ASHRAE transactions*, pp.484–490. Available at: http://www.osti.gov/energycitations/product.biblio.jsp?osti_id=5783875.

Phillips, E.G., Fisher, D.R. & Chant, R.E., 1992. Freeze-control strategy and air-to-air energy recovery performance. *ASHRAE journal*, pp.44–49. Available at: http://cat.inist.fr/?aModele=afficheN&cpsidt=4657461.

Qarnia, H.E., Lacroix, M. & Mercadier, Y., 2001. Use of a phase change material to prevent frosting in a compact crossflow air exchanger. *Energy conversion and management*, 42, pp.1277–1296. Available at: http://www.sciencedirect.com/science/article/pii/S0196890400000704 [Accessed November 11, 2012].

Rafati Nasr, M., Fauchoux, M., Besant, R.W., et al., 2014. A review of frosting in air-to-air energy exchangers. *Renewable and Sustainable Energy Reviews*, 30, pp.538–554.

Rafati Nasr, M., Kassai, M., et al., 2015. Evaluation of defrosting methods for air-to-air heat/energy exchangers on energy consumption of ventilation. *Journal of Applied Energy*, 151, p.35. Available at: http://dx.doi.org/10.1016/j.apenergy.2015.04.022.

Rafati Nasr, M., Fathieh, F., et al., 2015. Experimental methods of detecting frosting in cross-flow air-toair energy exchangers. *Under review in Experimental Thermal and Fluid Science*, p.38.

Rafati Nasr, M., Fauchoux, M., Kadylak, D., et al., 2014. Frosting limit in Air-to-Air Membrane Energy Exchangers. In *10th Nordic Symposium on Building Physics*. Lund, Sweden, pp. 774–781.

Rafati Nasr, M. & Simonson, C.J., 2016. Experimental Measurement of Frosting Limits in Cross-Flow Air-to-Air Energy Exchangers. In *under review ASHRAE Transactions*. st. Louis, Missouri: ASHRAE.

Rasouli, M. et al., 2013. Uncertainties in energy and economic performance of HVAC systems and energy recovery ventilators due to uncertainties in building and HVAC parameters. *Applied Thermal Engineering*, 50(1), pp.732–742. Available at: http://dx.doi.org/10.1016/j.applthermaleng.2012.08.021.

Rasouli, M., Simonson, C.J. & Besant, R.W., 2010. Applicability and optimum control strategy of energy recovery ventilators in different climatic conditions. *Energy and Buildings*, 42(9), pp.1376–1385. Available at: http://dx.doi.org/10.1016/j.enbuild.2010.03.006.

Reay, D.A., 1980. A Review of gas-gas heat recovery systems. *Heat Recorery Systems*, 1, pp.3–41.

Ruth, D.W., Fisher, D.R. & Gawley, H.N., 1975. Investigation of frosting in rotary air-to-air heat exchangers. *ASHRAE Transactions*, 81, pp.410–417.

Sauer, H.J., Howell, R.H. & Wray, J.R., 1981. Frosting and leak testing of air to air energy recovery systems. *ASHRAE Transactions*, 87, pp.211–234.

Shang, W., Chen, H. & Besant, R.W., 2005. Frost Growth in Regenerative Wheels. *Journal of Heat Transfer*, 127(9), p.1015.

Shoukri, M., 1979. The Use of a Regenerative Air-to-Air Rotary Heat Exchangers for Heat Recovery in Residential Ventilation Systems. In *American Society of Mechanical Engineers, Annual meeting*. New York, NY.

Simonson, C.J., 2007. Heat and energy wheels. *Encyclopedia of Energy Engineering and Technology*, pp.794–800.

Simonson, C.J. & Besant, R.W., 1998. Heat and Moisture Transfer in Energy Wheels During Sorption, Condensation, and Frosting Conditions. *Journal of Heat Transfer*, 120(3), p.699. Available at: http://link.aip.org/link/JHTRAO/v120/i3/p699/s1&Agg=doi.

Sisk, F.J., 1980. Apparatus for defrosting low temperature heat exchanger. *US Patent 4,191,026*, p.6.

Sonntag, R.E., Borgnakke, C. & Van Wylen, G.J., 2009. *Fundamentals of thermodynamics*,

Thomas, L., 1999. *Measurement of frost height on heat exchanger fins, M.Sc. Thesis*. University of Saskatchewan.

Tommerup, H. & Svendsen, S., 2005. Ventilation with heat recovery. In *Seventh Nordic Symposium on Building Physics in Nordic Countries*. TReykjavík, Iceland.

Voss, K. et al., 2009. IEA Joint Project: Towards Net Zero Energy Solar Buildings (NZEBs). *IEA Solar Heating & Cooling Programme - Task 40 and IEA Energy Conservation in Buildings and Community Systems Programme - Annex 52 Joint Project*, (February).

Wang, H. et al., 2007. Fabrication and anti-frosting performance of super hydrophobic coating based on modified nano-sized calcium carbonate and ordinary polyacrylate. *Applied Surface Science*, 253(22), pp.8818–8824.

Wang, W. et al., 2011. Field test investigation of the characteristics for the air source heat pump under two typical mal-defrost phenomena. *Applied Energy*, 88(12), pp.4470–4480.

White, F.M., 2011. *Fluid mechanics* 7th ed., New York, NY, USA: Mcgraw-Hill.

Wu, J. et al., 2011. Experimental investigation of frost formation on a parallel flow evaporator. *Applied Energy*, 88(5), pp.1549–1556.

Wu, Y. et al., 2001. Simulating the Performance of a Heat Exchanger During Frosting General Motors Corporation. *Air Conditioning and Refrigeration Center. College of Engineering. University of Illinois at Urbana-Champaign*.

Xiao, F., Ge, G. & Niu, X., 2011. Control performance of a dedicated outdoor air system adopting liquid desiccant dehumidification. *Applied Energy*, 88(1), pp.143–149. Available at: http://dx.doi.org/10.1016/j.apenergy.2010.06.019.

Zhang, J. & Fung, A.S., 2015a. Experimental study and analysis of an energy recovery ventilator and the impacts of defrost cycle. *Energy and Buildings*, 87, pp.265–271. Available at: http://www.sciencedirect.com/science/article/pii/S0378778814010068.

Zhang, J. & Fung, A.S., 2015b. Experimetnal and Numerical Investigation of the Thermal Impact of Defrost Cycle of Residential Heat and Energy Recovery Ventilators. *Energy and Buildings*, 97, pp.129–136. Available at: http://www.sciencedirect.com/science/article/pii/S0378778815002431.

Zhang, J., Fung, A.S. & Jhingan, S., 2014. Analysis and feasibility study of residential integrated heat and energy recovery ventilator with built-in economizer using an excel spreadsheet program. *Energy and Buildings*, 75, pp.430–438. Available at: http://www.sciencedirect.com/science/article/pii/S0378778814001509.

Zhang, L., 2008. *Total heat recovery: heat and moisture recovery from ventilation air*, New York, NY, USA: Nova Science Publishers, Inc.

Zhang, L.-Z. & Xiao, F., 2008. Simultaneous heat and moisture transfer through a composite supported liquid membrane. *International Journal of Heat and Mass Transfer*, 51(9-10), pp.2179–2189.

Zhang, L.-Z.Z., 2012. Progress on heat and moisture recovery with membranes: From fundamentals to engineering applications. *Energy Conversion and Management*, 63, pp.173–195. Available at: http://linkinghub.elsevier.com/retrieve/pii/S0196890412001203.

APPENDIX:

PERMISSIONS TO REPRODUCE

This appendix includes the copyright permissions for the published and co-authored manuscripts presented in this thesis. For manuscripts that form part of a thesis, the College of Graduate Studies and Research (CGSR) requires a written request from:

- the publisher (copyright holder) for previously published manuscripts, and
- the co-author(s) for unpublished manuscripts.

The permissions for using the published manuscripts in this thesis are presented in section A.1, and the permissions for using the unpublished manuscripts are presented in Sections A.2.

A.1 PERMISSIONS FOR THE MANUSCRIPTS USED IN CHAPTERS 2,3, 4, AND 6

The manuscripts used in Chapters 2, 4, and 6 are published by Elsevier. For manuscripts published by Elsevier, the authors retain the right to include their publication in a thesis without requesting a written permission as mentioned on the publisher's website as follows:

> *As an author, you retain rights for a large number of author uses, including use by your employing institute or company. These rights are retained and permitted without the need to obtain specific permission from Elsevier. These include:[…]The right to include the article in full or in part in a thesis or dissertation (provided that this is not to be published commercially)[…]*[1]

[1]~source: https://help.elsevier.com/app/answers/detail/a_id/565/session/L3RpbWUv/p/8045

A.2 PERMISSION FOR THE MANUSCRIPT USED IN CHAPTER 5

The manuscript used in Chapter 5 is unpublished, and thus copyright permissions are obtained from the co-author of the paper (Dr. Carey J. Simonson) as follows.

I am preparing the publication of a manuscript titled "**Frosting-defrosting and required defrosting time**" to be published as the 5th chapter of my Ph.D. thesis, and to be submitted to the Department of Mechanical Engineering at the University of Saskatchewan. The authors contributing in the completion of this manuscript are: Mohammad Rafati Nasr, Carey J. Simonson.

I am requesting permission to use the materials described in aforementioned manuscript in my Ph.D. thesis and all subsequent editions that may be prepared at the University of Saskatchewan. Please indicate agreement by signing below.

Sincerely,

Mohammad Rafati Nasr

March, 2016

Permission granted by: Carey J. Simonson Signature: Date: